Roger Ekseth

Uncertainties in connection with the determination of wellbore positions

NTNU Trondheim
Norges teknisk-naturvitenskapelige universitet

Doktor ingeniøravhandling 1998:24
Institutt for petroleumsteknologi og anvendt geofysikk

IPT-rapport 1998:2

UNCERTAINTIES IN CONNECTION WITH THE DETERMINATION OF WELLBORE POSITIONS

By

Roger Ekseth

A dissertation for the
partial fulfilment of requirements
for the degree of doktor ingeniør

Department of Petroleum Engineering and Applied Geophysics
The Norwegian University of Science and Technology

Trondheim, March 1998

Corrections

Page 12	Line 2+3 from bottom	*co-ordinate vector at station j* should be **the co-ordinate difference vector between station *j-1* and *j***
Page 13	Equation *{3.1-8}* line 1	$\varepsilon_X \varepsilon_X^T \approx [\ (\partial f_1/\partial I_0)^2 \varepsilon_{I0}^2 + (\partial f_1/\partial A_0)^2 \varepsilon_{A0}^2 + (\partial f_1/\partial D_0)^2 \varepsilon_{D0}^2\ ]$
Page 25	Equation *{3.5-2}*	all $\ldots \sum_{j=j+1}^{j+k_1} [\ldots$ should be $\ldots \sum_{j=\sum_{l=1}^{k}(k_{l-1})+1}^{\sum_{l=1}^{k}(k_l)} [\ldots$
Page 54	Equation *{5.1.1.3-2}*	second line should be $\approx \sqrt{\frac{d\eta_a^2}{G^2 \sin^2 I} + 2\sin^2\tau\cos^2\tau dv_a^2}$
Page 64	Line 2 chapter 5.2.1.1	*true magnetic north* should be **true north**
Page 89	Equation *{6.1.1.3-2}*	$d\tau \approx \sqrt{\frac{d\eta_a^2}{G^2 \sin^2 I} + 2\sin^2\tau\cos^2\tau dv_a^2}$
Page 92	Equation *{6.1.1.4-7}*	$T_{x,\tau+180} \approx -\Omega\cos\phi(\cos I\cos A\cos\tau - \sin A\sin\tau) - \Omega\sin\phi\sin I\cos\tau$
	Equation *{6.1.1.4-13}*	$T_{y,\tau+180} \approx \Omega\cos\phi(\cos I\cos A\sin\tau + \sin A\cos\tau) + \Omega\sin\phi\sin I\sin\tau$
Page 93	Line 1	*earth angular rate at the equator* should be **earth angular rate**
Page 94	Equation *{6.1.1.4-26}*	$T_{z,\tau+180} \approx -\Omega\cos\phi(\cos I\cos A\sin\tau + \sin A\cos\tau) + \Omega\sin\phi\sin I\sin\tau$
	Equation *{6.1.1.4-32}*	$T_{z,\tau+270} \approx \Omega\cos\phi(\cos I\cos A\cos\tau - \sin A\sin\tau) - \Omega\sin\phi\sin I\cos\tau$
Page 119	Equation *{7.1-3}*	$dD_I = i_s d\beta_2$
	Equation *{7.1-4}*	$dD_{II} = i_s\sqrt{d\beta_1^2 + d\beta_3^2}$
Page 120	Line 2 paragraph 4	*and 0°C.* should be **and the surface reference temperature for thermal drill string expansion.**
Page 124	Equation *{7.2.4-4}*	$dD_X = 0.125 dD_{IX}$
Page 126	Equation *{7.2.5-6}*	$dD_{XIV} = 0.5 dD_{XIII}$
Page 141	Equation *{8.1.1-8}*	$d\tau \approx \sqrt{\frac{d\eta_a^2}{G^2 \sin^2 I} + 2\sin^2\tau\cos^2\tau dv_a^2}$
	Equation *{8.1.1-9}* line 2	$\approx -(\Delta\tau_j \cos I_j + \Delta t(\omega_{x,j}\sin\tau_j + \omega_{y,j}\cos\tau_j)\sin I_j - \Delta t\omega_{z,j}\cos I_j - \Delta t\Omega\sin\phi)$
Page 144	Equation *{8.1.2-3}*	$dA_7 = \frac{\partial A}{\partial I} dI + \frac{\partial A}{\partial \tau} d\tau \approx \frac{\sin\phi}{\cos\phi} dI - \cos I d\tau$
Page 147	Line 2 paragraph 3	*factor is 2.49* should be **factor is 2.45**

Abstract

This theses presents the basic error propagation mechanisms for wellbore position surveying (often called directional surveying), gives an analysis of well known published error propagation theories, and gives a detailed theoretical error analysis of commonly used survey equipment and techniques.

To form a complete tool for wellbore position uncertainty studies, the theoretical error analysis has to be accompanied by estimated uncertainty figures for the different error sources, and by quality control procedures designed to assure survey results in accordance with these uncertainty figures. The latter two tasks are not part of this theses, but they have to be solved before wellbore position uncertainty studies can become a practical tool, for example in connection with risk based decision making and optimal planning of wellbore surveying programs.

Firstly, the derivation of the basic error propagation mechanisms for classical directional surveying techniques is presented. The basic error theory is visualised through numerical examples. The accuracy figures used are typical for what is expected in connection with high quality surveys in the North Sea region. They are not reflecting uncertainties that should be expected in connection with surveys taken anywhere in the world.

Published directional surveying error propagation theories, the Walstrom model, the Wolff deWardt model, and the Instrument performance model, are examined against this basic theory. It is concluded that available methods, at least their implementation in most of the oil industry, are too confined to give a realistic picture of wellbore position uncertainties for many present types of survey equipment and techniques, and for modern horizontal and designer wells. It is recommended that a new methodology is developed as soon as possible. Continued use of the old methods might lead to undesired consequences like wellbore intersections and loss of targets.

The new method is recommended to be an evolution (improved version) of the Wolff deWardt theory to reduce confusion and resistance within the drilling industry. It should be comprehensive enough to give a realistic picture of the position uncertainty for present and coming surveying instruments and techniques. It is further recommended to develop standard procedures on how to derive weighting functions and tool uncertainty parameters for new instruments and running procedures. This to assure the validity of the new method for a longer period. An improved theory is currently under development by the "Industry Steering Committee on Wellbore Survey Accuracy". Weighting functions presented in this theses are forming the framework of this work. It will be implemented in a major software for wellbore geometry design and anti collision studies.

At last, detailed theoretical error analyses are given for survey equipment commonly used in the Norwegian North Sea sector. Derivations of weighting functions, which describe how the different error sources propagate into inclination-, azimuth- and depth errors, are

integral parts of these analyses. Weighting functions are, according to the basic error propagation theory discussion, very important in the wellbore position uncertainty calculation. They should be derived with great care. It is especially important to assure that all singularities are reflected in the weighting functions. This is the case even for error sources that usually are without significance. This theses is the first known publication, which gives a complete overview of all relevant error sources, with the derivation of detailed weighting functions for all major types of wellbore surveying techniques (electronic magnetic, gyro compassing, continuous gyro and inertial).

Modern continuous high accuracy gyros and inertial systems are not discrete systems like traditional directional systems (magnetic- and gyro compassing systems). They are designed for continuously surveying of the entire wellbore profile, and they do therefore not fit directly into a station to station approach, which has to be used in connection with the improved Wolff deWardt method. It is in this theses proven that continuous gyro- and inertial wellbore positioning systems logically can be transformed to discrete systems in connection with position uncertainty studies without significant loss of precision. This means that it is possible to implement new wellbore position uncertainty prediction software with only one internal error propagation mechanism. This is a great breakthrough compared to what has been believed up to now.

Depth errors are currently handled as proportional with measured depth (MD) in wellbore position uncertainty studies. It is, in this theses, shown that this suggestion is to simple to avoid significant errors in the position uncertainty estimation. It is further shown that uncertainty estimation errors can be avoided if four different depth uncertainty components (a random reference-, a systematic reference-, a systematic proportional with MD-, and a bias proportional with MD and TVD component) are used in stead of the one currently used (proportional with MD). The four components are formed by lumping together the effect of twenty seven independent depth error sources. Weighting functions for all these are presented. A use of the total set of twenty seven weighting functions is, however, not recommended. Especially not in connection with uncertainty predictions, where many necessary input parameters, like detailed drill string properties, are unknown.

Acknowledgements

This work would not have been possible without the help and contribution from many persons and companies around the world. The support from the following persons have been of special great value, and is highly appreciated.

Erik Iversen Nakken, Statoil (Norway)
Leif Kristian Jensen, Statoil (Norway)
Ivar Haarstad, Statoil (former IKU Petroleum Research) (Norway)
Oddvar Lotsberg, Baker Hughes INTEQ (Norway)
David Roper, Sysdrill (UK)
Adam Henly, Sysdrill (UK)
Hugh Williamson, BP Exploration (UK)
Andy Brooks, Baker Hughes INTEQ (Texas)
Koen A. Noy, Baker Hughes INTEQ (former Gyrodata) (Texas)
Martyn I. Greensmith, Gyrodata (UK)
Brett H. van Steenwyk, Scientific Drilling International (California)

A special thank is given to my advisers

Professor Rune Martin Holt, NTNU (Norway), and
Torgeir Torkildsen, Statoil (former IKU Petroleum Research) (Norway)

for their guidance throughout the study.

A great thank is also given to Den Norske Stats Oljeselskap (Statoil) for raising resources to this study and for allowing it published.

Contents

1 Introduction

The drilling of modern advanced wellbores (extended reach-, horizontal-, and 3D wellbores) requires continuous measurements of the drill bit position and orientation in order to hit targets and avoid collision or interference with adjacent wellbores. The drill bit position is determined through wellbore positioning techniques, which often are called for directional surveying. Directional surveying is either run on wireline or while drilling (MWD).

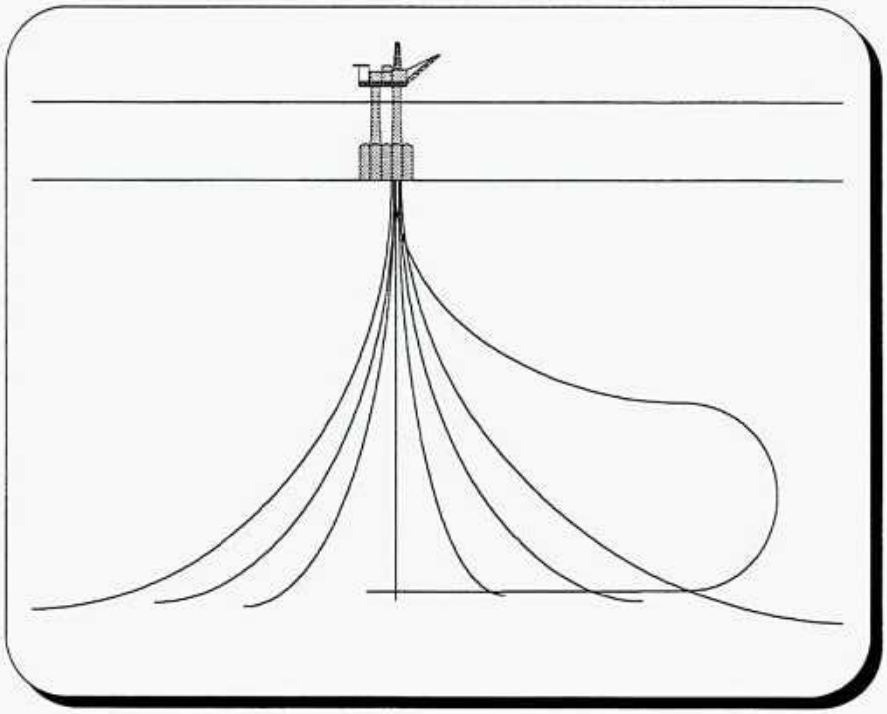

Figure 1-1 Example on an offshore platform wellbore cluster environment where new wellbores should be planned and drilled without the risk of collision with existing wellbores

Wellbore position surveys are, as all other types of measurements, affected by measurement errors. There are, because of this, uncertainties associated with an estimated wellbore profile. The uncertainties are dependent on the accuracy of the survey program in use. There will of course also be uncertainties associated with geological targets, which are to be hit, and with adjacent wellbores, which are to be avoided. The total accuracy requirement in connection with a drilling job is the combination of the target uncertainty

and the predicted position uncertainty of the wellbore under drilling. The requirement might vary during different phases of the drilling. The success in hitting a target or avoiding collision with adjacent wellbores, is therefore dependent on the availability of a prediction tool designed to optimise wellbore position survey programs with respect to needed accuracy. Up to now, different published error propagation theories like the Walstrom model [5], the Wolff deWardt model [6], and the Instrument performance model [7], have been used for this purpose. This theses is, however, showing that non of them are comprehensive enough for more advanced wellbore designs and surveying techniques. They do therefore have to be replaced by a new theory. The framework for such a theory will be given.

Directional surveys are usually affected by measurement errors which are of both random-, systematic-, and gross- (blunders) error types. The different error types propagate individually into derived quantities like the wellbore position. They are all subjected to different error propagation mechanisms. Gross errors are a problem in this regard. They can not be described in traditional error theory unless their presence are known. This is impossible prior to a survey, and it is therefore impossible to include them in a wellbore position uncertainty prediction theory. Any presence of gross errors in a survey must because of this be avoided if an underestimation of the predicted position uncertainty shall be avoided.

A study of the directional surveying performance achieved in the field [25], has shown that gross errors in connection with directional surveys are found at a much higher rate than expected. Azimuth errors of more than 15° over longer well sections have been experienced. Many of these gross errors should have been detected if adequate quality control procedures had been utilised. The study showed that today's level of quality control has to be improved if realistic wellbore position uncertainty predictions are to be obtained. The development of adequate quality control procedures is not a task in connection with this theses. It is too closely related to business policies within the different companies. It is, however, an important task, which has to be solved before wellbore position uncertainty predictions can be used in connection with for example risk based decision making.

2 Co-ordinate Systems

2.1 Instrument System

Three basic co-ordinate systems are in use in this document. It is the local earth based North/East/Vertical system (*NEV*), the instrument based *xyz*- system, and the magnetic reference system (next chapter). The *xyz*- system has its *z*- axis aligned along the instrument collar axis, which for an error free system is parallel to the wellbore axis. The *x*- and *y*- axis are normal to each other, and in a plane normal to the *z*- axis. Both co-ordinate systems are right handed, and tied to each other through three independent angles, the azimuth (*A*), the inclination (*I*) and the high-side toolface (τ).

The azimuth is defined as the angle between the north direction and the horizontal projection of the wellbore axis (*z*- axis).

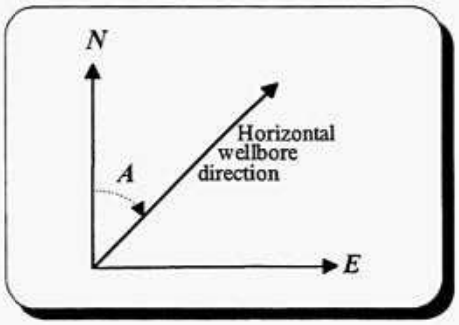

Figure 2.2-1 Definition of the azimuth (*A*)

The inclination is defined as the angle between the local vertical and the wellbore axis (*z*- axis).

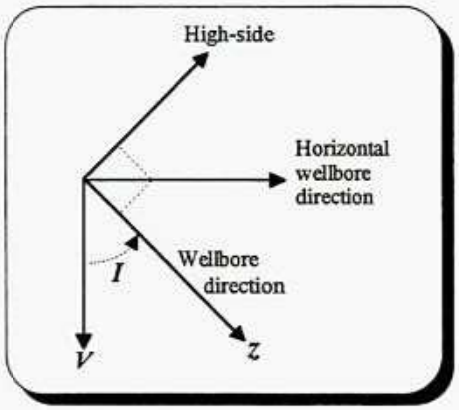

Figure 2.2-2 Definition of the inclination (*I*)

The high-side toolface is defined as the angle between the high-side direction and the *y*-axis. The high-side direction is given by the intersection between the plane normal to the wellbore axis (*z*- axis) and the vertical plane containing the wellbore axis. Positive direction is always up from the horizontal plane for non vertical wellbores.

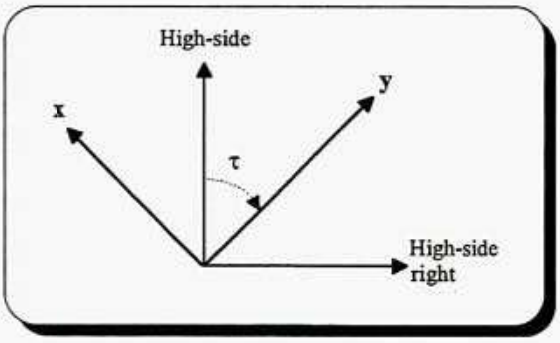

Figure 2.2-3 Definition of the high-side toolface (τ)

The azimuth, inclination and high-side toolface do not form a unique relationship between the two co-ordinate systems. The azimuth and the high-side toolface are not defined for vertical wellbores. This can create problems in kick-off operations etc., where orientation of the tool with respect to north / east are needed. An additional angle is introduced to solve this problem. It is call the north toolface (τ_A). Magnetic or gyro toolface are also commonly used expressions. Similar, the high-side toolface is often called the gravity toolface. The north toolface is for a vertical wellbore defined as the angle between the north axis and the y- axis. For small inclinations, the relationship between the azimuth and the north toolface is given by

$$\tau_A \approx A + \tau \qquad \{2.2\text{-}1\}$$

The undefined vertical azimuth and high-side toolface are, how ever, not a serious problem in wellbore position uncertainty analysis, and the introduction of a north toolface is not necessary. Large azimuth uncertainties do only have small influence on wellbore co-ordinates for vertical or near vertical wellbores. A 1000 meter deep 0.01 degree inclined wellbore with a toolface induced azimuth uncertainty of 5° will for example only have a horizontal co-ordinate uncertainty of approximately 0.2 meters. This is without significance compared to the inclination induced horizontal uncertainty, which in this case usually is greater than 5 meters.

2.2 Magnetic Reference System

Magnetic directional surveys are made with respect to the earth based magnetic field vector, which is linked to the *NEV*- system through two angles magnetic declination (δ) and the magnetic dip (Θ). The magnetic declination is defined as the horizontal angle between the north (*N*) and the magnetic north, where the magnetic north is equal to the horizontal direction of the magnetic field vector. The magnetic dip is defined as the angle between the horizontal plane and the magnetic field vector.

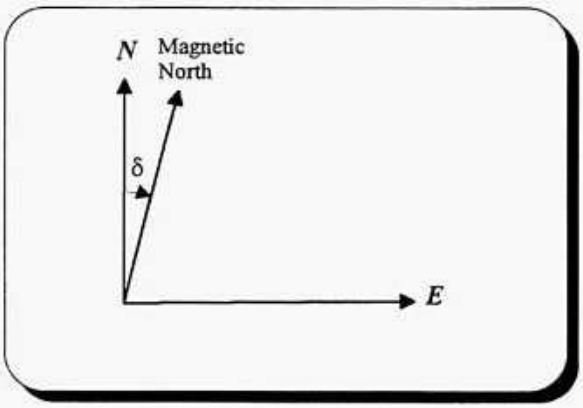

Figure 2.3-1 Definition of the magnetic declination (δ)

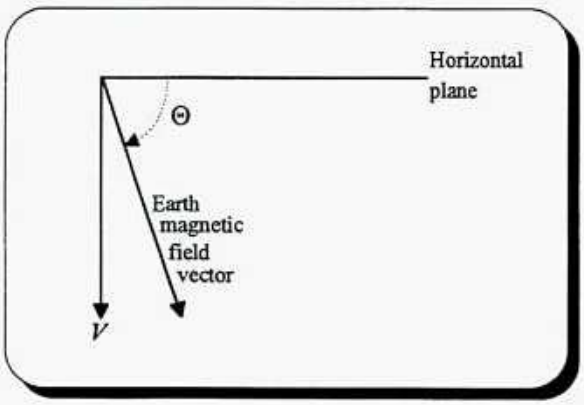

Figure 2.3-2 Definition of the magnetic dip (Θ)

3 Basic Error Theory

Both random- and systematic- errors are present in directional surveys. Even gross errors (blunders) can usually be found to some degree. It is necessary to have some knowledge about the nature and behaviour of all these three error types, if their individual and combined effect on a derived quantity (the wellbore position) shall be understood.

3.1 Random Errors

Random errors are per definition errors that can be averaged out through a large number of repeated measurements. Examples of random errors in directional surveys are

- Unpredictable environmental variations
- Round off errors
- Orthogonality errors when sensor is rotating
- Mud pump induced fluctuation in mud pressure

It is widely accepted, but not documented in the literature, that most random errors in connection with directional surveys follow the normal distribution. This will be taken for granted in the following. It means that it is possible to develop detailed theories on how to estimate or predict how random directional surveying errors propagate along different wellbore trajectories with associated confidence levels.

In the following, a development of a basic error propagation theory for random directional surveying errors is presented. The theory is designed for conventional directional surveying like magnetic north referencing and gyro compassing. More sophisticated methods must be used for inertial measurements and other direct methods that might be developed in the future. Only measurement errors are considered in this development. Mathematical model errors due to the use of a too simple mathematical model, or a too large station separation, are not included. Their behaviour are well known (Truex [9], Thorogood [10] and Guo [11]), and can easily be included into the theory if desired.

ΔX_j is the co-ordinate differences vector between measurement station *j-1* and *j*

I_j = inclination at station *j* $\quad$ ε_{Ij} = random inclination error at station *j*
A_j = azimuth at station *j* $\quad$ ε_{Aj} = random azimuth error at station *j*
D_j = depth at station *j* $\quad$ ε_{Dj} = random depth error at station *j*

f_j = the vector function relationships between measurements and co-ordinate vector at station *j*

$$\Delta X_j = \mathbf{f}_j(I_{j-1}, A_{j-1}, D_{j-1}, I_j, A_j, D_j) \qquad \{3.1\text{-}1\}$$

Page 12 Line 2+3 from bottom *co-ordinate vector at station j* should be the co-ordinate difference vector between station *j-1* and *j*

ΔX_j given on component form is then

$$\Delta N_j = f_{Nj}(\ I_{j-1},\ A_{j-1},\ D_{j-1},\ I_j,\ A_j,\ D_j\ ) \qquad \{3.1\text{-}2\}$$
$$\Delta E_j = f_{Ej}(\ I_{j-1},\ A_{j-1},\ D_{j-1},\ I_j,\ A_j,\ D_j\ ) \qquad \{3.1\text{-}3\}$$
$$\Delta V_j = f_{vj}(\ I_{j-1},\ A_{j-1},\ D_{j-1},\ I_j,\ A_j,\ D_j\ ) \qquad \{3.1\text{-}4\}$$

X is the co-ordinate vector at the last measurement station, station n.

$$X = \Sigma_{j=1}^{n}\ \Delta X_j \qquad \{3.1\text{-}5\}$$

$$X + \varepsilon_X = \Sigma_{j=1}^{n} f(\ I_{j-1}+\varepsilon_{Ij-1},\ A_{j-1}+\varepsilon_{Aj-1},\ D_{j-1}+\varepsilon_{Dj-1},\ \ I_j+\varepsilon_{Ij},\ A_j+\varepsilon_{Aj},\ D_j+\varepsilon_{Dj}\ ) \qquad \{3.1\text{-}6\}$$

1st order Taylor series and small errors give

$$\begin{aligned}\varepsilon_X = \Sigma_{j=1}^{n} (&\partial f_j/\partial I_{j-1}\varepsilon_{Ij-1}+\partial f_j/\partial A_{j-1}\varepsilon_{Aj-1}+\partial f_j/\partial D_{j-1}\varepsilon_{Dj-1}\\ &+\partial f_j/\partial I_j\varepsilon_{Ij}+\partial f_j/\partial A_j\varepsilon_{Aj}+\partial f_j/\partial D_j\varepsilon_{Dj})\end{aligned} \qquad \{3.1\text{-}7\}$$

The Gauss error propagation function is obtained by squaring equation *{3.1-7}*

$$\begin{aligned}\Sigma_X = [\ &(\partial f_1/\partial I_0)^2\varepsilon_{I0}^{\ 2}+(\partial f_1/\partial A_0)^2\varepsilon_{A0}^{\ 2}+(\partial f_1/\partial D_0)^2\varepsilon_{D0}^{\ 2}\ ]\\ &+\Sigma_{j=1}^{n-1}\ \{\ [\ (\partial f_j/\partial I_j)^2+2(\partial f_j/\partial I_j)(\partial f_{j+1}/\partial I_j)+(\partial f_{j+1}/\partial I_j)^2\ ]\varepsilon_{Ij}^{\ 2}\\ &\quad+[\ (\partial f_j/\partial A_j)^2+2(\partial f_j/\partial A_j)(\partial f_{j+1}/\partial A_j)+(\partial f_{j+1}/\partial A_j)^2\ ]\varepsilon_{Aj}^{\ 2}\\ &\quad+[\ (\partial f_j/\partial D_j)^2+2(\partial f_j/\partial D_j)(\partial f_{j+1}/\partial D_j)+(\partial f_{j+1}/\partial D_j)^2\ ]\varepsilon_{Dj}^{\ 2}\ \}\\ &+[\ (\partial f_n/\partial I_n)^2\varepsilon_{In}^{\ 2}+(\partial f_n/\partial A_n)^2\varepsilon_{An}^{\ 2}+(\partial f_n/\partial D_n)^2\varepsilon_{Dn}^{\ 2}\ ]\end{aligned} \qquad \{3.1\text{-}8\}$$

Where $(\partial f_1/\partial I_0)^2 = (\partial f_1/\partial I_0)^*(\partial f_1/\partial I_0)^T$ and $(\partial f_1/\partial I_0)(\partial f_1/\partial A_0) = (\partial f_1/\partial I_0)^*(\partial f_1/\partial A_0)^T$ etc. Sums including terms of the type $(\varepsilon_{Ij}\varepsilon_{Ij'})$, $(\varepsilon_{Ij}\varepsilon_{Aj'})$, $(\varepsilon_{Ij}\varepsilon_{Dj''})$, etc. where $0 <= j' <= n$, $0<= j'' <= n$, and j' is not equal to j, are set to zero because of the large number of stations in most directional surveys (usually more than one hundred) and the data randomness.

σ_{Ii}, etc. is the standard deviation of the associated parameter, and is the expectation of ε_{Ii} etc. Inserted into equation *{3.1-8}*, this gives

$$\begin{aligned}\Sigma_X = [\ &(\partial f_1/\partial I_0)^2\sigma_{I0}^{\ 2}+(\partial f_1/\partial A_0)^2\sigma_{A0}^{\ 2}+(\partial f_1/\partial D_0)^2\sigma_{D0}^{\ 2}\ ]\\ &+\Sigma_{j=1}^{n-1}\ \{\ [\ (\partial f_j/\partial I_j)^2+2(\partial f_j/\partial I_j)(\partial f_{j+1}/\partial I_j)+(\partial f_{j+1}/\partial I_j)^2\ ]\sigma_{Ij}^{\ 2}\\ &\quad+[\ (\partial f_j/\partial A_j)^2+2(\partial f_j/\partial A_j)(\partial f_{j+1}/\partial A_j)+(\partial f_{j+1}/\partial A_j)^2\ ]\sigma_{Aj}^{\ 2}\\ &\quad+[\ (\partial f_j/\partial D_j)^2+2(\partial f_j/\partial D_j)(\partial f_{j+1}/\partial D_j)+(\partial f_{j+1}/\partial D_j)^2\ ]\sigma_{Dj}^{\ 2}\ \}\\ &+[\ (\partial f_n/\partial I_n)^2\sigma_{In}^{\ 2}+(\partial f_n/\partial A_n)^2\sigma_{An}^{\ 2}+(\partial f_n/\partial D_n)^2\sigma_{Dn}^{\ 2}\ ]\end{aligned} \qquad \{3.1\text{-}9\}$$

Σ_X is the co-variance matrix of the estimated co-ordinate vector X at station n. The co-variance matrix shows how random errors in the individual directional survey measurements propagate into an error in the estimated vector X. The co-variance matrix can more easily be expressed as follows

Page 13 Equation *{3.1-8}* line 1 $\varepsilon_X\varepsilon_X^T \approx [\ (\partial f_1/\partial I_0)^2\varepsilon_{I0}^2+(\partial f_1/\partial A_0)^2\varepsilon_{A0}^2+(\partial f_1/\partial D_0)^2\varepsilon_{D0}^2\ ]$

$$\Sigma_X = \begin{bmatrix} \sigma_{NN}^2 & \sigma_{NE}^2 & \sigma_{NV}^2 \\ \sigma_{NE}^2 & \sigma_{EE}^2 & \sigma_{EV}^2 \\ \sigma_{NV}^2 & \sigma_{EV}^2 & \sigma_{VV}^2 \end{bmatrix} \qquad \{3.1\text{-}10\}$$

$$\begin{aligned}\sigma_{NN}^2 = {} & [\,(\partial f_{N1}/\partial I_0)^2\sigma_{I0}^2+(\partial f_{N1}/\partial A_0)^2\sigma_{A0}^2+(\partial f_{N1}/\partial D_0)^2\sigma_{D0}^2\,] \\ & + \Sigma_{j=1}^{n-1}\{\,[\,(\partial f_{Nj}/\partial I_j)^2+2(\partial f_{Nj}/\partial I_j)(\partial f_{Nj+1}/\partial I_j)+(\partial f_{Nj+1}/\partial I_j)^2\,]\sigma_{Ij}^2 \\ & \quad +[\,(\partial f_{Nj}/\partial A_j)^2+2(\partial f_{Nj}/\partial A_j)(\partial f_{Nj+1}/\partial A_j)+(\partial f_{Nj+1}/\partial A_j)^2\,]\sigma_{Aj}^2 \\ & \quad +[\,(\partial f_{Nj}/\partial D_j)^2+2(\partial f_{Nj}/\partial D_j)(\partial f_{Nj+1}/\partial D_j)+(\partial f_{Nj+1}/\partial D_j)^2\,]\sigma_{Dj}^2\,\} \\ & +[\,(\partial f_{Nn}/\partial I_n)^2\sigma_{In}^2+(\partial f_{Nn}/\partial A_n)^2\sigma_{An}^2+(\partial f_{Nn}/\partial D_n)^2\sigma_{Dn}^2\,] \end{aligned} \qquad \{3.1\text{-}11\}$$

$$\begin{aligned}\sigma_{NE}^2 = {} & [(\partial f_{N1}/\partial I_0)(\partial f_{E1}/\partial I_0)\sigma_{I0}^2+(\partial f_{N1}/\partial A_0)(\partial f_{E1}/\partial A_0)\sigma_{A0}^2+(\partial f_{N1}/\partial D_0)(\partial f_{E1}/\partial D_0)\sigma_{D0}^2] \\ & + \Sigma_{j=1}^{n-1}\{[(\partial f_{Nj}/\partial I_j)(\partial f_{Ej}/\partial I_j)+(\partial f_{Nj}/\partial I_j)(\partial f_{Ej+1}/\partial I_j)+(\partial f_{Ej}/\partial I_j)(\partial f_{Nj+1}/\partial I_j) \\ & \quad +(\partial f_{Nj+1}/\partial I_j)(\partial f_{Ej+1}/\partial I_j)]\sigma_{Ij}^2+[(\partial f_{Nj}/\partial A_j)(\partial f_{Ej}/\partial A_j)+(\partial f_{Nj}/\partial A_j) \\ & \quad +(\partial f_{Ej+1}/\partial A_j)+(\partial f_{Ej}/\partial A_j)(\partial f_{Nj+1}/\partial A_j)+(\partial f_{Nj+1}/\partial A_j)(\partial f_{Ej+1}/\partial A_j)]\sigma_{Aj}^2 \\ & \quad +[(\partial f_{Nj}/\partial D_j)(\partial f_{Ej}/\partial D_j)+(\partial f_{Nj}/\partial D_j)(\partial f_{Ej+1}/\partial D_j)+(\partial f_{Ej}/\partial D_j)(\partial f_{Nj+1}/\partial D_j) \\ & \quad +(\partial f_{Nj+1}/\partial D_j)(\partial f_{Ej+1}/\partial D_j)]\sigma_{Dj}^2\} \\ & +[(\partial f_{Nn}/\partial I_n)(\partial f_{En}/\partial I_n)\sigma_{In}^2+(\partial f_{Nn}/\partial A_n)(\partial f_{En}/\partial A_n)\sigma_{An}^2 \\ & \quad +(\partial f_{Nn}/\partial D_n)(\partial f_{En}/\partial D_n)\sigma_{Dn}^2] \end{aligned} \qquad \{3.1\text{-}12\}$$

Etc.

σ_{NN}^2 is the variance in the north direction, and σ_{NE}^2 is the co-variance between the north and east direction. The co-variance might also be expressed as follows:

$$\sigma_{NE}^2 = \sqrt{\sigma_{NN}^2}\,\sqrt{\sigma_{EE}^2}\,\rho_{NE} \qquad \{3.1\text{-}13\}$$

where ρ_{NE} is called the correlation coefficient between the north and east co-ordinates. A correlation coefficient equal to zero means totally independent quantities, while a coefficient equal to one means total dependency.

For a straight wellbore consisting of n stations with equal station separation, and repeated measurements with the same individual accuracy, equation *{3.1-9}* reduces to

$$\begin{aligned}\Sigma_X = n\,\{ & [(\partial f/\partial I)^2+(\partial f/\partial I\text{-})^2+2(1\text{-}1/n)(\partial f/\partial I)(\partial f/\partial I\text{-})]\sigma_I^2 \\ & +[(\partial f/\partial A)^2+(\partial f/\partial A\text{-})^2+2(1\text{-}1/n)(\partial f/\partial A)(\partial f/\partial A\text{-})]\sigma_A^2 \\ & +[(\partial f/\partial D)^2+(\partial f/\partial D\text{-})^2+2(1\text{-}1/n)(\partial f/\partial D)(\partial f/\partial D\text{-})]\sigma_D^2\,\} \end{aligned} \qquad \{3.1\text{-}14\}$$

Where *I*-, *A*- and *D*- is the inclination-, azimuth- and depth measurement at the previous station. $f = f_1$, $(\partial f/\partial I) = (\partial f_1/\partial I_1)$, $(\partial f/\partial I\text{-}) = (\partial f_1/\partial I_0)$, etc.

Equation *{3.1-14}* shows that the effect of random errors in traditional directional surveys are proportional to the square root of the number of measurement stations. Random errors will therefore not be averaged out for repeated measurements at consecutive stations as they will do for repeated measurements at the same station.

Example 3.1-1

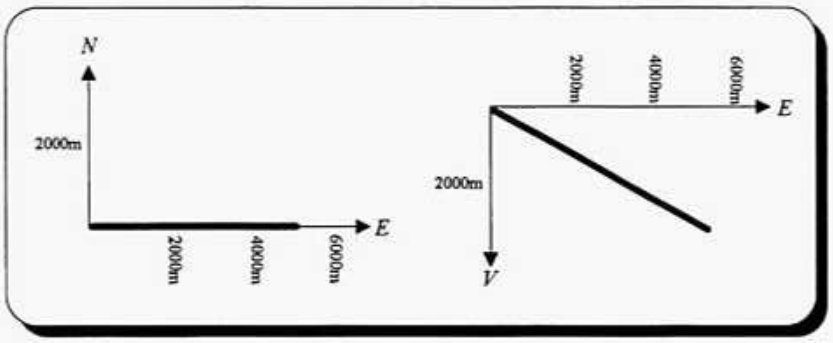

Figure 3.1-1 Sketch of wellbore profile used in this example

To visualise the effect of random directional surveying errors, a 6.0 km long straight artificial wellbore is analysed. The wellbore is directed due east at 60° inclination. Measurements are taken every 30 meters which almost is a standard for measurements while drilling (MWD), and wellbore co-ordinates are computed with the minimum curvature method. The following parameters are then valid for this survey

$$n = 200, \qquad I_j = I = 60°, \qquad A_j = A = 90°, \qquad D_j = j*30\text{m}, \qquad j = 1, 2, \ldots, n$$

$$f(I\text{-}, I, A\text{-}, A, D\text{-}, D) = F * \begin{bmatrix} [D_f\text{-}(D_f\text{-})]/2[\sin(I\text{-})\cos(A\text{-})+\sin(I)\cos(A)] \\ [D_f\text{-}(D_f\text{-})]/2[\sin(I\text{-})\sin(A\text{-})+\sin(I)\sin(A)] \\ [D_f\text{-}(D_f\text{-})]/2[\cos(I\text{-})+\cos(I)] \end{bmatrix} = \begin{bmatrix} 0 \\ 25.981 \\ 15 \end{bmatrix}$$

F is the minimum curvature multiplication constant, which for a straight wellbore is equal to one, and

$$I\text{-} = I, \quad A\text{-} = A, \quad D_f\text{-}(D_f\text{-}) = dD = 30\text{m}$$

Partial derivatives of the minimum curvature function for this wellbore are

$$(\partial f/\partial I\text{-}) = (\partial f/\partial I) = \begin{bmatrix} \frac{dD}{2}\cos(I)\cos(A) \\ \frac{dD}{2}\cos(I)\sin(A) \\ -\frac{dD}{2}\sin(I) \end{bmatrix} = \begin{bmatrix} 0 \\ 7.5 \\ -12.990 \end{bmatrix}$$

$$(\partial f/\partial A\text{-}) = (\partial f/\partial A) = \begin{bmatrix} -\frac{dD}{2}\sin(I)\sin(A) \\ \frac{dD}{2}\sin(I)\cos(A) \\ 0 \end{bmatrix} = \begin{bmatrix} -12.990 \\ 0 \\ 0 \end{bmatrix}$$

$$(\partial f/\partial D) = \begin{bmatrix} \sin(I)\cos(A) \\ \sin(I)\sin(A) \\ \cos(I) \end{bmatrix} = \begin{bmatrix} 0 \\ 0.886 \\ 0.5 \end{bmatrix}$$

$$(\partial f/\partial D\text{-}) = -(\partial f/\partial D)$$

The elements in the co-variance matrix will then be

$$\sigma_{NN}^2 = (4n\text{-}2)[(\partial f_N/\partial I)^2\sigma_I^2+(\partial f_N/\partial A)^2\sigma_A^2]+2[(\partial f_N/\partial D)^2\sigma_D^2] = 134654\sigma_A^2$$
$$\sigma_{EE}^2 = (4n\text{-}2)[(\partial f_E/\partial I)^2\sigma_I^2+(\partial f_E/\partial A)^2\sigma_A^2]+2[(\partial f_E/\partial D)^2\sigma_D^2] = 44887\sigma_I^2+1.57\sigma_D^2$$
$$\sigma_{VV}^2 = (4n\text{-}2)[(\partial f_V/\partial I)^2\sigma_I^2+(\partial f_V/\partial A)^2\sigma_A^2]+2[(\partial f_V/\partial D)^2\sigma_D^2] = 134654\sigma_I^2+0.5\sigma_D^2$$

$$\sigma_{NE}^2 = (4n\text{-}2)[(\partial f_N/\partial I)(\partial f_E/\partial I)\sigma_I^2+(\partial f_N/\partial A)(\partial f_E/\partial A)\sigma_A^2]+2[(\partial f_N/\partial D)(\partial f_E/\partial D)\sigma_D^2] = 0$$
$$\sigma_{NV}^2 = (4n\text{-}2)[(\partial f_N/\partial I)(\partial f_V/\partial I)\sigma_I^2+(\partial f_N/\partial A)(\partial f_V/\partial A)\sigma_A^2]+2[(\partial f_N/\partial D)(\partial f_V/\partial D)\sigma_D^2] = 0$$
$$\sigma_{EV}^2 = (4n\text{-}2)[(\partial f_E/\partial I)(\partial f_V/\partial I)\sigma_I^2+(\partial f_E/\partial A)(\partial f_V/\partial A)\sigma_A^2]+2[(\partial f_E/\partial D)(\partial f_V/\partial D)\sigma_D^2] = -77745\sigma_I^2+0.89\sigma_D^2$$

Magnetic measurements while drilling (MWD) is a commonly used wellbore position surveying technique. It is because of effects like time dependent variations in the earth magnetic field etc. not rated among the most accurate of today's surveying techniques. It is difficult to give global uncertainty estimates / predictions for the three different MWD measurement types. The uncertainty figures will be dependent on both running conditions and quality control procedures in use.

$2\sigma_I = 0.3°$, $2\sigma_A = 2.0°$, $2\sigma_D =$ 0.2% of the unit length (0.06m)

are an example on commonly used MWD uncertainty figures (95% confidence) in connection with wellbore planning in the Norwegian North Sea sector.

If we assume a survey where these figures are valid, and where all error components are random, which of course is not the case, we get the following co-variance matrix

$$\Sigma_X = \begin{bmatrix} 41.0 & 0 & 0 \\ 0 & 0.31 & -0.53 \\ 0 & -0.53 & 0.92 \end{bmatrix}$$

Maximum uncertainty is as expected parallel to the north axis, and $\sigma_{NN} = 6.40$m

North seeking gyro measurements in vertical- and slightly deviated wellbores are rated among the more accurate surveying techniques. It is also here difficult to give global uncertainty figures.

$2\sigma_I = 0.3°$, $2\sigma_A = 0.45°$, $2\sigma_D =$ 0.2% of the unit length = 0.06m

are an example on commonly used north seeking uncertainty figures (95% confidence) in connection with wellbore planning in the Norwegian North Sea sector.

If we, similar to the previous case, assume a survey where these figures are valid, and where all error components are random, we get the following co-variance matrix

$$\Sigma_X = \begin{bmatrix} 2.08 & 0 & 0 \\ 0 & 0.31 & -0.53 \\ 0 & -0.53 & 0.92 \end{bmatrix}$$

Now we get a maximum uncertainty $\sigma_{NN} = 1.44$m, which also is pointing to the north.

3.2 Gross Errors

Gross errors, which often are referred to as blunders, are usually caused by human faults or instrument failures. Examples of such errors in directional surveys are

- Use of wrong initialisation parameters
- Use of wrong calibration constants
- Instrument used beyond operational specifications
- Single channel failure in multi-channel equipment
- Memory or processor error in the computer

Gross errors are dangerous. They may range from very small errors without any significant effects to major errors that will be destructive to any survey. It is impossible to predict their appearance, and they are therefore usually not included in error propagation theories. Gross errors should be identified and corrected for by dedicated quality control (QC) procedures. None of the published directional surveying error propagation theories seem to include gross errors like human faults and instrument failures. They take it probably for granted that adequate QC has been applied to the measurements to secure against the appearance of gross errors at a very high confidence level. If large gross errors are present (probably the case in many existing directional surveys), the wellbore position uncertainty estimates obtained with these methods will be wrong and the error propagation models are not valid.

3.3 Systematic Errors

Systematic errors are all remaining errors when gross- and random- errors are removed. A systematic error has the same size, sign or geometric dependent nature for a given number of measurements. This means that some gross errors, like for instance use of wrong calibration constants, are systematic errors for all measurements of a given type. It is, however, not usual to include this kind of gross errors into the systematic error term, as opposed to for example residual errors after calibration, which are systematic errors as long as the same instrument is in use.

In directional drilling, some errors might be systematic at one level and random at another. The most usual case is errors that are systematic in one survey (at least in large parts of one survey), and random between different surveys.

Examples of errors that are systematic in one survey, and random between different surveys, are

- Reference errors in connection with free gyro surveys
- Residual errors in magnetic declination corrections
- Drill collar sag for MWD instruments

Examples of errors that are systematic for all surveys in a given region are

- Magnetic measurements without magnetic declination corrections
- Errors in the geodetic reference network

Error propagation of systematic directional survey errors

η_I = systematic inclination uncertainty
η_A = systematic azimuth uncertainty
η_D = systematic depth uncertainty

$$\Delta X_j + \eta_{\Delta X_j} = f_j(I_{j-1}+\eta_I, A_{j-1}+\eta_A, D_{j-1}+\eta_D, I_j+\eta_I, A_j+\eta_A, D_j+\eta_D) \qquad \{3.3\text{-}1\}$$

Reduced 1st order Taylor series gives

$$\eta_{\Delta Xj} = (\partial f_j/\partial I_{j-1})\eta_I + (\partial f_j/\partial A_{j-1})\eta_A + (\partial f_j/\partial D_{j-1})\eta_D + (\partial f_j/\partial I_j)\eta_I + (\partial f_j/\partial A_j)\eta_A + (\partial f_j/\partial D_j)\eta_D \quad \{3.3\text{-}2\}$$

$$\Sigma_X = \{\Sigma_{j=1}^{n}[(\partial f_j/\partial I_{j-1})\eta_I + (\partial f_j/\partial A_{j-1})\eta_A + (\partial f_j/\partial D_{j-1})\eta_D + (\partial f_j/\partial I_j)\eta_I + (\partial f_j/\partial A_j)\eta_A + (\partial f_j/\partial D_j)\eta_D]\}^2 \quad \{3.3\text{-}3\}$$

Sums including terms of the type $(\eta_{Ij}\eta_{Ij})$, $(\eta_{Ij}\eta_{Aj})$, $(\eta_{Ij}\eta_{Dj})$, etc. will not cancel out because of the systematic effect. They can therefore not be set to zero in this case.

Equation *{3.3-3}* shows how systematic errors in the individual measurements propagate into the estimated co-ordinate vector $\boldsymbol{X}$.

For a straight wellbore consisting of n stations with equal station separation, repeated angular measurements with the same systematic errors, and depth error proportional to the measured depth, *{3.3-3}* reduces to

$$\Sigma_X = \{n[(\partial f/\partial I)\eta_I + (\partial f/\partial I\text{-})\eta_I + (\partial f/\partial A)\eta_A + (\partial f/\partial A\text{-})\eta_A] + (n^2+n)/2(\partial f/\partial D)\eta_D + (n^2-n)/2(\partial f/\partial D\text{-})\eta_D\}^2 \quad \{3.3\text{-}4\}$$

Where $f = f_1$, $(\partial f/\partial I) = (\partial f_1/\partial I_1)$, $(\partial f/\partial I\text{-}) = (\partial f_1/\partial I_0)$, etc., and η_D is the systematic depth measurement uncertainty between two consecutive stations.

Equation *{3.3-4}* shows that the effect of systematic errors in traditional directional surveys are proportional to the number of measurement stations. This is a much more unfavourable error propagation than the random error propagation, which in chapter 3.1 where proven to be proportional to the square root of the number of measurement stations. There is, however, a basic difference between random and systematic error propagation, that leads to the conclusion that this larger error propagation rate not necessarily implies a greater resultant error. The reason is that systematic error propagation can be sign dependent while random is not. Equation *{3.3-3}* shows that a change in azimuth quadrant from 2 to 3 or 1 to 4 or visa versa, some distance out in the wellbore, will lead to a change in the sign of the upcoming systematic error terms to be added, compared to those added prior to the quadrant change. The absolute value of the resultant systematic position error will therefore start to decrease. It might in fact return back to zero before it start to grow again, if a 180° azimuth turn is performed. This behaviour applies, according to the discussion later on, to some systematic error terms like the gyro reference error, but not for others like the drill string magnetisation error term.

Example 3.3-1

The wellbore and survey frequency described in the example 3.1-1 is also used to visualise the effect of systematic directional surveying errors.

The elements of the co-variance matrix is now given by

$$\Sigma_X = n^2\{2[(\partial f/\partial I)\eta_I+(\partial f/\partial A)\eta_A]+(\partial f/\partial D)\eta_D\}^2$$

The same MWD uncertainties (95% confidence level) as used in example 3.1-1 are also used in this case, but they are now assigned to the systematic error class. That is

$$2\eta_I = 0.3°, \quad 2\eta_A = 2.0°, \quad 2\eta_D = 0.2\% \text{ of the unit length}$$

which gives the following co-variance matrix

$$\Sigma_X = \begin{bmatrix} 8221.1 & -1194.7 & 962.3 \\ -1194.7 & 173.6 & -139.8 \\ 962.3 & -139.8 & 112.6 \end{bmatrix}$$

Maximum uncertainty is parallel to the north axis (normal to the wellbore path), and σ_{NN}= 90.7m, which is more than ten times greater than the similar random uncertainty of 6.40m.

A north seeking gyro survey where all errors are assumed to be systematic, and where the different error sizes are equal to those used in example 3.1-1, gives

$$2\eta_I = 0.3°, \quad 2\eta_A = 0.45°, \quad 2\eta_D = 0.2\% \text{ of the unit length} = 0.06\text{m}$$

The following co-variance matrix is then obtained

$$\Sigma_X = \begin{bmatrix} 417.0 & -269.1 & 216.7 \\ -269.1 & 173.6 & -139.8 \\ 216.7 & -139.8 & 112.6 \end{bmatrix}$$

Maximum uncertainty is again to the north, and given by σ_{NN}= 20.4m.

Example 3.3-2

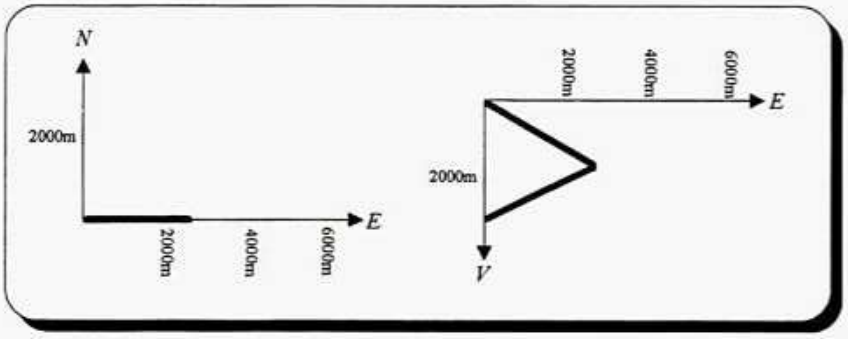

Figure 3.3-1 Sketch of wellbore profile used in this example

Let us now look at how systematic errors are behaving in a 6.0 km long constant 60° inclined wellbore that starts due east, and turns due west after 3.0 km. Measurements are like in the other examples taken every 30 meter, and wellbore co-ordinates are computed with the minimum curvature method. The following parameters are then valid for this survey

$n_1 = 100$, $I = 60°$, $A_1 = 90°$, $D_j = j$*30m where j = 1, 2, ..., $n = 30$m,
$n_2 = 100$, $A_2 = 270°$

$\partial f/\partial A_2 = -\partial f/\partial A_1 = -\partial f/\partial A$

$\Sigma_X = (n_1+n_2)^2[2(\partial f/\partial I)\eta_I+(\partial f/\partial D)\eta_D]^2$

A magnetic MWD-, or a north seeking gyro survey with uncertainties as defined in example 3.3-1, will both result in the same co-variance matrix. It is given by

$$\Sigma_X = \begin{bmatrix} 0 & 0 & 0 \\ 0 & 173.6 & -139.8 \\ 0 & -139.8 & 112.6 \end{bmatrix}$$

The north uncertainty $\sigma_{NN,syst} = 0$, which is significantly less than the similar random uncertainty of $\sigma_{NN,rand} = 6.40$m. The random error estimate is here identical to the result in the example in chapter 3.1.

These two examples show that the accumulated effect of systematic errors are extremely dependent on the wellbore geometry, and that the current practice, within most of the directional surveying industry, to disregard random errors from having any significant effect on the final result, might lead to serious underestimation of the estimated position accuracy.

The azimuth error due to drill string magnetic interference will, according to figure 3.3-2, always be pointing to the north on the northern hemisphere. The systematic magnetic interference error is because of this dependent on the azimuth quadrant in the same manner as the error propagation function. This is the case, even if the magnetic measurements are corrected based on a priori knowledge of the magnetic field, where it is impossible to tell whether the corrected vector is pointing to the north or to the south.

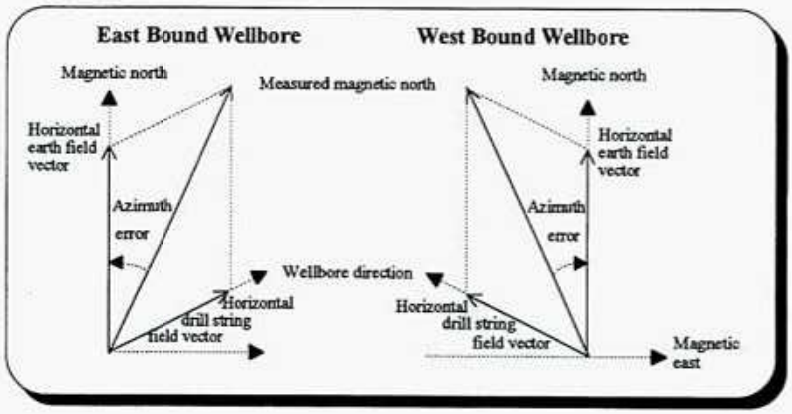

Figure 3.3-2 Magnetic azimuth errors for east and west bound wellbores caused by drill string magnetisation

Example 3.3-3

We shall now see what effect we get by taking the real magnetic drill string magnetisation error nature into account for the wellbore described in example 3.3-2.

For a magnetic MWD survey, the systematic azimuth error term is made up of two significant parts, the magnetic declination error and the drill string magnetisation error (see chapter 5). The total azimuth error, which is used in the uncertainty calculation, is the root sum square of these two components (plus a few other minor components).

Zijsling [30] is estimating the global declination uncertainty, with respect to a world declination chart or model, to 1.4° 2σ. This figure is based on the use of an updated version of the map or model. The present surveying practice is, however, not always securing this. Older charts / models are occasionally in use. The correct declination uncertainty is therefor probably slightly bigger than 1.4°. A commonly seen estimate for the magnetic declination uncertainty is 1.5°.

Assuming a total azimuth uncertainty of 2.0° (2σ) is then giving the following uncertainty components at a 95% confidence level

$2\eta_{A,d} = 1.5°$ (declination), $2\eta_{A,m} = 1.3°$ (drill string magnetisation)

Because the drill string magnetisation part is azimuth quadrant dependent, the current wellbore will have the following combined azimuth error terms and partial derivatives in the two wellbore sections

$2\eta_{A,1} = 2.0°$ (due east), $2\eta_{A,2} = 0.7°$ (due west)

and

$$\partial fl/\partial A_2 = -\partial fl/\partial A_1 = -\partial fl/\partial A$$

Combined, this gives

$$\Sigma_X = \{n_1\{2[(\partial fl/\partial I)\eta_I + (\partial fl/\partial A_1)\eta_{A,1})] + (\partial fl/\partial D)\eta_D\} + n_2\{2[(\partial fl/\partial I)\eta_I + (\partial fl/\partial A_2)\eta_{A2})] + (\partial fl/\partial D)\eta_D\}\}^2$$

which gives the following co-variance matrix

$$\Sigma_X = \begin{bmatrix} 1212.0 & -458.7 & 369.5 \\ -458.7 & 173.6 & -139.8 \\ 369.5 & -139.8 & 112.6 \end{bmatrix}$$

Maximum uncertainty is again to the north and given by $\sigma_{NN} = 34.8$m. This is dramatically different from the zero north uncertainty in the previous example.

Examples 3.3-1, 3.3-2 and 3.3-3 show that systematic errors are difficult to handle in wellbore position uncertainty studies, and that a detailed mapping of possible inclination-, azimuth- or high-side toolface dependencies are necessary to obtain realistic position uncertainty estimates.

3.4 Combination of Systematic and Random Errors

The total error budget in directional surveys (all errors associated with a survey) consists, as already mentioned, usually of both random and systematic errors.

The error propagation for such a combination is

$$\Delta X_j+\varepsilon_{\Delta Xj}+\eta_{\Delta Xj} = f_j(\, I_{j-1}+\varepsilon_{Ij-1}+\eta_I,\, A_{j-1}+\varepsilon_{Aj-1}+\eta_A,\, D_{j-1}+\varepsilon_{Dj-1}+\eta_D,\\ I_j+\varepsilon_{Ij}+\eta_I,\, A_j+\varepsilon_{Aj}+\eta_A,\, D_j+\varepsilon_{Dj}+\eta_D) \qquad \{3.4\text{-}1\}$$

A reduced 1st order Taylor series gives

$$\begin{aligned}\Sigma_X = {} & [(\partial f_1/\partial I_0)^2\sigma_{I0}^2+(\partial f_1/\partial A_0)^2\sigma_{A0}^2+(\partial f_1/\partial D_0)^2\sigma_{D0}^2]\\ & +[(\partial f_n/\partial I_n)^2\sigma_{In}^2+(\partial f_n/\partial A_n)^2\sigma_{An}^2+(\partial f_n/\partial D_n)^2\sigma_{Dn}^2]\\ & +\Sigma_{j=1}^{n-1}\{[(\partial f_j/\partial I_j)^2+2(\partial f_j/\partial I_j)(\partial f_{j+1}/\partial I_j)+(\partial f_{j+1}/\partial I_j)^2]\sigma_{Ij}^2\\ & \quad +[(\partial f_j/\partial A_j)^2+2(\partial f_j/\partial A_j)(\partial f_{j+1}/\partial A_j)+(\partial f_{j+1}/\partial A_j)^2]\sigma_{Aj}^2\\ & \quad +[(\partial f_j/\partial D_j)^2+2(\partial f_j/\partial D_j)(\partial f_{j+1}/\partial D_j)+(\partial f_{j+1}/\partial D_j)^2]\sigma_{Dj}^2\}\\ & +\{\Sigma_{j=1}^{n}[(\partial f_j/\partial I_{j-1})\eta_I+(\partial f_j/\partial A_{j-1})\eta_A+(\partial f_j/\partial D_{j-1})\eta_D\\ & \quad +(\partial f_j/\partial I_j)\eta_I+(\partial f_j/\partial A_j)\eta_A+(\partial f_j/\partial D_j)\eta_D]\}^2 \qquad \{3.4\text{-}2\}\end{aligned}$$

Sums including terms of the type $(\sigma_{Ij}\sigma_{If})$, $(\sigma_{Ij}\sigma_{Af})$, $(\sigma_{Ij}\sigma_{Df})$, $(\sigma_{Ij}\eta_I)$, $(\sigma_{Ij}\eta_A)$, $(\sigma_{Ij}\,\eta_D)$, $(\sigma_{Aj}\eta_I)$, $(\sigma_{Aj}\eta_A)$, $(\sigma_{Aj}\eta_D)$, $(\sigma_{Dj}\eta_I)$, $(\sigma_{Dj}\eta_A)$, $(\sigma_{Dj}\eta_D)$, etc. are set to zero because the large number of stations and the data randomness.

The first part of this vector equation is identical to the random co-variance matrix previously described, and the second part is identical to the systematic co-variance matrix. The introduction of both random- and systematic errors in a directional survey error analyses, is therefore basically the same as a summation of two independent covariance matrixes, one random and one systematic co-variance matrix.

$$\Sigma_X = \Sigma_{X,\sigma} + \Sigma_{X,\eta} \qquad \{3.4\text{-}3\}$$

For a straight wellbore consisting of n stations with equal station separation, and repeated measurements with same random and systematic errors (the systematic depth error is proportional to the measured depth), equation *{3.4-2}* reduces to

$$\begin{aligned}\Sigma_X = {} & n\{[(\partial f/\partial I)^2+(\partial f/\partial I\text{-})^2+2(1\text{-}1/n)(\partial f/\partial I)(\partial f/\partial I\text{-})]\sigma_I^2\\ & +[(\partial f/\partial A)^2+(\partial f/\partial A\text{-})^2+2(1\text{-}1/n)(\partial f/\partial A)(\partial f/\partial A\text{-})]\sigma_A^2\\ & +[(\partial f/\partial D)^2+(\partial f/\partial D\text{-})^2+2(1\text{-}1/n)(\partial f/\partial D)(\partial f/\partial D\text{-})]\sigma_D^2\}\\ & +\{n[(\partial f/\partial I)\eta_I+(\partial f/\partial I\text{-})\eta_I+(\partial f/\partial A)\eta_A+(\partial f/\partial A\text{-})\eta_A]\\ & \quad +(n^2+n)/2(\partial f/\partial D)\eta_D+(n^2-n)/2(\partial f/\partial D\text{-})\eta_D\}^2 \qquad \{3.4\text{-}4\}\end{aligned}$$

Example 3.4-1

To visualise the effect of combined random and systematic errors, let us once again look at the wellbore described in example 3.1-1, but now under the assumption that the resultant errors for the north seeking gyro consists of equal parts of random- and systematic angular errors and systematic depth errors proportional to the measured depth.

$2\sigma_I = 0.21°$, $2\sigma_A = 0.32°$,
$2\eta_I = 0.21°$, $2\eta_A = 0.32°$, $2\eta_D = 0.2\%$ of the unit length

These uncertainty figures used on the wellbore described in example 3.1-1 will give the following co-variance matrix

$$\Sigma_X = \Sigma_{X,\sigma} + \Sigma_{X,\eta}$$

$$\Sigma_X = \begin{bmatrix} 1.1 & 0 & 0 \\ 0 & 0.2 & -0.3 \\ 0 & -0.3 & 0.5 \end{bmatrix} + \begin{bmatrix} 210.2 & -156.7 & 94.4 \\ -156.7 & 116.8 & -70.3 \\ 94.4 & -70.3 & 42.4 \end{bmatrix} = \begin{bmatrix} 211.3 & -156.7 & 94.4 \\ -156.7 & 117.0 & -70.6 \\ 94.4 & -70.6 & 42.9 \end{bmatrix}$$

Maximum uncertainty $\sigma_{NN} = 14.5$m, and is again to the north. This uncertainty is about 70% of the similar uncertainty estimate obtained as if all errors where systematic.

Example 3.4-2

If we in the same survey as described in example 3.4-1 assume that the random errors are ten times greater than the systematic errors, we get the following situation

$2\sigma_I = 0.3°$, $2\sigma_A = 0.45°$,
$2\eta_I = 0.03°$, $2\eta_A = 0.045°$, $2\eta_D = 0.2\%$ of the unit length = 0.06m

$$\Sigma_X = \begin{bmatrix} 2.1 & 0 & 0 \\ 0 & 0.3 & -0.5 \\ 0 & -0.5 & 0.9 \end{bmatrix} + \begin{bmatrix} 4.2 & -12.5 & -3.3 \\ -12.5 & 37.2 & 10.0 \\ -3.3 & 10.0 & 2.7 \end{bmatrix} = \begin{bmatrix} 6.3 & -12.5 & -3.3 \\ -12.5 & 37.5 & 9.5 \\ -3.3 & 9.5 & 3.6 \end{bmatrix}$$

Maximum uncertainty $\sigma_{EE} = 6.2$m, and is this time directed to the east.

Based on equation *{3.4-3}* and examples 3.4-1 and 3.4-2, it is possible to draw the conclusion that inclusion of random errors into the systematic error term, only leads to over estimation of the real uncertainty when random errors are of the same magnitude or are greater than major systematic errors. Random errors, with exception of those that are grater than major systematic errors, can therefore usually be omitted in wellbore position uncertainty analyses. This is the case for all standard wellbore designs, but not necessarily for modern designer wells where the resultant effect of a specific systematic error source on the wellbore position can be near to zero in minor wellbore sections. It is, however, very unlikely that all systematic error sources effective in a given survey will show this kind of behaviour. There will usually be at least one systematic error source that is not sensitive to azimuth changes in this manner.

3.5 Consecutive Survey Sections

A total wellbore survey is often made up of consecutive independent directional surveys. In such combination surveys, we might have the following types of errors

- Errors that are random for all surveys
- Errors that are systematic for all surveys
- Errors that are systematic for one survey, and random between the other surveys
- Errors that are systematic for a given number of surveys
- Errors that are systematic for one survey, and random between some of the other surveys

The error propagation for a combination survey can be described by the following set of parameters

σ_{Ij} = random inclination uncertainty at station j for survey k
σ_{Aj} = random azimuth uncertainty at station j for survey k
σ_{Dj} = random depth uncertainty at station j for survey k

λ_I = systematic inclination uncertainty for one survey, random between surveys
λ_A = systematic azimuth uncertainty for one survey, random between surveys
λ_D = systematic depth uncertainty for one survey, random between surveys

ξ_{cI} = systematic inclination uncertainty between a given numbers of surveys, else zero
ξ_{cA} = systematic azimuth uncertainty between a given numbers of surveys, else zero
ξ_{cD} = systematic depth uncertainty between a given numbers of surveys, else zero

ζ_{cI} = systematic inclination uncertainty in one survey, random between a few surveys
ζ_{cA} = systematic azimuth uncertainty in one survey, random between a few surveys
ζ_{cD} = systematic depth uncertainty in one survey, random between a few surveys

η_I = systematic inclination uncertainty for all surveys
η_A = systematic azimuth uncertainty for all survey
η_D = systematic depth uncertainty for all surveys

k_n = the number of independent surveys
m_1 = the total number of different combinations of errors that are systematic for a given number of surveys (ξ)
m_2 = the total number of different combinations of errors that are systematic for one survey and random between a limited number of surveys (ζ)
k_k = the number of measurement stations in surveys
n = the total number of measurement stations

The position co-variance matrix is then given by

$$\Sigma_X = \{\Sigma_{j=1}^{n}\{\ (\partial f_j/\partial I_{j-1})[\sigma_{Ij-1}+\lambda_I+\Sigma_{c=1}^{m_1}\xi_{cI,\text{actual}}+\Sigma_{c=1}^{m_2}\zeta_{cI,\text{actual}}+\eta_I]$$
$$+(\partial f_j/\partial A_{j-1})[\sigma_{Aj-1}+\lambda_A+\Sigma_{c=1}^{m_1}\xi_{cA,\text{actual}}+\Sigma_{c=1}^{m_2}\zeta_{cA,\text{actual}}+\eta_A]$$
$$+(\partial f_j/\partial D_{j-1})[\sigma_{Dj-1}+\lambda_D+\Sigma_{c=1}^{m_1}\xi_{cD,\text{act}}+\Sigma_{c=1}^{m_2}\zeta_{cD,\text{act}}+\eta_D]$$
$$+(\partial f_j/\partial I_j)[\sigma_{Ij}+\lambda_I+\Sigma_{c=1}^{m_1}\xi_{cI,\text{actual}}+\Sigma_{c=1}^{m_2}\zeta_{cI,\text{actual}}+\eta_I]$$
$$+(\partial f_j/\partial A_j)[\sigma_{Aj}+\lambda_A+\Sigma_{c=1}^{m_1}\xi_{cA,\text{actual}}+\Sigma_{c=1}^{m_2}\zeta_{cA,\text{actual}}+\eta_A]$$
$$+(\partial f_j/\partial D_j)[\sigma_{Dj}+\lambda_D+\Sigma_{c=1}^{m_1}\xi_{cD,\text{actual}}+\Sigma_{c=1}^{m_2}\zeta_{cD,\text{actual}}+\eta_D]\ \}\ \}^2 \qquad \{3.5\text{-}1\}$$

Where sums of the type $(\sigma_{Ij}\sigma_{Aj})$, ..., $(\sigma_{Dj}\sigma_{Dj})$, $(\sigma_{Ij}\eta_I)$, ..., $(\sigma_{Ij}\ \lambda_D)$, $(\sigma_{Ij}\xi_{1I})$, ..., $(\sigma_{Dj}\xi_{m1D})$, $(\sigma_{Ij}\zeta_{1I})$, ..., $(\sigma_{Dj}\zeta_{m2D})$, etc. can be set to zero because of data randomness.

For a large number of independent consecutive surveys, also sums including terms of the form $(\eta_I\lambda_I)$, ..., $(\eta_D\lambda_D)$, $(\eta_I\zeta_{1I})$, ..., $(\eta_D\zeta_{m2D})$, $(\lambda_I\xi_{1I})$, ..., $(\lambda_D\xi_{m1D})$, $(\lambda_I\zeta_{1I})$, ..., $(\lambda_D\zeta_{m2D})$, $(\xi_{1I}\zeta_{1I})$, ..., $(\xi_{m1D}\zeta_{m2D})$, etc. might be set to zero. This leads to the simplified equation

$$\Sigma_X = [(\partial f_1/\partial I_0)^2\sigma_{I0}^2+(\partial f_1/\partial A_0)^2\sigma_{A0}^2+(\partial f_1/\partial D_0)^2\sigma_{D0}^2]$$
$$+[(\partial f_n/\partial I_n)^2\sigma_{In}^2+(\partial f_n/\partial A_n)^2\sigma_{An}^2+(\partial f_n/\partial D_n)^2\sigma_{Dn}^2]$$
$$+\Sigma_{j=1}^{n}\{[(\partial f_j/\partial I_j)^2+2(\partial f_j/\partial I_j)(\partial f_{j+1}/\partial I_j)+(\partial f_{j+1}/\partial I_j)^2]\sigma_{Ij}^2$$
$$+[(\partial f_j/\partial A_j)^2+2(\partial f_j/\partial A_j)(\partial f_{j+1}/\partial A_j)+(\partial f_{j+1}/\partial A_j)^2]\sigma_{Aj}^2$$
$$+[(\partial f_j/\partial D_j)^2+2(\partial f_j/\partial D_j)(\partial f_{j+1}/\partial D_j)+(\partial f_{j+1}/\partial D_j)^2]\sigma_{Dj}^2\}$$
$$+\Sigma_{k=1}^{k_n}\{\ \Sigma_{j=j+1}^{j+k_k}[(\partial f_j/\partial I_{j-1})\lambda_I+(\partial f_j/\partial A_{j-1})\lambda_A+(\partial f_j/\partial D_{j-1})\lambda_D$$
$$+(\partial f_j/\partial I_j)\lambda_I+(\partial f_j/\partial A_j)\lambda_A+(\partial f_j/\partial D_j)\lambda_D]\}^2$$
$$+\{\Sigma_{k=1}^{k_n}\Sigma_{j=j+1}^{j+k_k}[(\partial f_j/\partial I_{j-1})\zeta_{1I}+(\partial f_j/\partial A_{j-1})\zeta_{1A}+(\partial f_j/\partial D_{j-1})\zeta_{1D}$$
$$+(\partial f_j/\partial I_j)\zeta_{1I}+(\partial f_j/\partial A_j)\zeta_{1A}+(\partial f_j/\partial D_j)\zeta_{1D}]\}^2$$
$$+\ ....$$
$$+\{\Sigma_{k=1}^{k_n}\Sigma_{j=j+1}^{j+k_k}[(\partial f_j/\partial I_{j-1})\zeta_{m2I}+(\partial f_j/\partial A_{j-1})\zeta_{m2A}+(\partial f_j/\partial D_{j-1})\zeta_{m2D}$$
$$+(\partial f_j/\partial I_j)\zeta_{m2I}+(\partial f_j/\partial A_j)\zeta_{m2A}+(\partial f_j/\partial D_j)\zeta_{m2D}]\}^2$$
$$+\{\{\Sigma_{j=1}^{n}[(\partial f_j/\partial I_{j-1})\xi_{1I}+(\partial f_j/\partial A_{j-1})\xi_{1A}+(\partial f_j/\partial D_{j-1})\xi_{1D}$$
$$+(\partial f_j/\partial I_j)\xi_{1I}+(\partial f_j/\partial A_j)\xi_{1A}+(\partial f_j/\partial D_j)\xi_{1D}]\}$$
$$+\ ....$$
$$+\{\Sigma_{j=1}^{n}[(\partial f_j/\partial I_{j-1})\xi_{m1I}+(\partial f_j/\partial A_{j-1})\xi_{m1A}+(\partial f_j/\partial D_{j-1})\xi_{m1D}$$
$$+(\partial f_j/\partial I_j)\xi_{m1I}+(\partial f_j/\partial A_j)\xi_{m1A}+(\partial f_j/\partial D_j)\xi_{m1D}]\}$$
$$+\{\Sigma_{j=1}^{n}[(\partial f_j/\partial I_{j-1})\eta_I+(\partial f_j/\partial A_{j-1})\eta_A+(\partial f_j/\partial D_{j-1})\eta_D$$
$$+(\partial f_j/\partial I_j)\eta_I+(\partial f_j/\partial A_j)\eta_A+(\partial f_j/\partial D_j)\eta_D]\}\}^2 \qquad \{3.5\text{-}2\}$$

The three first lines of this vector equation system is identical to the random co-variance matrix previously described. Line four to seven is the co-variance matrixes of each of the error terms that are random between surveys. The last four lines are the resultant co-variance matrix from all error terms that are systematic between some or all surveys. The equation is only valid if non-existing uncertainties are set to zero. The overall uncertainty can then be looked upon as a summation of different co-variance matrixes.

For a straight wellbore consisting of k_n independent surveys each k stations long, and a total of n stations, with equal station separation and with angular measurements with the same random- and systematic- errors at the different levels, and depth errors proportional with measured depth, equation *{3.5-2}* reduces to

Page 25 Equation *{3.5-2}* all ... $\Sigma_{j=j+1}^{j+k_k}$[... should be ... $\Sigma_{j=\sum_{i=1}^{k}(k_{i-1})+1}^{\sum_{i=1}^{k}(k_i)}$[...

$$
\begin{aligned}
\Sigma_X = n\{&[(\partial f/\partial I)^2+(\partial f/\partial I\text{-})^2+2(1\text{-}1/n)(\partial f/\partial I)(\partial f/\partial I\text{-})]\sigma_I^2 \\
&+[(\partial f/\partial A)^2+(\partial f/\partial A\text{-})^2+2(1\text{-}1/n)(\partial f/\partial A)(\partial f/\partial A\text{-})]\sigma_A^2 \\
&+[(\partial f/\partial D)^2+(\partial f/\partial D\text{-})^2+2(1\text{-}1/n)(\partial f/\partial D)(\partial f/\partial D\text{-})]\sigma_D^2\} \\
&+k_n\{k[(\partial f/\partial I)\lambda_I+(\partial f/\partial I\text{-})\lambda_I+(\partial f/\partial A)\lambda_A+(\partial f/\partial A\text{-})\lambda_A] \\
&\quad+(k^2+k)/2(\partial f/\partial D)\lambda_D+(k^2-k)/2(\partial f/\partial D\text{-})\lambda_D\}^2 \\
&+b_1\{k[(\partial f/\partial I)\zeta_{1I}+(\partial f/\partial I\text{-})\zeta_{1I}+(\partial f/\partial \mathrm{A})\zeta_{1A}+(\partial f/\partial A\text{-})\zeta_{1A}] \\
&\quad+(k^2+k)/2(\partial f/\partial D)\zeta_{1D}+(k^2-k)/2(\partial f/\partial D\text{-})\zeta_{1D}\}^2 \\
&+ \ldots\ldots \\
&+b_{m2}\{k[(\partial f/\partial I)\zeta_{m2I}+(\partial f/\partial I\text{-})\zeta_{m2I}+(\partial f/\partial A)\zeta_{m2A}+(\partial f/\partial A\text{-})\zeta_{m2A}] \\
&\quad+(k^2+k)/2(\partial f/\partial D)\zeta_{m2D}+(k^2-k)/2(\partial f/\partial D\text{-})\zeta_{m2D}\}^2 \\
&+\{a_1\{k[(\partial f/\partial I)\xi_{1I}+(\partial f/\partial I\text{-})\xi_{1I}+(\partial f/\partial A)\xi_{1A}+(\partial f/\partial A\text{-})\xi_{1A}] \\
&\quad+(k^2+k)/2(\partial f/\partial D)\xi_{1D}+(k^2-k)/2(\partial f/\partial D\text{-})\xi_{1D}\} \\
&\quad+ \ldots\ldots \\
&\quad+a_{m1}\{k[(\partial f/\partial I)\xi_{m1I}+(\partial f/\partial I\text{-})\xi_{m1I}+(\partial f/\partial A)\xi_{m1A}+(\partial f/\partial A\text{-})\xi_{m1A}] \\
&\quad\quad+(k^2+k)/2(\partial f/\partial D)\xi_{m1D}+(k^2-k)/2(\partial f/\partial D\text{-})\xi_{m1D}\} \\
&\quad+n[(\partial f/\partial I)\eta_I+(\partial f/\partial I\text{-})\eta_I+(\partial f/\partial A)\eta_A+(\partial f/\partial A\text{-})\eta_A] \\
&\quad\quad+(n^2+n)/2(\partial f/\partial D)\eta_D+(n^2-n)/2(\partial f/\partial D\text{-})\eta_D\}^2
\end{aligned}
\qquad \{3.5\text{-}3\}
$$

$a_1, \ldots, a_{m1}, b_1, \ldots, b_{m2}$ is the number of surveys where the associated error is present.

Published error propagation theories do not give any description on how to handle this problem. An analysis of two major commercial software packages has shown that they are adding systematic error sources randomly between surveys regardless on the actual error propagation characteristics. All errors are therefor included in the ζ error type. Equation *{3.5-3}* is then simplified to

$$
\begin{aligned}
\Sigma_X = b_1\{&k[(\partial f/\partial I)\zeta_{1I}+(\partial f/\partial I\text{-})\zeta_{1I}+(\partial f/\partial A)\zeta_{1A}+(\partial f/\partial A\text{-})\zeta_{1A}] \\
&+(k^2+k)/2(\partial f/\partial D)\zeta_{1D}+(k^2-k)/2(\partial f/\partial D\text{-})\zeta_{1D}\}^2 \\
&+ \ldots\ldots \\
&+b_{m2}\{k[(\partial f/\partial I)\zeta_{m2I}+(\partial f/\partial I\text{-})\zeta_{m2I}+(\partial f/\partial A)\zeta_{m2A}+(\partial f/\partial A\text{-})\zeta_{m2A}] \\
&\quad+(k^2+k)/2(\partial f/\partial D)\zeta_{m2D}+(k^2-k)/2(\partial f/\partial D\text{-})\zeta_{m2D}\}^2
\end{aligned}
\qquad \{3.5\text{-}4\}
$$

The uncertainty predicted by equation *{3.5-4}* will always be less than what is predicted by equation *{3.5-3}* as long as significant systematic effects between surveys are present.

Example 3.5-1

We shall again look at the wellbore profile described in example 3.1-1. This time it is assumed that the wellbore is surveyed with four independent consecutive surveys with equal length. The first two sections is surveyed with the same north seeking gyro, and the latter two is surveyed with the same magnetic MWD. The following measurement uncertainty budget can be created if the same running conditions and quality control procedures are assumed.

$2\xi_{1I} = 2\xi_{2I} = 2\xi_{3I} = 2\xi_{4I} = 2\xi_I = 0.3°$,
$2\xi_{3A} = 2\xi_{4A} = 2\xi_A = 2.0°$, $\quad \xi_{1A} = \xi_{2A} = 0$,
$2\zeta_{1A} = 2\zeta_{2A} = 2\zeta_A = 0.45°$, $\quad \zeta_{3A} = \zeta_{4A} = 0$,

$2\eta_D = 0.2\%$ of the unit length,
$n = 200$, $k = 50$, $k_e = 4$, $a1 = a2 = b1 = b2 = 2$,

The following position co-variance matrix can then be created

$$\Sigma_X = \begin{bmatrix} 52.1 & 0 & 0 \\ 0 & 0 & 0 \\ 0 & 0 & 0 \end{bmatrix} + \begin{bmatrix} 2067.1 & -599.0 & 482.5 \\ -599.0 & 173.6 & -139.8 \\ 482.5 & -139.8 & 112.6 \end{bmatrix} = \begin{bmatrix} 2119.2 & -599.0 & 482.5 \\ -599.0 & 173.6 & -139.8 \\ 482.5 & -139.8 & 112.6 \end{bmatrix}$$

Maximum uncertainty is to the north and given by $\sigma_{NN} = 46.0$m.

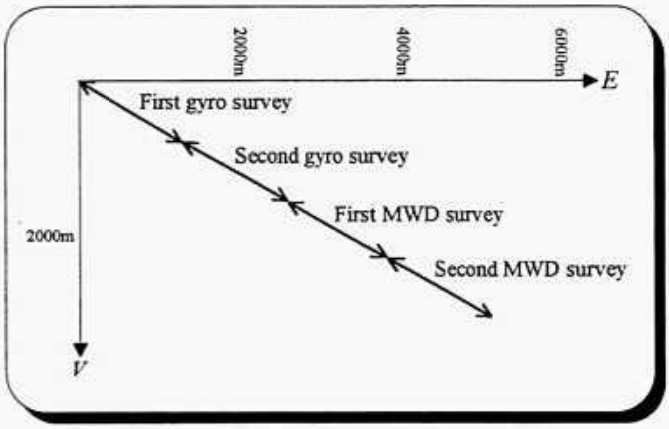

Figure 3.5-1 Survey program used in this example

Example 3.5-2

We shall look at the same survey program as described in example 3.5-1, but now with the current practice of handling consecutive surveys as if they where random with respect to each other. This gives the following uncertainty estimates

$2\zeta_{1I} = 2\zeta_{2I} = 0.3°$,
$2\zeta_{1A} = 2.0°$,
$2\zeta_{2A} = 0.45°$,
$2\zeta_{1S} = 2\zeta_{2S} = 0.2\%$ of the unit length,

$$\Sigma_X = \begin{bmatrix} 1085.7 & -183.4 & 147.7 \\ -183.4 & 43.4 & -35.0 \\ 147.7 & -35.0 & 28.2 \end{bmatrix}$$

Maximum uncertainty is now $\sigma_{NN} = 32.9$m.

This is very different from the result in example 3.5-1. The north uncertainty is reduced from 46.0m in the complete study to 32.9m in the simplified study. This represents an under estimation of the uncertainty of 28%.

3.6 Redundant Survey Programs

For longer extended reach- and designer- wells, it is a common practice to take multiple wellbore surveys, and / or to make overlapping sections between adjacent surveys as part of the QC procedure. This means that it usually are redundant survey information present in connection with these wellbores. The redundant information can be used for improvements the wellbore position estimate. Especially when different instruments, different bottom hole assemblies etc., are used in the different surveys. The value of redundant surveys taken with the same instrument are, however, more questionable. The effect of significant error sources which are systematic between surveys, for example the magnetic declination uncertainty, can then usually not be identified and removed. Today, redundant data are not used for other purposes than to identify gross errors. No statistical adjustment theory designed to make use of the redundancy has up to now been published. The final representation of a drilled wellbore is usually one single survey, or a few consecutive independent surveys tied together.

A simplified example based on a wellbore surveyed with m identical surface to bottom (TD) surveys will be used to prove that the current practice might produce position estimates with greater uncertainties than necessary. The different surveys are taken with different equal instruments, and each survey consists of n stations. The different measurements are assumed to be averaged at each station, and the averaged measurements are assumed to be used in the well path calculation. The following error terms are then of interest

σ_{Ij} = random inclination uncertainty
σ_{Aj} = random azimuth uncertainty
σ_{Dj} = random depth uncertainty
λ_{Ij} = systematic inclination uncertainty that is random between different surveys
λ_{Aj} = systematic azimuth uncertainty that is random between different surveys
λ_{Dj} = systematic depth uncertainty that is random between different surveys
η_{Ij} = systematic inclination uncertainty for all surveys
η_{Aj} = systematic azimuth uncertainty for all survey
η_{Dj} = systematic depth uncertainty for all surveys

and the following error propagation will be valid

$$\Delta X_j = f_j\left(\frac{\Sigma_{k=1}^{m} I_{j-1,k}}{m}, \frac{\Sigma_{k=1}^{m} A_{j-1,k}}{m}, \frac{\Sigma_{k=1}^{m} D_{j-1,k}}{m}, \frac{\Sigma_{k=1}^{m} I_{j,k}}{m}, \frac{\Sigma_{k=1}^{m} A_{j,k}}{m}, \frac{\Sigma_{k=1}^{m} D_{j,k}}{m} \right) \qquad \{3.6\text{-}1\}$$

Combined with equation *{3.5-2}*, this gives

$$\begin{aligned}
\Sigma_X = \Sigma_{j=1}^{n} [& (\partial f_j/\partial I_{j-1})^2 \frac{\sigma_{Ij-1}^2}{m} + (\partial f_j/\partial A_{j-1})^2 \frac{\sigma_{Aj-1}^2}{m} + (\partial f_j/\partial D_{j-1})^2 \frac{\sigma_{Dj-1}^2}{m} \\
& + (\partial f_j/\partial I_j)^2 \frac{\sigma_{Ij}^2}{m} + (\partial f_j/\partial A_j)^2 \frac{\sigma_{Aj}^2}{m} + (\partial f_j/\partial D_j)^2 \frac{\sigma_{Dj}^2}{m}] \\
& + \{ \Sigma_{j=1}^{n} [(\partial f_j/\partial I_{j-1}) \frac{\lambda_{Ij-1}}{\sqrt{m}} + (\partial f_j/\partial A_{j-1}) \frac{\lambda_{Aj-1}}{\sqrt{m}} + (\partial f_j/\partial D_{j-1}) \frac{\lambda_{Dj-1}}{\sqrt{m}} \\
& + (\partial f_j/\partial I_j) \frac{\lambda_{Ij}}{\sqrt{m}} + (\partial f_j/\partial A_j) \frac{\lambda_{Aj}}{\sqrt{m}} + (\partial f_j/\partial D_j) \frac{\lambda_{Dj}}{\sqrt{m}}] \}^2 \\
& + \{ \Sigma_{j=1}^{n} [(\partial f_j/\partial I_{j-1}) \eta_{Ij-1} + (\partial f_j/\partial A_{j-1}) \eta_{Aj-1} + (\partial f_j/\partial D_{j-1}) \eta_{Dj-1} \\
& + (\partial f_j/\partial I_j) \eta_{Ij} + (\partial f_j/\partial A_j) \eta_{Aj} + (\partial f_j/\partial D_j) \eta_{Dj}] \}^2
\end{aligned} \qquad \{3.6\text{-}2\}$$

For a straight well consisting of n stations with equal station separation, and repeated measurements with same random and systematic errors (systematic depth errors proportional to measured depth), equation *{3.6-2}* reduces to

$$\begin{aligned}\Sigma_X = \; & n/m \; \{[(\partial f/\partial I)^2+(\partial f/\partial I\text{-})^2+2(1\text{-}1/n)(\partial f/\partial I)(\partial f/\partial I\text{-})]\sigma_I^2 \\ & +[(\partial f/\partial A)^2+(\partial f/\partial A\text{-})^2+2(1\text{-}1/n)(\partial f/\partial A)(\partial f/\partial A\text{-})]\sigma_A^2 \\ & +[(\partial f/\partial D)^2+(\partial f/\partial D\text{-})^2+2(1\text{-}1/n)(\partial f/\partial D)(\partial f/\partial D\text{-})]\sigma_D^2\} \\ & + n^2/m \; \{[(\partial f/\partial I)\lambda_I+(\partial f/\partial I\text{-})\lambda_I+(\partial f/\partial A)\lambda_A+(\partial f/\partial A\text{-})\lambda_A] \\ & \quad +(n^2+n)/2(\partial f/\partial D)\lambda_D+(n^2-n)/2(\partial f/\partial D\text{-})\lambda_D\}^2 \\ & + n^2 \; \{[(\partial f/\partial I)\eta_I+(\partial f/\partial I\text{-})\eta_I+(\partial f/\partial A)\eta_A+(\partial f/\partial A\text{-})\eta_A] \\ & \quad +(n^2+n)/2(\partial f/\partial D)\eta_D+(n^2-n)/2(\partial f/\partial D\text{-})\eta_D\}^2 \end{aligned} \qquad \{3.6\text{-}3\}$$

Equation *{3.6-3}* shows that the contribution to the overall uncertainty from all errors which are random between different surveys, are reduced with one over the square root of the number of identical surveys. A use of the redundant information in multiple surveys can because of this represent a significant accuracy improvement, if random between surveys errors are major contributors to the wellbore position uncertainty. This is usually the case when different types of surveys, or different instruments of the same type, are used. For magnetic MWD, this is only partly true because of the presence of significant systematic between surveys errors (see chapter 5). An introduction of an adjustment theory into directional surveys has because of this a great potential as a low cost tool for accuracy improvements. The redundant measurements are already taken, and the additional cost is only a more complex data handling. Another great advantage with an adjustments approach, is a possibility to estimate some of the systematic error terms. The magnitude of these systematic uncertainty terms might then be reduced compared to the global numbers usually used in wellbore planning. This will reduce the predicted uncertainty estimate at the planning stage, which of course will be beneficial to the operations through a reduced need for high cost directional surveys, and a reduced number of closed in producing wells.

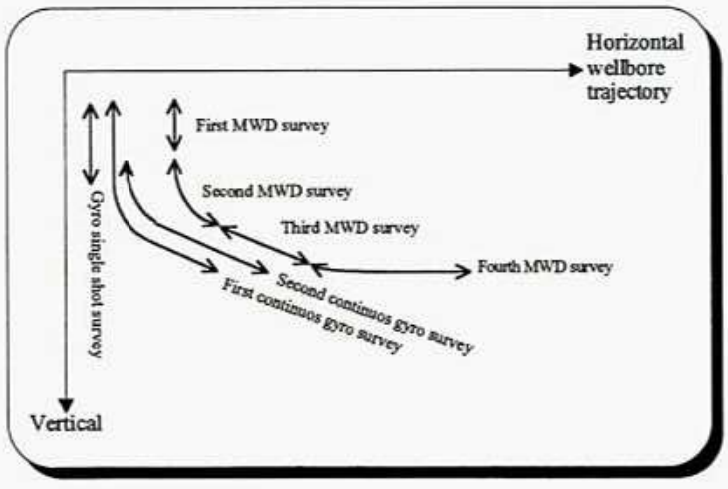

Figure 3.6-1 Example on redundant survey program

Example 3.6-1

Let us once again look at the wellbore described in example 3.1-1, but this time under the assumption that the wellbore is surveyed with four identical north seeking gyro surveys. Assuming same running conditions and quality control procedures as in example 3.1-1 gives the following measurement uncertainties

$n = 200$, $m = 4$,
$2\lambda_I = 0.3°$, $2\lambda_A = 0.45°$,
$2\eta_D = 0.2\%$ of the unit length,

This leads to the following co-variance matrix

$$\Sigma_X = n^2/m\,[2(\partial f/\partial I)\lambda_I + 2(\partial f/\partial A)\lambda_A]^2 + n^2[(\partial f/\partial D)\eta_D]^2$$

$$\Sigma_X = \begin{bmatrix} 104.2 & -40.1 & 69.5 \\ -40.1 & 15.4 & -26.8 \\ 69.5 & -26.8 & 46.3 \end{bmatrix} + \begin{bmatrix} 0 & 0 & 0 \\ 0 & 28.3 & 15.9 \\ 0 & 15.9 & 9.0 \end{bmatrix} = \begin{bmatrix} 104.2 & -40.1 & 69.5 \\ -40.1 & 43.7 & -10.8 \\ 69.5 & -10.8 & 55.3 \end{bmatrix}$$

This gives a north uncertainty of $\sigma_{NN} = 10.2$m.

Example 3.6-2

If the wellbore is surveyed as in example 3.6-1, but only represented with one of the four surveys (the current practice), the uncertainty is given by

$2\eta_I = 0.3°$, $2\eta_A = 0.45°$,
$2\eta_S = 0.2\%$ of the unit length,

$$\Sigma_X = n^2\,[2(\partial f/\partial I)\eta_I + 2(\partial f/\partial A)\eta_A + (\partial f/\partial D)\eta_D]^2$$

$$\Sigma_X = \begin{bmatrix} 417.0 & -269.1 & 216.7 \\ -269.1 & 173.6 & -139.8 \\ 216.7 & -139.8 & 112.6 \end{bmatrix}$$

This gives an north uncertainty of $\sigma_{NN} = 20.4$m, which is twice as big as the similar north uncertainty when all four surveys where used as in example 3.6-1.

3.7 Weighting Functions

It was in chapter 3.3 shown that the effect of systematic surveying errors on the inclination and the azimuth might be very dependent on wellbore geometry. The geometrical dependency is not only related to directional angles, but also to geographic location. The dependency can usually be described by one ore more of the following parameters

- azimuth
- inclination
- toolface
- latitude
- longitude
- elevation

Error sizes might also vary with other factors such as

- Bottom Hole Assembly (BHA)
- temperature
- pressure
- elastic properties

The way these factors affects the measurement accuracy, is known from physics or can be determined through tests, and can be expressed as error propagation functions. Wolff and deWardt called such functions as weighting functions. The Wolff deWardt terminology is well known within the drilling industry, and will therefore be used in the following. The actual measurement uncertainty might therefore be expressed by a weighting function and a reference variance

$$\sigma^2 = w(\text{dependency factors})^2\,\sigma_0^2 \qquad \{3.7\text{-}1\}$$

where σ_0^2 is the reference variance and w is the weighting function.

Weighting functions applied to a single directional survey with combined systematic and random errors leads to the following error propagation properties

$$\begin{aligned}\Sigma_X = {} & [(\partial f_1/\partial I_0)^2 u_{I0}^2 \sigma_{I0}^2 + (\partial f_1/\partial A_0)^2 u_{A0}^2 \sigma_{A0}^2 + (\partial f_1/\partial D_0)^2 u_{D0}^2 \sigma_{D0}^2] \\ & + [(\partial f_n/\partial I_n)^2 u_{In}^2 \sigma_{In}^2 + (\partial f_n/\partial A_n)^2 u_{An}^2 \sigma_{An}^2 + (\partial f_n/\partial D_n)^2 u_{Dn}^2 \sigma_{Dn}^2] \\ & + \Sigma_{j=1}^{n-1} \{[(\partial f_j/\partial I_j)^2 + 2(\partial f_j/\partial I_j)(\partial f_{j+1}/\partial I_j) + (\partial f_{j+1}/\partial I_j)^2]\, u_{Ij}^2 \sigma_{Ij}^2 \\ & \quad + [(\partial f_j/\partial A_j)^2 + 2(\partial f_j/\partial A_j)(\partial f_{j+1}/\partial A_j) + (\partial f_{j+1}/\partial A)^2] u_{Aj}^2 \sigma_{Aj}^2 \\ & \quad + [(\partial f_j/\partial D_j)^2 + 2(\partial f_j/\partial D_j)(\partial f_{j+1}/\partial D_j) + (\partial f_{j+1}/\partial D_j)^2] u_{Dj}^2 \sigma_{Dj}^2 \} \\ & + \{\Sigma_{j=1}^{n} [(\partial f_j/\partial I_{j-1}) w_{Ij-1} \eta_I + (\partial f_j/\partial A_{j-1}) w_{Aj-1} \eta_A + (\partial f_j/\partial D_{j-1}) w_{Dj-1} \eta_D \\ & \quad + (\partial f_j/\partial I_j) w_{Ij} \eta_I + (\partial f_j/\partial A_j) w_{Aj} \eta_A + (\partial f_j/\partial D_j) w_{Dj} \eta_D]\}^2 \end{aligned} \qquad \{3.7\text{-}2\}$$

u_{Ij} is the weighting function for the random inclination error at station j, and
w_{Aj} is the weighting function for the systematic azimuth error at station j, etc.

For a straight wellbore with equal station separation, and constant measurement accuracy (systematic depth errors proportional to measured depth), equation *{3.7-2}* reduces to

$$\begin{aligned}\Sigma_X = n\{&[(\partial f/\partial I)^2+(\partial f/\partial I\text{-})^2+2(1\text{-}1/n)(\partial f/\partial I)(\partial f/\partial I\text{-})]u_I^2\sigma_I^2\\ &+[(\partial f/\partial A)^2+(\partial f/\partial A\text{-})^2+2(1\text{-}1/n)(\partial f/\partial A)(\partial f/\partial A\text{-})]u_A^2\sigma_A^2\\ &+[(\partial f/\partial D)^2+(\partial f/\partial D\text{-})^2+2(1\text{-}1/n)(\partial f/\partial D)(\partial f/\partial D\text{-})]u_D^2\sigma_D^2\}\\ &+\{n[(\partial f/\partial I)w_I\eta_I+(\partial f/\partial I\text{-})w_I\eta_I+(\partial f/\partial A)w_A\eta_A+(\partial f/\partial A\text{-})w_A\eta_A]\\ &+(n^2+n)/2(\partial f/\partial D)w_D\eta_D+(n^2\text{-}n)/2(\partial f/\partial D\text{-})w_D\eta_D\}^2\end{aligned} \qquad \{3.7\text{-}3\}$$

A correct weighting function can be very complex and difficult to find. It may consist of both step functions and continuous functions. From equation *{3.7-3}* it is obvious that the accuracy of the chosen weighting function is critical for the accuracy of an wellbore position uncertainty estimate. Examples on the use of completely wrong weighting functions are known. The common use of *1/cosI* as weighting function for the Finder tool (a continuous gyro) is a good example on this. This is in sharp contrast with the correct weighting function which according to chapter 6.1.1.6 is proportional to *1/sinI*.

All mathematical derivations up to now have been made with the assumption that inclination-, azimuth-, and depth measurements at one single station are uncorrelated. For modern directional survey instruments, this is not necessary the case. In electronic instruments like magnetic MWD, north seeking gyros, continuous gyros etc. , accelerometer measurements are usually used as input in both inclination and azimuth calculations. These two measurements will therefore be correlated to some degree. Another example is electronic instruments where all sensor measurements are fed through the same analog-to-digital converter. The result must be some kind of correlation between all sensors, which lead to correlation between the inclination and the azimuth measurements. This and similar correlation should, if they are significant, be included in the error analysis to give an optimal result. This can be done by introducing a set of weighting matrixes instead of weighting functions. The different elements of each measurement co-variance matrixes will then be made up of the different weighting functions and the internal correlation between the different measurements.

Random Errors

The different measurement co-variance matrixes will then have the following form

$$\Lambda_j = \begin{bmatrix} u_{Ij\text{-}1}^2\sigma_{IIj\text{-}1}^2 & u_{Ij\text{-}1}u_{Aj\text{-}1}\sigma_{IAj\text{-}1}^2 & u_{Ij\text{-}1}u_{Dj\text{-}1}\sigma_{IDj\text{-}1}^2 & 0 & 0 & 0\\ u_{Ij\text{-}1}u_{Aj\text{-}1}\sigma_{IAj\text{-}1}^2 & u_{Aj\text{-}1}^2\sigma_{AAj\text{-}1}^2 & u_{Aj\text{-}1}u_{Dj\text{-}1}\sigma_{ADj\text{-}1}^2 & 0 & 0 & 0\\ u_{Ij\text{-}1}u_{Dj\text{-}1}\sigma_{IDj\text{-}1}^2 & u_{Aj\text{-}1}u_{Dj\text{-}1}\sigma_{ADj\text{-}1}^2 & u_{Dj\text{-}1}^2\sigma_{DDj\text{-}1}^2 & 0 & 0 & 0\\ 0 & 0 & 0 & u_{Ij}^2\sigma_{IIj}^2 & u_{Ij}u_{Aj}\sigma_{IAj}^2 & u_{Ij}u_{Dj}\sigma_{IDj}^2\\ 0 & 0 & 0 & u_{Ij}u_{Aj}\sigma_{IAj}^2 & u_{Aj}^2\sigma_{AAj}^2 & u_{Aj}u_{Dj}\sigma_{ADj}^2\\ 0 & 0 & 0 & u_{Ij}u_{Dj}\sigma_{IDj}^2 & u_{Aj}u_{Dj}\sigma_{ADj}^2 & u_{Dj}^2\sigma_{DDj}^2 \end{bmatrix} \qquad \{3.7\text{-}4\}$$

Equation *{3.1-6}* will then take the form

$$\Sigma_X = \Sigma_{j=1}^{n}(\Gamma_j\Lambda_j\Gamma_j^T) \qquad \{3.7\text{-}5\}$$

where the design matrixes Γ_j (related to the principal measurements inclination, azimuth and depth) have the following form

$$\Gamma_j = \begin{bmatrix} \partial f_{Nj}/\partial I_{j-1} & \partial f_{Nj}/\partial A_{j-1} & \partial f_{Nj}/\partial D_{j-1} & \partial f_{Nj}/\partial I_j & \partial f_{Nj}/\partial A_j & \partial f_{Nj}/\partial D_j \\ \partial f_{Ej}/\partial I_{j-1} & \partial f_{Ej}/\partial A_{j-1} & \partial f_{Ej}/\partial D_{j-1} & \partial f_{Ej}/\partial I_j & \partial f_{Ej}/\partial A_j & \partial f_{Ej}/\partial D_j \\ \partial f_{Vj}/\partial I_{j-1} & \partial f_{Vj}/\partial A_{j-1} & \partial f_{Vj}/\partial D_{j-1} & \partial f_{Vj}/\partial I_j & \partial f_{Vj}/\partial A_j & \partial f_{Vj}/\partial D_j \end{bmatrix} \quad \{3.7\text{-}6\}$$

Systematic Errors

It is in this case difficult to continue to make sequential computations. The best alternative is to change to a complete matrix computation. Equation *{3.3-3}* will then take the form

$$\Sigma'_X = \Gamma \Lambda \Gamma^T \quad \{3.7\text{-}7\}$$

Σ'_X is a complete position co-variance matrix for the entire survey, and has the dimension of $3n$ multiplied by $3n$.

The observation co-variance matrix Λ has the following form

$$\Lambda = \begin{bmatrix} \mathbf{w}_{00} & \mathbf{w}_{01} & \cdots & \mathbf{w}_{0k} & \cdots & \mathbf{w}_{0n} \\ \mathbf{w}_{10} & \mathbf{w}_{11} & \cdots & \mathbf{w}_{1k} & \cdots & \mathbf{w}_{1n} \\ \cdots & \cdots & \cdots & \cdots & \cdots & \cdots \\ \mathbf{w}_{j0} & \mathbf{w}_{j1} & \cdots & \mathbf{w}_{jk} & \cdots & \mathbf{w}_{jn} \\ \cdots & \cdots & \cdots & \cdots & \cdots & \cdots \\ \mathbf{w}_{n0} & \mathbf{w}_{n1} & \cdots & \mathbf{w}_{nk} & \cdots & \mathbf{w}_{nn} \end{bmatrix} \quad \{3.7\text{-}8\}$$

where

$$\mathbf{w}_{jk} = \begin{bmatrix} w_{Ij}w_{Ik}\eta_{II}^2 & w_{Ij}w_{Ak}\eta_{IA}^2 & w_{Ij}w_{Dk}\eta_{ID}^2 \\ w_{Ik}w_{Aj}\eta_{IA}^2 & w_{Aj}w_{Ak}\eta_{AA}^2 & w_{Aj}w_{Dk}\eta_{AD}^2 \\ w_{Ik}w_{Dj}\eta_{ID}^2 & w_{Ak}w_{Dj}\eta_{AD}^2 & w_{Dj}w_{Dk}\eta_{DD}^2 \end{bmatrix} \quad \{3.7\text{-}9\}$$

The design matrix Γ has the following form

$$\Gamma = \begin{bmatrix} \partial f''_{N1}/\partial I_0 .. \partial f''_{N1}/\partial D_0 & \partial f''_{N1}/\partial I_1 .. \partial f''_{N1}/\partial D_1 .. & 0 & .. & 0 & 0 & .. & 0 \\ \cdots & & & & & & & \\ \partial f''_{V1}/\partial I_0 .. \partial f''_{V1}/\partial D_0 & \partial f''_{V1}/\partial I_1 .. \partial f''_{V1}/\partial D_1 .. & 0 & .. & 0 & 0 & .. & 0 \\ \cdots & & & & & & & \\ \partial f''_{Vn}/\partial I_0 .. \partial f''_{Vn}/\partial D_0 & \partial f''_{Vn}/\partial I_1 .. \partial f''_{Vn}/\partial D_1 .. \partial f''_{Vn}/\partial I_{n-1} .. \partial f''_{Vn}/\partial D_{n-1} & \partial f''_{Vn}/\partial I_n .. & & & & & \partial f''_{Vn}/\partial D_n \end{bmatrix} \quad \{3.7\text{-}10\}$$

where $\partial f''_{Nj}/\partial I_0 = \partial(\Sigma_{k=1}^{j} f_{Nk})/\partial I_0$ etc.

By manipulating with the observation co-variance matrix Λ, it is possible to include all previously described effects with exception of redundancy. For a wellbore surveyed with many consecutive independent surveys (different degrees of correlation between the different surveys as described in chapter 3.5), Λ might become very complex.

3.8 Angular Uncertainty Components

Angular measurements (inclination, azimuth and toolface) are looked upon as fundamental measurements in traditional directional surveying. They are, however, not direct measurements. They are derived from other measurements, which are related to physical quantities like the earth gravity field, the earth magnetic field or the earth rotation rate. The uncertainties related to derived angular measurements are therefore the combined effect of uncertainties associated with the actual physical measurements, reference values used to calculate the angle, and wellbore misalignments. The error in derived angles at measurement station j, for example $\varepsilon_{I,j}$ in the inclination, is then given by

$$\varepsilon_{I,j} = \Sigma_{i=1}^{n} w_{I,ij} \varepsilon_{I,ij} \qquad \{3.8\text{-}1\}$$

where $\varepsilon_{I,ij}$ is the independent error source number i and $w_{I,ij}$ is a weighting function describing how $\varepsilon_{I,ij}$ is propagated into $\varepsilon_{I,j}$. Similar relationships are also valid for the azimuth and the toolface.

Measurement errors are usually unknown, but can, as shown in chapter 3.1, be substituted with an estimated uncertainty (standard deviation) in accuracy studies. The resulting inclination uncertainty dI at station j is then given by

$$dI_j = \sqrt{\Sigma_{i=1}^{n1} (w_{I,ij} d\sigma_{i,j})^2 + \Sigma_{i=n1+1}^{n} (w_{I,ij} d\eta_{i,j})^2} \qquad \{3.8\text{-}2\}$$

It is here assumed that all significant error sources affecting the inclination are broken down into uncorrelated components.

Equation *{3.8-2}* and similar azimuth and toolface equations give the angular measurement uncertainty at one single station. Such equations are very useful in uncertainty studies in connection with "kick off" operations etc., where the angular accuracy is the primary concern. They are, however, not so useful in connection with wellbore position uncertainty studies, and this is usually the principal task in directional surveying accuracy studies.

Most weighting functions ($w_{I,ij}$, $w_{A,ij}$, $w_{\tau,ij}$) are, as it will be shown in chapter 5 and 6, proportional to inclination-, azimuth- and toolface dependent trigonometric functions. The sign of the weighting function might therefore vary along the wellpath. It was in chapter 3.3 shown that the wellbore position uncertainty is very dependent on the weighting function sign if significant systematic errors are present. The sign information given in the weighting functions will get lost if equation *{3.8-2}* is used directly in the position uncertainty calculation.

The sign variation in the weighting functions can be preserved if each uncorrelated error source is handled independently. Each error source must then be summed into its own position co-variance matrix, and not combined with other error sources before at the investigation station. The different inclination uncertainty components are then given by

$$dI_{1,j} = w_{I,1j} d\sigma_1 \qquad \{3.8\text{-}3\}$$

$$dI_{2,j} = w_{I,2j} d\sigma_2 \qquad \{3.8\text{-}4\}$$

.....

$$dI_{n,j} = w_{I,nj} d\eta_n \qquad \{3.8\text{-}5\}$$

The total inclination uncertainty given in equation *{3.8-2}* is then equal to

$$dI = \sqrt{\Sigma_{i=1}^{n} (dI_{i,j})^2} \qquad \{3.8\text{-}6\}$$

Similar equations do also exist for the azimuth and the toolface.

The toolface (τ) is, as it will be shown in chapter 5 and 6, an important parameter in the estimation of many factors affecting the inclination and azimuth. For accuracy studies in connection with drilled wellbores, there is no critical problems related to this. The toolface is part of the survey result, and the toolface measurements can directly be used in the weighting functions. The toolface creates, however, problems in connection with uncertainty prediction in the planning stage.

It is impossible to predict the toolface, which therefore is an unknown quantity. One solution is to divide the surveys into two classes. One with constant or near constant toolface, and one with random toolface. The first class is for wireline measurements and while drilling (MWD) with a bent sub, and the second class is for MWD with a rotary bottom hole assembly (BHA). The constant toolface class can be treated as systematic errors between stations within one survey, and the random classes random errors between all stations.

The constant or near constant toolface assumption is probably not valid for longer sections surveyed with wirelines or bent subs, and should be substituted with a gradually changing toolface. This can be solved with the introduction of a randomisation distance, over which the toolface change from being nearly constant to being random.

An other solution is to generate artificial toolfaces to be used in the weighting functions based on a priori expectations about the toolface behaviour.

3.9 Co-variance Matrix and Confidence Level

It was shown in chapter 3.1 that the position uncertainty at a point on the wellbore trajectory is represented by the position co-variance matrix at this point. This co-variance matrix contain all known information regarding the position uncertainty, and should be used if a total uncertainty status is to be reported. To report a squared three dimensional matrix is, however, not very practical. Instead, a practice to report an ellipsoid (3D) of uncertainty, or projections of the ellipsoid (error ellipses 2D and error confidence intervals 1D), has evolved. The relationship between these figures and the position co-variance matrix will be shown in this chapter.

The position co-variance matrix in the NEV co-ordinate system, is a symmetrical matrix of the form

$$\Sigma_X = \begin{bmatrix} \sigma_{NN}^2 & \sigma_{NE}^2 & \sigma_{NV}^2 \\ \sigma_{NE}^2 & \sigma_{EE}^2 & \sigma_{EV}^2 \\ \sigma_{NV}^2 & \sigma_{EV}^2 & \sigma_{VV}^2 \end{bmatrix}$$

The matrix shows directly the uncertainty for directions originating from the point of investigation, which are parallel to the north east and vertical axis. The uncertainty along other directions can not be read directly out of the co-variance matrix, but is hidden within the total matrix content. An equation for computing the uncertainty in any given direction can be found by making use of the second Tienstra rule [3]. To find the link between the Tienstra rule and the equation shown below, it is necessary to know the basic definition of weight, which states that a weight is a relative accuracy measure between two given measurements. The weight is usually set equal to the inverse of its own variance. When more than two measurements are involved, it is common to weight the different measurements to a common reference measurement. The unit of the searched quantity is often chosen as the reference measurement, and given the weight of one. The uncertainty along a given *R*- direction is then according to Holsen [4] given by

$$\begin{aligned}\sigma_{RR}^2 = {} & \sigma_{NN}^2\cos^2(\alpha) + \sigma_{EE}^2\cos^2(\beta) + \sigma_{VV}^2\cos^2(\gamma) \\ & +2\sigma_{NE}^2\cos(\alpha)\cos(\beta) + 2\sigma_{NV}^2\cos(\alpha)\cos(\gamma) + 2\sigma_{EV}^2\cos(\beta)\cos(\gamma)\end{aligned} \qquad \{3.9\text{-}1\}$$

where cos(α), cos(β), and cos(γ) are the directional cosines to R in the *NEV* system.

As long as biases are removed to a degree where they act as random errors between a large number of independent surveys, the measurements are assumed to be normally distributed. A point with a co-ordinate *r* along the *R*- direction will then be a linear combination of the measurements, and therefore also normal distributed. This because of the linearisation process used in the error propagation function. r/σ_R will then be standard normal distributed N(0,1). This means that the uncertainty along a given direction can be scaled up according to a standard normal distribution table, to create a confidence interval at any significance level along this direction.

Examples on scaling factors

Significance level	Scaling factor
50%	0.667
95%	1.96
99.9%	3.29

A 95% symmetrical confidence interval for the estimated co-ordinate along the *R*-direction is then

$$-1.96\sigma_R <= r <= 1.96\sigma_R \qquad \{3.9\text{-}2\}$$

Since Σ_X is a squared diagonal matrix, it follows from the linear algebra that it is possible to find a new three dimensional orthogonal co-ordinate system, where Σ_X transforms into a diagonal matrix. This co-ordinate system, which can be called *STU*, has origin in the point of investigation, and will usually have an other orientation than the *XYZ* system. This matrix has the following form:

$$\Sigma_S = \begin{bmatrix} \sigma_{SS}^2 & 0 & 0 \\ 0 & \sigma_{TT}^2 & 0 \\ 0 & 0 & \sigma_{UU}^2 \end{bmatrix} \qquad \{3.9\text{-}3\}$$

σ_{SS}^2, σ_{TT}^2, σ_{UU}^2, are identical to the eigenvalues of the Σ_X matrix.

The co-variance matrix Σ_S, where all correlation terms are equal to zero, shows that the uncertainties along the *S*-, *T*-, and *U*- axis are uncorrelated.

The values σ_{SS}^2, σ_{TT}^2, σ_{UU}^2, and the orientation of the *STU* co-ordinate system relative to the *NEV* system, can be obtained in many ways. One possibility is to use a modified version of the method described by John Holsen (Holsen [4]), where the orientation is given by directional cosines to each of the *S*-, *T*-, and *U*- *axis* relative to the *NEV* co-ordinate system, and where the matrix diagonal elements is found through a cubic equation. The necessary computation steps are given below

1) Computation of the co-variance matrix elements σ_{SS}^2, σ_{TT}^2, σ_{UU}^2

$$a = -(\sigma_{NN}^2 + \sigma_{EE}^2 + \sigma_{VV}^2) \qquad \{3.9\text{-}4\}$$

$$b = \sigma_{NN}^2\sigma_{EE}^2 + \sigma_{NN}^2\sigma_{VV}^2 + \sigma_{EE}^2\sigma_{VV}^2 - \sigma_{NE}^4 - \sigma_{NV}^4 - \sigma_{EV}^4 \qquad \{3.9\text{-}5\}$$

$$c = -\sigma_{NN}^2\sigma_{EE}^2\sigma_{VV}^2 - 2\sigma_{NE}^2\sigma_{NV}^2\sigma_{EV}^2 + \sigma_{EV}^4\sigma_{NN}^2 + \sigma_{NV}^4\sigma_{EE}^2 + \sigma_{NE}^4\sigma_{VV}^2 \qquad \{3.9\text{-}6\}$$

$$p = -\left(b - \frac{a^2}{3}\right). \qquad \{3.9\text{-}7\}$$

$$q = c - \frac{a}{27}(9b - 2a^2) \qquad \{3.9\text{-}8\}$$

$$v = \frac{1}{3}\arcsin\left(\frac{3q}{2p^2}\sqrt{3p}\right) \qquad \{3.9\text{-}9\}$$

$$\sigma_{SS}^2 = -\sqrt{p}\left(\cos(v) + \frac{\sqrt{3}}{3}\sin(v)\right) - \frac{a}{3} \qquad \{3.9\text{-}10\}$$

$$\sigma_{TT}^2 = \sqrt{p}\left(\cos(v) - \frac{\sqrt{3}}{3}\sin(v)\right) - \frac{a}{3} \qquad \{3.9\text{-}11\}$$

$$\sigma_{UU}^2 = \frac{2}{3}\sqrt{3p}\,\sin(v) - \frac{a}{3} \qquad \{3.9\text{-}12\}$$

2) Computation of the directional cosine elements $\cos(\alpha_S)$, $\cos(\beta_S)$, and $\cos(\gamma_S)$

$$L_S = \left(\sigma_{EE}^2 - \sigma_{SS}^2\right)\sigma_{NV}^2 - \sigma_{NE}^2\sigma_{EV}^2 \qquad \{3.9\text{-}13\}$$

$$M_S = \left(\sigma_{NN}^2 - \sigma_{SS}^2\right)\sigma_{EV}^2 - \sigma_{NE}^2\sigma_{NV}^2 \qquad \{3.9\text{-}14\}$$

$$N_S = -\left(\sigma_{NN}^2 - \sigma_{SS}^2\right)\left(\sigma_{EE}^2 - \sigma_{SS}^2\right) + \sigma_{NE}^4 \qquad \{3.9\text{-}15\}$$

$$\cos(\alpha_S) = \frac{L_S}{\sqrt{L_S^2+M_S^2+N_S^2}} \qquad \{3.9\text{-}16\}$$

$$\cos(\beta_S) = \frac{M_S}{\sqrt{L_S^2+M_S^2+N_S^2}} \qquad \{3.9\text{-}17\}$$

$$\cos(\gamma_S) = \frac{N_S}{\sqrt{L_S^2+M_S^2+N_S^2}} \qquad \{3.9\text{-}18\}$$

3) Computation of the directional cosine elements $\cos(\alpha_T)$, $\cos(\beta_T)$, and $\cos(\gamma_T)$

$$L_T = \left(\sigma_{EE}^2 - \sigma_{TT}^2\right)\sigma_{NV}^2 - \sigma_{NE}^2\sigma_{EV}^2 \qquad \{3.9\text{-}19\}$$

$$M_T = \left(\sigma_{NN}^2 - \sigma_{TT}^2\right)\sigma_{EV}^2 - \sigma_{NE}^2\sigma_{NV}^2 \qquad \{3.9\text{-}20\}$$

$$N_T = -\left(\sigma_{NN}^2 - \sigma_{TT}^2\right)\left(\sigma_{EE}^2 - \sigma_{TT}^2\right) + \sigma_{NE}^4 \qquad \{3.9\text{-}21\}$$

$$\cos(\alpha_T) = \frac{L_T}{\sqrt{L_T^2+M_T^2+N_T^2}} \qquad \{3.9\text{-}22\}$$

$$\cos(\beta_T) = \frac{M_T}{\sqrt{L_T^2+M_T^2+N_T^2}} \qquad \{3.9\text{-}23\}$$

$$\cos(\gamma_T) = \frac{N_T}{\sqrt{L_T^2+M_T^2+N_T^2}} \qquad \{3.9\text{-}24\}$$

4) Computation of the directional cosine elements $\cos(\alpha_U)$, $\cos(\beta_U)$, and $\cos(\gamma_U)$ by making use of the fact that the *S*-, *T*- and *U*- axis are forming a right handed co-ordinate system.

It is already shown that r/σ_R for any given direction, is standard normal distributed N(0,1). If s is a co-ordinate along the *S*- axis, t the co-ordinate along the *T*- axis, and u the co-ordinate along the *U*- axis; s/σ_S, t/σ_T, and u/σ_U must also be standard normal distributed N(0,1). It follows then directly that

$(\frac{s^2}{\sigma_{SS}^2}+\frac{t^2}{\sigma_{TT}^2}+\frac{u^2}{\sigma_{UU}^2})$ must be chi squared distributed with three degrees of freedom, χ_3^2.

This chi squared variable has similar form as the left side of an ellipsoidal equation. A three dimensional confidence interval can therefore be represented by an ellipsoid of the form

$$\frac{s^2}{\sigma_{SS}^2}+\frac{t^2}{\sigma_{TT}^2}+\frac{u^2}{\sigma_{UU}^2}=k^2 \qquad \{3.9\text{-}25\}$$

where $k\sigma_S$, $k\sigma_T$, and $k\sigma_U$ are the three semi axis of the ellipsoid.

The confidence coefficient (significance level) for this interval is

$$\alpha = P(\chi_3^2 < \chi_{1-\alpha,3}^2) \qquad \{3.9\text{-}26\}$$

Because χ_3^2 is expressed with k^2, we have

$$\alpha = P(k^2 < \chi_{1-\alpha,3}^2) \qquad \{3.9\text{-}27\}$$

α and k will become equal by setting

$$k = \sqrt{\chi_{1-\alpha,3}^2} \qquad \{3.9\text{-}28\}$$

$\chi_{1-\alpha,3}^2$ can be picked from a chi squared distribution table as long as the significance level α is settled.

This leads to the following table between k and α

k	α	Comments
1.0	0.199	Equals the use of 1σ measurement uncertainties inputs
1.538	0.50	50% confidence uncertainty ellipsoid
2.0	0.739	Equals the use of 2σ measurement uncertainties inputs
2.796	0.95	95% confidence uncertainty ellipsoid
3.0	0.971	Equals the use of 3σ measurement uncertainties inputs
4.033	0.999	99.9% confidence uncertainty ellipsoid

The table shows that the error ellipsoid term has no quantitative meaning without a stated confidence level. This fact has up to now not been given enough attention in the directional survey industry. A 95% confidence level for input uncertainty parameters are for example believed to give 95% ellipsoid without scaling. This is according to the table not the case. The ellipsoid will in this case have a significance level of 74%.

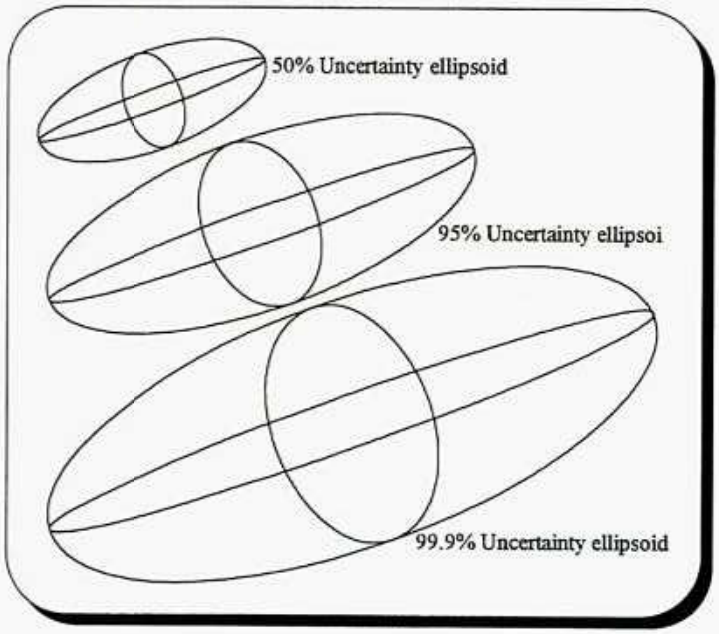

Figure 3.9-1 Examples on different uncertainty ellipsoids obtained from the same co-variance matrix

Equation *{3.9-1}* expresses, as already mentioned, the uncertainty in a given direction. This quantity is not equal to the radius of the uncertainty ellipsoid in the same direction. It has been a common misunderstanding within the directional surveying industry that this is the case. The uncertainty given by *{3.9-1}* will always be greater than the ellipsoid radius as long as the ellipsoid is not equal to a sphere, or the investigation direction is not equal to one of the three principal axis directions. For these special cases, the two quantities are equal. The validity of this can be examined by looking at the surface created by equation *{3.9-1}* for all possible directions in space. This surface is according to Holsen [4] given by the following equation

$$(s^2+t^2+u^2)^2-\left(s^2\sigma_{SS}^2+t^2\sigma_{TT}^2+u^2\sigma_{UU}^2\right)=0 \qquad \{3.9\text{-}29\}$$

This is the footprint spheroid of the error ellipsoid with $k = 1$, which is contained within the foot print spheroid for all other points than the six points where the principal axis meet the ellipsoid surface. These six points are common for both spheroids, and they will both have the same tangent plane. The footprint spheroid radius is grater than the ellipsoid radius for all other directions. The more elliptical the ellipsoid are, the bigger is the

difference. Maximum difference is found 45 degrees apart from the major ellipsoid axis. Examples on differences 45 degrees apart from the major axis in the minor / major plane are

Major axis	Minor axis	Foot print radius divided by ellipsoid radius
2	1	1.25
5	1	2.60
10	1	5.05

This example shows that the use of the error ellipsoid radius in connection with anti collision consideration etc., can lead to serious underestimation of the possibility for a collision. This is especially the case for magnetic measurements where the uncertainty ellipsoids tend to be very elliptical.

Directional drilling accuracy requirements are usually divided into two. A vertical tolerance, and lateral (horizontal) tolerance, which might be quite different from each other. To be able to compare the estimated directional surveying uncertainty with the required position tolerance, it is necessary to have the possibility to transform the content in the position co-variance matrix into uncertainties in any given plane. The position uncertainty in a plane is represented by a two dimensional squared symmetrical position co-variance matrix. The co-variance matrixes for planes parallel to the *NE*-, *NV*-, and *EV*-planes, can be found directly as the three two dimensional sub matrixes it is possible to extract from the Σ_X position co-variance matrix. Similarly it is possible to find two dimensional co-variance matrixes in planes parallel to the *ST*-, *SU*-, *TU*- planes by creating the three sub matrixes out of the Σ_S co-variance matrix. The uncertainty in other planes are not given directly by the Σ_X position co-variance matrix. The information has to be calculated out of the total position co-variance matrix content. This can be done by creating of an orthogonal PQ co-ordinate system in the desired plane, where the orientation of the P- and Q- axis in the NEV co-ordinate system are given by the directional cosines $\cos(\alpha_P)$, $\cos(\beta_P)$, $\cos(\gamma_P)$, $\cos(\alpha_Q)$, $\cos(\beta_Q)$, and $\cos(\gamma_Q)$. The uncertainty along the P- and Q- axis are then according to equation *{3.9-1}* given by

$$\sigma_{PP}^2 = \sigma_{NN}^2\cos^2(\alpha_P) + \sigma_{EE}^2\cos^2(\beta_P) + \sigma_{VV}^2\cos^2(\gamma_P) + 2\sigma_{NE}^2\cos(\alpha_P)\cos(\beta_P) + 2\sigma_{NV}^2\cos(\alpha_P)\cos(\gamma_P) + 2\sigma_{EV}^2\cos(\beta_P)\cos(\gamma_P) \quad \{3.9\text{-}30\}$$

$$\sigma_{QQ}^2 = \sigma_{NN}^2\cos^2(\alpha_Q) + \sigma_{EE}^2\cos^2(\beta_Q) + \sigma_{VV}^2\cos^2(\gamma_Q) + 2\sigma_{NE}^2\cos(\alpha_Q)\cos(\beta_Q) + 2\sigma_{NV}^2\cos(\alpha_Q)\cos(\gamma_Q) + 2\sigma_{EV}^2\cos(\beta_Q)\cos(\gamma_Q) \quad \{3.9\text{-}31\}$$

The P and Q correlation can be found by once again making use of the Tienstra rule

$$\begin{aligned}\sigma_{PQ}^2 = {} & \sigma_{NN}^2\cos(\alpha_P)\cos(\alpha_Q) + \sigma_{EE}^2\cos(\beta_P)\cos(\beta_Q) + \sigma_{VV}^2\cos(\gamma_P)\cos(\gamma_Q) \\ & + \sigma_{NE}^2(\cos(\alpha_P)\cos(\beta_Q) + \cos(\alpha_Q)\cos(\beta_P)) \\ & + \sigma_{NV}^2(\cos(\alpha_P)\cos(\gamma_Q) + \cos(\alpha_Q)\cos(\gamma_P)) \\ & + \sigma_{EV}^2(\cos(\beta_P)\cos(\gamma_Q) + \cos(\beta_Q)\cos(\gamma_P)) \end{aligned} \quad \{3.9\text{-}32\}$$

The uncertainty in the plane of investigation is now given by the following co-variance matrix

$$\Sigma_P = \begin{bmatrix} \sigma_{PP}^2 & \sigma_{PQ}^2 \\ \sigma_{PQ}^2 & \sigma_{QQ}^2 \end{bmatrix} \qquad \{3.9\text{-}33\}$$

This co-variance matrix contain all necessary information to create any uncertainty number related to this plane including a two dimensional confidence interval, which turn out to be the ellipse

$$\frac{s^2}{\sigma_{SS}^2} + \frac{t^2}{\sigma_{TT}^2} = k^2 \qquad \{3.9\text{-}34\}$$

ST is the orthogonal co-ordinate system in the investigation plane where there are no correlation between uncertainties along the two co-ordinate axis. σ_{SS}^2 and σ_{TT}^2 are the variance along the *S*- and *T*- axis, while *s* and *t* are the co-ordinates along the same two axis. σ_{SS}^2 and σ_{TT}^2 and the orientation elements of the *S*- and *T*- axis, can be found by using the same set of formulas as used in connection with the three dimensional ellipsoid ({3.9-4} - {3.9-24}). σ_{NN}^2, σ_{EE}^2, and σ_{NE}^2 used in these equations do then have to be substituted by σ_{PP}^2, $\sigma_{QQ}^2$and σ_{PQ}^2. σ_{VV}^2, σ_{NV}^2 and σ_{EV}^2 have to be set to zero. k^2 is because of the linear relationships described earlier in connection with the three dimensional error ellipsoid, a chi squared variable with two degrees of freedom.

$$k = \sqrt{\chi_{1-\alpha,2}^2} \qquad \{3.9\text{-}35\}$$

α is the confidence level of the uncertainty ellipse, and $\chi_{1-\alpha,2}^2$ can be picked from a chi squared distribution table.

This leads to the following table between *k* and α

k	α	Comments
1.0	0.394	Equals the use of 1σ measurement uncertainties inputs
1.177	0.50	50% confidence uncertainty ellipse
2.0	0.865	Equals the use of 2σ measurement uncertainties inputs
2.448	0.95	95% confidence uncertainty ellipse
3.0	0.989	Equals the use of 3σ measurement uncertainties inputs
3.717	0.999	99.9% confidence uncertainty ellipse

These numbers are different from the similar three dimensional ellipsoid numbers. It is therefore very important to distinguish between two and three dimensional problems when reporting uncertainties.

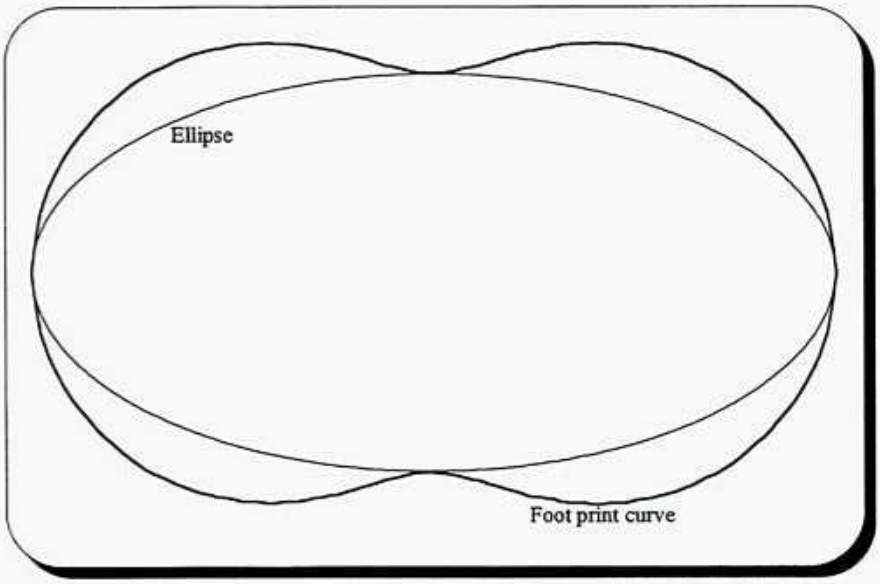

Figure 3.9-2 Example on the difference between a 2D uncertainty ellipse and the associated foot print curve

4 Error Propagation Theories

4.1 Published Theories

4.1.1 The Walstrom Model

The Walstrom error model (Walstrom [5]) is a random error propagation model dedicated for directional surveys. The model was first published in 1969, and its validity was questioned for many years. This because much greater directional errors are experienced in the field than predicted by the model. After the publication of the Wolff deWardt model (chapter 4.1.2), the Walstrom model has hardly never been used.

The reason for the problems with the Walstrom model, is that all directional survey error sources are treated as random between stations. According to a large number of publications, this is not the case. Major directional drilling error sources, like drill pipe stretch, magnetic declination etc., have significant systematic components. To treat systematic directional surveying errors as random will, as shown in chapter 3.1 and 3.3, lead to serious underestimation of the real position uncertainty for most wellbore trajectory designs. The Walstrom model should therefore not be used.

4.1.2 The Wolff deWardt Model

The Wolff deWardt model (Wolff [6]) is a systematic error propagation model developed by Shell KSEPL for use in connection with directional surveying. The model was first published in 1981, and is therefore based on the instruments present at that time, and on the simple vertical and slightly deviated wellbore profiles drilled in the early 80's. Since its publication, the Wolff deWardt model has become the most known and used error propagation model for directional surveys. It has in its basic published form (without major modifications) been regarded as an industry standard. The wide use of the published theory for many years without modifications is not according to Wolff and deWardt's recommendations. They are obviously looking at the published theory as a preliminary work, and are in their paper stating that further research is necessary.

In recent years, the validity of the Wolff deWardt model for modern instruments and wellbore profiles has been questioned in a couple of papers (Thorogood [7] and Lange [8]). No analysis or proof of model limitations are, however, presented. The model has therefore held its reputation. The following discussion will, however, show that the model in its basic form, as used in most of the surveying industry, should be improved or replaced by a more appropriate and accurate model.

The Wolff deWardt model is a pure systematic error propagation theory designed for one single survey in each wellbore. It has defined major error terms (size and weighting functions) for four different instrument classes; good (1) and poor (2) magnetic surveys,

and good (3) and poor (4) gyros surveys. The model seems to take it for granted, although not stated in the paper, that gross errors are not present in the survey data.

Based on the discussion in chapter 3, the following limitations to the basic Wolff deWardt theory are found

- Wolff and deWardt's assumption that random errors can be overlooked due to systematic error dominance is not always true. It is for example not valid for three dimensional wellbore trajectories (designer wells) where systematic errors are cancelled out due to azimuth changes of more than 90°. The Wolff deWardt theory may therefore underestimate the real position uncertainty (according to chapter 3.3, from 0 to 6m for a 4000m deep fish hook shaped wellbore surveyed with MWD).

- The Wolff deWardt weighting function *sin(I)* of the so called inclination error is not valid when bent subs are used. The *sin(I)* function is rooted in the gravity driven sag of the bottom hole assembly, and will lead to an underestimation of the position uncertainty due to collar misalignment for low inclination wellbores. A 0.5° systematic bent sub induced misalignment will for a 4000m deep and 15° inclined wellbore result in a position uncertainty of 35m. The use of the *sin(I)* function will indicate an uncertainty of 9m, which is only 1/4 of the real uncertainty.

- Major magnetic- and gyro error terms have a well known latitude / longitude dependency (see chapter 5 and 6). Chapter 5.1.1.5 is showing that magnetic measurement solutions have a singularity at the magnetic poles. Chapter 6.1.1.5 is further showing that north seeking gyro measurements have an accuracy which is proportional to *1/cos(latitude)*. These and other latitude / longitude dependencies are not included in the Wolff deWardt weighting functions. Chapter 3.7 is showing that accurate weighting functions are essential for a good result. The validity of the Wolff deWardt model is limited to the North Sea where the reference data where collected.

- The uncertainty associated with modern instruments like north seeking gyros, high accuracy continuous gyros and inertial systems (see chapter 6 and 8) can not be described by the limited numbers of error terms and the simple gyro weighting function of *1/cos(I)*, given by Wolff and deWardt. Modern continuous gyro instruments are designed to be run from vertical to horizontal (chapter 6.1.1.6), and they do not suffer from the horizontal wellbore singularity given in the Wolff deWardt weighting function. The Wolff deWardt model will give a recommendation on not to use these instruments in high inclined wellbores where they often are the most cost effective high accuracy alternative.

- Wolff and deWardt are in their model assuming a linear growth in the depth uncertainty with respect to the measured depth. This simplification to the real world is probably too large to give a realistic picture of the actual depth uncertainty (see chapter 7). Depth errors have a far more complicated nature. They are because of stretch- and temperature effects etc. a function of geometry and measurement technique. The MWD depth uncertainty for a 4000m deep vertical wellbore

computed with Wolff and deWardt's 0.1% proportionality factor is for example only 1/2 of what is obtained with the detailed depth uncertainty equations given in chapter 7.2.

- The Wolff deWardt theory is designed as a one survey per wellbore error propagation theory. This means that it is not applicable for extended reach- and designer wells, where a combination of many surveys is the standard. To come around this problem, some of the model users (for example Sysdrill Ltd.) have made modifications to incorporate combined survey analysis into the model. These modifications have not been published. Most of them seem, however, to randomise systematic uncertainties at survey tie points. It was in chapter 3.5 shown that this may lead to serious under estimation of the actual uncertainty. The magnetic declination error is according to chapter 5.2.1.1 a bias, which is systematic for all consecutive MWD surveys. A division of a 4000m long horizontal wellbore into four consecutive MWD sections will underestimate the position uncertainty caused by a declination uncertainty of 1.5° with 50m (100%).

- The Wolff deWardt model has because of the single survey per wellbore design, no possibility to estimate accuracy improvements related to the redundancy in multiple surveys and overlapping sections (see chapter 3.6). This has led to a practice of picking what is believed to be the best survey instead of finding the optimal solution.

- Wolff and deWardt have not given any confidence level for their estimated error parameters, which are said to be worst case figures. Worst case figures are, however, non converging statistical figures which are difficult to estimate. They are for example dependent on which quality control procedures that acctually are in use, and on how many gross errors that can be identified and corrected for. This has lead to confusion, and new instruments have been added to the model without securing the same confidence level as used by Wolff and deWardt in their study. Examples on totally different Wolff deWardt uncertainty figures (valid for the same instrument and running conditions, see figure 4.1.2-1) used in different assets within the same company are known.

	Org.1	Org.2	Org.3	Org.4
Error 1	0.35°	0.003°	0.35°	0.003°
Error 2	0.175°	0.03°	0.175°	0.03°
Error 3	0°	0°	0.175°	0.05°
Error 4	0.5°	0.5°	0.05°	0.1°

Figure 4.1.2-1 Examples on different Wolff deWardt uncertainty parameters used for the same instrument by three different assets within the same oil company and by the surveying company.

- Wolff and deWardt are, in addition to the already mentioned maximum errors, using an uncertainty ellipsoid scaling factor of one in their paper. This has led to unknown

confidence levels for wellbore position uncertainty figures obtained with the Wolff deWardt model. A consequence of this is the common misunderstanding that 95% (2σ) uncertainty inputs also are giving a 95% uncertainty ellipsoid. This is according to chapter 3.9 not the case. It is giving a 74% ellipsoid, which has 40% smaller axis than the real 95% ellipsoid.

The listed limitations show that the Wolff deWardt model, as it appears in the paper (Wolff [6]) or in later unpublished improvements, today only has a limited value as tool for wellbore position uncertainty studies. This is specially the case for the offshore environment, where collision avoidance in large wellbore clusters and targeting far away from the platform, are the major tasks.

4.1.3 The Instrument Performance Model

The Instrument Performance Model (IPM) (Thorogood [7]) is a combined random-, systematic- and bias error propagation theory developed by BP. Systematic errors are in this model divided into two parts. One part which is random between surveys, and one other which is systematic between surveys. The latter one is called bias, and is given a separate handling.

The model is probably the most comprehensive of all published directional surveying error propagation theories. It was presented in 1988 as an alternative to the Wolff deWardt model, which according to Thorogood's paper has some limitations with respect to modern instruments. The IPM has up to now only been used within BP.

The IPM model is, as already stated, a combined random-, systematic- and bias error propagation theory. The limitations that according to chapter 3.1 and 3.3 apply to pure random- or pure systematic models are therefore not any problem for the IPM model. This conclusion is drawn under the assumption that sign dependent systematic error terms, like the drill string magnetisation etc., are taken care of. The importance of this is not stated in the IPM paper, and is therefore a potential danger (see example 3 in chapter 3.3).

It can be questioned whether the introduction of the new bias term is beneficial or not. Biases are systematic between surveys. They do therefore have a gross error nature. The question is therefore: is it beneficial to make use of the bias term, or is it better to correct the measurements for bias effects before the position calculation is performed. The latter alternative yields uncertainty estimates which easily can be communicated through well known statistical quantities (the position co-variance matrix, the error ellipse or the error ellipsoid), while the first alternative is more difficult to communicate. Here it is necessary with a translation of the uncertainty quantity with respect to the computed wellbore position in addition to the uncertainty itself (see figure 4.1.3-1). Personnel without statistical knowledge can have problem understanding uncertainty reports containing both statistical values and translations without the help of a dedicated graphical presentation tool.

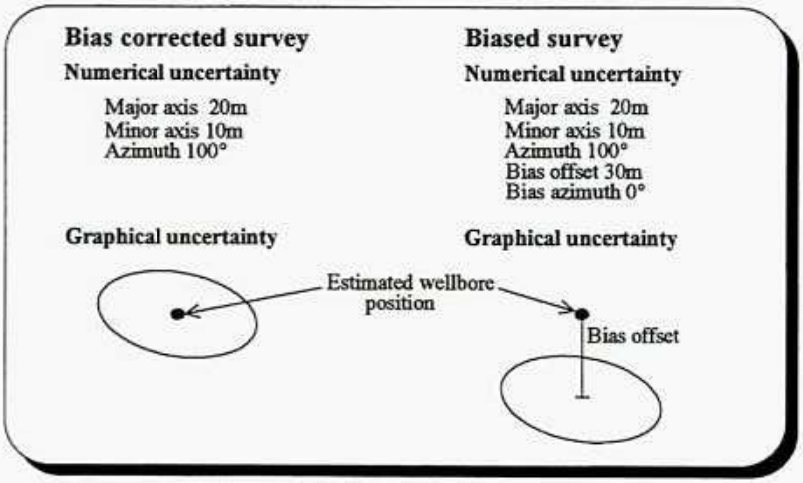

Figure 4.1.3-1 Examples on numerical and graphical presentation of biased and corrected uncertainties.

Thorogood is, in his paper, introducing a new concept for handling of depth errors. He does not evaluate the position uncertainty at physical measurement stations, but at theoretical stations with depths (as established through petrophysical logging) like the measured depths. The measurement will then be taken at points differing more or less from the defined survey points. The depth errors will in this case be transformed into additional inclination- and azimuth errors due to a change in curvature over the distance between the physical measurement stations and the theoretical stations. It can be shown that the "true depth" position uncertainty for all practical purposes is equal to the survey station uncertainty if the integrated along hole depth component is removed.

It is, according to the discussion in chapter 5 and 6, usually very little correlation between inclination- and azimuth measurements in traditional directional surveying. A transformation of the depth error into the two angular errors, the inclination- and the azimuth error, means a great change to this. It will then be a strong correlation, which has to be taken into consideration in the position uncertainty calculation if estimation errors are to be avoided. The IPM paper does not give any instruction on how to handle this problem. The model will further, because of the correlation introduced by depth error conversions, be difficult to modify and use in an adjustment theory to improve accuracy in redundant survey programs (see chapter 3.6). Mathematical expressions will become more complicated, and correlation coefficients calculations will become a complicating factor. These correlation coefficients will be dependent on wellbore geometry and relative depth accuracy between the different surveys.

The IPM model is not designed for inertial systems, which already are on the market. The final outputs from an inertial system is wellbore co-ordinates and not angular measurements. Wellbore co-ordinates have to be transformed into true depth, inclination and azimuth, if the IPM model is to be used on inertial data. This process will introduce additional errors (alignment and model errors) into the analysis, and should be avoided. The same problem will also be relevant for eventually future seismic positioning systems.

4.2 Recommendations for a new Theory

None of the three published directional surveying error propagation theories are found to be complex and accurate enough as planning tools for today's instruments and complicated wellbore profiles. The limitations are both related to accuracy and to the ability to design the most cost effective survey programs. A continued use of the Wolff deWardt theory, as implemented in most of the industry, and the Walstrom theory, if still used, may lead to underestimation of the real wellbore position uncertainty. This might in its worst consequence lead to wellbore intersections or loss of targets. Organisations still using the Wolff deWardt model are therefore advised to find a substitute. The Instrument Performance Model is here rated highest of the three published theories. But there are also serious limitations with this theory, which make it difficult to recommend it as an optimal replacement for the other two. Instead it is recommended to develop a completely new directional surveying error propagation theory. The new theory should be an evolution of the Wolff deWardt theory to reduce confusion and resistance within the drilling industry. It should nevertheless be comprehensive enough to give a realistic picture of the position uncertainty associated with wellbore surveying with present and future instruments and techniques. It should be designed to meet the following requirements

- Prediction of wellbore position uncertainties for standalone surveys with any tool configurations based on historical tool performance.
- Prediction of wellbore position uncertainties based on historical tool performance for any survey programs consisting of more than one consecutive section surveys.
- Prediction of wellbore position uncertainties based on historical tool performance for redundant survey programs with overlapping wellbore sections and multiple surveys. The possibility to or not to estimate systematic effects must be taking into consideration.
- Final wellbore positions error estimation based on least squares estimation of redundant survey programs. Unresolved systematic effects have to be included in the error estimation based on historical data.

It is important that a new error propagation model is followed by standard procedures on how to derive weighting functions and tool uncertainty parameters for new instruments and running procedures. This to secure the validity of the model for some years, and to avoid misuse similar to what have been seen with the Wolff deWardt theory.

A new expanded Wolff deWardt theory is currently under development by the "Industry Steering Committee on Wellbore Survey Accuracy" (Hugh Williamson BP is chairman). This new method will be a simplification of the basic theory presented in chapter 3. It will give results that are very near to what eventually would have been obtained by applying the basic theory presented here. The new theory will be the combination of the work of four different persons / groups. This study is one of these. Most weighting functions presented in this report will be used in this new theory. The steering committee work is not yet completed. A first version of the mathematical theory is, however, finished. It is currently under implementation in a major well planning software. This new method has to be accompanied by adequate quality control procedures and realistic uncertainty figures / predictions for all relevant error sources.

5 Errors in Electronic Magnetic Tools

Electronic magnetic tools are usually equipped with six sensors. Three accelerometers which are used to find inclination (I) and toolface (τ), and three fluxgate magnetometers which together with the accelerometers are used to find the magnetic azimuth (A_m). The inclination, azimuth and toolface are therefore partly correlated, and it is necessary to split the three resultant angular uncertainties into uncorrelated components to fit into a new expanded Wolff deWardt error propagation theory, which is recommended in chapter 4.2.

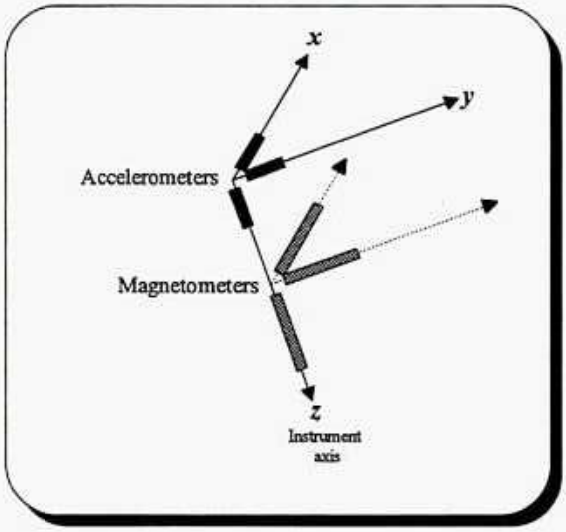

Figure 5-1 Example on sensor mounting in electronic magnetic tools

5.1 Tool Uncertainties

5.1.1 Sensor Uncertainties

It is, based on documentation given to the Industry Steering Committee on Wellbore Survey Accuracy (ISCWSA) by major survey companies, concluded that there are three principal types of sensor errors in electronic magnetic instruments. It is sensor reading errors, misalignments of the sensors within the instrument, and errors originating from instabilities in the electronics.

Sensor dependent errors are usually systematic within a survey as long as the instrument is working within specification and is undamaged. They will also be systematic between surveys if the same instrument is used in all surveys. This is the case even between different wellbores. Sensor errors will then be random between surveys, if different instruments are used in different surveys, or if the instrument has been recalibrated between surveys.

5.1.1.1 Accelerometers

Accelerometers are, according to William F. Lee at Allied Signal in Redmond, Washington (a major manufacturer), non linear sensors specified to work within given environmental limits (temperature, pressure, and vibrations), and calibrated to a pre defined accuracy level. Outside these environmental limits, the measurements are not valid. The same conclusion should be applied if calibration control measures are not met. As long as an instrument is operating as specified, the accelerometer error will consist of four independent components, a random component, a bias, a linear scale factor error, and a second order scale factor error. The second order scale factor error is according to Allied Signal not significant compared to the other three uncertainty terms unless very large accelerations are present (the manufacturing specification for the accelerometer QA-T150 <= 0.000048/G). Accelerometers used in directional surveying are only exposed to small accelerations during measurements. The second order term can therefore be neglected in uncertainty studies. The random uncertainty is usually small enough to be without significance in the wellbore position uncertainty compared to the bias and the linear scale factor uncertainty because of its favourable error propagation characteristics. It can therefore also be neglected in position uncertainty studies.

The two significant error terms, the bias (specification for QA-T150 η_a<= 0.0006G) and the linear scale factor error (specification for QA-T150 υ_a<= 0.0006), will usually be modelled and corrected for in a calibration process. The mechanical properties of accelerometers are, however, changing with time. This is resulting in accelerometer bias and scale factor errors even for calibrated instruments. To secure that the accuracy is held within given limits, accelerometers are recalibrated at regular intervals. The bias and scale factor uncertainties can then be defined as the standard deviations in bias and scale factor calibration updates at consecutive calibrations. Different time spans between consecutive calibrations, and a large number of identical instruments, should be used.

The local gravity ($9.78 <= G <= 9.83 m/s^2$) is usually not known as precise at a measurement station as at the calibration station. This give rise to an additional scale factor uncertainty, which is correlated between all accelerometers, and therefore a systematic error source for an entire field. This scale factor uncertainty is usually small, and is given by

$$d\upsilon_G = \frac{dG}{G} \qquad \{5.1.1.1\text{-}1\}$$

where G is the local gravity, and dG its uncertainty.

The uncertainty in an accelerometer measurement can therefore be divided into three independent parts, the bias uncertainty ($d\eta_a$), the linear scale factor uncertainty ($d\upsilon_a$) multiplied by the measurement itself, and the linear gravity induced scale factor uncertainty ($d\upsilon_G$) multiplied by the measurement itself.

Accelerometer errors are usually uncorrelated with respect to each other. The only expectation is for instruments where all accelerometer measurements are fed through the same analogue / digital converter. They are, however, rare, and will not be covered here.

Accelerometer bias and scale factor uncertainties can therefore be regarded as random between different instruments. They will because of this be systematic within surveys as long as the same instrument is in use. The gravity induced scale factor uncertainty is, as already mentioned, always systematic at the same location.

Electronic magnetic instruments are usually equipped with three equal and orthogonal accelerometers, each mounted along one of the principal axis. The nine independent uncertainties associated with the three accelerometer measurements (dg_{x1}, dg_{x2}, dg_{x3}, dg_{y1}, dg_{y2}, dg_{y3}, dg_{z1}, dg_{z2}, and dg_{z3}) can then be expressed as

$$dg_{x1} = d\eta_a \qquad \{5.1.1.1\text{-}2\}$$
$$dg_{x2} = g_x d\upsilon_a \approx -G \sin I \sin \tau d\upsilon_a \qquad \{5.1.1.1\text{-}3\}$$
$$dg_{x3} = g_{x3} d\upsilon_G \approx -G \sin I \sin \tau d\upsilon_G \qquad \{5.1.1.1\text{-}4\}$$

$$dg_{y1} = d\eta_a \qquad \{5.1.1.1\text{-}5\}$$
$$dg_{y2} = g_y d\upsilon_a \approx -G \sin I \cos \tau d\upsilon_a \qquad \{5.1.1.1\text{-}6\}$$
$$dg_{y3} = g_y d\upsilon_G \approx -G \sin I \cos \tau d\upsilon_G \qquad \{5.1.1.1\text{-}7\}$$

$$dg_{z1} = d\eta_a \qquad \{5.1.1.1\text{-}8\}$$
$$dg_{z2} = g_z d\upsilon_a \approx G \cos I d\upsilon_a \qquad \{5.1.1.1\text{-}9\}$$
$$dg_{z3} = g_z d\upsilon_G \approx G \cos I d\upsilon_G \qquad \{5.1.1.1\text{-}10\}$$

where G is the local gravity, I the inclination and τ the toolface.

Because of the presence of inclination and toolface dependent trigonometric functions in the scale factor equations, the accelerometer uncertainties should be kept in this form, and not lumped together to three resultant accelerometer errors. This is to secure against loss of sign information in the co-variance squaring process.

5.1.1.2 Gravity Inclination

Standard Three Accelerometer Systems

The following equations can be used to transform the accelerometer measurements into inclination measurements (I)

$$I = \arctan \frac{\sqrt{g_x^2 + g_y^2}}{g_z} \qquad \{5.1.1.2\text{-}1\}$$

Where g_x, g_y, and g_z are the three right handed orthogonal accelerometer measurements with g_z aligned along the wellbore axis.

Inclination uncertainty components (dI_i) due to the accelerometer uncertainties given in equation *{5.1.1.1-2}* to *{5.1.1.1-10}*, are then

$$dI_1 = \frac{\partial I}{\partial g_x} dg_{x1} = -\frac{\cos I \sin \tau}{G} dg_{x1} \qquad \{5.1.1.2\text{-}2\}$$

$$dI_2 = \frac{\partial I}{\partial g_x} dg_{x2} = -\frac{\cos I \sin \tau}{G} dg_{x2} \qquad \{5.1.1.2\text{-}3\}$$

$$dI_3 = \frac{\partial I}{\partial g_y} dg_{y1} = -\frac{\cos I \cos \tau}{G} dg_{y1} \qquad \{5.1.1.2\text{-}4\}$$

$$dI_4 = \frac{\partial I}{\partial g_y} dg_{y2} = -\frac{\cos I \cos \tau}{G} dg_{y2} \qquad \{5.1.1.2\text{-}5\}$$

$$dI_5 = \frac{\partial I}{\partial g_z} dg_{z1} = -\frac{\sin I}{G} dg_{z1} \qquad \{5.1.1.2\text{-}6\}$$

$$dI_6 = \frac{\partial I}{\partial g_z} dg_{z2} = -\frac{\sin I}{G} dg_{z2} \qquad \{5.1.1.2\text{-}7\}$$

Three accelerometer systems are not sensitive to gravity induced scale factor errors. They are therefore not included in these equations.

Three Accelerometer Systems with Axial Gravity Correction

Occasionally, there has been a discussion on whether a *z*- accelerometer correction should be applied to stationary three accelerometer magnetic measurements or not. This correction is developed for continuos gyro system suffering from large axial accelerations, and is based on estimation of the *z*- accelerometer measurement by the *x*- and *y*-accelerometer readings and a priori knowledge of the local gravity. The following equation can be used in this estimation

$$g_z = \pm\sqrt{G^2 - \left(g_x^2 + g_y^2\right)} \qquad \{5.1.1.2\text{-}8\}$$

which yields the following inclination equation

$$I = \arctan \frac{\sqrt{g_x^2+g_y^2}}{\sqrt{G^2-\left(g_x^2+g_y^2\right)}} = \arcsin \frac{\sqrt{g_x^2+g_y^2}}{G} \qquad \{5.1.1.2\text{-}9\}$$

This equation does not distinguish between *I* and *180°-I*. Additional information is necessary to pick the right inclination. This information is usually obtained through knowledge about the drilling performance higher up in the wellbore. Past drilling history is, however, not always possible to use. For example when drilling horizontal wellbores.

The inclination uncertainty components due to accelerometer uncertainties (equations *{5.1.1.1-2}* to *{5.1.1.1-7}*) are then

$$dI_1 = \frac{\partial I}{\partial g_x} dg_{x1} = -\frac{\sin \tau}{G \cos I} dg_{x1} \qquad \{5.1.1.2\text{-}10\}$$

$$dI_2 = \frac{\partial I}{\partial g_x} dg_{x2} = -\frac{\sin \tau}{G \cos I} dg_{x2} \qquad \{5.1.1.2\text{-}11\}$$

$$dI_3 = \frac{\partial I}{\partial g_y} dg_{y1} = -\frac{\cos \tau}{G \cos I} dg_{y1} \qquad \{5.1.1.2\text{-}12\}$$

$$dI_4 = \frac{\partial I}{\partial g_y} dg_{y2} = -\frac{\cos \tau}{G \cos I} dg_{y2} \qquad \{5.1.1.2\text{-}13\}$$

$$dI_7 = \frac{\partial I}{\partial g_x} dg_{x3} + \frac{\partial I}{\partial g_y} dg_{y3} = -\frac{\sin I}{G \cos I} dG \qquad \{5.1.1.2\text{-}14\}$$

The inclination uncertainty is according to these equations proportional to *1/cosI* , which lead to a rapid deterioration in inclination accuracy as the well approaches the horizontal. Stationary systems utilising the axial correction method should because of this only be used with great cause.

5.1.1.3 Gravity Toolface

The following equations can be used to transform the accelerometer outputs into highside toolface (τ)

$$\tau = \arctan\frac{g_x}{g_y} \qquad \{5.1.1.3\text{-}1\}$$

g_x and g_y are the two orthogonal accelerometer measurements made in the high-side toolface plane (the plane normal to the *z*- axis).

Toolface measurements do only have secondary effects on the wellbore position calculation. The toolface is not used directly in the minimum curvature calculation, only in intermediate azimuth calculations. Its error propagation nature is therefore of less importance than the inclination and azimuth error propagation, and its uncertainty components can be lumped together to reduce complexity. The lumped uncertainty in a highside toolface ($d\tau$) measurement due to accelerometer uncertainties (equations *{5.1.1.1-2}* to *{5.1.1.1-7}*) is then given by

$$\begin{aligned} d\tau &= \sqrt{\left(\frac{\partial\tau}{\partial g_x}\right)^2\left(dg_{x1}^2 + dg_{x2}^2\right) + \left(\frac{\partial\tau}{\partial g_y}\right)^2\left(dg_{y1}^2 + dg_{y2}^2\right) + \left(\frac{\partial\tau}{\partial g_x}dg_{x3} + \frac{\partial\tau}{\partial g_y}dg_{y3}\right)^2} \\ &= \sqrt{\frac{d\eta_a^2}{G\sin I} + 2\sin^2\tau\cos^2\tau d\upsilon_a^2} \end{aligned} \qquad \{5.1.1.3\text{-}2\}$$

It follows directly from this equation that vertical wellbores will have a infinite gravity based toolface uncertainty. This is in accordance with the definition of the highside toolface which is undefined in the horizontal plane.

5.1.1.4 Magnetometers

Similar to accelerometers, magnetometers are specified to work within given environmental limits (temperature, pressure, shocks, and vibrations), and calibrated to a predefined accuracy level. Outside these environmental limits, the measurements are not valid. The same conclusion should be applied if calibration control measures are not met. The magnetometer uncertainty can, according to Tensor in Austin, Texas (a major manufacturer), be represented with three independent components, a random component, a systematic bias, and a systematic resultant scale factor error. The random component can, like in the accelerometer case, be neglected in position uncertainty calculations due to favourable error propagation.

Page 54 Equation *{5.1.1.3-2}* second line should be $\approx \sqrt{\frac{d\eta_a^2}{G^2\sin^2 I} + 2\sin^2\tau\cos^2\tau d\upsilon_a^2}$

The local magnetic field is usually not known with the same accuracy at a measurement station as at a calibration station. This give rise to an additional scale factor uncertainty, which is correlated between different magnetometers. This scale factor uncertainty is given by

$$d\upsilon_B = \frac{dB}{B} \qquad \{5.1.1.4\text{-}1\}$$

where B the local magnetic field strength, and dB its uncertainty. The uncertainty in an magnetometer measurement can therefore be divided into three significant independent uncertainties, the bias uncertainty ($d\eta_m$), the linear scale factor uncertainty ($d\upsilon_m$) multiplied by the measurement itself, and the linear field strength induced scale factor uncertainty ($d\upsilon_B$) multiplied by the measurement itself.

Magnetometers will usually be uncorrelated with respect to each other. The bias uncertainty can therefore be regarded as a random error source between different magnetometers. This gives a systematic between stations uncertainty as long as the same instrument is in use. The same conclusion is valid for the sensor scale factor uncertainty, while the field induced scale factor uncertainty will have a time and location dependent propagation nature.

Electronic magnetic instruments are equipped with three equal and orthogonal magnetometers, each mounted along one of the principal axis. The nine independent magnetometer uncertainties (db_{x1}, db_{x2}, db_{x3}, db_{y1}, db_{y2}, db_{y3}, db_{z1}, db_{z2} and db_{z3}) can then be expressed as

$$db_{x1} = d\eta_m \qquad \{5.1.1.4\text{-}2\}$$
$$db_{x2} = b_x d\upsilon_m \qquad \{5.1.1.4\text{-}3\}$$
$$db_{x3} = b_x d\upsilon_B \qquad \{5.1.1.4\text{-}4\}$$
$$b_x \approx B(\cos\Theta\cos I\cos A_m\sin\tau - \sin\Theta\sin I\sin\tau + \cos\Theta\sin A_m\cos\tau) \qquad \{5.1.1.4\text{-}5\}$$

$$db_{y1} = d\eta_m \qquad \{5.1.1.4\text{-}6\}$$
$$db_{y2} = b_y d\upsilon_m \qquad \{5.1.1.4\text{-}7\}$$
$$db_{y3} = b_y d\upsilon_B \qquad \{5.1.1.4\text{-}8\}$$
$$b_y \approx B(\cos\Theta\cos I\cos A_m\cos\tau - \sin\Theta\sin I\cos\tau - \cos\Theta\sin A_m\sin\tau) \qquad \{5.1.1.4\text{-}9\}$$

$$db_{z1} = d\eta_m \qquad \{5.1.1.4\text{-}10\}$$
$$db_{z2} = b_z d\upsilon_m \qquad \{5.1.1.4\text{-}11\}$$
$$db_{z3} = b_z d\upsilon_B \qquad \{5.1.1.4\text{-}12\}$$
$$b_z \approx B(\cos\Theta\sin I\cos A_m + \sin\Theta\cos I) \qquad \{5.1.1.4\text{-}13\}$$

where B is the local earth magnetic field strength, A_m the magnetic azimuth, I the inclination, τ the toolface, and Θ the magnetic dip angle.

Magnetometer uncertainties should be kept in this form, and not lumped together to three resultant magnetometer errors, because of the presence of inclination-, azimuth-, toolface-, and magnetic dip angle dependent trigonometric functions in the scale factor equations.

5.1.1.5 *Magnetic Azimuth*

The following equation can be used to transform the magnetometer measurements into an azimuth (A)

$$A = \delta + A_m = \delta + \arctan \frac{b_x \cos\tau - b_y \sin\tau}{\cos I(b_x \sin\tau + b_y \cos\tau) + b_z \sin I} \qquad \{5.1.1.5\text{-}1\}$$

where δ is the magnetic declination and A_m the magnetic azimuth. b_x, b_y, and b_z are the magnetometer measurements along the principal tool axis. The inclination (I) and toolface (τ) are, as described earlier, determined through accelerometer measurements. Errors in the accelerometer measurements will because of this also have influence on the magnetic azimuth accuracy.

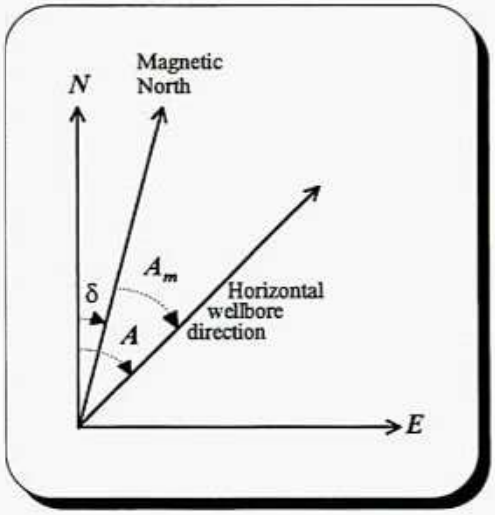

Figure 5.1.1.5-1 Definition of magnetic azimuth (A_m)

The azimuth uncertainty components (dA_i) due to magnetometer uncertainties given in equation *{5.1.1.4-2}* to *{5.1.1.4-13}*, and sensor dependent uncertainties in the inclination (dI_s) and toolface ($d\tau$), are then given by

$$dA_1 = \frac{\partial A_m}{\partial b_x} db_{x1} = \frac{\cos\tau\cos A_m - \cos I \sin\tau \sin A_m}{B\cos\Theta} db_{x1} \qquad \{5.1.1.5\text{-}2\}$$

$$dA_2 = \frac{\partial A_m}{\partial b_x} db_{x2} = \frac{\cos\tau\cos A_m - \cos I \sin\tau \sin A_m}{B\cos\Theta} db_{x2} \qquad \{5.1.1.5\text{-}3\}$$

$$dA_3 = \frac{\partial A_m}{\partial b_y} db_{y1} = -\frac{\sin\tau\cos A_m + \cos I \cos\tau \sin A_m}{B\cos\Theta} db_{y1} \qquad \{5.1.1.5\text{-}4\}$$

$$dA_4 = \frac{\partial A_m}{\partial b_y} db_{y2} = -\frac{\sin\tau\cos A_m + \cos I \cos\tau \sin A_m}{B\cos\Theta} db_{y2} \qquad \{5.1.1.5\text{-}5\}$$

$$dA_5 = \frac{\partial A_m}{\partial b_z} db_{z1} = -\frac{\sin I \sin A_m}{B \cos \Theta} db_{z1} \qquad \{5.1.1.5\text{-}6\}$$

$$dA_6 = \frac{\partial A_m}{\partial b_z} db_{z2} = -\frac{\sin I \sin A_m}{B \cos \Theta} db_{z2} \qquad \{5.1.1.5\text{-}7\}$$

$$dA_7 = \frac{\partial A_m}{\partial I} dI_s + \frac{\partial A_m}{\partial \tau} d\tau = -\frac{\sin \Theta \sin A_m}{\cos \Theta} dI_s + \frac{\sin \Theta \sin I \cos A_m - \cos \Theta \cos I}{\cos \Theta} d\tau \qquad \{5.1.1.5\text{-}8\}$$

where B is the local earth magnetic field strength and Θ the local magnetic dip angle. The toolface uncertainty ($d\tau$) is given by equation *{5.1.1.3-2}*, and the inclination uncertainty (dI_s) is the random sum of all significant sensor dependent inclination uncertainty components at the measurement station given by

$$dI_s = \sqrt{\Sigma_{i=1}^{7}\left(dI_i^2\right)} \qquad \{5.1.1.5\text{-}9\}$$

where dI_i is given by equations *{5.1.1.2-2}* to *{5.1.1.2-7}* (*{5.1.1.2-10}* to *{5.1.1.2-14}* if gravity correction is used). The effect of the inclination and the toolface uncertainties on the magnetic azimuth are combined into just one uncertainty term because of the high correlation that exists between these two terms (determined through common accelerometer measurements. db_{x3}, db_{y3} and db_{z3} are not found in equations *{5.1.1.5-2}* to *{5.1.1.5-8}*. This shows that three magnetometer systems are not sensitive to the accuracy of the local magnetic field strength estimate.

Equations *{5.1.1.5-2}* to *{5.1.1.5-8}* shows that the azimuth uncertainty tends towards infinity as the dip angle approaches the vertical. This is in agreement with no magnetic azimuth definition at the magnetic poles. The azimuth uncertainty do also, as expected, tend towards infinity for vertical wells. The highside toolface uncertainty in *{5.1.1.5-8}* reach infinity when vertical, and this is propagated into the azimuth uncertainty.

The inclination and toolface uncertainties used in equation *{5.1.1.5-8}* are originating from the same accelerometer errors, and are therefore correlated. A full correlation is assumed in this derivation. This will, however, not always be true. Estimation errors can be avoided by introduction of inclination- and toolface correlation coefficients, or by splitting the dA_7 term into six uncorrelated components. These uncertainty components will usually be systematic within and random between surveys, and are given by

$$dA_{7\_1} = \frac{\partial A_m}{\partial g_x} dg_{x1} = \frac{\sin \Theta \sin I(\sin \tau \cos I \sin A_m - \cos \tau \cos A_m) + \cos \Theta \cos \tau \cos I}{G \cos \Theta \sin I} dg_{x1} \qquad \{5.1.1.5\text{-}10\}$$

$$dA_{7\_2} = \frac{\partial A_m}{\partial g_x} dg_{x2} = \frac{\sin \Theta \sin I(\sin \tau \cos I \sin A_m - \cos \tau \cos A_m) + \cos \Theta \cos \tau \cos I}{G \cos \Theta \sin I} dg_{x2} \qquad \{5.1.1.5\text{-}11\}$$

$$dA_{7\_3} = \frac{\partial A_m}{\partial g_y} dg_{y1} = \frac{\sin \Theta \sin I(\cos \tau \cos I \sin A_m + \sin \tau \cos A_m) - \cos \Theta \sin \tau \cos I}{G \cos \Theta \sin I} dg_{y1} \qquad \{5.1.1.5\text{-}12\}$$

$$dA_{7\_4} = \frac{\partial A_m}{\partial g_y} dg_{y2} = \frac{\sin \Theta \sin I(\cos \tau \cos I \sin A_m + \sin \tau \cos A_m) - \cos \Theta \sin \tau \cos I}{G \cos \Theta \sin I} dg_{y2} \qquad \{5.1.1.5\text{-}13\}$$

$$dA_{7\_5} = \frac{\partial A_m}{\partial g_z} dg_{z1} = \frac{\sin \Theta \sin I \sin A_m}{G \cos \Theta} dg_{z1} \qquad \{5.1.1.5\text{-}14\}$$

$$dA_{7\_6} = \frac{\partial A_m}{\partial g_z} dg_{z2} = \frac{\sin \Theta \sin I \sin A_m}{G \cos \Theta} dg_{z2} \qquad \{5.1.1.5\text{-}15\}$$

Accelerometer uncertainties (dg_{x1}, dg_{x2}, dg_{y1}, dg_{y2}, dg_{z1} and dg_{z2}) are given by equation *{5.1.1.1-2}* to *{5.1.1.1-10}*.

Inclination and azimuth uncertainty components originating from the same accelerometer error source are correlated with each other, and should be treated as correlated errors in the position co-variance matrix calculation. The following uncertainty components are fully correlated in magnetic surveys

- dI_1 and dA_{7_1}
- dI_2 and dA_{7_2}
- dI_3 and dA_{7_3}
- dI_4 and dA_{7_4}
- dI_5 and dA_{7_5}
- dI_6 and dA_{7_6}

5.1.1.6 Sensor Misalignments

The sensor uncertainty equations presented in the previous chapter, are developed under the assumption that the principal instrument axis (x, y and z) are forming a perfect orthogonal co-ordinate system. This is usually not the case. Instrument axis are defined by the sensor mounting, and to mount small sensors perfectly orthogonal or parallel is nearly impossible. There will always be small misalignments left after a calibration. It will be shown that the resultant effect of this kind of errors usually are small, and that it is not necessary to include sensor misalignments in the inclination- (dI), toolface- ($d\tau$) and azimuth- (dA) uncertainty calculation as long as standard quality control procedures are used (regular tests of the calibration).

Accelerometers

Sensor misalignment might be expressed in many ways. A simple approach is to choose the z- accelerometer axis as an error free direction, and the x-z accelerometer plane as an error free plane. This can be done because the theoretical orthogonal x-, y- and z-co-ordinate system used in the angular calculation (I, A_m and τ), is related to the actual sensor mounting, and not to a predefined instrument co-ordinate system. Any single sensor direction or sensor plane (containing two sensor directions), can therefore be treated as error free. Other sensor axis and sensor planes will be misaligned with respect to this chosen axis and plane. The accelerometer misalignments can then be expressed by

$m_{a,xz}$ The difference between the x- and z- accelerometer axis angle (in the error free x-z plane) and 90° (the non orthogonal part).

$m_{a,yx}$ The non orthogonal part of the angle between the y- accelerometer axis component in the theoretical x-y plane and the x- axis.

$m_{a,yz}$ The non orthogonal part of the angle between the y- accelerometer axis component in the theoretical y-z plane and the z- axis.

With this definition of sensor misalignments, the *x*- and *y*- accelerometer outputs will be erroneous. The *x*- accelerometer will read a small component of the *z*- axis gravity in addition to a major component of the theoretical *x*- axis gravity. The *y*- accelerometer will read small components of both the theoretical *x*- axis and the theoretical *z*- axis gravity in addition to a major component of the theoretical *y*- axis gravity. The theoretical inclination is given by

$$I_0 = \arctan \frac{\sqrt{G_x^2+G_y^2}}{G_z} \qquad \{5.1.1.6\text{-}1\}$$

where G_x, G_y and G_z are the gravity components along the theoretical axis.

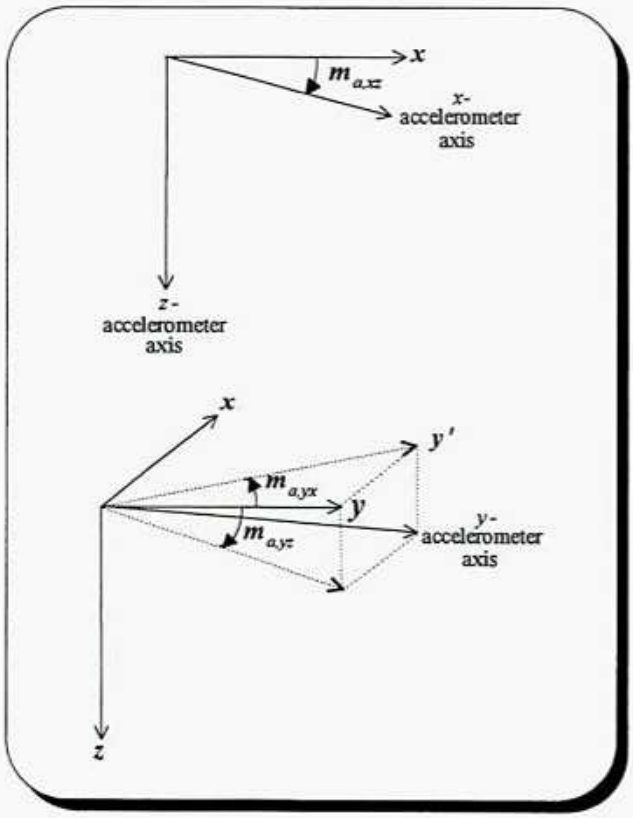

Figure 5.1.1.6-1 Definition of sensor misalignments

The measured inclination is

$$I = \arctan \frac{\sqrt{g_x^2+g_y^2}}{g_z} \qquad \{5.1.1.6\text{-}2\}$$

where g_x, g_y and g_z are the accelerometer measurements.

The measured inclination expressed through gravity component is then given by

$$I = \arctan \frac{\sqrt{(G_x \cos m_{a,xz} + G_z \sin m_{a,xz})^2 + (G_y \cos m_{a,yz} \cos m_{a,xz} + G_x \sin m_{a,yz} \cos m_{a,xz} + G_z \sin m_{a,yz})^2}}{G_z} \qquad \{5.1.1.6\text{-}3\}$$

For small misalignments, equation *{5.1.1.6-3}* can be simplified to

$$I \approx \arctan \frac{\sqrt{G_x^2 + G_y^2 + 2G_x G_y \sin m_{a,yz} + 2G_x G_z \sin m_{a,xz} + 2G_y G_z \sin m_{a,yz}}}{G_z} \qquad \{5.1.1.6\text{-}4\}$$

By assuming equal misalignments ($m_{a,xz} = m_{a,yz} = m_{a,yz} = m_a$), equation *{5.1.1.6-4}* can be simplified to

$$I \approx \arctan \sqrt{\frac{G_x^2 + G_y^2}{G_z^2} + 2\frac{G_x G_y + G_x G_z + G_y G_z}{G_z^2} \sin m_a} \qquad \{5.1.1.6\text{-}5\}$$

The inclination uncertainty caused by uncertainties in accelerometer misalignments (dm_a) is then given by

$$dI = \frac{\partial I}{\partial m_a} dm_a \approx \cos^2 I \frac{G_x G_y + G_x G_z + G_y G_z}{\sqrt{G_x^2 + G_y^2}\, G_z} dm_a \le \left(\frac{\sin I \cos I}{2} + \sqrt{2}\, \cos^2 I \right) dm_a \qquad \{5.1.1.6\text{-}6\}$$

Maximum inclination uncertainty is given by

$$\frac{\partial dI}{\partial I} = \frac{\cos^2 I - \sin^2 I}{2} - \sqrt{6}\, \cos I \sin I = 0 \qquad \{5.1.1.6\text{-}7\}$$

$$I_{extreme} = 9.7° \qquad \{5.1.1.6\text{-}9\}$$

$$dI_{max} = 1.44 dm_a \qquad \{5.1.1.6\text{-}10\}$$

Minimum uncertainty is zero, and is found at the gravity based inclination singularity at 90° inclination. The inclination uncertainty caused by accelerometer misalignments is then bounded by

$$0 \le dI \le 1.44 dm_a \qquad \{5.1.1.6\text{-}11\}$$

This show that accelerometer misalignments only have small effects on the inclination uncertainty for properly calibrated instruments. The inclination error turn out to be of about the same magnitude as the misalignments them selves. Misalignments are usually smaller than 0.01° for properly calibrated instruments. The effect on the inclination accuracy is therefore without significance compared to other error sources. Accelerometer misalignments can then be removed from the inclination error budget.

Magnetometers

A similar study of the effect of accelerometer and magnetometer misalignments on the azimuth uncertainty show that sensor misalignments also can be omitted in the azimuth uncertainty estimation for all practical purposes.

5.1.2 Electronics Dependent Uncertainties

Electronic dependent errors are related to instabilities in the electronics such as analogue / digital converters, down hole processors, etc. They give rise to systematic- and random errors, which are added to the sensor outputs. Electronic dependent errors have a very similar nature to the sensor errors mentioned previously, and consist of biases, scale factor errors, axial misalignments, and random noise. The electronic noise and misalignments are usually small compared to biases and scale factors errors for properly calibrated instruments. It is therefore not necessary to include them in the error budget. Electronic dependent biases and scale factor errors can be modelled by the same type of equations as for sensor biases and scale factor errors.

It is, however, very difficult to distinguish between sensor dependent- and electronic dependent errors in a calibration / qualification process, and thereby making estimates of the individual error components. It is therefore recommended to lump them together to combined biases ($d\eta_a$ for accelerometers and $d\eta_m$ for magnetometers) and combined scale factor uncertainties for ($d\upsilon_a$ accelerometers and $d\upsilon_m$ for magnetometers). These lumped quantities can easily be derived in a test stand during calibrations.

5.1.3 Instrument Misalignment

The misalignment between the z- axis of the sensor package and the principal axis of the instrument collar, is defined as the instrument misalignment. It is necessary to make use of two different angles to give a unique quantification of this error. One alternative is to split the random oriented misalignment angle (m) into two uncorrelated orthogonal components, the x-z plane component and the y-z plane component (m_x and m_y) (Brooks [12]). They will both have effects on the accuracy of both the inclination and the azimuth. The inclination and azimuth instrument misalignment uncertainty components originating from the same misalignment component will therefore be correlated with each other. It should be accounted for this effect in the position co-variance matrix calculation. Instrument misalignments are systematic for one instrument as long as it remains undamaged and not repaired. It is therefore usually a systematic within and random between surveys error source.

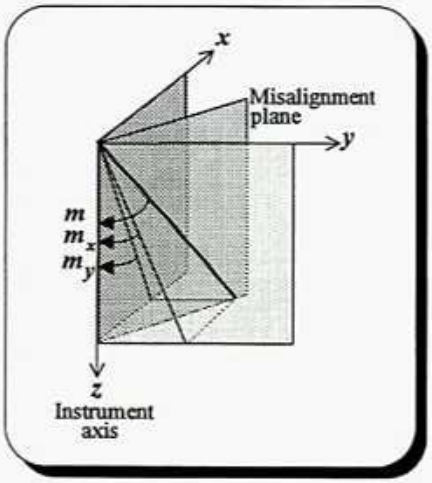

Figure 5.1.3-1 Definition of instrument misalignment

Inclination

The inclination uncertainty originating from the *x*- and the *y*- axis misalignment are given by

$$dI_8 = \sin\tau dm_x \qquad \{5.1.3\text{-}1\}$$

$$dI_9 = \cos\tau dm_y \qquad \{5.1.3\text{-}2\}$$

where dm_x and dm_y are the two instrument misalignment uncertainty components, and τ the toolface. The combined effect of these two inclination uncertainty components will, like anticipated, vary between $\sqrt{dm_x^2 + dm_y^2} = dm$ and $-\sqrt{dm_x^2 + dm_y^2} = -dm$, and it will cancel out when the toolface is reversed.

Azimuth

The azimuth uncertainty originating from the *x*- and the *y*- axis misalignment uncertainties (dm_x and dm_y) are further given by

$$dA_8 = -\frac{\cos\tau}{\sin I} dm_x \qquad \{5.1.3\text{-}3\}$$

$$dA_9 = \frac{\sin\tau}{\sin I} dm_y \qquad \{5.1.3\text{-}4\}$$

The azimuth uncertainty is not defined for vertical wellbores and is therefore unstable for near the vertical (a division with *sin(I)*). This should, however, not represent any problem. An increasing azimuth uncertainty with decreasing inclination has, as stated earlier, little influence on co-ordinate uncertainties.

5.2 Environmental Uncertainties

5.2.1 Earth Magnetic Field Uncertainties

The earth magnetic field at a point is usually described by the three parameters, the total magnetic field strength (B), the magnetic dip angle (Θ), and the magnetic declination (δ). The earth field is built up of three major sub fields. The earth principal field (the major contributor), the local crustal field (often called the local anomaly field), and the atmospheric field (including the effects from induced currents in the earth surface). Non of these fields are constant. They vary with both geographic position and time.

Magnetic field estimates are used directly in magnetic directional surveys. The accuracy of a magnetic survey is therefore very dependent on the accuracy of these estimates. They are usually obtained by one of the following methods

- Use of a recommended regional best fit value
- Use of a magnetic field prediction model
- Presurvey on the surface to correct the model for local magnetic anomalies
- Real time magnetic monitoring (at location or interpolated from reference stations)
- Real time monitoring and local pre survey

The three last examples are different versions of the new In-field referencing surveying technique, which is becoming more and more used.

Accuracy in magnetic field estimates will vary significantly with estimation method, both in size and propagation nature.

The principal field is most easily described by a strong magnetic dipole centred in the earth and a few secondary dipoles placed half inside the earth body. On the surface, this creates a magnetic field that varies with both latitude and longitude, with latitude as the dominant variable. The field can be described with spherical harmonic functions or look up tables (in latitude and longitude). The accuracy of magnetic models used in connection with directional surveying is so high that the principal field can be regarded as error free compared to other field errors.

The atmospheric field varies with time. It has significant daily-, yearly- and eleven yearly variations in addition to short term fluctuations cased by solar effects (magnetic storms etc.). Strong storms are in directional surveying regarded as gross errors, and should be controlled through quality control routines. Corrections based on local magnetic monitoring will remove all significant contribution from the atmospheric field. The reference station has to be near enough to the survey station to secure high correlation between the two stations (Torkildsen [13] is indicating 200km as a maximum distance).

Short term fluctuations and daily variations are not included in any other field estimates than those obtained by magnetic monitoring. They must therefore be regarded as error sources when magnetic models or best fit values are used. The size of random fluctuations can be large, but that is unusual. They are usually small. Short time fluctuations are only considered as a significant error source when working with high confidence levels (over 99.9%). It must be taken into account that random fluctuations probably not are normal distributed (Torkildsen [13]), if they are to be include in the uncertainty estimation. The daily variation has an amplitude of more than 0.1°, and must be considered as a significant error source in all types of magnetic surveys.

The yearly variations and the eleven yearly variations are usually accounted for in all estimation methods, and are therefore not regarded as significant error sources.

The local crustal field is created by magnetic minerals in the earth crust. Their effect can be very strong and local if ferric ore bodies are present. Anomalies created by such ore bodies are in fact used by the mining industry to find ferric minerals. Ferric ore bodies are, however, not especially common in sedimentary basis where drilling usually are performed. The principal source for local crustal fields is instead a variation in the depth down to and the field strength of the magnetic basement rocks. Local crustal fields must be regarded as measurement errors in magnetic surveys. They can be partly removed if corrections based on local anomaly determination are used, but there will always be some residual errors left. Vertical information in addition to surface survey data will reduce the residual error. Significant variations in the magnetic basement will usually have longer wave lengths than horizontal wellbore displacements. Errors associated with the local crustal field will therefore be systematic between stations for an entire field.

5.2.1.1 Magnetic Declination

The magnetic declination (δ) is by definition the horizontal angle between the earth magnetic north and the true magnetic north. The azimuth is then given by

$$A = A_m + \delta \qquad \{5.2.1.1\text{-}1\}$$

which gives the following azimuth uncertainty component

$$dA = \frac{\partial A_m}{\partial \delta} d\delta + \frac{\partial \delta}{\partial \delta} d\delta = d\delta \qquad \{5.2.1.1\text{-}2\}$$

$d\delta$ is a complicated quantity consisting of different time and geographic dependent components, which all have different error propagation characteristics. The different components must because of these different error propagation characteristics be treated separately. The number of significant components vary with different types of magnetic surveys.

Page 64 Line 2 chapter 5.2.1.1 *true magnetic north* should be **true north**

The most significant magnetic declination uncertainty components, which have to be included in wellbore position uncertainty studies, are

- The unmodelled declination uncertainty δ_l.

  This component, which is very near the modelled local declination value, shall only be used in uncertainty studies if no declination values are used in the azimuth calculations. It is a bias (gross error), which it ideally should have been corrected for. δ_l varies with geographic location, and is systematic between all stations within a field, both within surveys, between surveys, and between wellbores. The unmodelled declination uncertainty should be derived from a high accuracy global magnetic model. Although this is a bias, it is recommended to treat it as a dual signed uncertainty figure in accuracy studies. The position uncertainty will be slightly over estimated, but this is considered as a minor problem compared to the benefit of securing against human misinterpretation of of-centre uncertainties.

- The modelled declination uncertainty $d\delta_l$.

  This component is to be used when the local declination is established through a high accuracy magnetic model. It is equal to the uncertainty in the magnetic model, and is mainly caused by local crustal anomalies. $d\delta_l$ is mainly systematic between all survey stations in a field (Torkildsen [13]).

- The residual crustal declination uncertainty $d\delta_r$.

  $d\delta_r$ is equal to the residual uncertainty in the modelled declination after it has been corrected for estimated local crustal anomalies. Local crustal anomalies will usually be estimated through surface magnetic area surveys. It is difficult to settle the error propagation characteristics for this error source, since it is related to local geology and not to wellbore geometry. The magnetic basement (usually the primary source for this error), is relatively constant over a field, and the residual field is expected to be the same. It is therefore recommended to use a systematic within a field error propagation method for this error source as long as no detailed geological data are present to prove anything else.

- The daily declination variation $d\delta_d$.

  The daily declination variation is a 24 hour oscillating effect caused by solar effects and the earth rotation. Station based survey times will usually not be available during uncertainty studies, especially not in the planning stage. It is therefore difficult to establish exact size and station to station correlation properties for this error source. Simplifications are necessary. It is recommended to make use of the daily standard deviation as an estimate for $d\delta_d$, and to assign different error propagation to wireline- and in MWD surveys. Wireline surveys should be handled as if the daily variation is a systematic between stations uncertainty for single

surveys, while MWD surveys should be handled as random between stations uncertainties when drilling in medium and hard formations. Fast drilling (over ca 50 meters per hour) in soft formations necessitates the introduction of a station to station correlation coefficient. Both wireline and MWD surveys should be added randomly between surveys. These conclusions are based on a survey speed analysis (Torkildsen [13]).

The declination dependent azimuth uncertainty components to be used in connection with different surveying techniques are then given by

No Declination in Use

$$dA_{10} = \delta_I \qquad \{5.2.1.1\text{-}3\}$$
$$dA_{11} = d\delta_d \qquad \{5.2.1.1\text{-}4\}$$

The Use of a Magnetic Model

$$dA_{10} = d\delta_I \qquad \{5.2.1.1\text{-}5\}$$
$$dA_{11} = d\delta_d \qquad \{5.2.1.1\text{-}6\}$$

The Use of Magnetic Monitoring And a Magnetic Model

$$dA_{10} = d\delta_I \qquad \{5.2.1.1\text{-}7\}$$
$$dA_{11} \approx 0 \qquad \{5.2.1.1\text{-}8\}$$

Magnetic Monitoring And Local Crustal Correction

$$dA_{10} = d\delta_r \qquad \{5.2.1.1\text{-}9\}$$
$$dA_{11} \approx 0 \qquad \{5.2.1.1\text{-}10\}$$

5.2.1.2 *Magnetic Dip*

The magnetic dip angle (Θ) is per definition the angle between the total magnetic field direction at a given point and the local horizontal plane. The azimuth is given by

$$A = A_m + \delta \qquad \{5.2.1.2\text{-}1\}$$

which gives

$$dA_{12} = \frac{\partial A_m}{\partial \Theta} d\Theta + \frac{\partial \delta}{\partial \Theta} d\Theta = 0 \qquad \{5.2.1.2\text{-}2\}$$

Uncertainty in the magnetic dip angle estimate has therefore no effect on the azimuth accuracy in standard magnetic surveys.

5.2.1.3 *Earth Magnetic Field Strength*

The total magnetic field strength estimate (B) has, according to the discussion in chapter *{5.1.1.5}*, no effect on the magnetic azimuth uncertainty in standard magnetic surveys. The azimuth is also in this case given by *{5.2.1.2-1}*, which differentiated with respect to the total field strength scale factor uncertainty gives

$$dA_{13} = \frac{\partial A_m}{\partial b_x} db_{x3} + \frac{\partial A_m}{\partial b_y} db_{y3} + \frac{\partial A_m}{\partial b_z} db_{z3} + \frac{\partial \delta}{\partial b_x} db_{x3} + \frac{\partial \delta}{\partial b_y} db_{y3} + \frac{\partial \delta}{\partial b_z} db_{z3} = 0 \qquad \{5.2.1.3\text{-}1\}$$

5.2.2 *External Magnetic Field Uncertainties*

The total magnetic field at a given location is the vector sum of the local earth magnetic field and other significant man made local magnetic fields. In directional surveying, platforms, templates, casings (both in the drilled or in nearby wellbores), the drill string, and the bottom hole assembly (BHA), can be the origin of such external magnetic fields. A wireline can also create a local field. Simulations have, however, shown that this field usually is small. It is not regarded as a significant error source in directional surveying. It is convenient to divide man made magnetic fields into two classes, one drill string class (drill string plus BHA), and one external structure class.

5.2.2.1 *Drill string Magnetisation*

Most drill string parts included in the BHA consists usually of, or have components with ferromagnetic materials. They will be magnetised by the earth magnetic field or by other major magnetic fields. There will always be some remanent magnetisation left after a field has been removed or is weakened, for example due to change in direction. The single most important non earth magnetic field to cause drill string magnetisation is, according to McElhinney [14], generated by equipment for non destructive testing (X-ray etc.). This field can be between fifty and hundred thousand times bigger than the earth field, and leave remanent magnetisation in the drill pipe or collar that are greater than the earth induced field. This remanent field is characterised by two equal magnetic poles with opposite sign, each situated approximately fifty cm from the two pipe ends. Lotsberg [15] has found pole strengths of up to 1100 μWb while the induced pole strength according to McElhinney usually is less than 60 μWb. The induced component will usually because of this be without significance compared to the permanent part, and can be omitted in position uncertainty studies.

The permanent magnetisation can be divided into an axial and a cross axial component. The axial component will not generate any toolface dependency in the azimuth calculations, while the cross axial component will. It has its origin in magnetic poles not centralised along the drill string axis, which take part in the drill string rotation. The permanent cross axial magnetisation will usually, because of a small off centre distance compared to normal non magnetic distances between drill string poles and magnetic instruments, be much smaller than the axial magnetisation. It is therefore without significance in the magnetic azimuth determination.

To reduce the azimuth uncertainty caused by drill string magnetisation down to an acceptable level, the practice is to mount the magnetic tool within non magnetic drill collars (NMDC). The necessary NMDC length on each side of the instrument has to be determined for each individual survey. This length is dependent on latitude, wellbore geometry, etc. (Grindrod [31]).

Due to drilling requirements (steering ability etc.), shorter non magnetic drill collars can be used in connection with axial correction algorithms to get a similar effect. The use of axial corrections are very common, and they are in fact often used even when enough nonmagnetic collars are installed. Surveying techniques involving axial corrections have very different error characteristics compared to standard methods. It is therefore important to distinguish between the different methods in uncertainty studies.

MWD without Correction for Axial Magnetisation

The cross axial magnetisation is, as already mentioned, usually without significance in this case where the axial component is dominant. It is therefore enough to evaluate the effect on the magnetic azimuth determination of the axial magnetisation. The axial magnetisation is usually not known at the planning stage. It is recommended to use the standard deviation of magnetic pole strengths of a large number of BHA components as input in uncertainty predictions. The standard deviation should be established by pole strength measurements on many different types of BHA components. It is important that each component type is populated with individual components exposed to different downhole- and stock conditions.

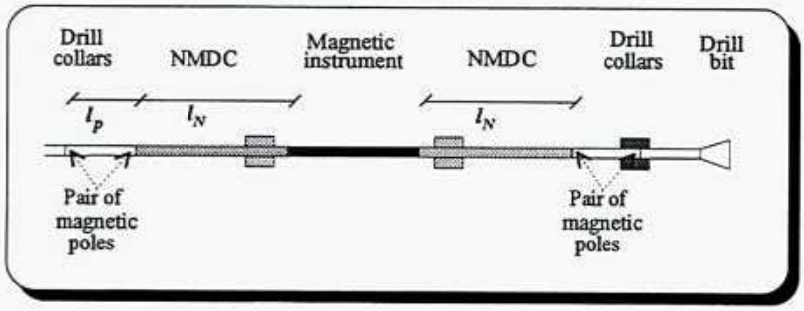

Figure 5.2.2.1-1 Magnetic conditions in a drill string

The field strength at the magnetic instrument is created by pairs of magnetic poles in the non magnetic drill pipes / collars. Poles in the nearest pipes / collars to the instrument are, as it will be shown, most significant.

The axial field strength uncertainty at the magnetic sensors (dB_{a1}) caused by the nearest preceding magnetic drill pipe / collar is given by

$$dB_{a1} = \left(\frac{1}{l_N^2} - \frac{1}{(l_N+l_p)^2}\right)\frac{dp_{mp}}{4\pi} = 0.08\left(\frac{1}{l_N^2} - \frac{1}{(l_N+l_p)^2}\right)dp_{mp} \qquad \{5.2.2.1\text{-}1\}$$

where dP_{mp} is the uncertainty in the magnetic pole strengths of different BHA components (standard deviation), l_p the average distance between two complementary poles (usually the length of one drill pipe or collar), and l_N the length between the magnetic instrument and the nearest magnetic pole (length of non magnetic collars presiding the instrument).

The axial field strength uncertainty at the magnetic sensors ($dB_{a'}$) caused by all magnetic drill pipe / collars installed higher up in the drill string is then given by

$$dB_{a'} = 0.08\sqrt{\left(\frac{1}{l_N^2} - \frac{1}{(l_N+l_p)^2}\right)^2 + \left(\frac{1}{(l_N+l_p)} - \frac{1}{(l_N+2l_p)^2}\right)^2 + \ldots\ldots}\, dp_{mp} \approx \frac{0.08}{l_N^2} dp_{mp} \qquad \{5.2.2.1\text{-}2\}$$

The axial field strength uncertainty at the magnetic sensors caused by all the following non magnetic drill pipe / collar will be given by the same expression as long as equal amount of non magnetic material is used on both sides of the instrument. Its sign will, however, be random with respect to the first case. The total drill string induced axial field strength (dB_a) can then be found by multiplying equation *{5.2.2.1-2}* with the square root of two.

$$dB_a = \sqrt{2}\,\frac{0.08}{l_N^2} dp_{mp} = \frac{0.11}{l_N^2} dp_{mp} \qquad \{5.2.2.1\text{-}3\}$$

The magnetic field sensed by the magnetic instrument is the combined effect of the earth magnetic field and the axial drill string magnetisation field (dB_a). The combined field will only differ from the earth field in the axial direction (the z- axis). The axial magnetisation will therefore have the same effect in the magnetic azimuth determination as a z-magnetometer bias. The axial azimuth uncertainty is then given by

$$dA_{14} = \frac{\partial A_m}{\partial b_z} dB_a = -\frac{\sin I \sin A_m}{B \cos\Theta} dB_a \qquad \{5.2.2.1\text{-}4\}$$

where B is the earth magnetic field strength, Θ is the magnetic dip angle, I is the inclination, and A_m is the magnetic azimuth.

The axial drill string magnetisation azimuth error is a bias type error, where the sign is totally governed by the sign of the magnetic pole strength. The error can because of this be regarded as systematic between stations within the same survey and random between different surveys as long as the BHA is changed. This is usually the case. New surveys are usually initialised at bit runs, and causes the pole strength to become random between different surveys.

MWD with Correction for Axial Magnetisation

There are many algorithms available for correction of axial drill string magnetisation. Many different MWD companies have developed and patented their own algorithms (Coles [16], Engebretson [17] and Russell [18]). Even though different patents are present, most algorithms seem not to be differing very much. Most standard axial correction methods are ignoring or making adjusts to the z- magnetometer readings through an

introduction of external data (the local magnetic dip and total field strength) in the azimuth calculation. A couple of new and more sophisticated methods involving trend analyses between consecutive measurement stations are also available. They will, due to confidentiality considerations, not be covered here. It is, however, recommended to make use of the same uncertainty equations as for standard corrections. This is justified by the fact that these new methods also suffer from the same type of singularity. They have, however, proven to be more accurate before the singularity is reach, a fact that should be reflected in the use of more accurate uncertainty inputs.

Standard axial correction methods are, as already stated, not very different from each other. Weighting functions derived from one method will also be valid for the other. In the following, the derivation will be shown for one method. It is making use of a calculated *z*-magnetometer reading instead of the measured one. The new *z*- reading is obtained by a minimising of the difference between the given earth magnetic field vector and the measured (corrected) total field vector. Ignoring the real *z*- magnetometer measurements means that the magnetometer azimuth uncertainty equations given in chapter 5.1.1.5 (equation *{5.1.1.5-2}* to *{5.1.1.5-15}*) are not valid. A new set of weighting functions have to be derived. The azimuth accuracy is in this case sensitive to dip and total field strength errors.

The *x*- and *y*- magnetometer measurements are given by

$$b_x \approx B(\cos\Theta\cos I\cos A_m\sin\tau - \sin\Theta\sin I\sin\tau + \cos\Theta\sin A_m\cos\tau) \qquad \{5.2.2.1\text{-}5\}$$

$$b_y \approx B(\cos\Theta\cos I\cos A_m\cos\tau - \sin\Theta\sin I\cos\tau - \cos\Theta\sin A_m\sin\tau) \qquad \{5.2.2.1\text{-}6\}$$

where B is the local earth magnetic field strength, A_m the magnetic azimuth, I the inclination, τ the toolface, and Θ the estimated magnetic dip angle.

The minimisation constraint with respect to the total magnetic field strength and the dip angle can be expressed as

$$(b_h - B\cos\Theta)^2 + (b_v - B\sin\Theta)^2 = \min \qquad \{5.2.2.1\text{-}7\}$$

where b_h is the horizontal component and b_v the vertical component of the measured field given by

$$b_h = \frac{b_x\cos\tau - b_y\sin\tau}{\sin A_m} \qquad \{5.2.2.1\text{-}8\}$$

$$b_v = \frac{\frac{b_x\cos\tau - b_y\sin\tau}{\sin A_m}\cos I\cos A_m - b_x\sin\tau - b_y\cos\tau}{\sin I} \qquad \{5.2.2.1\text{-}9\}$$

Substituting b_h and b_v in equation *{5.2.2.1-7}* with b_x and b_y in equation *{5.2.2.1-5}* and *{5.2.2.1-6}* yields an equation in the magnetic azimuth A_m, which differentiated with respect to A_m gives the following result

$$(b_h - B\cos\Theta)\sin I\cos A_m + (b_v - B\sin\Theta)\cos I = 0 \qquad \{5.2.2.1\text{-}10\}$$

Equation *{5.2.2.1-10}* can be solved with respect to A_m and then partially differentiated with respect to the inputs (the two magnetometer measurements, the inclination, the toolface, the dip and the total field strength). This yields the following magnetic azimuth uncertainty components for magnetic measurements with axial corrections. The measured horizontal and vertical components are estimated by their a priori estimated counterparts in these equations.

$$dA_1 = \frac{\partial A_m}{\partial b_x} db_{x1} \approx \frac{\cos A_m \cos\tau - \cos I \sin A_m \sin\tau}{B\cos\Theta\left(1-\sin^2 I \sin^2 A_m\right)} db_{x1} \qquad \{5.2.2.1\text{-}11\}$$

$$dA_2 = \frac{\partial A_m}{\partial b_x} db_{x2} \approx \frac{\cos A_m \cos\tau - \cos I \sin A_m \sin\tau}{B\cos\Theta\left(1-\sin^2 I \sin^2 A_m\right)} db_{x2} \qquad \{5.2.2.1\text{-}12\}$$

$$dA_3 = \frac{\partial A_m}{\partial b_y} db_{y1} \approx -\frac{\cos I \sin A_m \cos\tau + \cos A_m \sin\tau}{B\cos\Theta\left(1-\sin^2 I \sin^2 A_m\right)} db_{y1} \qquad \{5.2.2.1\text{-}13\}$$

$$dA_4 = \frac{\partial A_m}{\partial b_y} db_{y2} \approx -\frac{\cos I \sin A_m \cos\tau + \cos A_m \sin\tau}{B\cos\Theta\left(1-\sin^2 I \sin^2 A_m\right)} db_{y2} \qquad \{5.2.2.1\text{-}14\}$$

$$dA_5 = 0 \qquad \{5.2.2.1\text{-}15\}$$

$$dA_6 = 0 \qquad \{5.2.2.1\text{-}16\}$$

$$dA_7 = \frac{\partial A_m}{\partial I} dI_s + \frac{\partial A_m}{\partial \tau} d\tau \approx -\frac{\cos I \sin A_m (\cos\Theta \sin I \cos A_m + \sin\Theta \cos I)}{\cos\Theta\left(1-\sin^2 I \sin^2 A_m\right)} dI_s - \frac{\cos\Theta \cos I - \sin\Theta \sin I \cos A_m}{\cos\Theta\left(1-\sin^2 I \sin^2 A_m\right)} d\tau \qquad \{5.2.2.1\text{-}17\}$$

$$dA_{12} = \frac{\partial A_m}{\partial \Theta} d\Theta \approx -\frac{\sin I \sin A_m (\cos\Theta \cos I - \sin\Theta \sin I \cos A_m)}{\cos\Theta\left(1-\sin^2 I \sin^2 A_m\right)} d\Theta \qquad \{5.2.2.1\text{-}18\}$$

$$dA_{13} = \frac{\partial A_m}{\partial b_x} db_{x3} + \frac{\partial A_m}{\partial b_y} db_{y3} \approx -\frac{\sin I \sin A_m (\sin\Theta \cos I + \cos\Theta \sin I \cos A_m)}{B\cos\Theta\left(1-\sin^2 I \sin^2 A_m\right)} dB \qquad \{5.2.2.1\text{-}19\}$$

$$dA_{14} = 0 \qquad \{5.2.2.1\text{-}20\}$$

Magnetometer uncertainties (db_{x1}, db_{x2}, db_{x3}, db_{y1}, db_{y2} and db_{y3}) are given in equation *{5.1.1.4-2}* to *{5.1.1.4-9}*.

It follows directly from these equations that the accuracy of axial magnetisation correction algorithms tends towards infinity at the magnetic poles and for horizontal wellbores in the magnetic east or west direction. It should also be noted that the magnetic azimuth equation derived from equation *{5.2.2.1-10}* does not distinguish between A_m and 180°-A_m. The correct quadrant has to be chosen from other inputs like earlier drilling performance etc. There is therefore a real possibility to pick the wrong solution near the horizontal magnetic east / west direction when significant azimuth changes take place between two consecutive survey stations. This problem has been experienced in the field from time to time, and has therefore to be taken seriously. One example is presented in Ekseth [25]. It shows azimuth errors, which over a longer wellbore section increase from nearly zero to more than 20°. The unpublished consequence of this was that all three targets where lost. Axial corrections should not be used if the uncertainty after correction is larger than the uncertainty without correction, or if it is a realistic possibility to pick the wrong quadrant.

The toolface uncertainty ($d\tau$) is given by equation *{5.1.1.3-2}*, and the inclination uncertainty (dI_s) is given by equation *{5.1.1.5-9}*. The effect of the inclination and the toolface uncertainties on the magnetic azimuth are, as in the uncorrected case, combined into just one uncertainty term because of the high correlation that exists between these two terms.

Magnetometer dependent equations (*{5.2.2.1-11}* to *{5.2.2.1-14}*) are, as shown earlier, systematic within surveys, and random between surveys as long as different instruments are used in different surveys. The same conclusion is valid for the inclination and toolface dependent equation (*{5.2.2.1-17}*), which are rooted in accelerometer errors. Magnetic dip and total field strength equations (*{5.2.2.1-18}* and *{5.2.2.1-19}*) should be given the same error propagation as the declination dependent equations given in chapter 5.2.1.1. This recommendation is based on the fact that the magnetic field vector is described by the three values, the total field strength, the dip and the declination. Any error source affecting the magnetic field vector should therefore be reflected in all three parameters.

It is of course possible to substitute the inclination and toolface used in these mathematical derivations with the basic accelerometer measurements. The dA_7 uncertainty component given in equation *{5.2.2.1-17}* will then be divided into six uncorrelated components, which have to be treated separately. These six uncertainty components will usually be systematic within and random between surveys, and are given by

$$dA_{7\_1} = \frac{\partial A_m}{\partial g_x} dg_{x1} = \frac{\sin I \cos^2 I \sin A_m \sin\tau(\sin\Theta\cos I + \cos\Theta\sin I\cos A_m) - \cos\tau(\sin\Theta\sin I\cos A_m - \cos\Theta\cos I)}{G\cos\Theta\sin I\left(1-\sin^2 I\sin^2 A_m\right)} dg_{x1} \quad \{5.2.2.1\text{-}21\}$$

$$dA_{7\_2} = \frac{\partial A_m}{\partial g_x} dg_{x2} = \frac{\sin I \cos^2 I \sin A_m \sin\tau(\sin\Theta\cos I + \cos\Theta\sin I\cos A_m) - \cos\tau(\sin\Theta\sin I\cos A_m - \cos\Theta\cos I)}{G\cos\Theta\sin I\left(1-\sin^2 I\sin^2 A_m\right)} dg_{x2} \quad \{5.2.2.1\text{-}22\}$$

$$dA_{7\_3} = \frac{\partial A_m}{\partial g_y} dg_{y1} = \frac{\sin I \cos^2 I \sin A_m \cos\tau(\sin\Theta\cos I + \cos\Theta\sin I\cos A_m) + \sin\tau(\sin\Theta\sin I\cos A_m - \cos\Theta\cos I)}{G\cos\Theta\sin I\left(1-\sin^2 I\sin^2 A_m\right)} dg_{y1} \quad \{5.2.2.1\text{-}23\}$$

$$dA_{7\_4} = \frac{\partial A_m}{\partial g_y} dg_{y2} = \frac{\sin I \cos^2 I \sin A_m \cos\tau(\sin\Theta\cos I + \cos\Theta\sin I\cos A_m) + \sin\tau(\sin\Theta\sin I\cos A_m - \cos\Theta\cos I)}{G\cos\Theta\sin I\left(1-\sin^2 I\sin^2 A_m\right)} dg_{y2} \quad \{5.2.2.1\text{-}24\}$$

$$dA_{7\_5} = \frac{\partial A_m}{\partial g_z} dg_{z1} = \frac{\sin I \cos I \sin A_m(\sin\Theta\cos I + \cos\Theta\sin I\cos A_m)}{G\cos\Theta\left(1-\sin^2 I\sin^2 A_m\right)} dg_{z1} \quad \{5.2.2.1\text{-}25\}$$

$$dA_{7\_6} = \frac{\partial A_m}{\partial g_z} dg_{z2} = \frac{\sin I \cos I \sin A_m(\sin\Theta\cos I + \cos\Theta\sin I\cos A_m)}{G\cos\Theta\left(1-\sin^2 I\sin^2 A_m\right)} dg_{z2} \quad \{5.2.2.1\text{-}26\}$$

Accelerometer uncertainties (dg_{x1}, dg_{x2}, dg_{y1}, dg_{y2}, dg_{z1} and dg_{z2}) are given by equation *{5.1.1.1-2}* to *{5.1.1.1-10}*.

These azimuth uncertainty components will, as in the uncorrected case, be correlated with their inclination counterparts. The following uncertainty components should therefore be treated as correlated errors in the position co-variance matrix calculation

- dI_1 and dA_{7_1}
- dI_2 and dA_{7_2}
- dI_3 and dA_{7_3}
- dI_4 and dA_{7_4}
- dI_5 and dA_{7_5}
- dI_6 and dA_{7_6}

EMS on Wireline

Electronic multishot surveys (EMS) are usually run on wirelines. This is either done in open hole or in the BHA. It was in chapter 5.2.2 shown that a wireline can be regarded as non magnetic in connection with wellbore surveying. EMS surveys taken in open holes do therefore not suffer significantly from drill string magnetisation like error sources. dA_{12}, dA_{13} and dA_{14} are therefore not to be used in EMS uncertainty studies in open hole.

5.2.2.2 *External Structure Magnetic Fields*

Magnetic fields generated by external structures made up of ferromagnetic materials like casings, templates, etc., can be very strong, and destroy the quality of any magnetic measurement. These errors are therefore to be defined as gross errors. Magnetic directional surveys should because of this be avoided if strong external fields are present. This should be controlled through quality control routines designed to secure against surveying in areas with external fields over a given limit. Such quality control routines should be possible to implement. Magnetic fields around external structures can be estimated. There are, however, two situations where it will be difficult to always avoid the use of magnetic instruments in potential significant external field areas. It is when drilling out of an existing casing, or near and parallel to existing casings. It is in these two cases necessary to account for the expected external field in position uncertainty calculations. Drilling out of an existing casing means either out of the casing shoe or out of a milled window. The error characteristics are, unless the new wellbore is parallel to the old one over longer distances, not differing much. It is therefore regarded as sufficient to analyse only the casing shoe- and the parallel to existing casings cases, to derive necessary weighting functions for wellbore position uncertainty estimations.

The magnetic nature of installed casing strings is not known well enough to give final conclusions on this error term. Casing pole detection performed by Pratt and Hartmann [32] show significant magnetic poles near the ends of individual casing pipes. Pratt and Hartmann did, however, not perform any quantitative pole detection. Further research is therefore needed. It is, however, reasonable to expect a behaviour not far away from the drill pipe behaviour (described in the previous chapter). Both string types are made up of joined ferric pipes, which are exposed to the earth field for longer time periods, and which might have been heavily magnetised as part of the manufacturing quality control. It is therefore assumed that the principal source of casing induced magnetic fields are remanent magnetisation after man made induction, and that each casing pipe is believed to be an

independent magnet bar. Whether installed casing strings actually have such a high frequency of significant magnetic poles is still an unanswered question, but this assumption is regarded as sufficient as a first order approximation. It represents a worst case solution when drilling parallel to existing casings (the only case where the pole frequency is important).

Drilling out of an Existing Casing

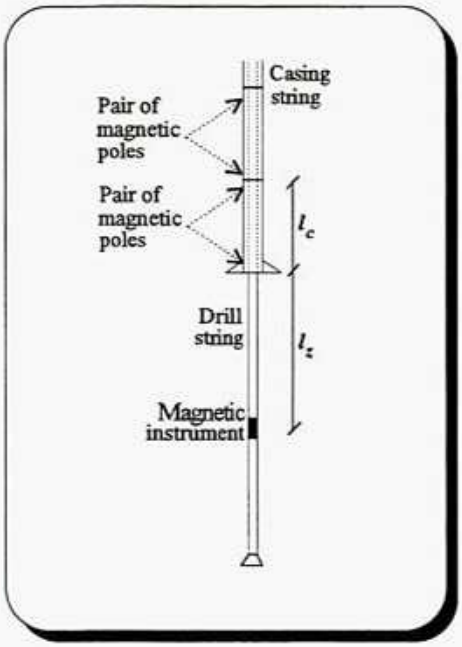

Figure 5.2.2.2-1 Magnetic conditions while drilling out of an existing casing shoe

The field strength at the magnetic instrument is created by pairs of magnetic poles in the casing string. The pole at the casing shoe will be most significant. The associated axial field strength uncertainty at the magnetic sensors (dB_{cs}) is according to the derivation for the drill pipe induced magnetisation given by

$$dB_{cs} = \frac{0.08}{l_z^2} dp_{mc} \qquad \{5.2.2.2\text{-}1\}$$

where dP_{mc} is the uncertainty in casing magnetic pole strengths (standard deviation), l_z the length between the magnetic instrument and the casing shoe and l_c the length of one casing pipe (average).

The magnetic azimuth uncertainty in the distance l_z below the casing shoe is then given by

$$dA_{15} = \frac{\partial A_m}{\partial b_z} dB_{cs} = -\frac{\sin I \sin A_m}{B \cos \Theta} dB_{cs} \qquad \{5.2.2.2\text{-}2\}$$

B is the local earth magnetic field strength, A_m the magnetic azimuth, I the inclination, and Θ the magnetic dip angle. Equation *{5.2.2.2-2}* can also be used when drilling out of a milled casing window, if the new wellbore is significantly deflected from the old one.

dA_{I5} will because of the inverse squared length effect decrease rapidly with increasing distance, and will, at most, only be significant in one or two measurement stations (30 - 60 meters). It will have very little effect on the wellbore position accuracy, and can usually be omitted. The error propagation is systematic between stations and random between surveys.

Drilling Near and Parallel to an Existing Casing

The knowledge of the magnetic behaviour of installed casing strings are not good enough to establish accurate uncertainty estimates when drilling parallel to existing wellbores. Magnetic pole strengths and pole frequencies, which are fundamental inputs in the uncertainty estimation, are more or less unknown. Field experience have, however, shown that significant errors can be present. It is therefore recommended to include this error source in the total error budget, and to make use of a temporary uncertainty estimation method until the true magnetic nature of installed casing strings have been settled.

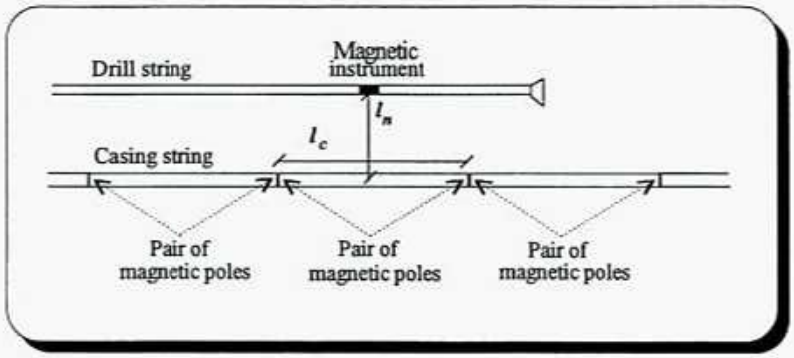

Figure 5.2.2.2-2 Average casing induced magnetic conditions while drilling parallel to an existing casing

A simplified model can be created by assuming that each piece of the casing acts as an independent magnet bar, where the magnetisation is permanent and caused by non destructive testing. This is identical to the proven magnetic nature of drill pipes (McElhinney [14] and Lotsberg [15]), and will result in a random distribution of pairs of magnetic poles within the installed casing string. The resultant casing field will result in correlated axial and cross axial effects at the magnetic sensors. There will be a random between stations error propagation due to the random pole distribution.

The axial field strength uncertainty at the magnetic instrument caused by casing interference (dB_{ca}) is given by

$$dB_{ca} = \sqrt{\left(\frac{2l_c dP_{mc}}{\pi\sqrt{\left(4l_n^2+l_c^2\right)^3}}\right)^2 + 2\left(\frac{l_c dP_{mc}}{\pi\sqrt{\left(4l_n^2+l_c^2\right)^3}} - \frac{3l_c dP_{mc}}{\pi\sqrt{\left(4l_n^2+9l_c^2\right)^3}}\right)^2 + \cdots\cdots}$$

$$\approx \sqrt{\left(\frac{2l_c dP_{mc}}{\pi\sqrt{\left(4l_n^2+l_c^2\right)^3}}\right)^2 + 2\left(\frac{l_c dP_{mc}}{\pi\sqrt{\left(4l_n^2+l_c^2\right)^3}}\right)^2} = \frac{0.8l_c}{\sqrt{\left(4l_n^2+l_c^2\right)^3}} dP_{mc} \qquad \{5.2.2.2\text{-}3\}$$

where dP_{mc} is the casing magnetic pole strengths uncertainty, l_n the minimum distance between the old casing and the magnetic instrument, and l_c the average length of casing pipes.

The cross axial field strength uncertainty at the magnetic instrument (dB_{cc}) is further given by

$$dB_{cc} = \sqrt{2\left(\frac{2l_n dP_{mc}}{\pi\sqrt{\left(4l_n^2+l_c^2\right)^3}} - \frac{2l_n dP_{mc}}{\pi\sqrt{\left(4l_n^2+9l_c^2\right)^3}}\right)^2 + 2\left(\frac{2l_n dP_{mc}}{\pi\sqrt{\left(4l_n^2+9l_c^2\right)^3}} - \frac{2l_n dP_{mc}}{\pi\sqrt{\left(4l_n^2+25l_c^2\right)^3}}\right)^2 + \cdots\cdots}$$

$$\approx \sqrt{2\left(\frac{2l_n dP_{mc}}{\pi\sqrt{\left(4l_n^2+l_c^2\right)^3}}\right)^2} = \frac{0.9l_n}{\sqrt{\left(4l_n^2+l_c^2\right)^3}} dP_{mc} \qquad \{5.2.2.2\text{-}4\}$$

This field uncertainty will affect both the x- and the y- magnetometer readings. Their orientation with respect to cross axial field direction are unknown. It is therefore assumed equal contribution on both magnetometers.

For measurements without axial corrections, the azimuth uncertainty caused by an old parallel casing is given by

$$dA_{15} = \frac{\partial A_m}{\partial b_x}\frac{dB_{cc}}{\sqrt{2}} + \frac{\partial A_m}{\partial b_y}\frac{dB_{cc}}{\sqrt{2}} + \frac{\partial A_m}{\partial b_z} dB_{ca}$$

$$= \sqrt{2}\left(\frac{\cos\tau\cos A_m - \cos I\sin\tau\sin A_m}{B\cos\Theta} - \frac{\sin\tau\cos A_m + \cos I\cos\tau\sin A_m}{B\cos\Theta}\right) dB_{cc} - \frac{\sin I\sin A_m}{B\cos\Theta} dB_{ca} \quad \{5.2.2.2\text{-}5\}$$

B is the local earth magnetic field strength, A_m the magnetic azimuth, I the inclination, and Θ the magnetic dip angle. This uncertainty is random between stations.

For measurements with axial corrections, the similar azimuth uncertainty is given by

$$dA_{15} = \frac{\partial A_m}{\partial b_x}\frac{dB_{cc}}{\sqrt{2}} + \frac{\partial A_m}{\partial b_y}\frac{dB_{cc}}{\sqrt{2}}$$

$$= \sqrt{2}\left(\frac{\cos A_m\cos\tau - \cos I\sin A_m\sin\tau}{B\cos\Theta\left(1-\sin^2 I\sin^2 A_m\right)} - \frac{\cos I\sin A_m\cos\tau + \cos A_m\sin\tau}{B\cos\Theta\left(1-\sin^2 I\sin^2 A_m\right)}\right) dB_{cc} \qquad \{5.2.2.2\text{-}6\}$$

5.2.3 *Collar Misalignments*

There are three fundamental types of misalignments associated with directional surveys. The first two have already been covered, the sensor misalignments (chapter 5.1.1.6) and the instrument misalignment (chapter 5.1.3). The third type is the misalignment between the wellbore axis and the instrument axis. This error is created by borehole deformations or by mechanical forces acting on the drill string or wireline, and is a function of the wellbore geometry and the bottom hole assembly (BHA). Measurements are often correct for this error source with help of special programs, which estimates the actual error size.

It is difficult to model this misalignment exactly. Especially at the planning stage, where no detailed BHA and deformation information are present. The collar misalignment is, however, a significant contributor in the total error budget, and has to be included in wellbore position uncertainty studies. This is usually the case even for corrected measurements where residual errors after correction can have a systematic nature.

Borehole deformations will usually have a random behaviour (wash outs etc.) or be systematic over longer wellbore sections (key-seats, horizontal stress breakouts, etc.). Random borehole deformations will because of the systematic error dominance have little effect compared to systematic gravity and bent sub driven misalignments. Longer key-seats and systematic breakouts are only resulting in negligible differences between the direction of a wellbore axis and the direction of an instrument axis. Borehole deformations are therefore not regarded as a significant error source in wellbore positioning.

Mechanical forces are in directional surveying usually divided into vertical and horizontal components to simplify the gravity treatment. It is therefore also convenient to split the collar alignment error into vertical and horizontal components.

5.2.3.1 *Vertical Collar Misalignment*

Vertical collar alignment errors are usually rooted in gravity, stabiliser forces, axial forces, and bending moments. The gravity effect should be considered as a bias and corrected for.

Wireline

Magnetic wireline surveys are usually performed in open hole, and centralizers are hardly never used. The instrument collar will have less diameter than the wellbore, and will usually rest on the bottom if normal wellbore curvatures are assumed. The vertical collar alignment error is therefore usually caused by roughness in the borehole surface, and will, because a random roughness distribution, be random between stations. It is given by

$$dI_{10} = \arctan\frac{dr_i}{l_m} \approx 0 \qquad \{5.2.3.1\text{-}1\}$$

where dr_i is the average wellbore radius difference over the actual wireline magnetic collar length l_m.

MWD

The vertical MWD collar alignment error is often called the sag error. This error is more complicated than the similar wireline error because it is dependent on the actual used bottom hole assembly (BHA). Factors that have first order effects on the sag error are the drill collar stiffness, weight on bit (bending moment), stabilisers, drill bit location (with respect to the magnetic instrument), and whether or not a bent sub is in use. There is a variety of different possible BHA configurations. It should, ideally, have been differentiated between all of them in uncertainty studies. This is, however, impossible. Necessary inputs will usually not be available to persons at the planning stage.

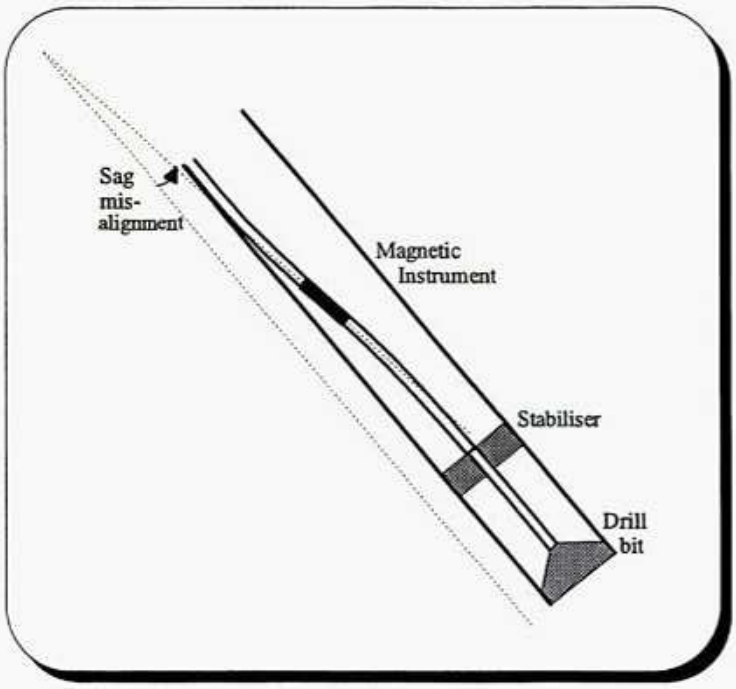

Figure 5.2.3.1-2 Definition of the sag misalignment

The gravity component normal to the wellbore profile is the fundamental force associated with the sag error, at least for standard rotary drilling where no bent sub is in use. The inclination uncertainty caused by the sag is therefore assumed to be proportional to *sin(I)* (Wolff [6]), and is given by

$$dI_{10} = \sin I ds_v \qquad \{5.2.3.1\text{-}2\}$$

where ds_v is the average sag for a large number of surveys reduced to the horizontal.

The sag error is a bias, and will therefore always be systematic.

The sag error has, however, for many years been recognised as a major contributor to the inclination uncertainty. It is therefore a common practice to make estimates and correct for this error. Corrections are usually calculated with specially designed computer programs. They are based on the same theory as used in programs for drill string design. No available sag correction method is capable of removing all errors. There is always some residual sag left after correction. This residual sag is caused by a natural spread in material properties etc. It is therefore gravity dependent, and will have the same *sin(I)* dependency as the uncorrected error. The residual error will remain nearly constant as long as the drill string, the mud, etc., are unchanged. Residual errors after sag correction will be systematic between stations within surveys, and random between surveys. The corrected sag uncertainty is then given by

$$dI_{10} = \sin I ds_r \qquad \{5.2.3.1\text{-}3\}$$

where ds_r is the expected residual sag uncertainty after a sag correction in horizontal wellbores.

5.2.3.2 *Horizontal Collar Misalignment*

Horizontal collar alignment errors are caused by bending moments due to horizontal wellbore curvatures and drill string buckling. Buckling is an unpredictable gross error condition, which it is impossible to include in uncertainty estimations. It must be controlled through quality control procedures. Bending moments is only significant for large horizontal curvatures. Large horizontal curvatures is, however, unusual, and horizontal collar alignment uncertainties can be omitted for all practical purposes.

6 Errors in Gyro Tools

Gyro tools are usually equipped with two or three accelerometers, and one, two or three rotor gyros. The accelerometers are used to find the inclination (I) and the high-side toolface (τ). The gyros are together with the accelerometers used to find the true north azimuth (A). One instrument type do also, as it will be shown, make use of gyro measurements in the inclination determination.

Weighting functions will in the following be derived for the most commonly used gyro instruments in the Norwegian North Sea sector. The different uncertainty equations will because of similarities be organised after error sources, and not after instrument type. It is therefore necessary to pick equations from different sub chapters to form a complete set of weighting functions for a given instrument.

6.1 Tool Uncertainties

6.1.1 Sensor Uncertainties

There are three principal sensor dependent error types associated with gyro instruments. It is errors within the accelerometers and gyros themselves, errors associated with the alignment of the sensors within the instrument, and errors originating from the electronics.

6.1.1.1 Accelerometers

Gyro instruments are designed to be run both stationary and continuous. Accelerometers react differently in stationary measurements and in measurements taken during significant movements. It is therefore necessary to distinguish between stationary and continuous measurements in uncertainty studies.

Stationary Measurements

Accelerometer errors in gyro instruments consist, like in the magnetic case, of random components, biases (η_a), sensor induced linear scale factors (υ_a), gravity induced linear scale factors (υ_G), and second order scale factors. The second order- and the random components are, as for magnetic instruments, without significance in wellbore positioning. This conclusion is based on the assumption that instruments are run according to standard operational procedures, which include repeated initialisation measurements (to force the resultant random effect down to a level where it is without significance) etc.

The gravity induced scale factor uncertainty is given by

$$d\upsilon_G = \frac{dG}{G} \qquad \{6.1.1.1\text{-}1\}$$

where G is the local gravity, and dG its uncertainty.

The bias and the sensor induced scale factor uncertainty are again systematic between measurement stations as long as the same instrument is in use.

Most gyro instruments are equipped with from one to three accelerometers mounted along different principal axis. The equations derived for magnetic instruments to find the different accelerometer uncertainties can therefore also be used for gyro instruments. The gyro accelerometer uncertainties are then given by

$$dg_{x1} = d\eta_a \qquad \{6.1.1.1\text{-}2\}$$
$$dg_{x2} = g_x d\upsilon_a \approx -G\sin I \sin\tau d\upsilon_a \qquad \{6.1.1.1\text{-}3\}$$
$$dg_{x3} = g_x d\upsilon_G \approx -G\sin I \sin\tau d\upsilon_G \qquad \{6.1.1.1\text{-}4\}$$

$$dg_{y1} = d\eta_a \qquad \{6.1.1.1\text{-}5\}$$
$$dg_{y2} = g_y d\upsilon_a \approx -G\sin I \cos\tau d\upsilon_a \qquad \{6.1.1.1\text{-}6\}$$
$$dg_{y3} = g_y d\upsilon_G \approx -G\sin I \cos\tau d\upsilon_G \qquad \{6.1.1.1\text{-}7\}$$

$$dg_{z1} = d\eta_a \qquad \{6.1.1.1\text{-}8\}$$
$$dg_{z2} = g_z d\upsilon_a \approx G\cos I d\upsilon_a \qquad \{6.1.1.1\text{-}9\}$$
$$dg_{z3} = g_z d\upsilon_G \approx G\cos I d\upsilon_G \qquad \{6.1.1.1\text{-}10\}$$

All nine equations have to be used in connection with standard three accelerometer systems, while the six first are necessary for standard two accelerometer systems, and only the latter three for single accelerometer systems.

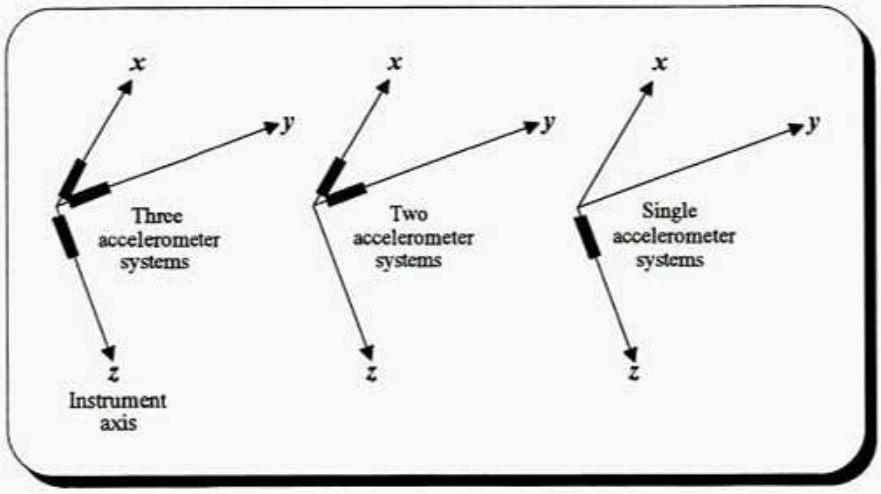

Figure 6.1.1.1-1 Accelerometer mounting in standard three-, two- and single accelerometer gyro instruments

Continuous Measurements

Continuous gyro tools run in-hole might suffer from large acceleration if they temporarily get stuck etc. It is impossible to distinguish between such accelerations and the z-component of the gravity field. Axial accelerations will therefore act as an additional accelerometer error. This error will have a random between stations behaviour, and is given by

$$dg_{z4} = da_z \qquad \{6.1.1.1\text{-}11\}$$

where da_z is the standard deviation of the expected axial acceleration.

Bias and scale factor uncertainties are also for continuous measurements given by equation *{6.1.1.1-1}* to *{6.1.1.1-10}*.

Canted Scientific Drilling Controls Systems

The accelerometers in Scientific Drilling Controls (SDC) gyro instruments are mounted in a non orthogonal co-ordinate frame (Van Steenwyk [19]), and they are therefore called canted systems. The x- accelerometer (x'- accelerometer) is canted in the x-z plane, and its uncertainties are given by

$$dg_{x'1} = d\eta_a \qquad \{6.1.1.1\text{-}12\}$$
$$dg_{x'2} = g_{x'}d\upsilon_a \approx -G(\sin I \sin\tau\cos\gamma + \cos I \sin\gamma)d\upsilon_a \qquad \{6.1.1.1\text{-}13\}$$
$$dg_{x'3} = g_{x'}d\upsilon_G \approx -G(\sin I \sin\tau\cos\gamma + \cos I \sin\gamma)d\upsilon_G \qquad \{6.1.1.1\text{-}14\}$$

$g_{x'}$ is the canted accelerometer measurement and γ is the cant angle (the angle between the theoretical x- axis and the accelerometer axis).

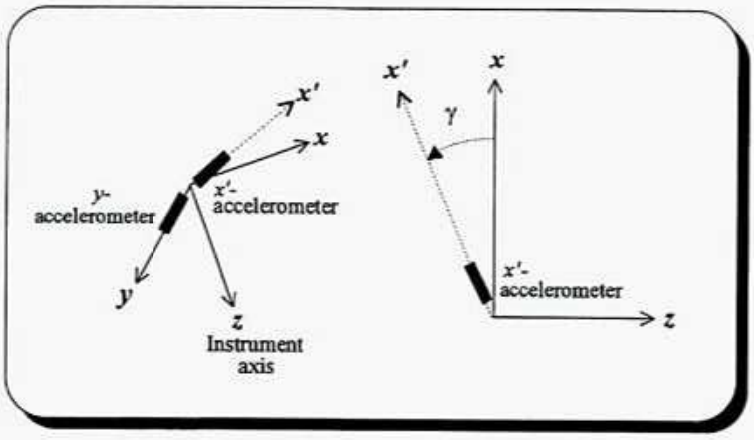

Figure 6.1.1.1-2 Accelerometer mounting in canted systems

Canted systems are also equipped with one *y*- accelerometer. The uncertainties associated with this *y*- accelerometer are equal to those obtained for standard systems, and are given by equation *{6.1.1.1-5}* to *{6.1.1.1-7}*.

For continuous measurements, the axial acceleration effect must also be included in the uncertainty study. It is given by

$$dg_{x'4} = -\sin\gamma da_z \qquad \{6.1.1.1\text{-}15\}$$

6.1.1.2 *Gravity Inclination*

There are many known accelerometer arrangements used in different types of directional surveying gyro instruments. The inclination uncertainty associated with the most common instruments used in the Norwegian North Sea sector will in the following be presented on an instrument type basis. The optimal three accelerometer configuration known from magnetic instruments is not very common for gyro instruments. It is, however, known in for example the Sperry-Sun G2 (Russell [20]). This instrument is unusual in Norway, and is therefore not a part of this study. It is expected that the majority of high accuracy gyro instruments will be transformed to three accelerometer systems in the near future. It is a strong request for this in the marked, and three accelerometer systems are therefore included to simplify uncertainty software adjustment when this change take place.

Three Accelerometer Systems

Available three accelerometer gyro systems do have the accelerometers mounted along the principal axes (*x, y, z*). The uncertainty in inclination (*dI*) due to accelerometer uncertainties, can therefore be estimated with the same type of equations as for magnetic instruments. Accelerometer uncertainties (dg_{xi}, dg_{yi}, and dg_{zi}) are given in equations *{6.1.1.1-2}* to *{6.1.1.1-11}*.

$$dI_1 = -\frac{\cos I \sin\tau}{G} dg_{x1} \qquad \{6.1.1.2\text{-}1\}$$

$$dI_2 = -\frac{\cos I \sin\tau}{G} dg_{x2} \qquad \{6.1.1.2\text{-}2\}$$

$$dI_3 = -\frac{\cos I \cos\tau}{G} dg_{y1} \qquad \{6.1.1.2\text{-}3\}$$

$$dI_4 = -\frac{\cos I \cos\tau}{G} dg_{y2} \qquad \{6.1.1.2\text{-}4\}$$

$$dI_5 = -\frac{\sin I}{G} dg_{z1} \qquad \{6.1.1.2\text{-}5\}$$

$$dI_6 = -\frac{\sin I}{G} dg_{z2} \qquad \{6.1.1.2\text{-}6\}$$

Continuous tool suffering from larger axial accelerations will need an additional uncertainty term given by

$$dI_{11} = \frac{\partial I}{\partial g_z} dg_{z4} = -\frac{\sin I}{G} dg_{z4} \qquad \{6.1.1.2\text{-}7\}$$

Traditional Free Gyros

Old free gyros do usually have two accelerometers mounted along the *x*- and *y*- axis. The inclination uncertainty components caused by accelerometer uncertainties (dg_{xi} and dg_{yi}) given in equations *{6.1.1.1-2}* to *{6.1.1.1-7}* can be estimated with the same set of equations as for magnetic instruments with axial corrections. The mathematical solution turn out to be identical. The same equations must of course also be used for continuous three accelerometer gyro systems when axial gravity corrections are applied.

$$dI_1 = -\frac{\sin\tau}{G\cos I}dg_{x1} \qquad \{6.1.1.2\text{-}8\}$$

$$dI_2 = -\frac{\sin\tau}{G\cos I}dg_{x2} \qquad \{6.1.1.2\text{-}9\}$$

$$dI_3 = -\frac{\cos\tau}{G\cos I}dg_{y1} \qquad \{6.1.1.2\text{-}10\}$$

$$dI_4 = -\frac{\cos\tau}{G\cos I}dg_{y2} \qquad \{6.1.1.2\text{-}11\}$$

$$dI_7 = -\frac{\sin I}{G\cos I}dG \qquad \{6.1.1.2\text{-}12\}$$

Stationary Gyrodata Instruments

The Gyrodata Wellbore Surveyor and the Gyrodata Continuous Tool, are both in the traditional design equipped with one dual axis accelerometer package with the two sensitive axis directed along the *x*- and *y*- axis. The design of the new small diameter version is, however, different from this. It is equipped with two single axis accelerometers (same sensitivity axis). There is no error theoretical difference between these two configurations. The dual axis accelerometer has according to documentation given by Gyrodata very little correlation between the two sensitivity axis.

The Wellbore Surveyor is a stationary instrument (Uttecht [21]), and the Continuous Tool has two operational modes (Noy [22]). Stationary measurements used up to about 15°, and continuous high speed measurements above 15°. Stationary measurements can be used at higher inclinations if desired. The two instrument types have identical sensor packages, which means that the Continuous Tool can be looked on as a Wellbore Surveyor, if used to stationary measurements at higher inclinations. The accelerometer measurements are the principal source for inclination determination in stationary mode, while both inclination and / or gyro measurements can be used in continuous mode. The continuous inclination uncertainty will therefore be covered in the gyro uncertainty chapter (6.1.1.6). Stationary Gyrodata tools make use of two combined accelerometer measurements in the inclination determination. The two measurements are taken at different toolfaces (180° apart from each other). They are obtained by rotation (indexing) of the sensor package inside the instrument collar, and not by rotation of the collar it self. The following equation is used to compute the inclination

$$I = \arcsin\frac{\sqrt{\left(g_{x,\tau}-g_{x,\tau+180}\right)^2+\left(g_{y,\tau}-g_{y,\tau+180}\right)^2}}{2G} \qquad \{6.1.1.2\text{-}13\}$$

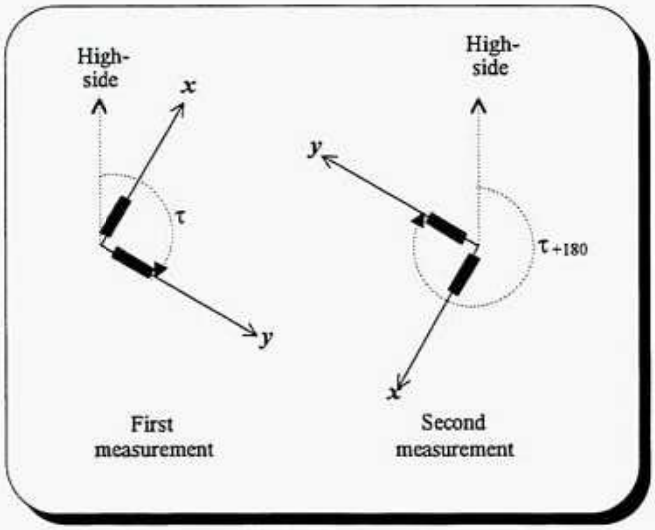

Figure 6.1.1.2-1 Relationship between the two measurements at each station in stationary Gyrodata mode

This gives the following inclination uncertainty components when the correlation between the two measurements originating from the same sensors are taken into consideration

$$dI_1 = \frac{\partial I}{\partial g_{x,\tau}} dg_{x1,\tau} + \frac{\partial I}{\partial g_{x,\tau+180}} dg_{x1,\tau+180} = 0 \qquad \{6.1.1.2\text{-}14\}$$

$$dI_2 = \frac{\partial I}{\partial g_{x,\tau}} dg_{x2,\tau} + \frac{\partial I}{\partial g_{x,\tau+180}} dg_{x2,\tau+180} = \frac{\sin I \sin^2 \tau}{\cos I} d\upsilon_a \qquad \{6.1.1.2\text{-}15\}$$

$$dI_3 = \frac{\partial I}{\partial g_{y,\tau}} dg_{y1,\tau} + \frac{\partial I}{\partial g_{y,\tau+180}} dg_{y1,\tau+180} = 0 \qquad \{6.1.1.2\text{-}16\}$$

$$dI_4 = \frac{\partial I}{\partial g_{y,\tau}} dg_{y2,\tau} + \frac{\partial I}{\partial g_{y,\tau+180}} dg_{y2,\tau+180} = \frac{\sin I \cos^2 \tau}{\cos I} d\upsilon_a \qquad \{6.1.1.2\text{-}17\}$$

$$dI_7 = \frac{\partial I}{\partial g_{x,\tau}} dg_{x3,\tau} + \frac{\partial I}{\partial g_{x,\tau+180}} dg_{x3,\tau+180} + \frac{\partial I}{\partial g_{y,\tau}} dg_{y3,\tau} + \frac{\partial I}{\partial g_{y,\tau+180}} dg_{y3,\tau+180}$$
$$= -\frac{\sin I}{G \cos I} dG \qquad \{6.1.1.2\text{-}18\}$$

This shows that the accelerometer biases are without significance for this type of measurements.

Scientific Drilling Controls Instruments (SDC)

Finder and Keeper (gyro instruments from SDC) are usually built with two accelerometer mounted in a non orthogonal co-ordinate system. The standard design is one *y*-accelerometer and one accelerometer (*x'*) canted in the *x-z* plane. Both systems have different operational modes depending on wellbore inclination. Finder has two modes, and Keeper has three.

The two Finder modes are stationary (up to ca 15° wellbore inclinations) and continuous high speed mode (above 15°). The stationary mode (often referred to as gyro compassing or north seeking) makes use of rotation of the sensor package (carouselling). Four measurements taken at different toolfaces (90° apart from each other). The *y*-accelerometer is connected to a servo motor, which is forcing the *y*- accelerometer output to always be as near zero as possible in the continuous mode. The *y*- accelerometer is because of this aligned in the horizontal plane during continuous measurements, which therefore is call the vertical stabilised mode.

The three Keeper modes are stationary (used for initialisation at inclinations below 2°), continuous high speed low angle (used from initialisation to ca 20°) and continuous high speed high angle (used above 20°). The stationary and high angle modes are identical to similar Finder modes. The low angle mode is an inertial stabilised mode where the azimuth toolface is held fixed in space by a servo motor steered by gyro outputs.

If desired, both Finder and Keeper can be used for stationary measurements at higher inclinations than the upper limits outlined in these standard operational procedures.

Continuous Finder and High Angle Keeper

The inclination is in the vertical stabilised case (Brown [23]) calculated by the following equation

$$I = \arcsin\left(-\frac{g_{x'}}{G}\right) - \gamma \qquad \{6.1.1.2\text{-}19\}$$

where γ is the x'- accelerometer cant angle.

The inclination uncertainty due to the accelerometer uncertainties and the cant angle uncertainty are then given by

$$dI_1 = \frac{\partial I}{\partial g_{x'}} dg_{x'1} = -\frac{1}{G\cos(I+\gamma)} dg_{x'1} \qquad \{6.1.1.2\text{-}20\}$$

$$dI_2 = \frac{\partial I}{\partial g_{x'}} dg_{x'2} = -\frac{1}{G\cos(I+\gamma)} dg_{x'2} \approx \frac{\sin(I+\gamma)}{\cos(I+\gamma)} d\upsilon_a \qquad \{6.1.1.2\text{-}21\}$$

$$dI_7 = \frac{\partial I}{\partial g_{x'}} dg_{x'3} = -\frac{\sin(I+\gamma)}{G\cos(I+\gamma)} dG \qquad \{6.1.1.2\text{-}22\}$$

$$dI_{11} = \frac{\partial I}{\partial g_{x'}} dg_{x'4} = -\frac{1}{G\cos(I+\gamma)} dg_{x'4} \qquad \{6.1.1.2\text{-}23\}$$

$$dI_{12} = \frac{\partial I}{\partial \gamma} d\gamma = -d\gamma \qquad \{6.1.1.2\text{-}24\}$$

$d\gamma$ the cant misalignment angle. $dg_{x'1}$, $dg_{x'2}$, $dg_{x'3}$ and $dg_{x'4}$ are given in equations *{6.1.1.1-12}* to *{6.1.1.1-15}* when the toolface is set to 90°. $dg_{x'2}$ is for example equal to

$$dg_{x'2} = g_{x'}d\upsilon_a \approx -G\sin(I+\gamma)d\upsilon_a \qquad \{6.1.1.2\text{-}21\}$$

dI_{12} is usually systematic for all measurements with one instrument, at least in periods between mechanical adjustments. This means a systematic within surveys and random between surveys error propagation nature.

Given a negative cant angle, there is no breakdown in the accuracy for horizontal wellbores in this case.

Stationary SDC Instruments

The stationary SDC inclination is calculated by the following equation

$$I = \arcsin\frac{\sqrt{\left(g_{x',\tau}-g_{x',\tau+180}\right)^2+\left(g_{x',\tau+90}-g_{x',\tau+270}\right)^2}}{2G\cos\gamma} \qquad \{6.1.1.2\text{-}25\}$$

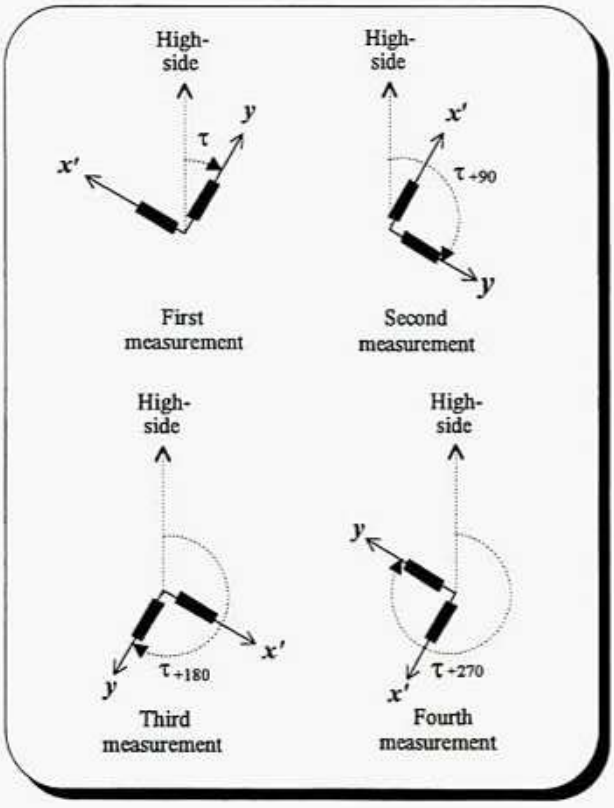

Figure 6.1.1.2-2 Relationship between the four measurements at each station in stationary SDC modes

This gives the following inclination uncertainties when the correlation between the four measurements is taken into consideration

$$dI_1 = \frac{\partial I}{\partial g_{x',\tau}} dg_{x'1,\tau} + \frac{\partial I}{\partial g_{x',\tau+180}} dg_{x'1,\tau+180} + \frac{\partial I}{\partial g_{x',\tau+90}} dg_{x'1,\tau+90} + \frac{\partial I}{\partial g_{x',\tau+270}} dg_{x'1,\tau+270} = 0 \qquad \{6.1.1.2\text{-}26\}$$

$$dI_2 = \frac{\partial I}{\partial g_{x',\tau}} dg_{x'2,\tau} + \frac{\partial I}{\partial g_{x',\tau+180}} dg_{x'2,\tau+180} + \frac{\partial I}{\partial g_{x',\tau+90}} dg_{x'2,\tau+90} + \frac{\partial I}{\partial g_{x',\tau+270}} dg_{x'2,\tau+270} \approx \frac{\sin I}{\cos I} d\omega_a \qquad \{6.1.1.2\text{-}27\}$$

$$dI_7 = \frac{\partial I}{\partial g_{x',\tau}} dg_{x'3,\tau} + \frac{\partial I}{\partial g_{x',\tau+180}} dg_{x'3,\tau+180} + \frac{\partial I}{\partial g_{x',\tau+90}} dg_{x'3,\tau+90} + \frac{\partial I}{\partial g_{x',\tau+270}} dg_{x'3,\tau+270} = -\frac{\sin I}{G\cos I} dG \qquad \{6.1.1.2\text{-}28\}$$

$$dI_{12} = \frac{\sin I \sin\gamma}{\cos I \cos\gamma} d\gamma \qquad \{6.1.1.2\text{-}29\}$$

This shows that the accelerometer biases is without significance also for SDC tools while gyro compassing.

Continuous Low Angle Keeper

The inclination is in the inertial stabilised mode calculated by

$$I = \arctan \frac{\sqrt{\left(g_{x'}\cos\gamma + \sqrt{G^2 - g_{x'}^2 - g_y^2}\,\sin\gamma\right)^2 + g_y^2}}{\sqrt{G^2 - g_{x'}^2 - g_y^2}\,\cos\gamma - g_{x'}\sin\gamma} \qquad \{6.1.1.2\text{-}30\}$$

where γ again is the cant angle, and τ the toolface ($\tau \approx 90°$). The inclination uncertainty is then given by

$$dI_1 = \frac{\partial I}{\partial g_{x'}} dg_{x'1} = -\frac{\sin\tau}{G(\cos I\cos\gamma - \sin I\sin\tau\sin\gamma)} dg_{x'1} \approx -\frac{1}{G\cos(I+\gamma)} dg_{x'1} \qquad \{6.1.1.2\text{-}31\}$$

$$dI_2 = \frac{\partial I}{\partial g_{x'}} dg_{x'2} = -\frac{\sin\tau}{G(\cos I\cos\gamma - \sin I\sin\tau\sin\gamma)} dg_{x'2} \approx -\frac{1}{G\cos(I+\gamma)} dg_{x'2} \qquad \{6.1.1.2\text{-}32\}$$

$$dI_3 = \frac{\partial I}{\partial g_y} dg_{y1} = -\frac{\cos\tau}{G(\cos I\cos\gamma - \sin I\sin\tau\sin\gamma)} dg_{y1} \approx 0 \qquad \{6.1.1.2\text{-}33\}$$

$$dI_4 = \frac{\partial I}{\partial g_y} dg_{y2} = -\frac{\cos\tau}{G(\cos I\cos\gamma - \sin I\sin\tau\sin\gamma)} dg_{y2} \approx 0 \qquad \{6.1.1.2\text{-}34\}$$

$$dI_7 = \frac{\partial I}{\partial g_{x'}} dg_{x'3} + \frac{\partial I}{\partial g_{y3}} dg_{y3} = \frac{\cos I\sin\tau\sin\gamma + \sin I\cos\gamma}{G(\cos I\cos\gamma - \sin I\sin\tau\sin\gamma)} dG \approx -\frac{\sin(I+\gamma)}{G\cos(I+\gamma)} dG \qquad \{6.1.1.2\text{-}35\}$$

$$dI_{11} = \frac{\partial I}{\partial g_{x'}} dg_{x'4} = -\frac{\sin\tau}{G(\cos I\cos\gamma - \sin I\sin\tau\sin\gamma)} dg_{x'4} \approx -\frac{1}{G\cos(I+\gamma)} dg_{x'4} \qquad \{6.1.1.2\text{-}36\}$$

$$dI_{12} = \frac{\partial I}{\partial \gamma} d\gamma = -\sin\tau\, d\gamma \approx -d\gamma \qquad \{6.1.1.2\text{-}37\}$$

Canted accelerometer uncertainties are given in equations *{6.1.1.1-12}* to *{6.1.1.1-15}*.

6.1.1.3 *Gravity Toolface*

The high-side toolface uncertainty will in this chapter be presented for the same instrument types as presented in the previous chapter (6.1.1.2).

Three Accelerometer Systems, Free Gyros, and Continuous Gyrodata Instruments

The high-side toolface (τ) is for all these instruments given by

$$\tau = \arctan\frac{-g_x}{-g_y} \qquad \{6.1.1.3\text{-}1\}$$

The high-side toolface uncertainty ($d\tau$) is then given by

$$d\tau \approx \sqrt{\frac{d\eta_a^2}{G\sin I} + \sin^2\tau\cos^2\tau d\upsilon_a^2} \qquad \{6.1.1.3\text{-}2\}$$

where G is the local gravity and I the inclination.

Stationary Gyrodata Instruments

The high-side toolface for these high-side plane indexing systems is given by

$$\tau = \arctan\frac{-g_{x,\tau}+g_{x,\tau+180}}{-g_{y,\tau}+g_{y,\tau+180}} \qquad \{6.1.1.3\text{-}3\}$$

which gives the following toolface uncertainty

$$d\tau = \sqrt{\left(\frac{\partial\tau dg_{x1}}{\partial g_{x,\tau}} + \frac{\partial\tau dg_{x1,\tau+180}}{\partial g_{x,\tau+180}}\right)^2 + \left(\frac{\partial\tau dg_{x2}}{\partial g_{x,\tau}} + \frac{\partial\tau dg_{x2,\tau+180}}{\partial g_{x,\tau+180}}\right)^2 + \left(\frac{\partial\tau dg_{y1}}{\partial g_{y,\tau}} + \frac{\partial\tau dg_{y1,\tau+180}}{\partial g_{y,\tau+180}}\right)^2 + \left(\frac{\partial\tau dg_{y2}}{\partial g_{y,\tau}} + \frac{\partial\tau dg_{y2,\tau+180}}{\partial g_{y,\tau+180}}\right)^2}$$

$$\approx 0 \qquad \{6.1.1.3\text{-}4\}$$

This equation does not give any toolface uncertainty, which it obviously should have done. Random measurement errors will always be present. They should therefore have been included in the error budget in this case when biases and scale factor uncertainties turn out to be without significance. The toolface uncertainty caused by random accelerometer uncertainties are given by

$$d\tau = \sqrt{\left(\frac{\partial\tau d\sigma_a}{\partial g_{x,\tau}}\right)^2 + \left(\frac{\partial\tau d\sigma_a}{\partial g_{x,\tau+180}}\right)^2 + \left(\frac{\partial\tau d\sigma_a}{\partial g_{y,\tau}}\right)^2 + \left(\frac{\partial\tau d\sigma_a}{\partial g_{y,\tau+180}}\right)^2} = \frac{1}{\sqrt{2}\,G\sin I}d\sigma_a \qquad \{6.1.1.3\text{-}5\}$$

where $d\sigma_a$ is the random between stations accelerometer uncertainty.

Page 89 Equation *{6.1.1.3-2}* $d\tau \approx \sqrt{\frac{d\eta_a^2}{G^2\sin^2 I} + 2\sin^2\tau\cos^2\tau d\upsilon_a^2}$

Continuous Finder and High Angle Keeper

The theoretical *x*- axis is in the continuous Finder and the high angle Keeper modes kept vertical by *z*- axis rotations with respect to the instrument housing. The inertial toolface is measured with a *z*- axis rotation angle sensor. This angle, which might be important for steering applications, is not very interesting in connection with position uncertainty studies. It is not used as input in any angular or position calculations. The "sensor package gravity toolface", which is maintained to about 90° by *z*- axis rotations, is , on the other hand, needed in the gyro azimuth calculation. The "sensor package gravity toolface" for a vertical stabilised canted system, is then given by

$$\tau = \arccos\left(-\frac{g_y}{G\sin I}\right) \qquad \{6.1.1.3\text{-}6\}$$

and the toolface uncertainty is given by

$$d\tau = \sqrt{\left(\frac{\partial\tau}{\partial g_y}\right)^2\left(dg_{y1}^2 + dg_{y2}^2 + dg_{y3}^2\right)^2} \approx \frac{1}{G\sin I}d\eta_a \qquad \{6.1.1.3\text{-}7\}$$

Stationary Scientific Drilling Controls Instruments

The high-side toolface for these canted high-side plane carouselling systems is given by

$$\tau = \arctan\frac{-g_{x',\tau}+g_{x',\tau+180}}{-g_{x',\tau+90}+g_{x',\tau+270}} \qquad \{6.1.1.3\text{-}8\}$$

The toolface uncertainty is then given by

$$d\tau = \sqrt{\left(\frac{\partial\tau d g_{x'1,\tau}}{\partial g_{x',\tau}} + \frac{\partial\tau d g_{x'1,\tau+180}}{\partial g_{x',\tau+180}} + \frac{\partial\tau d g_{x'1,\tau+90}}{\partial g_{x',\tau+90}} + \frac{\partial\tau d g_{x'1,\tau+270}}{\partial g_{x',\tau+270}}\right)^2 + \left(\frac{\partial\tau d g_{x'2,\tau}}{\partial g_{x',\tau}} + \frac{\partial\tau d g_{x'2,\tau+180}}{\partial g_{x',\tau+180}} + \frac{\partial\tau d g_{x'2,\tau+90}}{\partial g_{x',\tau+90}} + \frac{\partial\tau d g_{x'2,\tau+270}}{\partial g_{x',\tau+270}}\right)^2}$$

$$\approx 0 \qquad \{6.1.1.3\text{-}9\}$$

As in the stationary Gyrodata case, this equation indicates error free toolface determinations. Random accelerometer uncertainties must therefore be included in the error budget. This gives the following toolface uncertainty

$$d\tau = \sqrt{\left(\frac{\partial\tau d\sigma_a}{\partial g_{x',\tau}}\right)^2 + \left(\frac{\partial\tau d\sigma_a}{\partial g_{x',\tau+180}}\right)^2 + \left(\frac{\partial\tau d\sigma_a}{\partial g_{x',\tau+90}}\right)^2 + \left(\frac{\partial\tau d\sigma_a}{\partial g_{x',\tau+270}}\right)^2} = \frac{1}{\sqrt{2}\,G\sin I\cos\gamma}d\sigma_a \qquad \{6.1.1.3\text{-}10\}$$

6.1.1.4 Rotor Gyros

Gyros are designed for measurement of angular rates. Many gyro types are available, but rotor gyros are with one exception the only used type in wellbore surveying. The orientation of a rotor gyro is defined by its input-, output- and spin axis (usually aligned along the *x*-, *y*- and *z*- axis). The input- and output axes are placed in the gyro rotation plane, and the spin axis is identical to the gyro rotation axis. The output axis is the sensitive axis where measurements are taken. These measurements, which actually are torque measurements, are proportional to the angular rate around the input axis. Directional gyro instruments are usually equipped with one or two rotor gyros. There is, however, a marked demand for three gyro systems, and such instruments are likely to be available in the near future. Both single axis and dual axis gyros are in use.

Gyro measurements are together with inclination and toolface measurements used to calculate the azimuth. This is either done in a stationary north seeking mode (gyro compassing), or in a continuous mode where relative changes in azimuth are measured. Modern high accuracy continuous gyro system have the possibility to work in both modes. Error characteristics are quite different in stationary and continuous modes, and they will be handled separately.

For properly calibrated instruments with adequate quality control procedures, gyro sensor errors can be divided into two classes, mass unbalances and sensor reading errors. Mass unbalances are a result of imperfect gyro manufacturing, and consists of three parts (spin axis (M_s), input axis (M_i) and output axis (M_o) mass unbalances). Their effects on the azimuth determination are relatively large, and mass unbalances are because of this modelled in the motion equations. Mass unbalances are changing with time due to time dependent effects like creep, thermal expansion etc. The uncertainty this creates with respect to the modelled mass unbalance has to be included in the gyro error budget.

Mass unbalances are usually determined during instrument calibration. Their uncertainties can therefore be defined as the standard deviation in mass unbalance updates determined through multiple calibrations with different instruments and variable calibration cycles. This definition is adequate for surveys with older gyro instruments, but not for modern high accuracy gyro surveys where the effect of mass unbalance uncertainties can be reduced through zero velocity updates at regular intervals etc. The effective mass unbalance uncertainties (dM_s, dM_i and dM_o) are then reduced compared to what is given by the definition. For modern high accuracy gyro surveys, it is convenient to define mass unbalance uncertainties as the standard deviation in calibration mass unbalance updates for gyro compassing surveys (dM_{ns}, dM_{ni} and dM_{no}), and as half the standard deviation in consecutive zero velocity mass unbalance updates for continuous measurements (dM_{cs}, dM_{ci} and dM_{co}). Half is used for continuous measurements because effective mass unbalance uncertainties are near zero immediately after an update, and near the next measured mass unbalance update immediately before the next update. The measured update values should be used in stead of statistical figures in final survey studies.

As for mass unbalances, biases and scale factors do also change with time, and the effect of their uncertainties are reduced through zero velocity updates in high accuracy

continuous surveys. It is therefore necessary to distinguish between gyro compassing- and continuous reading errors. North seeking related error sources are the bias north seeking $d\eta_{ng}$ and the linear north seeking scale factor $d\upsilon_{ng}$, and continuous gyro related error sources are the continuous bias $d\eta_{cg}$ and the linear continuous scale factor $d\upsilon_{cg}$.

Random components are, because of the systematic error dominance in longer wellbore sections, usually without significance in position uncertainty studies.

The principal output from an error free rotor gyro is, according to Savage [24], the torque vector **T** (torque on the spinning mass), which is given by

$$\mathbf{T} = \omega_H \times \mathbf{H} \qquad \{6.1.1.4\text{-}1\}$$

H is the angular momentum vector of the spinning mass, and ω_H the angular rotation perpendicular to **H**. This torque can easily be scaled to an angular rate equivalent, which is the actual gyro measurement used in this document.

Gyro dependent bias and scale factor uncertainties are in the following given for the instruments covered in the inclination chapter (6.1.1.2). Scale factor equations are derived with the assumption that the expectation of mass unbalances are equal to zero for a large population of tools. This assumption is confirmed by Brett H. van Steenwyk at Scientific Drilling Controls.

Stationary Gyrodata Instruments

This is a one dual axis gyro instrument with the spin axis aligned along the *z*- axis (Noy [22]), see figure 6.1.1.5-1. The scaled stationary Gyrodata gyro uncertainties are given by

$$dT_{nx1} = dT_{nx1,\tau} = d\eta_{ng} \qquad \{6.1.1.4\text{-}2\}$$
$$dT_{nx2} = dT_{nx2,\tau} = T_{x,\tau} d\upsilon_{ng} \qquad \{6.1.1.4\text{-}3\}$$
$$T_{x,\tau} \approx \Omega\cos\phi(\cos I\cos A\cos\tau - \sin A\sin\tau) + \Omega\sin\phi\sin I\cos\tau \qquad \{6.1.1.4\text{-}4\}$$

$$dT_{nx1,\tau+180} = dT_{nx1} \qquad \{6.1.1.4\text{-}5\}$$
$$dT_{nx2,\tau+180} = T_{x,\tau+180} d\upsilon_{ng} = -dT_{nx2} \qquad \{6.1.1.4\text{-}6\}$$
$$T_{x,\tau+180} \approx -\Omega\cos\phi(\cos I\cos A\cos\tau - \sin A\sin\tau) + \Omega\sin\phi\sin I\cos\tau \qquad \{6.1.1.4\text{-}7\}$$

$$dT_{ny1} = dT_{ny1,\tau} = d\eta_{ng} \qquad \{6.1.1.4\text{-}8\}$$
$$dT_{ny2} = dT_{ny2,\tau} = T_{y,\tau} d\upsilon_{ng} \qquad \{6.1.1.4\text{-}9\}$$
$$T_{y,\tau} \approx -\Omega\cos\phi(\cos I\cos A\sin\tau + \sin A\cos\tau) - \Omega\sin\phi\sin I\sin\tau \qquad \{6.1.1.4\text{-}10\}$$

$$dT_{ny1,\tau+180} = dT_{ny1} \qquad \{6.1.1.4\text{-}11\}$$
$$dT_{ny2,\tau+180} = T_{y,\tau+180} d\upsilon_{ng} = -dT_{ny2} \qquad \{6.1.1.4\text{-}12\}$$
$$T_{y,\tau+180} \approx \Omega\cos\phi(\cos I\cos A\sin\tau + \sin A\cos\tau) - \Omega\sin\phi\sin I\sin\tau \qquad \{6.1.1.4\text{-}13\}$$

Page 92 Equation {6.1.1.4-7} $T_{x,\tau+180} \approx -\Omega\cos\phi(\cos I\cos A\cos\tau - \sin A\sin\tau) - \Omega\sin\phi\sin I\cos\tau$
Equation {6.1.1.4-13} $T_{y,\tau+180} \approx \Omega\cos\phi(\cos I\cos A\sin\tau + \sin A\cos\tau) + \Omega\sin\phi\sin I\sin\tau$

Ω is the earth angular rate at the equator, and ϕ the local latitude.

The $T_{x,\tau+180}$ and $T_{y,\tau+180}$ measurements are obtained by a 180° indexing from the $T_{x,\tau}$ and $T_{y,\tau}$ measurements in the high-side toolface plane. The two T_x measurements are because of this fully correlated. The same is the case for the two T_y measurements.

Continuous Gyrodata Instruments

The continuous sensor package is identical to the stationary package, and the continuous Gyrodata gyro uncertainties (dT_{cx1}, dT_{cx2}, dT_{cy1} and dT_{cy2}) are then given by

$$dT_{cx1} = d\eta_{cg} \qquad \{6.1.1.4\text{-}14\}$$

$$dT_{cx2} = T_x d\upsilon_{cg} \qquad \{6.1.1.4\text{-}15\}$$

$$T_x \approx \frac{\Delta I \sin\tau - \Delta A \sin I \cos\tau + \Omega \cos\phi(\cos I \cos A \cos\tau - \sin A \sin\tau)\Delta t + \Omega \sin\phi \sin I \cos\tau \Delta t}{\Delta t} \qquad \{6.1.1.4\text{-}16\}$$

$$dT_{cy1} = d\eta_{cg} \qquad \{6.1.1.4\text{-}17\}$$

$$dT_{cy2} = T_y d\upsilon_{cg} \qquad \{6.1.1.4\text{-}18\}$$

$$T_y \approx \frac{\Delta I \cos\tau + \Delta A \sin I \sin\tau - \Omega \cos\phi(\cos I \cos A \sin\tau + \sin A \cos\tau)\Delta t - \Omega \sin\phi \sin I \sin\tau \Delta t}{\Delta t} \qquad \{6.1.1.4\text{-}19\}$$

Δt is the time difference between two consecutive measurement recordings, ΔI and ΔA the inclination and azimuth change between the same two recordings (stations). It is, with reference to the standard high continuous measurement recording frequency (5 to 30 meters for standard wellbore curvatures, and 1 to 5 meters for short radius curvatures), assumed small angular changes and a relative uniform wellbore geometry between the two stations (no corkscrewing effects etc.). ΔI and ΔA can therefore without loss of accuracy be estimated with the actual survey results in final survey accuracy studies, and by the planned wellbore profile in uncertainty predictions.

Δt is usually an unknown quantity in directional surveying. It can roughly be estimated by the planned or experienced average logging speed (v), and the measured depths at the two consecutive measurement stations (D_j and D_{j+1}). Their difference can for standard operations (with nearly constant output frequency) be substituted with the average station separation (ΔD). Δt is then given by

$$\Delta t \approx \frac{D_{j+1} - D_j}{v} \approx \frac{\Delta D}{v} \qquad \{6.1.1.4\text{-}20\}$$

Stationary Finder and Keeper

These are in stationary mode basically single axis single gyro instruments, with the spin axis aligned along the y- axis and the output axis along the z- axis (Brown [23]), see figure 6.1.1.5-2. The stationary SDC scaled gyro uncertainties are given by

Page 93 Line 1 *earth angular rate at the equator* should be **earth angular rate**

$$dT_{nz1} = dT_{nz1,\tau} = d\eta_{ng} \qquad \{6.1.1.4\text{-}21\}$$
$$dT_{nz2} = dT_{nz2,\tau} = T_{z,\tau} d\upsilon_{ng} \qquad \{6.1.1.4\text{-}22\}$$
$$T_{z,\tau} \approx \Omega\cos\phi(\cos I\cos A\sin\tau + \sin A\cos\tau) + \Omega\sin\phi\sin I\sin\tau \qquad \{6.1.1.4\text{-}23\}$$

$$dT_{nz1,\tau+180} = dT_{nz1} \qquad \{6.1.1.4\text{-}24\}$$
$$dT_{nz2,\tau+180} = T_{z,\tau+180} d\upsilon_{ng} = -dT_{nz2} \qquad \{6.1.1.4\text{-}25\}$$
$$T_{z,\tau+180} \approx -\Omega\cos\phi(\cos I\cos A\sin\tau + \sin A\cos\tau) + \Omega\sin\phi\sin I\sin\tau \qquad \{6.1.1.4\text{-}26\}$$

$$dT_{nz1,\tau+90} = dT_{nz1} \qquad \{6.1.1.4\text{-}27\}$$
$$dT_{nz'2} = dT_{nz2,\tau+90} = T_{z,\tau+90} d\upsilon_{ng} \qquad \{6.1.1.4\text{-}28\}$$
$$T_{z,\tau+90} \approx -\Omega\cos\phi(\cos I\cos A\cos\tau - \sin A\sin\tau) - \Omega\sin\phi\sin I\cos\tau \qquad \{6.1.1.4\text{-}29\}$$

$$dT_{nz1,\tau+270} = dT_{nz1} \qquad \{6.1.1.4\text{-}30\}$$
$$dT_{nz2,\tau+270} = T_{z,\tau+270} d\upsilon_{ng} = -dT_{nz'2} \qquad \{6.1.1.4\text{-}31\}$$
$$T_{z,\tau+270} \approx \Omega\cos\phi(\cos I\cos A\cos\tau - \sin A\sin\tau) - \Omega\sin\phi\sin I\cos\tau \qquad \{6.1.1.4\text{-}32\}$$

The $T_{z,\tau+90}$, $T_{z,\tau+180}$ and $T_{z,\tau+270}$ measurements are obtained by 90°, 180° and 270° carouselling from the $T_{z,\tau}$ measurement in the high-side toolface plane. These four measurements are obtained by the same sensor, and will be fully correlated.

Continuous Finder and High Angle Keeper

These two instruments are in this mode basically functioning as a vertical stabilised single axis single gyro instruments with the spin axis aligned along the *y*- axis and the output axis along the *z*- axis (Brown [23]), see figure 6.1.1.6-3. The continuous high angle SDC scaled gyro uncertainties (dT_{nz1} and dT_{nz2}) are then given by

$$dT_{cz1} = d\eta_{cg} \qquad \{6.1.1.4\text{-}33\}$$
$$dT_{cz2} = T_z d\upsilon_{cg} \qquad \{6.1.1.4\text{-}34\}$$
$$T_z \approx \frac{-\Delta A\sin I + \Omega(\cos\phi\cos I\cos A + \sin\phi\sin I)\Delta t}{\Delta t} \qquad \{6.1.1.4\text{-}35\}$$

Continuous Low Angle Keeper

This is basically an inertial stabilised single axis single gyro instrument with the spin axis aligned along the *y*- axis and the output axis along the *x*- axis (Brown [23]), see figure 6.1.1.6-4. The scaled continuous low angle Keeper gyro uncertainties (dT_{nx1} and dT_{nx2}) are then given by

$$dT_{cx1} = d\eta_{cg} \qquad \{6.1.1.4\text{-}36\}$$
$$dT_{cx2} = T_x d\upsilon_{cg} \qquad \{6.1.1.4\text{-}37\}$$
$$T_x \approx \frac{-\Delta A\cos I - \Omega(\cos\phi\sin I\cos A - \sin\phi\cos I)\Delta t}{\Delta t} \qquad \{6.1.1.4\text{-}38\}$$

Page 94 Equation {6.1.1.4-26} $T_{z,\tau+180} \approx -\Omega\cos\phi(\cos I\cos A\sin\tau + \sin A\cos\tau) + \Omega\sin\phi\sin I\sin\tau$
Equation {6.1.1.4-32} $T_{z,\tau+270} \approx \Omega\cos\phi(\cos I\cos A\cos\tau - \sin A\sin\tau) - \Omega\sin\phi\sin I\cos\tau$

6.1.1.5 *North Seeking Gyro Azimuth*

North seeking gyro measurements, also commonly referred to as gyro compassing, are stationary measurements. The directional tool has to stop and rest for a small period at each survey station. It is therefore like magnetic MWD a discrete surveying technique, which it is easy to model error theoretically.

North seeking gyros make use of the horizontal earth rotation in their determination. This is a much more stable reference than the magnetic field used for magnetic MWD.

Stationary Gyrodata Instruments

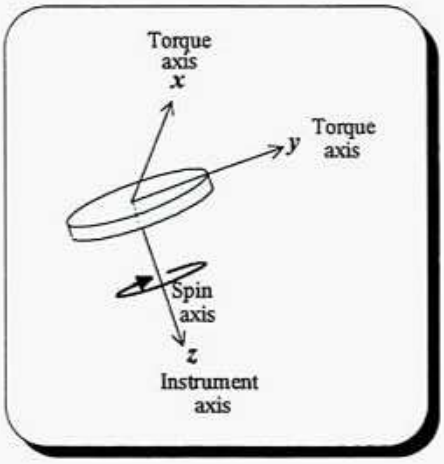

Figure 6.1.1.5-1 Gyro orientation in Gyrodata instruments

The Gyrodata Wellbore Surveyor and the Gyrodata Continuous Tool are both equipped with one dual axis gyro aligned with the spin axis parallel to the *z*- axis. Two measurements are taken at each station (Uttecht [21]). The gyro is indexed 180° in the high-side toolface plane between the two measurements. The azimuth is then calculated with the following equation

$$A = \arctan\frac{\left[\left(T_{x,\tau}-T_{x,\tau+180}\right)\sin\tau+\left(T_{y,\tau}-T_{y,\tau+180}\right)\cos\tau\right]\cos I}{\left(T_{x,\tau}-T_{x,\tau+180}\right)\cos\tau-\left(T_{y,\tau}-T_{y,\tau+180}\right)\sin\tau-2(\Omega\sin\phi+M_{su})\sin I} \qquad \{6.1.1.5\text{-}1\}$$

$T_{x,\tau}$, $T_{x,\tau+180}$, $T_{y,\tau}$ and $T_{y,\tau+180}$ are the *x*- and *y*- gyro measurements taken 180° apart from each other, τ the toolface, I the inclination, Ω the earth rotation rate, ϕ the latitude at the observation point, and M_{su} the gyro compassing spin axis mass unbalance.

The azimuth uncertainty is a function of the combined gyro measurement uncertainties given in equations *{6.1.1.4-2}* to *{6.1.1.4-13}*, the toolface uncertainty ($d\tau$), the sensor dependent inclination uncertainty (dI_s), the latitude uncertainty ($d\phi$), and the gyro compassing spin axis mass unbalance uncertainty (dM_{ns}). The earth rotation rate is well known, and its variations are so small that the uncertainty is without significance in the azimuth calculation. The azimuth uncertainty consists then of the following components (the correlation in each pair of measurements is taken into consideration)

$$dA_7 = \frac{\partial A}{\partial I}dI + \frac{\partial A}{\partial \tau}d\tau = -\frac{\sin A(\cos\phi\sin I\cos A - \sin\phi\cos I)}{\cos\phi\cos I}dI_s - \frac{\cos\phi\left(\sin^2 A + \cos^2 I\cos^2 A\right) + \sin\phi\sin I\cos I\cos A}{\cos\phi\cos I}d\tau$$
$$\approx -\frac{\sin A(\cos\phi\sin I\cos A - \sin\phi\cos I)}{\cos\phi\cos I}dI_s \qquad \{6.1.1.5\text{-}2\}$$

$$dA_{16} = \frac{\partial A}{\partial T_{x,\tau}}dT_{nx1,\tau} + \frac{\partial A}{\partial T_{x,\tau+180}}dT_{nx1,\tau+180} = 0 \qquad \{6.1.1.5\text{-}3\}$$

$$dA_{17} = \frac{\partial A}{\partial T_{x,\tau}}dT_{nx2,\tau} + \frac{\partial A}{\partial T_{x,\tau+180}}dT_{nx2,\tau+180} = -\frac{\cos I\cos A\sin\tau + \sin A\cos\tau}{\Omega\cos\phi\cos I}dT_{nx2} \qquad \{6.1.1.5\text{-}4\}$$

$$dA_{18} = \frac{\partial A}{\partial T_{y,\tau}}dT_{ny1,\tau} + \frac{\partial A}{\partial T_{y,\tau+180}}dT_{ny1,\tau+180} = 0 \qquad \{6.1.1.5\text{-}5\}$$

$$dA_{19} = \frac{\partial A}{\partial T_{y,\tau}}dT_{ny2,\tau} + \frac{\partial A}{\partial T_{y,\tau+180}}dT_{ny2,\tau+180} = -\frac{\cos I\cos A\cos\tau - \sin A\sin\tau}{\Omega\cos\phi\cos I}dT_{ny2} \qquad \{6.1.1.5\text{-}6\}$$

$$dA_{20} = \frac{\partial A}{\partial M_{ns}}dM_{ns} = -\frac{\sin I\sin A}{\Omega\cos\phi\cos I}dM_{ns} \qquad \{6.1.1.5\text{-}7\}$$

$$dA_{21} = \frac{\partial A}{\partial \phi}d\phi = -\frac{\sin I\sin A}{\cos I}d\phi \qquad \{6.1.1.5\text{-}8\}$$

dI_s is given by

$$dI_s = \sqrt{dI_2^2 + dI_4^2 + dI_7^2} \qquad \{6.1.1.5\text{-}9\}$$

The sensor dependent inclination uncertainty components dI_i are given in equations *{6.1.1.2-15}*, *{6.1.1.2-17}* and *{6.1.1.2-18}*.

Equations *{6.1.1.5-2}* to *{6.1.1.5-8}* show that the uncertainty associated with this type of north seeking operations tends towards infinity as the wellbore approaches the horizontal or the latitude approaches the poles.

The inclination and toolface uncertainties used in equation *{6.1.1.5-2}* are, as in the magnetometer case, correlated. It is therefore recommended to divided the dA_7 term into three uncorrelated accelerometer uncertainty components. They are given by

$$dA_{7\_2} = \frac{\partial A}{\partial g_{x,\tau}}dg_{x2,\tau} + \frac{\partial A}{\partial T_{x,\tau+180}}dg_{x2,\tau+180} \approx -\sin I\sin A\sin^2\tau\frac{\cos\phi\sin I\cos A - \sin\phi\cos I}{\cos\phi\cos^2 I}d\upsilon_a$$
$$-\sin\tau\cos\tau\frac{\cos\phi\left(\sin^2 A + \cos^2 I\cos^2 A\right) + \sin\phi\sin I\cos I\cos A}{\cos\phi\cos I}d\upsilon_a \qquad \{6.1.1.5\text{-}10\}$$

$$dA_{7\_4} = \frac{\partial A}{\partial g_{x,\tau}} dg_{y2,\tau} + \frac{\partial A}{\partial T_{y,\tau+180}} dg_{y2,\tau+180} \approx -\sin I \sin A \cos^2\tau \frac{\cos\phi \sin I \cos A - \sin\phi \cos I}{\cos\phi \cos^2 I} d\upsilon_a$$
$$+\sin\tau \cos\tau \frac{\cos\phi\left(\sin^2 A + \cos^2 I \cos^2 A\right) + \sin\phi \sin I \cos I \cos A}{\cos\phi \cos I} d\upsilon_a \qquad \{6.1.1.5\text{-}11\}$$

$$dA_{7\_7} = \frac{\partial I}{\partial G} dG = \sin I \sin A \frac{\cos\phi \sin I \cos A - \sin\phi \cos I}{G \cos\phi \cos^2 I} dG \qquad \{6.1.1.5\text{-}12\}$$

$d\upsilon_a$ is the accelerometer scale factor uncertainty, and dG the uncertainty in the gravity.

Accelerometer biases do not result in any gyro compassing azimuth uncertainty for carouselling systems. They where in chapter 6.1.1.2 and 6.1.1.3 proven not to have any influence on the inclination or toolface accuracy, and can because of the relationships in equation *{6.1.1.5-1}* neither affect the azimuth accuracy.

dA_{7_2} and dA_{7_4} are systematic within surveys and random between surveys as long as different instruments are in use. dA_{7_7} is systematic within an entire field.

Inclination and azimuth uncertainty components originating from the same error source are correlated with each other, and should be treated as correlated errors in the position co-variance matrix calculation. The following uncertainty components are correlated in this case

- dI_2 and dA_{7_2} (Both caused by the *x*- accelerometer scale factor uncertainty)
- dI_4 and dA_{7_4} (Both caused by the *y*- accelerometer scale factor uncertainty)
- dI_7 and dA_{7_7} (Both caused by the uncertainty in the local gravity)

The Gyrodata Continuous Tool are mechanically identical to the Gyrodata Wellbore Surveyor, which is purely a gyro compassing instrument. The standard Continuous Tool running procedure is, however, to make north seeking measurements only at low inclinations below ca 15°. The presented uncertainty equations will therefore mostly be used in connection with Wellbore Surveyor surveys and Continuous Tool surveys below 15°.

Stationary Finder and Keeper

Finder is according to Brown [23] equipped with one single axis *y*- spin gyro with *z*- axis output, and Keeper with two single axis *y*- spin gyros with orthogonal outputs. The Keeper does, however, only make use of the *z*- gyro output in connection with north seeking measurements. Finder and Keeper are therefore mechanically identical in stationary mode. Four *z*- gyro measurements are taken at each stationary station. The gyro is carouselled 90° in the high-side toolface plane between each measurement. The azimuth is then calculated with the following equation

$$A = \arctan \frac{\left[\left(T_{z,\tau+90} - T_{z,\tau+270}\right)\sin\tau + \left(T_{z,\tau} - T_{z,\tau+180}\right)\cos\tau\right) + 2M_{ni}\sin I\Big]\cos I}{-\left(T_{z,\tau+90} - T_{z,\tau+270}\right)\cos\tau + \left(T_{z,\tau} - T_{z,\tau+180}\right)\sin\tau - 2(\Omega\sin\phi + M_{ns})\sin I} \qquad \{6.1.1.5\text{-}13\}$$

$T_{z,\tau}$, $T_{z,\tau+90}$, $T_{z,\tau+180}$ and $T_{z,\tau+270}$ are the four gyro measurements taken at different toolfaces, M_{ns} the gyro compassing spin axis mass unbalance, and M_{ni} the gyro compassing input axis mass unbalance.

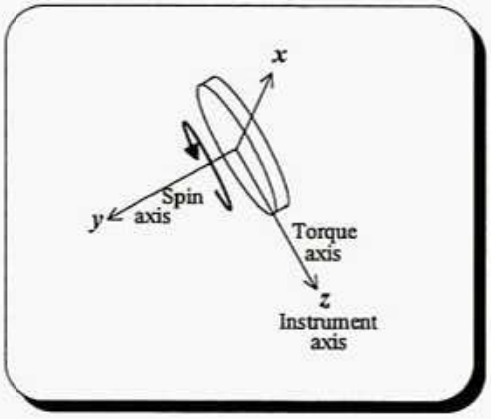

Figure 6.1.1.5-2 Gyro orientation in Finder and Keeper during gyro compassing

The azimuth uncertainty will consist of the following terms, when the correlation at each station is taken into consideration. Gyro uncertainties are given in equations *{6.1.1.4-21}* to *{6.1.1.4-32}*.

$$dA_7 = \frac{\partial A}{\partial I}dI_s + \frac{\partial A}{\partial \tau}d\tau = -\frac{\sin A(\cos\phi\sin I\cos A + \sin\phi\cos I)}{\cos\phi\cos I}dI_s - \frac{\cos\phi\left(\sin^2 A + \cos^2 A\cos^2 I\right) + \sin\phi\cos A\sin I\cos I}{\cos\phi\cos I}d\tau$$
$$\approx -\frac{\sin A(\cos\phi\sin I\cos A + \sin\phi\cos I)}{\cos\phi\cos I}dI_s \qquad \{6.1.1.5\text{-}14\}$$

$$dA_{16} = \frac{\partial A}{\partial T_{z,\tau}}dT_{nz1,\tau} + \frac{\partial A}{\partial T_{z,\tau+180}}dT_{nz1,\tau+180} + \frac{\partial A}{\partial T_{z,\tau+90}}dT_{nz'1,\tau+90} + \frac{\partial A}{\partial T_{z,\tau+270}}dT_{nz'1,\tau+270} = 0 \qquad \{6.1.1.5\text{-}15\}$$

$$dA_{17} = \frac{\partial A}{\partial T_{z,\tau}}dT_{nz2,\tau} + \frac{\partial A}{\partial T_{z,\tau+180}}dT_{nz2,\tau+180} + \frac{\partial A}{\partial T_{z,\tau+90}}dT_{nz'2,\tau+90} + \frac{\partial A}{\partial T_{z,\tau+270}}dT_{nz'2,\tau+270} \approx -\frac{\sin\phi\sin I\sin A}{\cos\phi\cos I}d\omega_{ng} \qquad \{6.1.1.5\text{-}16\}$$

$$dA_{20} = \frac{\partial A}{\partial M_{ns}}dM_{ns} = -\frac{\sin I\sin A}{\Omega\cos\phi\cos I}dM_{ns} \qquad \{6.1.1.5\text{-}17\}$$

$$dA_{21} = \frac{\partial A}{\partial \phi}d\phi = -\frac{\sin I\sin A}{\cos I}d\phi \qquad \{6.1.1.5\text{-}18\}$$

$$dA_{22} = \frac{\partial A}{\partial M_{ni}}dM_{ni} = \frac{\sin I\cos A}{\Omega\cos\phi}dM_{ni} \qquad \{6.1.1.5\text{-}19\}$$

$d\phi$ is the latitude uncertainty, $d\upsilon_{sg}$ the gyro compassing gyro scale factor uncertainty, dM_{sa} the gyro compassing spin axis mass unbalance uncertainty, and dM_{ia} the gyro compassing input axis mass unbalance uncertainty. dI_s is given by

$$dI_s = \sqrt{dI_2^2 + dI_7^2 + dI_{12}^2} \qquad \{6.1.1.5\text{-}20\}$$

where the sensor dependent uncertainty components (dI_2, dI_7 and dI_{12}) are given by equations *{6.1.1.2-27}*, *{6.1.1.2-28}* and *{6.1.1.2-29}*.

Equations *{6.1.1.5-14}* to *{6.1.1.5-19}* show again that the uncertainty tends towards infinity as the wellbore approaches the horizontal or the latitude approaches the poles.

The inclination and toolface uncertainties used in equation *{6.1.1.5-14}* can of course, like in the Gyrodata case, be substituted with uncorrelated accelerometer uncertainties to overcome the problem with inclination and toolface correlation. dA_7 will then be divided into three uncorrelated terms, which are given by

$$\begin{aligned} dA_{7\_2} &= \frac{\partial A}{\partial g_{x',\tau}} dg_{x'2,\tau} + \frac{\partial A}{\partial g_{x',\tau+180}} dg_{x'2,\tau+180} + \frac{\partial A}{\partial g_{x',\tau+90}} dg_{x'2,\tau+90} + \frac{\partial A}{\partial g_{x',\tau+270}} dg_{x'2,\tau+270} \\ &\approx -\sin I \sin A \frac{\cos\phi \sin I \cos A - \sin\phi \cos I}{\cos\phi \cos^2 I} d\upsilon_a \end{aligned} \qquad \{6.1.1.5\text{-}21\}$$

$$dA_{7\_7} = \sin I \sin A \frac{\cos\phi \sin I \cos A - \sin\phi \cos I}{G \cos\phi \cos^2 I} dG \qquad \{6.1.1.5\text{-}22\}$$

$$dA_{7\_12} = -\frac{\sin I \sin A(\cos\phi \sin I \cos A + \sin\phi \cos I)\sin\gamma}{\cos\phi \cos^2 I \cos\gamma} d\gamma \qquad \{6.1.1.5\text{-}23\}$$

$d\upsilon_a$ is the accelerometer scale factor uncertainty, dG the gravity uncertainty, and $d\gamma$ the cant angle uncertainty.

dA_{7_2} and dA_{7_12} are systematic within surveys and random between surveys as long as different instruments are used. dA_{7_7} is systematic within an entire field.

The following uncertainty components are correlated, and should be treated uncorrelated in the position co-variance matrix calculation.

- dI_2 and dA_{7_2} (Both caused by the x'- accelerometer scale factor uncertainty)
- dI_7 and dA_{7_7} (Both caused by the uncertainty in the local gravity)
- dI_{12} and dA_{7_12} (Both caused by the x'- accelerometer cant angle uncertainty)

The Keeper is according to the manufacturer (Brett H. van Steenwyk) designed mainly as a continuous tool, and is normally not used for Gyro compassing although it has the possibility to function also in this mode. The presented equations will because of this mostly be used in connection with Finder surveys for inclinations up to ca 15° (where gyro compassing is the preferred running mode), and during initialisation of both systems.

6.1.1.6 *Continuous Gyro Inclination and Azimuth*

Continuous gyro systems do not like gyro compassing systems stop at each survey station to take direct azimuth measurements. They do instead measure a continuous change in azimuth (ΔA) as the instrument moves down the wellbore. These systems have therefore a fundamental different behaviour compared to what was expected in the derivation of the Wolff deWardt theory. It will, however, in the following be shown that it error theoretically is possible to describe continuous gyro instruments as discrete measurement system. This will make it possible to include them in an new improved Wolff deWardt theory. Necessary weighting functions will be derived in the coming sub chapters.

By knowing an initial reference direction (A_0), the azimuth can be calculated by

$$A = A_0 + \Delta A \qquad \{6.1.1.6\text{-}1\}$$

The azimuth change over a time period t sensed by a continuous gyro is given by

$$\Delta A = {}_0\int^{t}\left(\frac{\partial A}{\partial t}\right)dt \qquad \{6.1.1.6\text{-}2\}$$

where $\frac{\partial A}{\partial t}$ is the time derivative of the azimuth.

The azimuth change over the small wellbore section between measurement station j-1 and j is then given by

$$\Delta A_j = {}_{t_{j-1}}\int^{t_j}\left(\frac{\partial A}{\partial t}\right)dt \qquad \{6.1.1.6\text{-}3\}$$

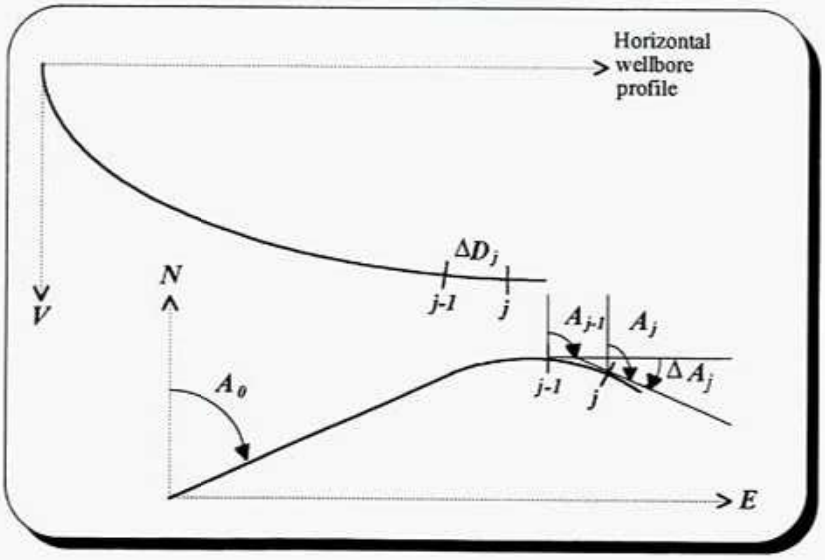

Figure 6.1.1.6-1 Definitions of station based measurements in connection with continuous gyro surveys

Equation *{6.1.1.6-3}* can be simplified if it is taken into consideration that the azimuth change between two consecutive stations (j and $j+1$) usually is small (maximum a few degrees) and uniform (no significant angular oscillations and cork screwing effects etc.) in directional surveys. This is the case even for short radius wellbore sections, where the standard station separation of 10 or 30 meters usually is reduced to avoid large model errors in the minimum curvature calculation.

$$\Delta A_j \approx \frac{\partial A_j}{\partial t}\Delta t_j \qquad \{6.1.1.6\text{-}4\}$$

Δt_j is defined by $\Delta t_j = t_j - t_{j-1}$ where t_{j-1} and t_j are the recording times of two consecutive recorded measurements.

Similar simplifications are done inside the instrument, but at a much higher frequency (smaller time increments). To duplicate this high survey frequency in position uncertainty calculations is, however, not recommended. Calculations will become time consuming, and there will be produced a huge amount of data that never will be used. The wellbore profile is only represented by angular measurements at recording stations, and it is only angular uncertainties at these points that are transferred into position uncertainties.

Recording times (t_{j-1} and t_j) will usually be unknown in connection with continuous gyro uncertainty studies. The time difference can, however, as in the continuous gyro scale factor uncertainty calculation, be estimated by the average logging speed (v) and the measured or planned depth difference between consecutive recording stations (ΔD_j).

$$\Delta t_j = \frac{\Delta D_j}{v} \qquad \{6.1.1.6\text{-}5\}$$

It will usually not be necessary to distinguish between different time increments. There will only be minor differences due to standard running procedures that shall secure against unwanted axial accelerations and large differences in the spacing between measurement recordings. The individual time increments Δt_j can because of this be substituted by an average time increment Δt in error analysis. The azimuth at time t_j (measurement station j) is then given by

$$A_j = A_0 + \Sigma_{k=1}^{j}\Delta A_k \approx A_0 + \Delta t\Sigma_{k=1}^{j}\left(\frac{\partial A_k}{\partial t}\right) \qquad \{6.1.1.6\text{-}6\}$$

The total azimuth uncertainty at station j caused by gyro errors will then become

$$dA_j = \sqrt{(dA_0)^2 + \left(\Sigma_{k=1}^{j} d\Delta A_k\right)^2} \approx \sqrt{(dA_0)^2 + \left(\Delta t\Sigma_{k=1}^{j} d\left(\frac{\partial A_k}{\partial t}\right)\right)^2} \qquad \{6.1.1.6\text{-}7\}$$

The reference uncertainty (dA_0) will be described in the reference error chapter (6.2.1), and the continuous uncertainty ($\Delta t\Sigma_{k=1}^{j} d\left(\frac{\partial A_k}{\partial t}\right)$) will be described in the following sub chapters. The continuous uncertainty is made up of many independent error sources. It should be divided into uncorrelated uncertainty components. Each component should be propagated independently to the final position, and then root sum squared (RSS).

Some continuous gyro systems can also measure changes in inclination and toolface with the gyros. Similar mathematical derivations as for the azimuth change yields

$$I_j = I_0 + \Sigma_{k=1}^{j} \Delta I_k \approx I_0 + \Delta t \Sigma_{k=1}^{j} \left(\frac{\partial I_k}{\partial t} \right) \qquad \{6.1.1.6\text{-}8\}$$

$$\tau_j = \tau_0 + \Sigma_{k=1}^{j} \Delta \tau_k \approx \tau_0 + \Delta t \Sigma_{k=1}^{j} \left(\frac{\partial \tau_k}{\partial t} \right) \qquad \{6.1.1.6\text{-}9\}$$

$$dI_j \approx \sqrt{(dI_0)^2 + \left(\Delta t \Sigma_{k=1}^{j} d\left(\frac{\partial I_k}{\partial t} \right) \right)^2} \qquad \{6.1.1.6\text{-}10\}$$

$$d\tau_j \approx \sqrt{(d\tau_0)^2 + \left(\Delta t \Sigma_{k=1}^{j} d\left(\frac{\partial \tau_k}{\partial t} \right) \right)^2} \qquad \{6.1.1.6\text{-}11\}$$

Gyrodata Continuous Tool

The Gyrodata Continuous Tool is, as stated earlier, equipped with one strap down dual axis gyro aligned with its spin axis parallel to the *z*- axis. This system do in continuous mode, measure both azimuth and inclination changes with this gyro. The initial azimuth is found by gyro compassing, and the initial inclination by indexing accelerometer measurements. The continuous azimuth (initial azimuth plus accumulated change in azimuth) can at any time be reset to the result of a new gyro compassing measurement. This measurement should be taken with initialisation quality. Similar can the continuous inclination be rest to the result of a new indexed accelerometer based inclination measurement. It is in both cases important to be aware of the horizontal wellbore singularity.

Making use of equation *{6.1.1.4-1}* gives the following changes in inclination ΔI_j and azimuth ΔA_j between measurement station *j-1* and *j* (time difference Δt).

$$\Delta I_j = \int_{t_{j-1}}^{t_j} \left(\frac{\partial I_j}{\partial t} \right) dt$$
$$\approx \Delta t (T_{x,j} \sin \tau_j + T_{y,j} \cos \tau_j + \Omega \cos \phi \sin A_j + M_x \cos \tau_j \cos I_j - M_y \sin \tau_j \cos I_j) \qquad \{6.1.1.6\text{-}12\}$$

$$\Delta A_j = \int_{t_{j-1}}^{t_j} \left(\frac{\partial A_j}{\partial t} \right) dt$$
$$\approx \Delta t \frac{-T_{x,j} \cos \tau_j + T_{y,j} \sin \tau_j + \Omega \cos \phi \cos I_j \cos A_j + \Omega \sin \phi \sin I_j + M_x \sin \tau_j \cos I_j + M_y \cos \tau_j \cos I_j + M_z \sin I_j}{\sin I_j} \qquad \{6.1.1.6\text{-}13\}$$

$T_{x,j}$, $T_{y,j}$, I_j, A_j and τ_j are the two gyro outputs, the inclination, the azimuth and the toolface at measurement station *j*; ϕ the local latitude, Ω the earth rotation rate, and M_x, M_y and M_z the mass unbalances.

The sensor dependent continuous inclination uncertainty components at measurement station *j* are then given by the following set of equations. It is in the mathematical derivation assumed that mass unbalances are small compared to earth rate, that the change in azimuth between two measurements is relatively small, and that the geometry of the traversed wellbore section is relatively uniform.

$$dI_{13,j} = \Delta t \Sigma_{k=1}^{j}\left(\frac{\partial \frac{\partial I_k}{\partial t}}{\partial \tau} d\tau_k\right) = dI_{13,j-1} + \Delta t \frac{\partial \frac{\partial I_j}{\partial t}}{\partial \tau} d\tau_j$$
$$\approx dI_{13,j-1} - (\Delta A_j \sin I_j - \Delta t \Omega(\cos\phi \cos I_j \cos A_j + \sin\phi \sin A_j)) d\tau_j \qquad \{6.1.1.6\text{-}14\}$$

$$dI_{14,j} = dI_{14,j-1} + \Delta t \frac{\partial \frac{\partial I_j}{\partial t}}{\partial T_x} dT_{cx1} \approx dI_{14,j-1} + \Delta t \sin\tau_j dT_{cx1} \qquad \{6.1.1.6\text{-}15\}$$

$$dI_{15,j} = dI_{15,j-1} + \Delta t \frac{\partial \frac{\partial I_j}{\partial t}}{\partial T_x} dT_{cx2} \approx dI_{15,j-1} + \Delta t \sin\tau_j dT_{cx2} \qquad \{6.1.1.6\text{-}16\}$$

$$dI_{16,j} = dI_{16,j-1} + \Delta t \frac{\partial \frac{\partial I_j}{\partial t}}{\partial T_y} dT_{cy1} \approx dI_{16,j-1} + \Delta t \cos\tau_j dT_{cy1} \qquad \{6.1.1.6\text{-}17\}$$

$$dI_{17,j} = dI_{17,j-1} + \Delta t \frac{\partial \frac{\partial I_j}{\partial t}}{\partial T_y} dT_{cy2} \approx dI_{17,j-1} + \Delta t \cos\tau_j dT_{cy2} \qquad \{6.1.1.6\text{-}18\}$$

$$dI_{18,j} = dI_{18,j-1} + \Delta t \frac{\partial \frac{\partial I_j}{\partial t}}{\partial \phi} d\phi \approx dI_{18,j-1} - \Delta t \Omega \sin\phi \sin A_j d\phi \qquad \{6.1.1.6\text{-}19\}$$

$$dI_{19,j} = dI_{19,j-1} + \Delta t \frac{\partial \frac{\partial I_j}{\partial t}}{\partial M_x} dM_{ci} \approx dI_{19,j-1} + \Delta t \cos I_j \cos\tau_j dM_{ci} \qquad \{6.1.1.6\text{-}20\}$$

$$dI_{20+j} = dI_{20,j-1} + \Delta t \frac{\partial \frac{\partial I_j}{\partial t}}{\partial M_y} dM_{ci} \approx dI_{20,j-1} - \Delta t \cos I_j \sin\tau_j dM_{ci} \qquad \{6.1.1.6\text{-}21\}$$

$$dI_{21,j} = dI_{21,j-1} + \Delta t \frac{\partial \frac{\partial I_j}{\partial t}}{\partial A} dA_{s,j} \approx dI_{21,j-1} + \Delta t \Omega \cos\phi \cos A_j dA_{s,j-1} \qquad \{6.1.1.6\text{-}22\}$$

ΔA_j can be estimated by the measured or planed azimuth change between measurement station *j-1* and *j*. dT_{cx1}, dT_{cx2}, dT_{cy1} and dT_{cy2} are the continuous gyro bias and scale factor uncertainties. They are given in equations *{6.1.1.4-14}* to *{6.1.1.4-19}*. $d\phi$ is the latitude uncertainty, and dM_{ci} the continuous input axis mass unbalance uncertainty. The toolface uncertainty ($d\tau$) is given by equation *{6.1.1.3-2}*, and the sensor dependent azimuth uncertainty at measurement station *j* is given by

$$dA_{s,j-1} = \sqrt{\Sigma_{i=16}^{23}\left(dA_{i,j-1}^2\right)} \qquad \{6.1.1.6\text{-}23\}$$

where the different $dA_{i,j-1}$ are given in equations *{6.1.1.6-25}* to *{6.1.1.6-32}*.

The previous station uncertainty components ($dI_{i,j-1}$) used in the gyro based inclination uncertainty equations (*{6.1.1.6-14}* to *{6.1.1.6-22}*) do all have to be reset to zero at zero velocity update stations where indexed accelerometer measurements are taken. A new inclination reference uncertainty has, however, to be calculated. The gyro based inclination uncertainty equations do not show any inclination dependent singularities for horizontal wellbores. The Gyrodata Continuous Tool can therefore measure inclinations with high accuracy even in horizontal wellbores.

Continuous inclination uncertainty components are, due to the time integrating process, systematic between stations. Gyrodata claims that the systematic effect is effective only between zero velocity update stations, and not during complete surveys. This conclusion is

based on gyro drifts seen at update stations in the field (totally random). This random effect is, however, not necessarily caused by random drift in the different error components, as claimed by Gyrodata. It is just as likely that it is caused by toolface dependent effects. Many errors, which are lumped together into the field derived drift term, are toolface dependent. Field data show that gyro instruments change toolface between zero velocity update stations, even if centalizers are used. More research is therefore necessary to solve this question. It is recommended to treat continuous inclination uncertainty components as systematic within surveys and random between surveys until this is done. This to secure against underestimation of the uncertainty.

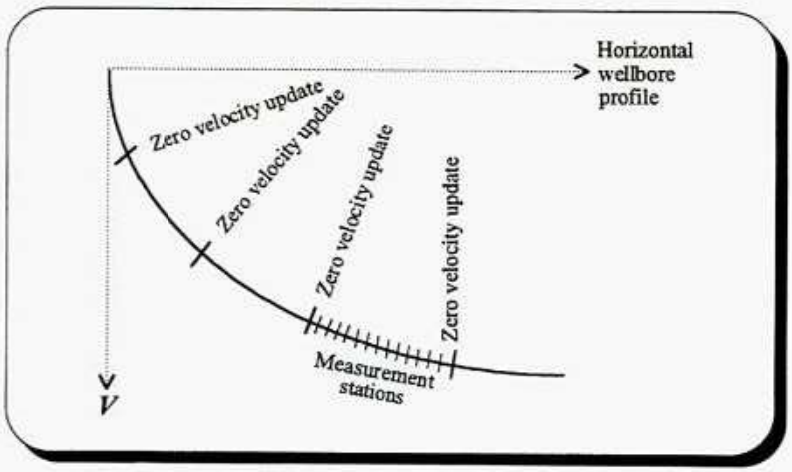

Figure 6.1.1.6-2 Relationship between zero velocity update stations and measurement stations in high accuracy continuous gyro surveys

Similar conclusions can be drawn for continuous azimuth uncertainty components, which are given by

$$dA_{7,j} = dA_{7,j-1} + \Delta t \frac{\frac{\partial A_j}{\partial t}}{\partial \tau} d\tau_j \approx dA_{7,j-1} + \frac{\Delta I_j - \Delta t \Omega \cos\phi \sin A_j}{\sin I_j} d\tau_j \qquad \{6.1.1.6\text{-}24\}$$

$$dA_{16,j} = dA_{16,j-1} + \Delta t \frac{\frac{\partial A_j}{\partial t}}{\partial T_x} dT_{cx1} \approx dA_{16,j-1} - \Delta t \frac{\cos\tau_j}{\sin I_j} dT_{cx1} \qquad \{6.1.1.6\text{-}25\}$$

$$dA_{17,j} = dA_{17,j-1} + \Delta t \frac{\frac{\partial A_j}{\partial t}}{\partial T_x} dT_{cx2} \approx dA_{17,j-1} - \Delta t \frac{\cos\tau_j}{\sin I_j} dT_{cx2} \qquad \{6.1.1.6\text{-}26\}$$

$$dA_{18,j} = dA_{18,j-1} + \Delta t \frac{\frac{\partial A_j}{\partial t}}{\partial T_y} dT_{cy1} \approx dA_{18,j-1} + \Delta t \frac{\sin\tau_j}{\sin I_j} dT_{cy1} \qquad \{6.1.1.6\text{-}27\}$$

$$dA_{19,j} = dA_{19,j-1} + \Delta t \frac{\frac{\partial A_j}{\partial t}}{\partial T_y} dT_{cy2} \approx dA_{19,j-1} + \Delta t \frac{\sin\tau_j}{\sin I_j} dT_{cy2} \qquad \{6.1.1.6\text{-}28\}$$

$$dA_{20,j} = dA_{20,j-1} + \Delta t \frac{\frac{\partial A_j}{\partial t}}{\partial M_z} dM_{cz} \approx dA_{20,j-1} + \Delta t dM_{cz} \qquad \{6.1.1.6\text{-}29\}$$

$$dA_{21,j} = dA_{21,j-1} + \Delta t \frac{\frac{\partial A_j}{\partial t}}{\partial \phi} d\phi \approx dA_{21,j-1} + \Delta t \Omega \frac{\cos\phi \sin I_j - \sin\phi \cos I_j \cos A_j}{\sin I_j} d\phi \qquad \{6.1.1.6\text{-}30\}$$

$$dA_{22,j} = dA_{22,j-1} + \Delta t \frac{\partial \frac{\partial A_j}{\partial t}}{\partial M_x} dM_{ci} \approx dA_{22,j-1} + \Delta t \frac{\cos I_j \sin \tau_j}{\sin I_j} dM_{ci} \qquad \{6.1.1.6\text{-}31\}$$

$$dA_{23,j} = dA_{23,j-1} + \Delta t \frac{\partial \frac{\partial A_j}{\partial t}}{\partial M_y} dM_{ci} \approx dA_{23,j-1} + \Delta t \frac{\cos I_j \cos \tau_j}{\sin I_j} dM_{ci} \qquad \{6.1.1.6\text{-}32\}$$

$$\begin{aligned} dA_{24,j} &= dA_{24,j-1} + \Delta t \frac{\partial \frac{\partial A_j}{\partial t}}{\partial I} dI_{s,j} + \Delta t \frac{\partial \frac{\partial A_j}{\partial t}}{\partial A} dA_{s,j} \\ &\approx dA_{24,j-1} - \left(\frac{\Delta A_j \cos I_j + \Delta t \Omega \left(\cos \phi \sin I_j \cos A_j - \sin \phi \cos I_j \right)}{\sin I_j} \right) dI_{s,j-1} \\ &\quad - \Delta t \frac{\Omega \cos \phi \cos I_j \sin A_j}{\sin I_j} dA_{s,j-1} \end{aligned} \qquad \{6.1.1.6\text{-}33\}$$

ΔI_j and ΔA_j can for accuracy studies be estimated by the measured or planed inclination and azimuth changes between measurement station *j-1* and *j*. dM_{ci} is the continuous spin axis mass unbalance uncertainty, and $dI_{s,j-1}$ is given by

$$dI_{s,j-1} = \sqrt{\Sigma_{i=14}^{20} \left(dI_{i,j-1}^2 \right)} \qquad \{6.1.1.6\text{-}34\}$$

where the different $dI_{i,j-1}$ are given in equations *{6.1.1.6-15}* to *{6.1.1.6-21}*. The other uncertainty figures are identical to those used in the inclination uncertainty equations.

The previous station uncertainty components ($dA_{i,j}$) used in the gyro based azimuth uncertainty equations (*{6.1.1.6-24}* to *{6.1.1.6-33}*) should be reset to the actual gyro compassing uncertainty if intermediate gyro compassing (with initialisation quality) is performed.

It follows directly from these equations that the azimuth uncertainty tends towards infinity for vertical wellbores. This effect explains way the Gyrodata Continuous Tool is not used as a continuous tool for inclinations below 15°. The presented equations should therefore only be used in connection with Continuous Tool surveys when the inclination exceed 15°.

The inclination and azimuth uncertainty components at station *j-1* ($dI_{s,j-1}$ and $dA_{s,j-1}$) are handled as fully correlated errors when used as input in the station *j* azimuth uncertainty calculation. This because of the high correlation that exist between these two figures. They are both based on the same gyro measurements. The correlation between continuous inclination and azimuth measurements should also be reflected in the position uncertainty calculation. The following uncertainty components are assumed to be correlated

- dI_{13} and dA_7 (Both caused by the toolface uncertainty)
- dI_{14} and dA_{16} (Both caused by the *x*- gyro bias uncertainty)
- dI_{15} and dA_{17} (Both caused by the *x*- gyro scale factor uncertainty)
- dI_{16} and dA_{18} (Both caused by the *y*- gyro bias uncertainty)
- dI_{17} and dA_{19} (Both caused by the *y*- gyro scale factor uncertainty)
- dI_{18} and dA_{21} (Both caused by the latitude uncertainty)
- dI_{19} and dA_{22} (Both caused by the *x*- gyro input axis mass unbalance uncertainty)
- dI_{20} and dA_{23} (Both caused by the *y*- gyro input axis mass unbalance uncertainty)
- dI_{21} and dA_{24} (Both caused by the last inclination- and azimuth uncertainty)

The toolface uncertainty ($d\tau$) is derived from accelerometer measurements. dI_{13} (equation *{6.1.1.6-14}*) and dA_7 (equation *{6.1.1.6-24}*) can therefore be substituted with eight uncorrelated accelerometer uncertainty components.

$$dI_{13\_1,j} \approx dI_{13\_1,j-1} - \frac{\left(\Delta A_j \sin I_j - \Delta\Omega\left(\cos\phi \cos I_j \cos A_j + \sin\phi \sin A_j\right)\right)\cos\tau_j}{G \sin I_j} dg_{x1} \qquad \{6.1.1.6\text{-}35\}$$

$$dI_{13\_2,j} \approx dI_{13\_2,j-1} - \frac{\left(\Delta A_j \sin I_j - \Delta\Omega\left(\cos\phi \cos I_j \cos A_j + \sin\phi \sin A_j\right)\right)\cos\tau_j}{G \sin I_j} dg_{x2} \qquad \{6.1.1.6\text{-}36\}$$

$$dI_{13\_3,j} \approx dI_{13\_3,j-1} + \frac{\left(\Delta A_j \sin I_j - \Delta\Omega\left(\cos\phi \cos I_j \cos A_j + \sin\phi \sin A_j\right)\right)\sin\tau_j}{G \sin I_j} dg_{y1} \qquad \{6.1.1.6\text{-}37\}$$

$$dI_{13\_4,j} \approx dI_{13\_4,j-1} + \frac{\left(\Delta A_j \sin I_j - \Delta\Omega\left(\cos\phi \cos I_j \cos A_j + \sin\phi \sin A_j\right)\right)\sin\tau_j}{G \sin I_j} dg_{y2} \qquad \{6.1.1.6\text{-}38\}$$

$$dA_{7\_1,j} \approx dA_{7\_1,j-1} + \frac{\left(\Delta I_j - \Delta\Omega \cos\phi \sin A_j\right)\cos\tau_j}{G \sin^2 I_j} dg_{x1} \qquad \{6.1.1.6\text{-}39\}$$

$$dA_{7\_2,j} \approx dA_{7\_2,j-1} + \frac{\left(\Delta I_j - \Delta\Omega \cos\phi \sin A_j\right)\cos\tau_j}{G \sin^2 I_j} dg_{x2} \qquad \{6.1.1.6\text{-}40\}$$

$$dA_{7\_3,j} \approx dA_{7\_3,j-1} - \frac{\left(\Delta I_j - \Delta\Omega \cos\phi \sin A_j\right)\sin\tau_j}{G \sin^2 I_j} dg_{y1} \qquad \{6.1.1.6\text{-}41\}$$

$$dA_{7\_4,j} \approx dA_{7\_4,j-1} - \frac{\left(\Delta I_j - \Delta\Omega \cos\phi \sin A_j\right)\sin\tau_j}{G \sin^2 I_j} dg_{y2} \qquad \{6.1.1.6\text{-}42\}$$

Accelerometer uncertainties (dg_{x1}, dg_{x2}, dg_{y1} and dg_{y2}) are given in equations *{6.1.1.1-2}* to *{6.1.1.1-7}*.

dI_{13_1} through dI_{13_4} and dA_{7_1} through dA_{7_4} are systematic within surveys and random between surveys.

The following error components should be treated as correlated errors in the position co-variance calculation if accelerometer uncertainties are used as input in the azimuth uncertainty calculation

- dI_{13_1} and dA_{7_1} (Both caused by the *x*- accelerometer bias uncertainty)
- dI_{13_2} and dA_{7_2} (Both caused by the *x*- accelerometer scale factor uncertainty)
- dI_{13_3} and dA_{7_3} (Both caused by the *y*- accelerometer bias uncertainty)
- dI_{13_4} and dA_{7_4} (Both caused by the *y*- accelerometer scale factor uncertainty)

Continuous Finder and High Angle Keeper

Finder is, as stated in the gyro compassing chapter, equipped with one *z*- axis (*y*- spin) rotor gyro, and Keeper with one *x*- and one *z*- axis gyro, both with *y*- spin. The Keeper do mainly make use of the *z*- gyro at inclinations above ca 20° (15° for earlier versions). This makes it nearly identical to the Finder at higher inclinations. The *z*- gyro is for both systems mounted on a controlled motor driven rotary *z*- axis. This rotary axis is in continuous mode (high angle mode for the Keeper) forced to maintain a horizontal *y*- spin through a feedback loop governed by the *y*- accelerometer. The two accelerometers are also mounted on the rotary axis, and the *z*- axis rotation is controlled by maintaining the *y*- accelerometer output as near zero as possible. Vertical stabilised systems are practically not sensitive to collar rotations, and do only sense azimuth changes. Making use of equation *{6.1.1.4-1}* gives the following change in azimuth (ΔA_j) between measurement station *j-1* and *j* (time difference Δt).

$$\Delta A_j = \Delta t \frac{-\frac{\partial I_j}{\partial t}\cos\tau_j - T_{z,j} + \Omega\left(\cos\phi\left(\cos I_j \cos A_j \sin\tau_j + \sin A_j \cos\tau_j\right) + \sin\phi \sin I_j \sin\tau_j\right) - \sin I_j\left(M_x \cos\tau_j - M_y \sin\tau_j\right)}{\sin I_j \sin\tau_j}$$

$$\approx \Delta t \frac{-T_{z,j} + \Omega\left(\cos\phi \cos I_j \cos A_j + \sin\phi \sin I_j\right) + M_y \sin I_j}{\sin I_j} \qquad \{6.1.1.6\text{-}43\}$$

$T_{z,j}$, I_j, A_j and τ_j are the gyro output, the inclination, the azimuth and the toolface at measurement station *j*; ϕ the local latitude, Ω the earth rotation rate, and M_x and M_y the *x*- and *y*- mass unbalances.

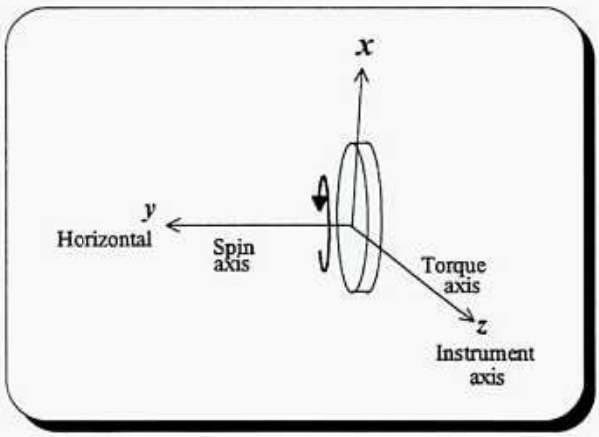

Figure 6.1.1.6-3 Gyro orientation for continuous Finder and high angle Keeper

The continuous azimuth uncertainty components at measurement station *j* are then given by the following equations. They are, like in the continuous Gyrodata case, based on the assumption that mass unbalances are small compared to earth rate, that the change in azimuth is relatively small, and that the geometry of the traversed wellbore section is relatively uniform.

$$dA_{7,j} = \Delta t \Sigma_{k=1}^{j}\left(\frac{\partial\frac{\partial A_k}{\partial t}}{\partial I}dI_{s,k} + \frac{\partial\frac{\partial A_k}{\partial t}}{\partial \tau}d\tau_k\right) = dA_{7,j-1} + \Delta t\frac{\partial\frac{\partial A_j}{\partial t}}{\partial I}dI_{s,j} + \Delta t\frac{\partial\frac{\partial A_j}{\partial t}}{\partial \tau}d\tau_j$$

$$\approx dA_{7,j-1} - \frac{\Delta A_j \cos I_j + \Delta t\Omega\left(\cos\phi\sin I_j\cos A_j - \sin\phi\cos I_j\right)}{\sin I_j}dI_{s,j}$$

$$+(\Delta I_j - \Delta t\Omega\cos\phi\sin A_j)d\tau_j \qquad \{6.1.1.6\text{-}44\}$$

$$dA_{16,j} = dA_{16,j-1} + \Delta t\frac{\partial\frac{\partial A_j}{\partial t}}{\partial T_z}dT_{cz1} \approx dA_{16,j-1} + \frac{\Delta t}{\sin I_j}dT_{cz1} \qquad \{6.1.1.6\text{-}45\}$$

$$dA_{17,j} = dA_{17,j-1} + \Delta t\frac{\partial\frac{\partial A_j}{\partial t}}{\partial T_z}dT_{cz2} \approx dA_{17,j-1} + \frac{\Delta t}{\sin I_j}dT_{cz2} \qquad \{6.1.1.6\text{-}46\}$$

$$dA_{20,j} = dA_{20,j-1} + \Delta t\frac{\partial\frac{\partial A_j}{\partial t}}{\partial M_y}dM_{cs} \approx dA_{20,j-1} + \Delta t dM_{cs} \qquad \{6.1.1.6\text{-}47\}$$

$$dA_{21,j} = dA_{21,j-1} + \Delta t\frac{\partial\frac{\partial A_j}{\partial t}}{\partial \phi}d\phi \approx dA_{21,j-1} + \Delta t\Omega\left(\frac{\cos\phi\sin I_j - \sin\phi\cos I_j\cos A_j}{\sin I_j}\right)d\phi \qquad \{6.1.1.6\text{-}48\}$$

$$dA_{24,j} = dA_{24,j-1} + \Delta t\frac{\partial\frac{\partial A_j}{\partial t}}{\partial A}dA_{s,j} \approx dA_{24,j-1} - \Delta t\frac{\Omega\cos\phi\cos I_j\sin A_j}{\sin I_j}dA_{s,j-1} \qquad \{6.1.1.6\text{-}49\}$$

ΔI_j and ΔA_j can be estimated by the measured or planed inclination and azimuth changes between measurement station *j-1* and *j*. dT_{cz1} and dT_{cz2} are the continuous gyro bias and scale factor uncertainties given in equations *{6.1.1.4-33}* to *{6.1.1.4-35}*. $d\phi$ is the latitude uncertainty, and dM_{cs} the continuous spin axis mass unbalance uncertainty. The toolface uncertainty ($d\tau_j$) is given by equation *{6.1.1.3-6}*, and the sensor dependent inclination and azimuth uncertainties ($dI_{s,j}$and $dA_{s,j-1}$) are given by

$$dI_{s,j} = \sqrt{dI_{1,j}^2 + dI_{2,j}^2 + dI_{7,j}^2 + dI_{11,i}^{j} + dI_{12,j}^2} \qquad \{6.1.1.6\text{-}50\}$$

$$dA_{s,j-1} = \sqrt{dA_{16,j-1}^2 + dA_{17,j-1}^2 + dA_{20,j-1}^2 + dA_{21,j-1}^2} \qquad \{6.1.1.6\text{-}51\}$$

$dI_{i,j}$ is the sensor induced azimuth uncertainty components at station *j* given by equations *{6.1.1.2-20}* to *{6.1.1.2-24}*, and $dA_{i,j-1}$ the sensor induced azimuth uncertainty components at station *j-1* given in equations *{6.1.1.6-44}* to *{6.1.1.6-49}*.

These equations show, like in the continuous Gyrodata case, that the Finder and the high angle Keeper azimuth uncertainty tends towards infinity for vertical wellbores. The Finder is because of this usually not used as a continuous tool for inclinations below ca 15°, and the Keeper is usually run in a low angle mode up to about 20°. Equations *{6.1.1.6-44}* to *{6.1.1.6-49}* should therefore only be used in connection with continuous Finder or Keeper surveys when the inclination is greater than 15° (Finder) or 20° (Keeper).

The continuous azimuth uncertainty components have a recursive nature, and will because of this be systematic between stations. It is therefore recommended to treat them as systematic within surveys and random between surveys errors.

The inclination and toolface uncertainties (dI and $d\tau$) are once again derived from accelerometer measurements. dA_7 (equation *{6.1.1.6-44}*) can therefore be substituted with six uncorrelated accelerometer uncertainty components (the y- accelerometer scale factor uncertainty has no effect).

$$dA_{7\_1,j} = dA_{7\_1,j-1} + \frac{\Delta A_j \cos I_j + \Delta\Omega\left(\cos\phi \sin I_j \cos A_j - \sin\phi \cos I_j\right)}{G \sin I_j \cos\left(I_j + \gamma\right)} dg_{x'1} \qquad \{6.1.1.6\text{-}52\}$$

$$dA_{7\_2,j} = dA_{7\_2,j-1} + \frac{\Delta A_j \cos I_j + \Delta\Omega\left(\cos\phi \sin I_j \cos A_j - \sin\phi \cos I_j\right)}{G \sin I_j \cos\left(I_j + \gamma\right)} dg_{x'2} \qquad \{6.1.1.6\text{-}53\}$$

$$dA_{7\_3,j} = dA_{7\_3,j-1} + \frac{\Delta I_j - \Delta\Omega \cos\phi \sin A_j}{G \sin I_j} dg_{y1} \qquad \{6.1.1.6\text{-}54\}$$

$$dA_{7\_7,j} = dA_{7\_7,j-1} + \frac{\left(\Delta A_j \cos I_j + \Delta\Omega(\cos\phi \sin I_j \cos A_j - \sin\phi \cos I_j)\right) \sin\left(I_j + \gamma\right)}{G \sin I_j \cos\left(I_j + \gamma\right)} dG \qquad \{6.1.1.6\text{-}55\}$$

$$dA_{7\_11,j} = dA_{7\_11,j-1} + \frac{\Delta A_j \cos I_j + \Delta\Omega\left(\cos\phi \sin I_j \cos A_j - \sin\phi \cos I_j\right)}{G \sin I_j \cos\left(I_j + \gamma\right)} dg_{x'4} \qquad \{6.1.1.6\text{-}56\}$$

$$dA_{7\_12,j} = dA_{7\_12,j-1} + \frac{\Delta A_j \cos I_j + \Delta\Omega\left(\cos\phi \sin I_j \cos A_j - \sin\phi \cos I_j\right)}{\sin I_j} d\gamma \qquad \{6.1.1.6\text{-}57\}$$

Accelerometer uncertainties (dg_{y1}, $dg_{x'1}$, $dg_{x'2}$ and $dg_{x'4}$) can be found by setting $\sin\tau = 1$ ($\tau = 90°$ for vertical stabilised systems) in equations *{6.1.1.1-5}*, *{6.1.1.1-12}*, *{6.1.1.1-13}* and *{6.1.1.1-15}*. dG is the gravity uncertainty, and $d\gamma$ the cant angle uncertainty.

dA_{7_11} is random between stations, and dA_{7_1}, dA_{7_2}, dA_{7_3} and dA_{7_12} are systematic within surveys and random between surveys. dA_{7_7} is usually systematic within an entire field, but can with special pre-job calibrations be partly randomised. The following components should be treated correlated in the co-variance calculation

- dI_1 and dA_{7_1} (Both caused by the x'- accelerometer bias uncertainty)
- dI_2 and dA_{7_2} (Both caused by the x'- accelerometer scale factor uncertainty)
- dI_7 and dA_{7_7} (Both caused by the uncertainty in the local gravity)
- dI_{11} and dA_{7_11} (Both caused by random axial accelerations)
- dI_{12} and dA_{7_12} (Both caused by the x'- accelerometer cant angle uncertainty)

Continuous Low Angle Keeper

Keeper is, as already mentioned, equipped with one x- and one z- axis (y- spin) gyro. The two gyros are dedicated to different parts of the wellbore. The z- gyro is the principal device for azimuth determination for inclinations greater than 20°. The x- gyro is similarly dedicated as the principal azimuth device for inclinations lower than ca 20°. Both gyros are mounted on the motor driven rotary z- axis. The rotary axis is in low angle mode controlled by the x- gyro in such a manner that no z- axis rotations take place with respect to inertial space. The gyro toolface (τ_4) is then measured by the z- axis rotation angle sensor. The azimuth can then for small inclinations be found by

$$A \approx \tau_A - \tau \qquad \{6.1.1.6\text{-}58\}$$

or by a more complicated equation for higher inclinations. The inclination (I) and high-side toolface (τ) are determined through accelerometer measurements.

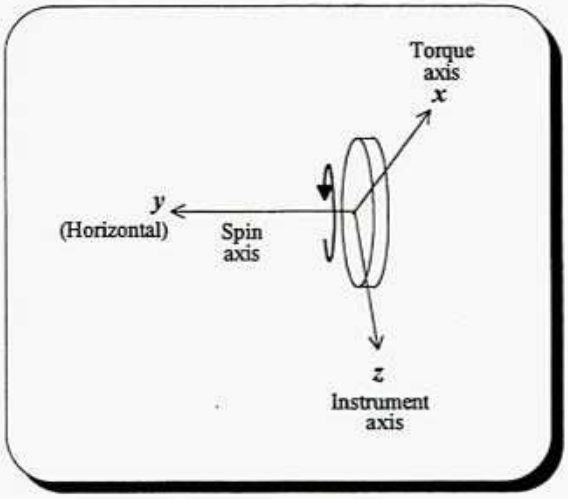

Figure 6.1.1.6-4 Gyro orientation for continuous low angle Keeper

This functionality is difficult to describe error theoretically in the same manner as used previously in this document. Principal error sources are not related to the measuring device itself (the rotation angle sensor), but to the gyro that is controlling the inertial reference of the measuring sensor. An indirect approach is chosen in the mathematical derivation to overcome this problem. It is assumed that the high-side toolface is held at 90° (within the accuracy of the rotation sensor), and that the x- gyro measures changes in the azimuth. Such an artificial functionality is found to generate almost the same azimuth uncertainty as the true functionality, and is much more easy to work with.

Making use of equation *{6.1.1.4-1}* gives then the following azimuth change ΔA between measurement station j-1 and j (time difference Δt)

$$\begin{aligned}\Delta A_j &= \Delta t \frac{-\frac{\partial \tau_j}{\partial t} - T_{x_j} - \Omega\left(\cos\phi \sin I_j \cos A_j - \sin\phi \cos I_j\right) + \cos I_j M_y + \sin I_j \cos \tau_j M_z}{\cos I_j} \\ &\approx \Delta t \frac{-T_{x_j} - \Omega\left(\cos\phi \sin I_j \cos A_j - \sin\phi \cos I_j\right) + \cos I_j M_y}{\cos I_j}\end{aligned} \qquad \{6.1.1.6\text{-}59\}$$

τ_j is the artificial sensor package toolface at station j, which is near to 90°.

The low angle azimuth uncertainty components at measurement station j are then given by the following equations. They are, once again, based on the assumption about small mass unbalances, small azimuth changes, and uniform wellbore geometry.

$$dA_{7,j} = \Delta t \Sigma_{k=1}^{j} \frac{\partial \frac{\partial A_k}{\partial t}}{\partial I} dI_{s,k} = dA_{7,j-1} + \Delta t \frac{\partial \frac{\partial A_j}{\partial t}}{\partial I} dI_{s,j}$$
$$\approx dA_{7,j-1} + \frac{\Delta A_j \sin I_j - \Delta t \Omega \left(\cos\phi \cos I_j \cos Aj + \sin\phi \sin I_j \right)}{\cos I_j} dI_{s,j} \qquad \{6.1.1.6\text{-}60\}$$

$$dA_{16,j} = dA_{16,j-1} + \Delta t \frac{\partial \frac{\partial A_j}{\partial t}}{\partial T_x} dT_{cx1} \approx dA_{16,j-1} - \frac{\Delta t}{\cos I_j} dT_{cx1} \qquad \{6.1.1.6\text{-}61\}$$

$$dA_{17,j} = dA_{17,j-1} + \Delta t \frac{\partial \frac{\partial A_j}{\partial t}}{\partial T_x} dT_{cx2} \approx dA_{16,j-1} - \frac{\Delta t}{\cos I_j} dT_{cx2} \qquad \{6.1.1.6\text{-}62\}$$

$$dA_{20,j} = dA_{20,j-1} + \Delta t \frac{\partial \frac{\partial A_j}{\partial t}}{\partial M_y} dM_{cs} \approx dA_{20,j-1} + \Delta t dM_{cs} \qquad \{6.1.1.6\text{-}63\}$$

$$dA_{21,j} = dA_{21,j-1} + \Delta t \frac{\partial \frac{\partial A_j}{\partial t}}{\partial \phi} d\phi \approx dA_{21,j-1} + \Delta t \frac{\Omega \left(\cos\phi \cos I_j + \sin\phi \sin I_j \cos A_j \right)}{\cos I_j} d\phi \qquad \{6.1.1.6\text{-}64\}$$

$$dA_{24,j} = dA_{24,j-1} + \Delta t \frac{\partial \frac{\partial A_j}{\partial t}}{\partial A} dA_{s,j} \approx dA_{24,j-1} + \Delta t \frac{\Omega \cos\phi \sin I_j \sin A_j}{\cos I_j} dA_{s,j-1} \qquad \{6.1.1.6\text{-}65\}$$

ΔA_j can be estimated by the measured or planed azimuth change between measurement station *j-1* and *j*. dT_{cx1} and dT_{cx2} are the continuous gyro bias and scale factor uncertainties given in equation *{6.1.1.4-24}* to *{6.1.1.4-26}*. $d\phi$ is the latitude uncertainty, and dM_{cs} the continuous spin axis mass unbalance uncertainty.

The sensor dependent inclination and azimuth uncertainties ($dI_{s,j}$and $dA_{s,j-1}$) are given by

$$dI_{s,j} = \sqrt{dI_{1,j}^2 + dI_{2,j}^2 + dI_{7,j}^2 + dI_{11,j}^2 + dI_{12,j}^2} \qquad \{6.1.1.6\text{-}66\}$$

$$dA_{s,j-1} = \sqrt{dA_{16,j-1}^2 + dA_{17,j-1}^2 + dA_{20,j-1}^2 + dA_{21,j-1}^2} \qquad \{6.1.1.6\text{-}67\}$$

where $dI_{i,j}$ is the sensor induced azimuth uncertainty components at station *j* given in equations *{6.1.1.2-30}* to *{6.1.1.2-34}*, and $dA_{i,j-1}$ the sensor induced azimuth uncertainty components at station *j-1* given in equations *{6.1.1.6-61}* to *{6.1.1.6-63}*.

This shows that the low angle Keeper azimuth uncertainty tends towards infinity for horizontal wellbores, which is in total contradiction to the high angle mode that tends towards infinity for vertical wellbores.

The low angle azimuth uncertainty components are, like in the high angle mode, usually systematic between stations within surveys, and random between surveys.

The toolface uncertainty is not included in these equations, but must of course affect the azimuth accuracy as for other gyro based azimuths. It has its origin in the accuracy of the *z*- axis rotation sensor, and will therefore not be part of the gyro integration process. The low angle toolface dependent azimuth uncertainty can therefore be estimated by

$$dA_{25,j} \approx \cos I_j d\tau_r \qquad \{6.1.1.6\text{-}68\}$$

where $d\tau_z$ is the uncertainty associated with the z- axis rotation sensor readings when the control loop is active and regarded as free from gyro errors.

The inclination (I) is derived from accelerometer measurements. dA_7 used in equation *{6.1.1.6-60}* can therefore be substituted with five uncorrelated accelerometer uncertainty equations.

$$dA_{7\_1,j} \approx dA_{7\_1,j-1} - \frac{\Delta A_j \sin I_j - \Delta t\Omega\left(\cos\phi\cos I_j\cos A_j + \sin\phi\sin I_j\right)}{G\cos I_j\cos(I_j+\gamma)} dg_{x'1} \qquad \{6.1.1.6\text{-}69\}$$

$$dA_{7\_2,j} \approx dA_{7\_2,j-1} - \frac{\Delta A_j \sin I_j - \Delta t\Omega\left(\cos\phi\cos I_j\cos A_j + \sin\phi\sin I_j\right)}{G\cos I_j\cos(I_j+\gamma)} dg_{x'2} \qquad \{6.1.1.6\text{-}70\}$$

$$dA_{7\_7,j} \approx dA_{7\_7,j-1} - \frac{\left(\Delta A_j \sin I_j - \Delta t\Omega(\cos\phi\cos I_j\cos A_j + \sin\phi\sin I_j)\right)\sin(I_j+\gamma)}{G\cos I_j\cos(I_j+\gamma)} dG \qquad \{6.1.1.6\text{-}71\}$$

$$dA_{7\_11,j} \approx dA_{7\_11,j-1} - \frac{\Delta A_j \sin I_j - \Delta t\Omega\left(\cos\phi\cos I_j\cos A_j + \sin\phi\sin I_j\right)}{G\cos I_j\cos(I_j+\gamma)} dg_{x'4} \qquad \{6.1.1.6\text{-}72\}$$

$$dA_{7\_12,j} \approx dA_{7\_12,j-1} - \frac{\Delta A_j \sin I_j - \Delta t\Omega\left(\cos\phi\cos I_j\cos A_j + \sin\phi\sin I_j\right)}{\cos I_j} d\gamma \qquad \{6.1.1.6\text{-}73\}$$

The three accelerometer uncertainties ($dg_{x'1}$, $dg_{x'2}$ and $dg_{x'4}$), are given in equations *{6.1.1.1-12}*, *{6.1.1.1-13}* and *{6.1.1.1-15}* when $\cos\tau = 0$.

dA_{7_11} is random between stations, dA_{7_1} and dA_{7_2} are systematic within surveys and random between surveys, and dA_{7_7} is systematic within an entire field.

The following error components should, like in the high angle case, be treated as correlated errors in the position co-variance calculation

- dI_1 and dA_{7_1} (Both caused by the x'- accelerometer bias uncertainty)
- dI_2 and dA_{7_2} (Both caused by the x'- accelerometer scale factor uncertainty)
- dI_7 and dA_{7_7} (Both caused by the uncertainty in the local gravity)
- dI_{11} and dA_{7_11} (Both caused by axial accelerations)
- dI_{12} and dA_{7_12} (Both caused by the x'- accelerometer cant angle uncertainty)

6.1.1.6 *Sensor Misalignments*

Accelerometers

Like in the magnetic case, accelerometer misalignments are usually not significant error sources in gyro systems. The only exception is for canted systems, where the canted accelerometer misalignment must be considered. This error source is, however, due to its direct input into the inclination equation, already covered together with other accelerometer errors in chapter 6.1.1.2.

Gyros

A study similar to the magnetic accelerometer misalignment study, shows that gyro sensor misalignments in most cases also can be omitted. This is the case even for vertical stabilised systems like the Finder system from Scientific Drilling Controls, where the high-side toolface plane misalignment turn out to be a significant error source. This error is, however, identical to the toolface uncertainty, and is already included in the total error budget (chapter 6.1.1.3).

6.1.2 Electronics Dependent Uncertainties

Gyro errors connected to the electronics can also be described in form of biases, scale factor errors, and random noise, where the noise usually is without significance in the total error budget. Electronics biases and scale factors can be modelled by the same kind of equations as for magnetic instruments.

It is once again difficult to distinguish between sensor errors and electronic dependent errors in the calibration / qualification process, and it is therefore recommended to lump them together to combined axial biases and scale factor uncertainties.

6.1.3 Instrument Misalignment

The misalignment between the sensor package *z*- axis and the principal instrument axis is an identical error source to the similar magnetic error source. It can therefore also be described by two uncorrelated orthogonal components. This results in two uncorrelated inclination uncertainties (identical to the two similar magnetic inclination uncertainties given in equation *{5.1.3-1}* and equation *{5.1.3-2}*), and two uncorrelated azimuth uncertainties (identical to the two similar magnetic azimuth uncertainties given in equation *{5.1.3-3}* and equation *{5.1.3-4}*).

6.2 Environmental Uncertainties

6.2.1 Continuous Reference Uncertainties

It is earlier shown (chapter 6.1.1.6) that continuous gyro systems perform indirect azimuth measurements, and that the azimuth is given by

$$A = A_0 + \Delta A \qquad \{6.2.1\text{-}1\}$$

where ΔA is the measured change in azimuth from the starting point, and A_0 an independent derived initial azimuth (at the starting point). The azimuth uncertainty is given by

$$dA = dA_0 + d\Delta A \qquad \{6.2.1\text{-}2\}$$

where dA_0 is the reference azimuth uncertainty, and $d\Delta A$ the continuous azimuth uncertainty (described in chapter 6.1.1.6). The reference direction is usually the same during an entire survey. The only exception is when intermediate gyro compassing with initialisation accuracy is performed. This is, however, not a standard operational procedure, and it is therefore regarded as sufficient to treat the reference azimuth error as systematic during surveys and random between surveys. Two methods of reference direction determination are in use. It is optical referencing and independent north seeking (gyro compassing), which both will be random for a large number of surveys. A tie to old gyro or magnetic surveys is sometimes also used. This latter method will, however, not be covered here. It is totally dependent on the accuracy in the old survey, and is not recommended. Realistic uncertainty figures can not be established without detailed knowledge about the old survey. Expected gross error controls needed to validate a survey, like comparison of the known horizontal earth rotation rate with the measured rate, are also lost.

The Gyrodata Continuous Tool do also make use of the gyro outputs to determine relative change in the inclination. The inclination uncertainty is then given by

$$dI = dI_0 + d\Delta I \qquad \{6.2.1\text{-}3\}$$

where dI_0 is the reference inclination uncertainty, and $d\Delta I$ the continuous measurement uncertainty described in chapter 6.1.1.6. The reference inclination may be recalculated at zero velocity update stations up to a given inclination. Update stations will be unknown at the planning stage, but can be simulated at regular intervals up to the given inclination limit. The different inclination references will in a given survey be based on the same accelerometers. Their uncertainties are therefore systematic within and random between surveys as long as only one referencing is performed.

Reference errors for continuous gyro instruments covered in chapter 6.1.1.6 are given in the following subchapters.

Referencing of Free Gyros

The optical referencing method is measurement of the horizontal direction of the gyro spin plane with respect to a known reference direction with an external horizontal angle measuring device. This method is usually not very accurate, and is a method that traditionally has been used in connection with free gyro surveys. The reference uncertainty is systematic between stations within surveys and random between surveys, and is given by

$$dA_{26} = dA_r \qquad \{6.2.1\text{-}4\}$$

where dA_r is the uncertainty in the determination of the horizontal angle between the optical reference direction and the horizontal spin plane.

Referencing of Finder and Keeper

Repeated gyro compassing measurements prior to switching to continuous mode is called a continuous gyro initialisation. All known systems from Scientific Drilling Controls (Finder and Keeper), make use of this technique. The total gyro compassing uncertainty at the initialisation station is then equal to the reference uncertainty, and is given by

$$dA_{26} = \sqrt{dA_7^2 + dA_{17}^2 + \Sigma_{i=20}^{22}(dA_i^2)} \qquad \{6.2.1\text{-}5\}$$

where dA_i are significant uncertainty components in the north seeking reference measurements given in equations *{6.1.1.5-14}*, and *{6.1.1.5-16}* to *{6.1.1.5-19}*. It is assumed that the different error terms are independent of each other at the initialisation station. Systematic environmental error terms that also are effective after switching to continuous mode, are not included in this reference uncertainty. Their effect will be take care of in the respective systematic error terms.

dA_{26} is a reference error, and therefore systematic within and random between surveys.

Referencing of Gyrodata Continuous Tool

The Gyrodata Continuous Tool do also make use of repeated gyro compassing measurements as initialisation prior to switching to continuous mode. The reference uncertainty is then given by

$$dA_{26} = \sqrt{dA_7^2 + dA_{17}^2 + \Sigma_{i=19}^{21} dA_i^2} \qquad \{6.2.1\text{-}6\}$$

where dA_i are significant uncertainty components in the north seeking reference measurements given by equations *{6.1.1.5-2}*, *{6.1.1.5-4}*, and *{6.1.1.5-6}* to *{6.1.1.5-8 }*.

dA_{26} is once again systematic within and random between surveys.

New inclination references can be established at zero velocity update stations through indexed accelerometer measurements as long as not coming into conflict with the horizontal wellbore singularity. The associated uncertainty is then given by

$$dI_{22} = \sqrt{dI_2^2 + dI_4^2 + dI_7^2} \qquad \{6.2.1\text{-}7\}$$

where dI_i are significant inclination uncertainty components given in equations *{6.1.1.2-15}*, *{6.1.1.2-17}* and *{6.1.1.2-18}*. It is also here assumed that the different error terms are independent of each other at the initialisation stations.

dI_{22} is, like dA_{26}, systematic within and random between surveys as long as only one referencing is performed. The error propagation will be more complicated in connection with consecutive accelerometer based updates at zero velocity update stations.

6.2.2 *Free Gyro Uncertainty*

Free gyro is an old instrument class, which nowadays is unusual in the North Sea area. It is nevertheless included in this study. It is intended as a worst case instrument class to be assigned to old gyro surveys with unknown quality. Such a class is needed for realistic anti collision studies when planning new wellbores in areas with old existing wells.

Free gyros consist of one rotor gyro which is mounted on a double axis gimballed platform. The gyro is then allowed to maintain its direction in space as the tool is moving down the wellbore. The directional change between the gyro and the horizontal component of the tool axis is a direct estimate of the relative azimuth change. The azimuth change is measured by sensing the relative position of the horizontal gyro spin axis with respect to the instrument housing. By knowing an initial instrument reference azimuth (A_0), which usually is established through optical referencing, the momentary azimuth can be found by

$$A = A_0 + \Delta A \qquad \{6.2.2\text{-}1\}$$

The uncertainty is then given by

$$dA = dA_0 + d\Delta A \qquad \{6.2.2\text{-}2\}$$

where dA_o (the optical referencing error) was covered in the previous chapter.

A free gyro maintains its orientation in the inertial space and not to the earth surface, which the azimuth is linked to. This means that the horizontal component of the earth rotation must be looked at as an error source for these instruments. It is often called gyro drift, and is strongly latitude dependent (15°/hr at the equator and zero at the poles). Free gyros do of course also suffer from error sources like mass unbalances etc., but these are not regarded as significant compared to the earth rotation (usually less than 0.5°/hr). At least not at some distance from the poles (10 to 15°).

Free gyros are, as already mentioned, not used in connection with high accuracy work any more. It is therefore not necessary with any accurate uncertainty estimation technique for this instrument class. The equation proposed by Wolff [6] is regarded as sufficient to keep track of the position uncertainties associated with old existing wellbores surveyed with this technique. Old available surveys are located sufficiently far away from the poles (20° or more) to avoid the polar azimuth singularity, which is not reflected in Wolff's equation. The free gyro drift uncertainty is then given by

$$dA_{27} = d\Delta A = \frac{1}{\cos I} dA_f \qquad \{6.2.2\text{-}3\}$$

where dA_f is the free gyro azimuth drift for near vertical wellbores at a given location. dA_f is latitude dependent.

6.2.3 Collar Misalignments

Directional gyro surveys are traditionally a wireline technique. Surveys have been taken both in cased and open holes. Newer surveys inside drill pipes, both on wireline and with battery, are also well known, while surveying while drilling seems to be more unusual. This fact will probably change in the near future. There are indications that MWD gyros will become an alternative in the near future. The market seems to be demanding this solution the sooner the better. MWD surveys will be run on drill pipes, and will therefore suffer from the same collar misalignments as magnetic MWD surveys.

6.2.3.1 Vertical Collar Misalignment

Casing or Open Hole

The vertical collar alignment uncertainty is, as for magnetic wireline surveys, usually also very small for wireline based gyro surveys when run inside casings or in open holes. It can therefore in most cases be omitted in wellbore position uncertainty studies.

Drill Pipe Wireline Surveys and MWD

The vertical collar uncertainty for continuous wireline gyro surveys run inside drill pipes is caused by the vertical deflection between the drill string and the casing or the open hole. Little is known about this deflection, except that the resultant effect must be averaged out over longer wellbore sections. The drill string can not disappear out of the wellbore, and the total contribution to the wellbore position uncertainty must therefore be without significance.

The vertical collar uncertainty for battery or wet connect gyro surveys run stationary inside the bottom hole assembly is usually caused by the bottom hole assembly sag near the sensor package. The uncertainty is therefore identical to the magnetic sag uncertainty presented in chapter 5.2.3.1, and is given in equation *{5.2.3.1-2}* or *{5.2.3.1-3}*. A future MWD gyro sag uncertainty will also be given by the same equations.

6.2.3.2 Horizontal Collar Misalignment

Horizontal collar alignment uncertainties can, like in the magnetic case, usually be omitted in wellbore position uncertainty studies.

7 Depth Uncertainties

Wellbore depth measurements are affected by major error sources. A priori and real time estimates of depth error terms are usually not of the same quality as similar inclination and azimuth uncertainty estimates. The main problem is that depth measurements are corrupted by large biases and human gross errors, which have proven to be a significant problem (Ekseth [25]), especially in connection with drill string depth measurements. Human gross errors can usually not be predicted, and will therefore not be included in the following depth uncertainty analysis. The result of this analysis must therefore only be used when adequate quality control routines are implemented to secure against human errors. Biases are included, but should ideally have been corrected for.

The different depth error terms, which are analysed in the following, are in contrast to angular error terms in chapter 5 and 6 quantified. These uncertainty figures are needed as input in the derivation of simplified depth uncertainty equations (chapter 7.4 and 7.5). The simplified weighting functions have the potential of becoming helpful tools at the planning stage, when the use of the detailed weighting functions are difficult due to unknown input parameters like drill string properties etc.

It is convenient to divide the different depth error sources into two classes, one reference error class and one deformation error class. The reference class is dependent on the type of rig the wellbore is drilled from, and not on the used type of depth measurement, which the deformation class mostly is dependent on.

7.1 Reference Depth

Land rigs and rigs installed on the sea bottom have a fixed depth reference point with respect to the underlying rock formation. The relative distance between the reference point and the formation is not significantly affected by earth tides (0.2m), which is the only possible reference error contributor for these types of rigs. Errors in the determination of the reference depth are mainly caused by human faults, and are therefore classified as gross errors and not taken into consideration. The reference uncertainty is therefore without interest when drilling from land- and sea bottom rigs, and can be omitted in position uncertainty studies.

The position of a reference point for depth measurements on floaters is not constant with respect to the underlying rock formation due to water tides (β_1), rig heave (β_2) and varying rig ballast (β_3). The first two effects do both have a high frequency compared to the duration of MWD surveys, the second one also compared to the duration of wireline surveys. The reference depth uncertainty components are then for a MWD survey given by

$$dD_I = i_s \sqrt{d\beta_1^2 + d\beta_2^2} \qquad \{7.1\text{-}1\}$$

$$dD_{II} = i_s d\beta_3 \qquad \{7.1\text{-}2\}$$

and for a wireline survey

$$dD_I = i_s d\beta_1 \qquad \{7.1\text{-}3\}$$

$$dD_{II} = i_s \sqrt{d\beta_2^2 + d\beta_3^2} \qquad \{7.1\text{-}4\}$$

i_s is a survey type identifier, which is one for depth measurements taken on a floater and zero else.

$d\beta_1$ is the ocean tide uncertainty (estimated to 1.5m 2σ), $d\beta_2$ the rig heave uncertainty (estimated to 4.0m 2σ), and $d\beta_3$ the rig ballast depth uncertainty (estimated to 2.0m 2σ).

dD_I is usually random between stations, and dD_{II} is usually systematic between stations and random between surveys.

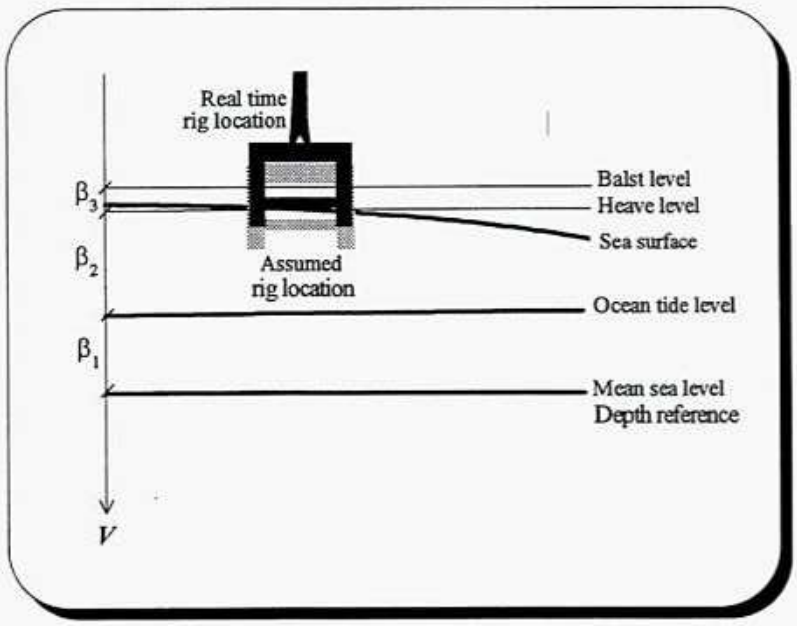

Figure 7.1-1 Depth reference errors for floater depth measurements

7.2 MWD Depth

Depth measurements in connection with MWD are usually drill pipe length measurements taken at the surface with a measuring tape. The depth measurement will because of downhole pipe deformations and uncertainties associated with the measuring tape, be erroneous. Special drill string equipment like jars etc. and lift-off procedures, adds extra uncertainty to the depth measurement. Size and error propagation characteristics of the different MWD depth error sources are discussed in the following.

Page 119 Equation {7.1-3} $dD_I = i_s d\beta_1$

Equation {7.1-4} $dD_{II} = i_s \sqrt{d\beta_2^2 + d\beta_3^2}$

7.2.1 *Measuring Tape*

High accuracy length measurements with measuring tapes are dependent on a number of corrections, where the scale factor error, the temperature expansion and the tape sag, are most important. Such corrections are usually not performed in connection with drill pipe length measurements, which therefore might have a relatively high uncertainty.

Measuring tapes are made of steel or a combination of steel and plastic materials. They are therefore subject to temperature expansion (α_t=1.2*10^{-5}/°C), which create a thermal dependent tape scale factor error. This error source is without significance. The drill pipes will usually be affected by the same thermal expansion as the tape.

A tape scale factor error ($d\upsilon_t$) is to some degree present in all measuring tapes (Holsen [1]), and varies slowly with time due to inelastic deformations. The tape scale factor error will be nearly constant as long as the same tape is used. The tape scale factor uncertainty is regarded as systematic between wellbores due to a high probability of using the same tape for a longer time period at the same platform. The tape scale factor error can be substituted with a thermal scale factor error. The reference temperature of the tape has then to be changed to the temperature where the tape is giving correct measurements. The accumulated tape scale factor error at measured depth D is then given by

$$dD_{III} = T_t \alpha_t D \qquad \{7.2.1\text{-}1\}$$

Where T_t is the difference between the zero tape scale factor error reference temperature and 0°C.

Free hanging horizontal tapes are subjected to a sagging effect, and therefore stretched. The same is the case for free vertical tapes if wind is present during the measurements. This sag can be up to half a meter, but is in average small since most drill pipes are measured at the rig floor and therefore free from tape sag. The tape sag depth uncertainty for one drill pipe can be estimated through an equation given by Holsen [1]. Multiplied by the number of pipes in the string, this gives the total tape sag error.

$$dD_{IV} = \frac{8s^2}{3l_p^2} D \qquad \{7.2.1\text{-}2\}$$

Where s is the sag and l_p is the average drill pipe length. The tape sag uncertainty is because of its bias nature, systematic between surveys.

7.2.2 *Telescopic and Suspension Effects*

Depth measurements have significant uncertainties due to jar-, accelerator-, pipe tally- and slips effects. Drilling jars and accelerators have often working areas of approximately 25" and 17", the pipe tally is often rounded towards whole meters, and slips are set randomly on the upper pipe. All these four error sources are random between stations and free from

Page 120 Line 2 paragraph 4 *and 0°C.* should be and the surface reference temperature for thermal drill string expansion.

angular- and geographical dependencies. They can therefore be added randomly together into one combined suspension depth error term given by

$$dD_V = \sqrt{\beta_4^2 + \beta_5^2 + \beta_6^2 + \beta_7^2} \qquad \{7.2.2\text{-}1\}$$

where β_4 is the drilling jar position uncertainty (0.3m 2σ), β_5 the accelerator position uncertainty (0.2m 2σ), β_6 the average pipe tally uncertainty (0.5m 2σ), and β_7 the slips position uncertainty (0.3m 2σ).

7.2.3 *Drill String Stretch*

A drill string hanging down the wellbore will because of gravity be significantly stretched compared to its measured surface length. The stretch is a function of drill pipe type, load and wellbore friction. The stretch (ε_{sk}) of drill pipe number k is found to be given by

$$\varepsilon_{sk} = \frac{l_{pk} G}{E_T a_{pk}} \left(\Sigma_{n=k}^{j} ((\cos I_n - \mu_n)(\rho_s - \rho_m) a_{pn} l_{pn}) - (W_b + F_Q) \right) \qquad \{7.2.3\text{-}1\}$$

It is here assumed that the station separation between station k-1 and k is equal to the length of pipe k. A different station separation will lead to an other upper summation index than j (the MWD survey station number), which is used here. G (9.78 - 9.83m/s^2) is the local gravity, E_T (2 - 2.25*10^{11}N/m^2) Young's modulus of steel, a_{pk} the cross sectional area of drill pipe k (drill pipe of a particular type shall according to the API standard have a 5% uncertainty in thickness), l_{pk} the nominal length of pipe k, μ_k the downhole friction factor acting on pipe k, I_k the downhole inclination of pipe k, ρ_s (7.8 - 7.9 kg/dm^3) the specific weight of steel, ρ_m (1.4 - 1.8 kg/dm^3) the density of mud, W_b the weight on bit, and F_Q the total mud flow induced lift force. These figures are collected by Ivar Haarstad and Atle Martinsen at IKU Petroleum Research, Trondheim, in an unpublished study for Statoil.

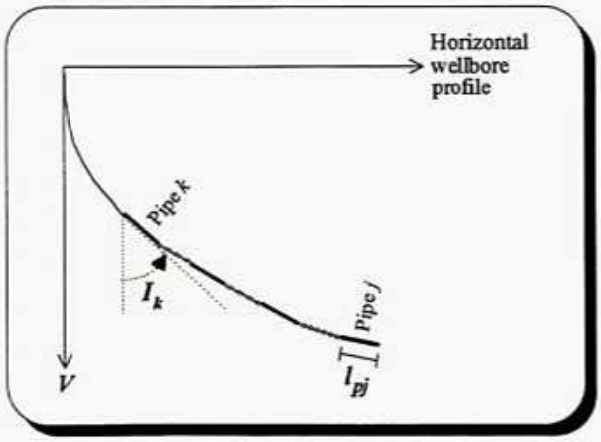

Figure 7.2.3-1 Drill pipes generating stretch in drill pipe k at measurement station j

Little is known about downhole friction factors, but it is believed that it is increasing in building sections (both inclination and azimuth) compared to straight hole sections due to side wall effects. It is therefore assumed that the friction factor for pipe number k can be estimated by an equation of the following type

$$\mu_k = \mu_{m1}\sin I_k + \mu_{m2}\frac{abs(I_k - I_{k-1}) + abs(A_k - A_{k-1})}{l_{pk}} \qquad \{7.2.3\text{-}2\}$$

where μ_{m1} (0.15 - 0.20) is the friction factor for a straight horizontal wellbore section, and μ_{m2} (0.1, only a guess because of no available data) is the additional friction factor due to wellbore curvature for a wellbore section with doglegs of 1° per unit length (pipe).

MWD depth measurements taken when the mud pump is turned on, are subject to three significant lifting forces that tend to reduce the length of the drill string. The three forces are the drill bit jet lifting force, the collar buoyancy force, and the outer mud induced pipe shear force. The resultant lift force is according to Rogaland Research (Kyllingstad [26]) given by

$$F_Q = (a_{po} + x a_a)\Psi_o D + \frac{\rho_m Q^2 \cos\alpha}{a_n} \qquad \{7.2.3\text{-}3\}$$

where a_{po} is the outer pipe area, a_a is the annular area, a_n the total bit nozzle area, x the fraction of drill string shear force relative to total shear force, Ψ_o the annulus pressure loss gradient, ρ_m the specific weight of mud, Q the mud flow rate, α the bit nozzle angle, and D the depth. The use of this equation is not very practical in directional surveying uncertainty estimation. This because many parameters needed in the computation usually will be unknown. Simulations done by Rogaland Research indicate an increase to the static buoyancy effect of approximately 1.5% (ρ_Q=0.015). It is possible to approximate the flow lifting force effect by making use of this rough estimate.

The stretch is always positive, and is therefore a biased type error, which it ideally should have been corrected for. A full correction is, however, not possible because of the indicated variations in fundamental parameters. There will always be remaining systematic errors left. The drill pipe stretch uncertainty must because of this be divided into tree parts. One constant part (always systematic, even between fields), one systematic part (systematic within and random between surveys), and one random part (random between stations). The random between station part is mainly caused by variations in drill pipe properties and local friction. The systematic bias stretch uncertainty at measurement station j is given by

$$dD_{VT} = \Sigma_{k=1}^{j}\frac{l_{pk}G}{E_T a_{pk}}\left(\Sigma_{n=k}^{j}((\cos I_n - \mu_n)(\rho_s - (1 + p_c\rho_Q)\rho_m)a_{pn}l_{pn}) - W_b\right) \qquad \{7.2.3\text{-}4\}$$

where the total number of pipes down to station j is equal to j.

The following input parameters can be used in uncertainty predictions if detailed drill string and mud information are unclear: $G = 9.81\text{m/s}^2$, $E_T = 2.12*10^{11}\text{N/m}^2$, $\mu_{m1} = 0.17$, $\mu_{m2} = 0.10$, $\rho_s = 7.85\text{kg/dm}^3$, $\rho_m = 1.6\text{kg/dm}^3$, $W_b = 0\text{kg}$ (20000 kg for floaters), $\rho_Q = 0.015$, and $p_c = 1$ for MWD measurements with the pump turned on and $p_c = 0$ if the pump are

turned off. Standard operational procedure is to lift the drill bit off bottom and work out torque before taking MWD measurements. There is because of this usually not any weight on bit when the MWD depths are recorded. The only exception is for floaters where some weight on bit are left during MWD measurement to secure against downhole movements during measurements. Cross sectional areas are difficult to generalise on. The distribution of drill collars, heavy weight drill pipes, standard drill pipes and thin drill pipes can be very different from well to well, an is usually a function of both wellbore type and rock formation.

Equation *{7.2.3-4}* shows that the stretch is nearly proportional to the product of the measured depth and the difference between the vertical- and the average vertical depth for standard wellbore profiles like vertical and extended reach.

The systematic within and random between surveys stretch depth uncertainty can be found by making use of equation *{7.2.3-4}* twice with different input parameters. Once with average inputs, and once with maximum 95% confidence interval inputs. The average result must be subtracted from the maximum result to give the random between surveys uncertainty. The random between stations stretch uncertainty can be computed by a similar approach.

With the same input parameters as given for equation *{7.2.3-1}* and an assumed 50% variation in weight on bit and flow induced lifting forces, the 2σ systematic within a survey drill pipe stretch uncertainty is given by

$$dD_{VII} = \Sigma_{k=1}^{j} \frac{l_{pk}1.13G}{E_T a_{pk}} \left(\Sigma_{m=k}^{j} \left(\left(\cos I_n - \frac{\mu_n}{1.12} \right) \left(\rho_s - \left(1 + \frac{p_c \rho_Q}{2} \right) \rho_m \right) \frac{a_{pm}}{0.8} l_{pm} \right) - \frac{W_b}{2} \right) - dD_{VI} \quad \{7.2.3\text{-}5\}$$

The 2σ random between station drill pipe stretch uncertainty is further given by

$$dD_{VIII} = \Sigma_{k=1}^{j} \frac{l_{pk}1.10G}{E_T a_{pk}} \left(\Sigma_{m=k}^{j} \left(\left(\cos I_n - \frac{\mu_n}{1.12} \right) (\rho_s - (1 + p_c \rho_Q) \rho_m) \frac{a_{pm}}{0.91} l_{pm} \right) - W_b \right) - dD_{VI} \quad \{7.2.3\text{-}6\}$$

7.2.4 *Drill String Temperature Expansion*

The downhole formation temperature is usually much higher than the surface temperature where the drill pipe lengths are measured. The formation temperature will propagate through the annulus mud to the drill string and thereby induce a thermal expansion. It is complicated to find an exact estimate for this expansion since it involves both the annulus and the pipe mud temperature gradients. Experience has shown that the two mud temperature gradients becomes nearly identical after a few full cycles of mud circulation, and that their average value equals the average formation gradient. The drill string temperature can therefore for all practical purposes be set to the average mud temperature, and the thermal expansion of drill pipe *k* is then given by

$$\varepsilon_{tk} = \alpha_p T_g D_{Vk} l_{pk} \quad \{7.2.4\text{-}1\}$$

where α_p (α_p=1.2*10^{-5}/°C) is the thermal expansion coefficient of steel, l_{pk} the length of drill pipe k, T_g the vertical formation temperature gradient, and D_{vk} the average vertical depth of pipe k given by

$$D_{Vk} = \frac{l_{pk}}{2}\cos I_k + \Sigma_{n=1}^{k-1} l_{pn}\cos I_n \qquad \{7.2.4\text{-}2\}$$

where I_k is the downhole inclination of pipe k.

The vertical thermal gradient is a statistical quantity. It can be quantified with three figures. One global linear geothermal gradient (T_{gb}), a linear systematic wellbore based departure from the global trend (T_{gs}), and wellbore based random fluctuations (T_{gr}). The last term is usually without significance compared to the other two when a nearly constant mud thermal gradient has been achieved. The global trend is a bias, which it ideally should have been corrected for. The thermal gradient parameters are estimated to 0.04°C/m (T_{gb}), and 0.005°C/m 2σ (T_{gs}) or 12.5% of T_{gc}. These figures are based on North Sea area data, and is collected by Ivar Haarstad and Atle Martinsen at IKU Petroleum Research.

The global systematic between surveys drill pipe thermal expansion uncertainty is then given by

$$dD_{IX} = \alpha_p T_{gb} \Sigma_{k=1}^{j} l_{pk}\left(\frac{l_{pk}}{2}\cos I_k + \Sigma_{n=1}^{k-1} l_{pn}\cos I_n\right) \qquad \{7.2.4\text{-}3\}$$

and the systematic within and random between wellbores thermal uncertainty is given by

$$dD_X = 0.125 dD_X \qquad \{7.2.4\text{-}4\}$$

These two equations show that the thermal expansion depth uncertainty is near to proportional to the product of the measured depth and the average vertical depth for traditional wellbore designs.

7.2.5 *Mud Pressure Effects*

Downhole drill pipes will be exposed to a hydrostatic pressure due to the in-hole mud, and thereby compressed in all three dimensions. The axial compression of drill pipe k is given by

$$\varepsilon_{pk} = l_{pk} G \frac{(1-2\nu_p)}{E_Y} \rho_m D_{Vk} \qquad \{7.2.5\text{-}1\}$$

where G is the gravity constant, E_Y Young's modulus of steel, ν_p Poisson ratio of steel, ρ_m the specific weight of mud, and D_{vk} the average vertical depth of pipe k.

Page 124 Equation {7.2.4-4} $dD_X = 0.125 dD_{IX}$

The hydrostatic pressure induced depth uncertainty will because of variations in input figures consist of a bias, a systematic within surveys, and a very little significant random between station part. The bias is given by

$$dD_{XI} = \Sigma_{k=1}^{j} l_{pk} G \frac{(1-2\nu_p)}{E_Y} \rho_m \left(\frac{l_{pk}}{2} \cos I_k + \Sigma_{n=1}^{k-1} l_n \cos I_n \right) \qquad \{7.2.5\text{-}2\}$$

This uncertainty is also near to proportional to the product of the measured depth and the average vertical depth for traditional wellbores.

The following input parameters can, according to chapter 7.2.3, be used for uncertainty predictions if detailed drill string and mud information are unknown: $G = 9.81\text{m/s}^2$, $E = 2.12*10^{11}\text{N/m}^2$, $\nu_p = 0.3$, and $\rho_m = 1.6\text{kg/dm}^3$.

The 2σ systematic between survey part is further given by

$$dD_{XII} = \left(\Sigma_{k=1}^{j} l_{pk} 1.41 G \frac{(1-2\nu_p)}{E_Y} \rho_m \left(\frac{l_{pk}}{2} \cos I_k + \Sigma_{n=1}^{k-1} l_n \cos I_n \right) \right) - dD_{XI} \qquad \{7.2.5\text{-}3\}$$

There will be an additional pressure inside the drill string that will cause an expansion when mud is circulated (the ballooning effect). This error source is only applicable for MWD tools that take measurements with the pumps turned on. The expansion is a function of mud pump pressure, friction losses, bit pressure drop, and is according to Kyllingstad [26] given by

$$\varepsilon_b = (1 - 2\nu_p)\kappa a_p \left(1 - \frac{D}{2(D+l_{d/2})} \right) \frac{P_p D}{E_Y} \qquad \{7.2.5\text{-}4\}$$

where E_Y is Young's modulus of steel, ν Poisson ratio of steel, a_p the average cross sectional drill pipe area, κ the surface pressure loss factor, $l_{d/2}$ half the normalised pressure loss length, P_p the stand pipe pressure, and D the measured depth.

Equation *{7.2.5-4}* is not practical in connection with position uncertainty estimations. It involves hydraulic parameters that usually will be unknown to the directional surveyor. This is special the case in connection with uncertainty predictions at the wellbore planning stage. Simulations with realistic hydraulic inputs show, however, a trend that does not differ much from a linear trend for typical wellbore lengths (Kyllingstad [26]). This fact can be used to create a simplified formula for planning purposes

$$dD_{XIII} = i_p f_b D \qquad \{7.2.5\text{-}5\}$$

where f_b is the ballooning factor, D the measured depth, and $i_p = 1$ if mud pumps are turned on during measurements and $i_p = 0$ if pumps are turned off. The ballooning factor is estimated to 0.08/1000m (Kyllingstad [26]) in a standard case where the measured depth is 4000m, the drill pipes 5", the mud weight 1.5kg/dm^3, the flow rate 2500 l/min, and there is used a three 16/32" bit nozzles.

dD_{XIII} is a bias type uncertainty, which means that it is a systematic between fields uncertainty. In addition, there will also be random between stations and systematic within and random between surveys ballooning uncertainties. The random between stations uncertainty is mainly caused by fluctuations in the flow rate and variations in drill pipe properties. It is usually without significance compared to the two systematic uncertainties due to favourable error propagation characteristics. The systematic within and random between surveys uncertainty is to a large degree caused by change of bit and major adjustments of mud and flow rates at bit runs when new MWD surveys usually are initialised. A 50% variation at both sides of the estimated bias uncertainty seem to be a reasonable 2σ estimate when the large variation in drilling conditions in different wellbore sections is taken into consideration. The systematic within and random between surveys ballooning uncertainty is then given by

$$dD_{XIV} = 0.5D_{XIV} \qquad \{7.2.5\text{-}6\}$$

7.3 Wireline Depth

Depth measurements in connection with magnetic electronic multishot measurements (EMS) and gyro measurements are usually performed with wireline length measurements at the surface. The depth measurement will because of downhole wireline deformation and uncertainties associated with the measuring device be erroneous. Size and error propagation characteristics of the different error sources will be discussed in the following. Two types of wireline depth systems are available. The most common type makes use of measuring wheels, while the other makes use of magnetic markers installed on the wireline. The second type is unusual in connection with directional surveying, and will not be covered here.

7.3.1 Suspension Effects

Wireline depth measurements will usually have a significant random between station uncertainty due to the wireline suspension (tension sensor etc.) given by

$$dD_{XV} = \beta_8 \qquad \{7.3.1\text{-}1\}$$

β_8 is roughly estimated to 0.3m 2σ.

7.3.2 Wireline Stretch

A wireline hanging down in a wellbore will because of gravity be significantly stretched compared to its measured surface length. The stretch is a function of wireline type, wireline and collar load, wellbore friction, and previous deformation history. The wireline stretch consists of two significant parts. An elastic part which always is present, and an inelastic part which is the dominant on newer wirelines.

Page 126 Equation {7.2.5-6} $dD_{XIV} = 0.5dD_{XIII}$

The elastic wireline stretch (ε_{sk}) acting on a short (usually equal to the station separation) wireline element k can be found by the same type of stretch equation as for drill pipes.

$$\varepsilon_{sk} = \frac{l_{wk}G}{E_w a_w}\left(\Sigma_{n=k}^{j}((\cos I_n - \mu_n)(\rho_w - \rho_m)a_w l_{wn}) + W_s\right) \qquad \{7.3.2\text{-}1\}$$

where G (9.78 - 9.83m/s^2) is the local gravity, E_w (0.90 - 1.15*10^{11}N/m^2) Young's modulus of standard wirelines, a_w the cross sectional wireline area (8 - 12 mm in diameters), l_{wk} the separation between station k-1 and k, μ_k the downhole friction factor acting on element k, I_k the average downhole inclination of element k, ρ_w (4.4 - 5.2 kg/dm^3) the specific weight of standard wirelines, ρ_m (1.4 - 1.8 kg/dm^3) the specific weight of mud, and W_s (100 - 400kg) the total instrument collar weight.

The friction factor acting on element k can be estimated through

$$\mu_k = \mu_m \sin I_k \qquad \{7.3.2\text{-}2\}$$

where μ_m (0.15 - 0.20) is the friction factor for a straight horizontal wellbore section.

The wireline stretch uncertainty must similarly to the drill string case be divided into tree parts. One bias (always systematic, even between fields), one systematic part (systematic within and random between surveys), and one random between stations part. The random between station part is mainly caused by variations in wireline properties and local friction.

The systematic between field wireline elastic stretch bias uncertainty at station j is given by

$$dD_{XVI} = \frac{G}{E_w a_w}\Sigma_{k=1}^{j} l_{wk}\left(\Sigma_{n=k}^{j}((\cos I_n - \mu_n)(\rho_w - \rho_m)a_w l_{wn}) + W_s\right) \qquad \{7.3.2\text{-}3\}$$

For uncertainty predictions, the following input parameters can be used if detailed drill string and mud information still are unknown: G = 9.81m/s^2, E_w = 1.04*10^{11}N/m^2, μ_m = 0.17, ρ_w = 4.8kg/dm^3, ρ_m = 1.6kg/dm^3, W_s = 250kg, and a_w = 78.5 mm^2.

Wireline properties can as indicated vary significantly depending on manufacturer, number of conductors etc. The 2σ systematic within a survey elastic wireline stretch uncertainty can be estimated by

$$dD_{XVII} = \frac{1.85G}{E_w a_w}\Sigma_{k=1}^{j} l_{wk}\left(\Sigma_{n=k}^{j}\left(\left(\cos I_n - \frac{\mu_n}{1.12}\right)\left(\rho_w - \frac{\rho_m}{0.8}\right)\frac{a_w l_{wn}}{0.64}\right) - \frac{W_s}{2.5}\right) - dD_{XVI} \qquad \{7.3.2\text{-}4\}$$

It is here assumed a 50% variation in the mud flow induced uncertainties from survey to survey.

Similar is the 2σ random between station drill pipe stretch uncertainty given by

$$dD_{XVIII} = \frac{1.05G}{E_w a_w}\Sigma_{k=1}^{j} l_{wk}\left(\Sigma_{n=k}^{j}\left(\left(\cos I_k - \frac{\mu_n}{1.12}\right)(\rho_w - \rho_m)\frac{a_w l_{wn}}{0.95}\right) - W_s\right) - dD_{XVI} \qquad \{7.3.2\text{-}5\}$$

Inelastic wireline stretch is more complicated to handle since it is a time dependent error source. New unused wirelines will get a large inelastic stretch, which gradually will decrease to zero with repeated use. Theys [27] estimates the inelastic stretch at the first run to about 0.6m per 1000m. How long the inelastic stretch remains a problem is, however, still not answered. The inelastic stretch will therefore be included in an empirical error term called repeatability errors, which is based on real measurements, and which is explained in chapter 7.3.8.

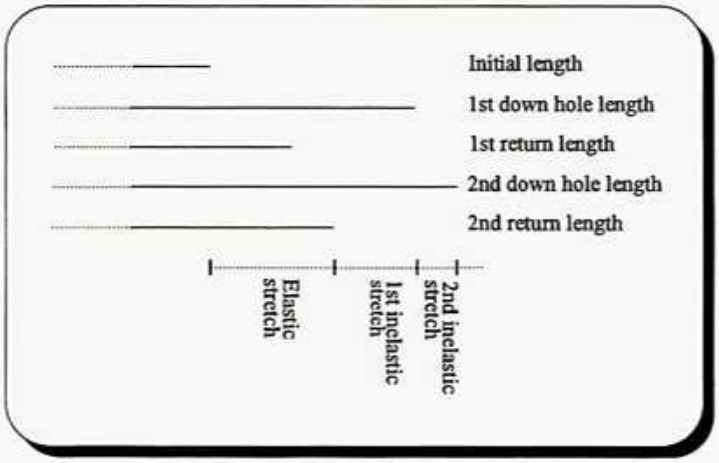

Figure 7.3.2-1 Typical wireline stretch behaviour

7.3.3 *Wireline Temperature Expansion*

The downhole formation temperature is greater than the surface temperature at which the wireline length is measured. The formation temperature will propagate into the wireline through the mud, and thereby induce a thermal expansion. Ander [28] gives a wireline thermal expansion constant expressed in *1/°C/N*. The wireline thermal expansion must therefore be proportional to the tension in addition to the temperature. The depth bias at measurement station *j* is then given by

$$dD_{XIX} = \alpha_w T_{gb} \Sigma_{k=1}^{j} (l_{wk} W_k D_{Vk}) \qquad \{7.3.3\text{-}1\}$$

where α_w = 1.5 - 2.5*10^{-10}/°C/N, l_{wk} is the station separation between station *k-1* and *k*, T_{gb} the global vertical formation temperature gradient (0.04°C/m), W_k the average wireline tension in element *k* and D_k the average measured vertical depth in element *k*. The tension in element *k* is given by

$$W_k = G\Sigma_{m=k}^{j}((\cos I_n - \mu_n)(\rho_w - \rho_m)a_w l_{wn} + W_s) \qquad \{7.3.3\text{-}2\}$$

and the vertical depth is given by

$$D_{Vk} = l_{wk}\frac{\cos I_k}{2} + \Sigma_{n=1}^{k-1} l_{wn}\cos I_n \qquad \{7.3.3\text{-}3\}$$

The systematic within and random between wellbores thermal wireline uncertainty is like in the drill pipe case given by

$$dD_{XX} = 0.125 dD_{XX} \qquad \{7.3.3\text{-}4\}$$

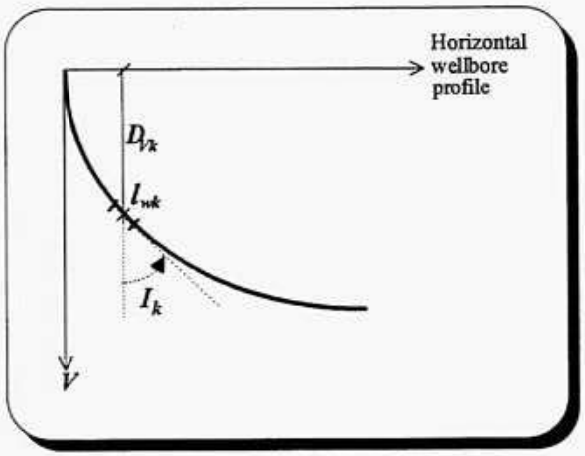

Figure 7.3.3-1 Vertical depth at wireline element *k*

7.3.4 *Measuring Wheel Effects*

Wearing of a measurement wheel and calibration inaccuracies give rise to a significant systematic within and random between surveys wireline scale factor depth uncertainty. It is given by

$$dD_{XXI} = d\upsilon_{ww} D \qquad \{7.3.4\text{-}1\}$$

where $d\upsilon_{ww}$ is the 95% wireline wheel scale factor uncertainty, and D the total depth. $d\upsilon_{w}$ is according to Theys [27] 0.0013.

7.3.5 *Wireline Twisting*

Due to coiling effects, the wireline will be twisted while running into the hole resulting in a to large depth measurement. Theys [27] estimates this wireline scale factor uncertainty $d\upsilon_{wt}$ to between 0.2 and 0.5 per 1000, which means that it both has a mean and a spread. It consists therefore of a bias and a systematic component. The systematic between surveys uncertainty (bias) is then given by

$$dD_{XXII} = d\upsilon_{wt,b}D \qquad \{7.3.5\text{-}1\}$$

and the systematic within and random between surveys uncertainty by

$$dD_{XXIII} = d\upsilon_{wt,s}D \qquad \{7.3.5\text{-}2\}$$

$d\upsilon_{wt,b} = 0.0003$, $d\upsilon_{wt,s} = 0.0002$, and D is the measured depth.

7.3.6 *Yo-yoing*

Dynamic effects in the wireline will result in position oscillations while stopping to take a measurement if the instrument is not clamped to the casing or the open hole. The same effect will also be noticeable in continuous measurements because of random variation in tension due to temporary stuck pipe etc. The exact nature of this error is unknown, but it is believed to act as a random between stations wireline scale factor error. Theys [27] estimates it to about 0.4m per 1000m leading to the following random between stations depth uncertainty

$$dD_{XXIV} = d\upsilon_{wy}D \qquad \{7.3.6\text{-}1\}$$

where D is the measured depth, and $d\upsilon_{wy} = 0.0004$.

7.3.7 *Viscous Drag*

Wireline depth measurements taken while continuously running into the hole are subjected to viscous drag errors. The viscous drag leads to a reduction in the measured depth while running into the hole and to an increase while pulling out. The error has known sign, and is therefore a bias. It is, however, a complex error source, which is dependent on mud viscosity, logging speed, and wireline properties. The error is not among the largest wireline depth errors, and detailed modelling is therefore not necessary. Theys [27] has estimated it to a wireline scale factor error varying between 0.2 and 0.4 per 1000. This give rise to a systematic between fields uncertainty given by

$$dD_{XXV} = d\upsilon_{wd,b}D \qquad \{7.3.7\text{-}1\}$$

where $d\upsilon_{wd,b} = 0.0003$, and a systematic within and random between surveys uncertainty given by

$$dD_{XXVI} = d\upsilon_{wd,s}D \qquad \{7.3.7\text{-}2\}$$

where $d\upsilon_{wd,s} = 0.0002$.

7.3.8 *Repeatability Uncertainties*

There are a number of error sources associated with wireline depth measurements, that are extremely difficult to quantify without major research projects. Examples on such errors are inelastic wireline stretch, slippage between wireline and measurement wheel, wireline buckling, etc. Common for most of these errors are that most of the effect will appear as a difference between the total inrun depth measurement and the total outrun depth measurement. Field data supplied by major wireline operators indicate that the combined effect creates a significant artificial repeatability scale factor error, which is systematic within and random between surveys. This field data set is made up of about 40 in / out runs with different measured depths and wellbore geometry. The scale factor uncertainty estimated out of these 40 surveys is
$d\upsilon_{wr} = 0.00082$ (2σ). The repeatability depth uncertainty is then given by

$$dD_{XXVII} = d\upsilon_{wr} D \qquad \{7.3.8\text{-}1\}$$

7.4 Simplified Depth Uncertainty Equations

Most depth uncertainty equations presented in the previous depth uncertainty chapters involve factors that are directly related to the drilling process (mechanical drill string or wireline properties, mud programs, formation temperatures, etc.). This is the case even for the most dominant error sources like the stretch and the temperature expansion. Accurate input figures, which are necessary to justify the use of such complex equations, are usually not available during directional uncertainty estimations. In stead of making use of average values with large uncertainties in these equations, it is recommended to develop simplified depth uncertainty equations generating the same accuracy. The aim should be to reproduce the total effect (as given by the accurate set of equations) to within a few decimetres or ca 80%, for all major wellbore designs. Simulations performed with help of equations *{7.1.1-1}* through *{7.3.3-4}* (see next chapter) indicates that this goal can be fulfilled by a simple random summation function in the measured depth (D) and in the product of the measured depth (D) and the vertical depth (D_v).

$$dD = \sqrt{k_1^2 + (k_2 D)^2 + (k_3 D_v D)^2} \qquad \{7.4\text{-}1\}$$

This equation is based on the fact that major depth error sources, according to the depth error discussion, can be divided into three classes. One reference class proportional to one, one scale class nearly proportional to the measured depth, and one stretch / temperature class nearly proportional to the product of the measured depth and the average vertical depth or the difference between the vertical- and the average vertical depth.

The average vertical depth is, however, difficult to incorporate in the proposed uncertainty estimation method. Information from below the point of investigation will be necessary, but is usually not available. This problem can be bypassed by substituting the average vertical depth with the actual measured vertical depth (or planned depth). This is a major simplification, but seems nevertheless to give an accuracy within the desired 80%.

The result obtained with equation *{7.4-1}* is the total depth uncertainty at a given survey station. It is made up of both random, systematic and bias uncertainties. The equation is therefore not suited for use in connection with wellbore position uncertainty calculations, where the error propagation nature of independent error components are a major concern. To solve this problem, the equation has to be divided into the following three independent classes

- the reference class (proportional to one)
- the scale class (proportional to the measured depth D)
- the stretch / temperature class (proportional to the product of the measured depth D and the vertical depth D_v)

Each of these three classes might further have to be divided into independent error propagation components. The reference class must, according the discussion in previous chapters, be divided into a random between stations error component and a systematic within and random between surveys component. The scale class must also be divided into two major components, a systematic within and random between surveys component, and a bias component. The scale bias component is only significant for wireline measurements, where it is caused by wireline twisting and instrument collar loads. The stretch class has therefore only one significant component, a bias. This leaves five significant depth uncertainty components, which it is necessary to treat separately in wellbore position uncertainty studies. This number can be reduced to four for MWD depth measurements by making use of the fact that the scale bias is without significance. A similar reduction to four for wireline depth measurements will lead to increased model uncertainty, because the scale bias has to be incorporated in the systematic scale and bias stretch components. The simulations in the next chapter are, however, indicating that the searched accuracy level of 80% can be reached even with this simplification. It will reduce complexity, and is therefore recommended.

The four necessary independent depth uncertainty components are then given by

- the random between stations reference component	$dD_1 = dk_{rr}$	*{7.4 -2}*
- the systematic within surveys reference component	$dD_2 = dk_{rs}$	*{7.4-3}*
- the systematic within surveys scale component	$dD_3 = Ddk_{ss}$	*{7.4-4}*
- the bias stretch component	$dD_4 = D_V Ddk_{sb}$	*{7.4-5}*

where dk_{rr} is the random between stations reference depth error, dk_{rs} the systematic within surveys reference depth error, dk_{ss} the systematic within surveys scale depth error, and dk_{sb} the bias stretch depth error.

The stretch bias can in the future be reduced and transformed to a small systematic within and random between surveys uncertainty component, if stretch and temperature corrections are introduced to the depth measurements. This will because of favourable error propagation characteristics lead to major improvements in the wellbore position accuracy.

7.5 Depth Uncertainty Simulations

To test the quality of the combined effect of equations *{7.4-2}* to *{7.4-5}* with respect to the combined effect of the more detailed depth uncertainty equations, simulations where made for three different wellbore profiles. A 4000 meter deep vertical wellbore (*a*), a 4000 meter deep 45° inclined wellbore (*b*), and a 4000 meter long simplified real wellbore with both horizontal and vertical sections (*c*). First, all uncertainty components given in equations *{7.1.1-1}* through *{7.3.3-4}* where calculated for four different scenarios, MWD drill pipe depth measurements for land / sea bottom rigs (1) and for floaters (2), and wireline depth measurements for land / sea bottom rigs (3) and for floaters (4). This was done for each of the three given profiles. Input parameters given in chapters 7.1, 7.2 and 7.3 where used in these calculations. The different uncertainty components where then summed randomly (root sum square) into the random reference class, the systematic reference class, the systematic scale class, and the bias stretch class (standard summing where used for the bias), based on their dominant error propagation nature. The four constants dk_{rr}, dk_{rs}, dk_{ss} and dk_{sb} where then optimised with respect to the simulated results for the three given profiles. This was done for each of the four scenarios (1, 2, 3 and 4). At last, the total depth error was calculated by summation of depth error components given in equations *{7.1.1-1}* through *{7.3.3-4}* (random or linear summation based on error type), and compared against the root sum square of equations *{7.4-2}* to *{7.4-5}*.

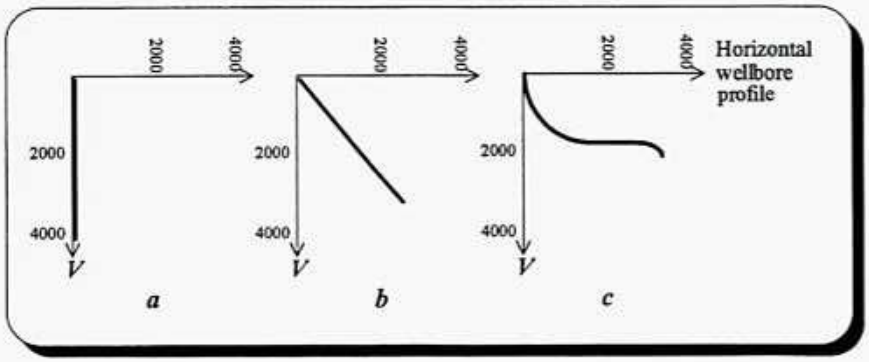

Figure 7.5-1 Wellbore profiles used in depth simulations

The results from the simulations are given in the following two sub chapters. The differences between the use of the whole range of accurate equations and the use of the four simplified equations are, as it will be shown, never greater than 6% of the actual error for MWD depth measurements, and never greater than 15% for wireline measurements. This is well within the desired 80% accuracy level, and proves that it should be sufficient to use the four artificial depth error components dk_{rr}, dk_{rs}, dk_{ss} and dk_{sb} in wellbore position uncertainty studies.

The constants presented in the next two chapters are not meant as inputs in uncertainty estimations. They are derived only to be used for this confirmation study. Input parameters must be based on a wider range of wellbore profiles and drill string- and wireline designs. This will probably increase the uncertainty created by the simplified model slightly compared to what is seen here, but probably not enough to question the 80% accuracy level. The number of unusual wellbore designs and drill string combinations with major deviations from what is used here, are to small.

7.5.1 MWD Simulations

The following depth uncertainty constants for MWD depth measurements on drill pipes are estimated through a least square fitting of simulations described in the previous chapter

Depth Constant	Land- / Sea Bottom Rig	Floater
k_{ra}	0.7	4.4
k_{rb}	0	2
k_{ia}	$4.8*10^{-4}$	$4.2*10^{-4}$
k_{ib}	$4.4*10^{-7}$	$3.0*10^{-7}$

which gives the following differences between the simplified depth estimation method and the optimal solution using the whole range of detailed depth uncertainty equations

Measured Depth [m]	Land / Bottom Rig				Floater			
	Estimated Depth Error [m]		Deviation		Estimated Depth Error [m]		Deviation	
	Precise	Simp-lified	Meter	%	Precise	Simp-lified	Meter	%
Vertical Wellbore								
1.000	1.4	1.3	0.1	6	5.0	5.2	-0.1	-3
2.000	3.0	3.0	0.0	0	6.1	6.2	-0.1	-1
3.000	5.3	5.6	-0.2	-4	7.9	7.9	0.1	1
4.000	8.6	9.1	-0.5	-5	10.6	10.2	0.4	4
45° Inclined Wellbore								
1.000	1.3	1.2	0.1	6	4.9	5.1	-0.2	-4
2.000	2.5	2.4	0.0	1	5.7	5.8	-0.2	-3
3.000	4.3	4.4	-0.1	-3	6.9	7.0	-0.1	-2
4.000	6.8	7.0	-0.2	-3	8.8	8.7	0.1	1
Real Horizontal Wellbore								
1.000	1.4	1.3	0.1	6	5.0	5.1	-0.1	-3
2.000	2.7	2.6	0.1	2	5.8	6.0	-0.1	-2
3.000	4.0	3.8	0.2	5	6.6	6.6	0.0	0
4.000	5.8	5.5	0.2	4	7.7	7.6	0.1	2

7.5.2 *Wireline Simulations*

The following depth uncertainty constants for wireline depth measurements are estimated through a least square fitting of simulations described in chapter 7.5

Depth Constant	Land- / Sea Bottom Rig	Floater
k_{ra}	0.4	4.3
k_{rb}	0	2
k_{aa}	$22*10^{-4}$	$22*10^{-4}$
k_{ab}	$4.1*10^{-7}$	$4.7*10^{-7}$

which give the following differences between the simplified depth estimation method and the optimal solution using the whole range of detailed depth uncertainty equations

Measured Depth [m]	Land / Bottom Rig				Floater			
	Estimated Depth Error [m]		Deviation		Estimated Depth Error [m]		Deviation	
	Precise	Simp-lified	Meter	%	Precise	Simp-lified	Meter	%
Vertical Wellbore								
1.000	3.0	2.7	0.4	13	6.4	5.7	0.7	12
2.000	6.3	6.1	0.2	3	8.8	8.3	0.5	5
3.000	9.8	10.3	-0.5	-6	11.7	12.4	-0.6	-5
4.000	13.7	15.4	-1.7	-12	15.3	17.5	-2.2	-15
45° Inclined Wellbore								
1.000	3.1	2.5	0.5	17	6.5	5.6	0.9	14
2.000	6.0	5.6	0.4	7	8.6	7.8	0.8	9
3.000	8.8	9.2	-0.4	-5	10.8	11.1	-0.4	-3
4.000	12.6	13.5	-0.8	-7	14.2	15.3	-1.1	-8
Real Horizontal Wellbore								
1.000	3.1	2.6	0.5	15	6.5	5.7	0.8	13
2.000	6.2	5.8	0.4	6	8.7	8.0	0.7	8
3.000	9.3	8.6	0.7	7	11.3	10.4	0.9	8
4.000	12.3	12.0	0.3	2	13.9	13.7	0.2	2

8 Error Propagation in Inertial Tools

Inertial navigation systems (INS) are navigation instruments widely used in the aerospace industry. Examples on use in connection with land surveying and wellbore positioning are also known. INS systems are built with at least 3 sensitive accelerometer- and gyro axis. Both strapped down and gimballed systems are known. Many gyro types are used in INS systems ranging from standard rotor gyros, through ring laser gyros to hemispherical resonator gyros. Two systems designed for wellbore applications are known. It is the FINDS and the Rigs system. Both are operated by Baker Hughes INTEQ.

FINDS is an old gimballed system equipped with three accelerometers and three rotor gyros. The system has a large outer diameter (10"), and can therefore only be used in the top hole section. It is because of this operational limitation seldom in use, and will therefore not be included in this document.

Rigs (Gibbons [27]) is a strapped down three accelerometers and three ring laser gyros system. It is smaller than FINDS (5"), and has therefore a wider use. It fits into intermediate sections, but this system is also to large to fit into many bottom hole sections.

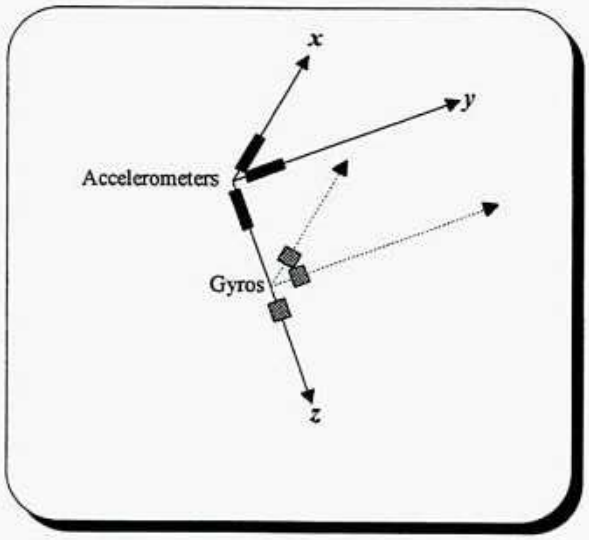

Figure 8-1 Example on sensor mounting in INS systems

INS systems are continuous instruments, that estimate the wellbore co-ordinates directly through a double integration of sensed accelerations. The gyros are used to keep track on accelerometer orientations, and not for inclination and azimuth determination as in traditional directional surveying. Inclinations and azimuths given by INS systems are derived from the measured wellbore co-ordinates, and it is therefore very important to distinguish between directional instruments and INS instruments in wellbore position uncertainty studies.

The error behaviour of inertial systems are well known and documented. The need for some kind of aiding to control a rapid accuracy deterioration is the most dominant factor. This deterioration is caused by the double integration process, which lead to an exponential growth of the resultant error. FINDS make use of zero velocity updates for aiding, while RIGS make use of the wireline speed. Zero velocity updates are the most precise of the two methods, but has the disadvantage that it leads to increased survey time.

A number of INS error analysing software packages are commercially available (for example one made by Paul G. Savage Minnetonka, Minnesota). They are usually based on some kind of Kalman filter based Monte Carlo simulations, which are rigid and time consuming calculations. These programs can of course be used directly in connection with wellbore positioning uncertainty studies, but this is not recommended. The use of different program packages are not practical, and should be avoided. A wellbore is often surveyed with a combination of many instrument types. An integration of INS systems into uncertainty programs designed for gyro and magnetic instruments is therefore more suitable. Especially at the planning stage where a large number of wellbore profiles and survey programs are to be evaluated within a short time period. A quick interactive response is then also of great importance.

The INS module in an integrated wellbore planning software should be as similar to other directional uncertainty modules as possible (improved Wolff deWardt methods). This to secure easy maintenance and introduction of new instrument types. A simplified recording station to recording station approach should therefore be used instead of time demanding Monte Carlo and Kalman filter simulations. It will in the following be shown that it is possible to develop such a method for strapped down systems. Gimballed systems will not be covered. They are becoming more and more rare in the aerospace industry. New wellbore INS instruments are therefore likely to be of the strapped down type.

Two different station to station solutions are identified. One co-ordinate based method, and one inclination, azimuth and relative depth method. The latter alternative is most like the improved Wolff deWardt theory that is recommended for conventional gyros and magnetic instruments. The mathematical derivation, including the derivation of weighting functions, will be given for this method.

Strapped down INS systems make use of gyros to measure changes in principal axis orientations as the instrument moves down the wellbore. The orientations are usually given in attitude angles to avoid problems with singularities, but any orthogonal set like for example inclination / azimuth / toolface can be used. This latter alternative is used in this study to secure as little difference from gyro instruments as possible. The measured changes in the orientation of the instrument is then given as a change in inclination (ΔI), a change in azimuth (ΔA) and a change in high-side toolface ($\Delta\tau$). By knowing the associated initial inclination, azimuth and toolfaces (I_0, A_0 and τ_0), the momentary orientation can be found by

$$I = I_0 + \Delta I \qquad \{8\text{-}1\}$$

$$A = A_0 + \Delta A \qquad \{8\text{-}2\}$$

$$\tau = \tau_0 + \Delta\tau \qquad \{8\text{-}3\}$$

The inclination and toolface can also be derived from accelerometer measurements. Either from all three, or just from the *x*- and *y*- accelerometer to secure against large axial accelerations. INS filters are optimising the inclination and toolface with respect to both gyro and accelerometer measurements. This process can be simplified for the uncertainty estimation by assuming that the *z*- accelerometer get less weight than the other two by introduction of axial acceleration noise, and that the real inclination and toolface uncertainty are near to the uncertainty of the optimal choice of accelerometer or gyro based angles.

The gyro based inclination, azimuth and toolface at measurement at station *j* are, if the same assumptions are used as for continuous gyros (chapter 6.1.1.6), given by

$$I_j \approx I_0 + \Delta t \Sigma_{k=i}^{j} \left(\frac{\partial I_k}{\partial t} \right) \qquad \{8\text{-}4\}$$

$$A_j \approx A_0 + \Delta t \Sigma_{k=i}^{j} \left(\frac{\partial A_k}{\partial t} \right) \qquad \{8\text{-}5\}$$

$$\tau_j \approx \tau_0 + \Delta t \Sigma_{k=i}^{j} \left(\frac{\partial \tau_k}{\partial t} \right) \qquad \{8\text{-}6\}$$

where $\frac{\partial I_j}{\partial t}$, $\frac{\partial A_j}{\partial t}$ and $\frac{\partial \tau_j}{\partial t}$ are the time derivatives of the inclination, azimuth and toolface at station *j*, and Δt the average time difference between two consecutive result recordings.

Equations *{8-4}* to *{8-6}* are showing a continuous accumulation of angular uncertainties as the survey progress down the wellbore. A continuous accumulation of angular errors throughout the survey may, however, not always reflect the actual error theoretical behaviour of INS systems. This is especially the case at zero velocity update stations for zero velocity update systems, where the accumulated gyro based inclination- and toolface uncertainties should be reset to the accelerometer based stationary inclination- and toolface uncertainties. The azimuth uncertainty should simultaneously be reset to the gyro compassing uncertainty. Wireline aided systems do not have the possibility for these stationary accuracy improvements, and will therefore have a continuous angular uncertainty growth throughout the survey as indicated in equations *{8-4}* to *{8-5}*.

Sensor misalignments are, as they where for other types of wellbore surveying equipment, small and without significance in INS systems. The instrument and collar misalignments, which are important error sources in traditional directional surveying, are of little interest in connection with INS systems. The misalignment will be estimated and corrected for in the optimisation of the *z*- axis movement, leaving only a negligible residual error.

The measured depth (travelled distance from time 0 to time *t*) sensed by an INS system is further given by

$$D = {}_0\int^t \left({}_0\int^{t'} \sqrt{a_N^2 + a_E^2 + a_V^2}\, dt' \right) dt \qquad \{8\text{-}7\}$$

where a_N, a_E and a_V are the momentary earth fixed north, east and vertical accelerations.

The depth change over the wellbore section between measurement station *j-1* and *j* is then given by (v_{j-1} is the momentary velocity at station *j-1*)

$$\Delta D_j = \int_{t_{j-1}}^{t_j} \left(\int_{t_{j-1}}^{\tau'} \sqrt{a_N^2 + a_E^2 + a_V^2}\, d\tau' + v_{j-1} \right) dt \qquad \{8\text{-}8\}$$

Accelerometers do not sense earth fixed accelerations, but inertial acceleration. Measured accelerations must therefore be corrected for the attraction from the earth, the earth centrifugal force and the Coriolis force. The Coriolis acceleration can be neglected in wellbore positioning uncertainty studies. It is usually less than 0.0015m/s^2, which is in the range of good accelerometer biases (0.002m/s^2). The uncertainty in the Coriolis acceleration estimation, which always is performed in INS systems, is much smaller than this, and therefore without significance compared to the accelerometer biases. The centrifugal acceleration can be more than 0.03m/s^2, which is about 15 times the accelerometer bias. Uncertainties of a few percent in the centrifugal force estimation might therefore be significant, and should be included in the error budget. The local gravity in use (G) is the combined effect of the earth attraction and the centrifugal force. Equation *{8-8}* substituted with the three accelerometer measurements (g_x, g_y and g_z) and the gravity (G) at measurement station *j* is then giving

$$\Delta D_j = \int_{t_{j-1}}^{t_j} \left(\int_{t_{j-1}}^{\tau'} \sqrt{(g_x - G_x)^2 + (g_y - G_y)^2 + (g_z - G_z)^2}\, d\tau' + v_{j-1} \right) dt \qquad \{8\text{-}9\}$$

where

$$G_x = -G \sin I \sin \tau \qquad \{8\text{-}10\}$$
$$G_y = -G \sin I \cos \tau \qquad \{8\text{-}11\}$$
$$G_z = G \cos I \qquad \{8\text{-}12\}$$

The output rate from existing wellbore INS systems is high enough to justify a no toolface rotation and straight line approximation between two consecutive measurement stations. Equation *{8-9}* can therefore be simplified to

$$\Delta D_j \approx \Delta t \left(\frac{\Delta t \sqrt{(g_{x,j} - G_{x,j})^2 + (g_{y,j} - G_{y,j})^2 + (g_{z,j} - G_{z,j})^2}}{2} + v_j \right) \qquad \{8\text{-}13\}$$

where $g_{x,j}$, $g_{y,j}$, $g_{z,j}$ are the three accelerometer measurements at station *j*, and v_j the instrument velocity at station *j*.

The instrument velocity is controlled by the wireline operator or through zero velocity updates, and is under normal running conditions nearly constant and directed along the wellbore axis (*z*- axis). The Rigs filters are for example designed to optimise for *z*- axis movements. v_j can therefore be substituted with an average theoretical *z*- axis velocity measurement (v_z) in wellbore position uncertainty studies. The accuracy of v_z (dv_z), which

is needed in this approach of position uncertainty calculations, will be dependent on the aiding system in use. It can be estimated as the uncertainty of wireline velocity measurements, or half the standard deviation of sensed velocities at zero velocity update stations. The wireline velocity uncertainty will have the same type of independent components as the wireline depth uncertainty (a random reference component, a systematic reference component, a systematic scale component proportional to the measured depth, and a bias stretch term proportional to the product of the depth and the vertical depth). The nature of the zero velocity uncertainty is not known, but is believed to consist of two independent systematic between stations components. One that is random between zero velocity update stations, and one that is random between surveys.

The measured depth at station j is then given by

$$D_j \approx \Sigma_{k=1}^{j} \left(\frac{\sqrt{\left(g_{x,k}-G_{x,k}\right)^2+\left(g_{y,k}-G_{y,k}\right)^2+\left(g_{z,k}-G_{z,k}\right)^2}\,\Delta t^2}{2} + v_z \Delta t \right) \qquad \{8\text{-}14\}$$

Schouler oscillations and other well known inertial error propagation effects (Savage [24]) are lost in this process, but this is not expected to introduce unacceptable model errors into the wellbore position uncertainty estimation process. The Schouler oscillation has a much smaller frequency compared to the zero velocity update frequency that will be needed, making the Schouler oscillation without significance for zero velocity systems. The same conclusion can be drawn for wireline systems, where the wireline velocity uncertainty will dominate over the Schouler effect.

8.1 The Rigs System

Two different Rigs systems are currently available. They are equipped with ring laser gyros from two different vendors. They have different design, and might therefore also have different error characteristics. The first ring laser gyro type (taken out of production) is used in all older Rigs system, while the second one will be used in coming tools. All Rigs surveys older than a couple of years are with the first type, while newer are questionable. A track of tool information is therefore needed for final survey accuracy analyses.

The error characteristics of ring laser gyros are well known and documented. Gibbons [27] indicates that biases and random errors are the dominant error types in wellbore surveying. Random errors turn out to be big enough to result in a random walk effects that are significant compared to the systematic bias effect. Scale factor and higher orders errors are not significant for this gyro type, and should not be included in the total error budget.

Two sets of uncertainty equations are necessary to establish Rigs uncertainties. It is stationary measurement equations and continuous equations. The stationary equations are used for initialisation.

8.1.1 *Continuous Uncertainties*

The resultant effect of the Rigs filter is that inclination and toolface mainly are determined through the accelerometer measurements, and the azimuth through gyro measurements. The inclination and toolface uncertainties are therefore given by similar equations as standard three accelerometer gyro instruments. The inclination uncertainty components at station *j* are then

$$dI_1 = -\frac{\cos I \sin\tau}{G} dg_{x1} \qquad \{8.1.1\text{-}1\}$$

$$dI_2 = -\frac{\cos I \sin\tau}{G} dg_{x2} \qquad \{8.1.1\text{-}2\}$$

$$dI_3 = -\frac{\cos I \cos\tau}{G} dg_{y1} \qquad \{8.1.1\text{-}3\}$$

$$dI_4 = -\frac{\cos I \cos\tau}{G} dg_{y2} \qquad \{8.1.1\text{-}4\}$$

$$dI_5 = -\frac{\sin I}{G} dg_{z1} \qquad \{8.1.1\text{-}5\}$$

$$dI_6 = -\frac{\sin I}{G} dg_{z2} \qquad \{8.1.1\text{-}6\}$$

$$dI_{11} = -\frac{\sin I}{G} dg_{z4} \qquad \{8.1.1\text{-}7\}$$

Accelerometer uncertainties (dg_{xi}, dg_{yi}, and dg_{zi}) are given in equations *{6.1.1.1-2}* to *{6.1.1.1-11}*. The last inclination uncertainty component is random between stations, while the rest usually are systematic within and random between surveys.

The toolface uncertainty is given by

$$d\tau = \sqrt{\frac{d\eta_a^2}{G\sin I} + 2\sin^2\tau\cos^2\tau d\upsilon_a^2} \qquad \{8.1.1\text{-}8\}$$

where G is the local gravity.

Making use of the same approach as for continuous gyros gives the following changes in azimuth ΔA_j between measurement station *j-1* and *j* (time difference Δt).

$$\Delta A_j = \int_{t_{j-1}}^{t_j} \left(\frac{\partial A}{\partial t}\right) dt \approx \Delta t \left(-\frac{\Delta\tau_j \cos I_j + \Delta t\left(\omega_{x,j}\sin\tau_j + \omega_{y,j}\cos\tau_j\right)\sin I_j - \Delta t\omega_{z,j}\cos I_j - \Delta t\Omega\sin\phi}{\Delta t} \right) \qquad \{8.1.1\text{-}9\}$$

where $\omega_{x,j}$, $\omega_{y,j}$ and $\omega_{z,j}$ are the three continuous ring laser gyro measurements (rotation rates around the three principal axis) at station *j*, and $\Delta\tau_j$ the measured change in toolface between station *j-1* and *j*.

The azimuth uncertainty components at measurement station *j* are then given by the following equations. They are based on the assumption that the change in azimuth and toolface is relatively small, and that the geometry of the traversed wellbore section is relatively uniform.

Page 141 Equation *{8.1.1-8}* $d\tau \approx \sqrt{\frac{d\eta_a^2}{G^2\sin^2 I} + 2\sin^2\tau\cos^2\tau d\upsilon_a^2}$

Equation *{8.1.1-9}* line 2 $\approx -(\Delta\tau_j\cos I_j + \Delta t(\omega_{x,j}\sin\tau_j + \omega_{y,j}\cos\tau_j)\sin I_j - \Delta t\omega_{z,j}\cos I_j - \Delta t\Omega\sin\phi)$

$$dA_{7,j} = dA_{7,j-1} + \Delta t \frac{\partial \frac{\partial A_j}{\partial t}}{\partial I} dI_{s,j} + \Delta t \frac{\partial \frac{\partial A_j}{\partial t}}{\partial \tau} d\tau_j$$
$$\approx dA_{7,j-1} - \Delta t \Omega \cos\phi \cos A_j dI_{s,j} + \sin I_j (\Delta I_j - \Delta t \Omega \cos\phi \sin A_j) d\tau_j \qquad \{8.1.1\text{-}10\}$$

$$dA_{21,j} = dA_{21,j-1} + \Delta t \frac{\partial \frac{\partial A_j}{\partial t}}{\partial \phi} d\phi \approx dA_{21,j-1} + \Delta t \Omega \cos\phi d\phi \qquad \{8.1.1\text{-}11\}$$

$$dA_{28,j} = dA_{28,j-1} + \Delta t \frac{\partial \frac{\partial A_j}{\partial t}}{\partial \omega_x} d\sigma_r \approx dA_{28,j-1} - \Delta t \sin I_j \sin\tau_j d\sigma_r \qquad \{8.1.1\text{-}12\}$$

$$dA_{29,j} = dA_{29,j-1} + \Delta t \frac{\partial \frac{\partial A_j}{\partial t}}{\partial \omega_x} d\eta_r \approx dA_{29,j-1} - \Delta t \sin I_j \sin\tau_j d\eta_r \qquad \{8.1.1\text{-}13\}$$

$$dA_{30,j} = dA_{30,j-1} + \Delta t \frac{\partial \frac{\partial A_j}{\partial t}}{\partial \omega_y} d\sigma_r \approx dA_{30,j-1} - \Delta t \sin I_j \cos\tau_j d\sigma_r \qquad \{8.1.1\text{-}14\}$$

$$dA_{31,j} = dA_{31,j-1} + \Delta t \frac{\partial \frac{\partial A_j}{\partial t}}{\partial \omega_y} d\eta_r \approx dA_{31,j-1} - \Delta t \sin I_j \cos\tau_j d\eta_r \qquad \{8.1.1\text{-}15\}$$

$$dA_{32,j} = dA_{32,j-1} + \Delta t \frac{\partial \frac{\partial A_j}{\partial t}}{\partial \omega_z} d\sigma_r \approx dA_{32,j-1} + \Delta t \cos I_j d\sigma_r \qquad \{8.1.1\text{-}16\}$$

$$dA_{33,j} = dA_{33,j-1} + \Delta t \frac{\partial \frac{\partial A_j}{\partial t}}{\partial \omega_z} d\eta_r \approx dA_{33,j-1} + \Delta t \cos I_j d\eta_r \qquad \{8.1.1\text{-}17\}$$

$d\sigma_r$ and $d\eta_r$ are the ring laser gyro random and bias uncertainties, and $d\phi$ the latitude uncertainty. The toolface uncertainty ($d\tau_j$) is given by equation *{8.1.1-8}*, and the sensor dependent inclination uncertainty are given by

$$dI_{s,j} = \sqrt{\Sigma_{i=1}^{6} dI_{i,j}^2 + dI_{11,j}^2} \qquad \{8.1.1\text{-}18\}$$

$dI_{i,j}$ are the sensor induced inclination uncertainty components at station j given by equations *{8.1.1-1}* to *{8.1.1-7}*.

It is, like for the continuous gyro tools, recommended to treat the bias components as systematic within surveys and random between surveys. The random components are of course random between stations.

The systematic within and random between surveys reference uncertainty is given by

$$dA_{26} = \sqrt{dA_7^2 + \Sigma_{i=28}^{33} (dA_i^2)} \qquad \{8.1.1\text{-}19\}$$

where dA_i are significant uncertainty components in the north seeking reference measurements given in equations *{8.1.2-2}* and *{8.1.2-4}* to *{8.1.2-9}* (next chapter).

The depth uncertainty components can be found by partial differentiation of equation *{8-14}* with respect to the four wireline aided logging speed uncertainty components (the random reference component dv_{z1}, the systematic reference component dv_{z2}, the systematic scale component proportional to the measured depth dv_{z3}, and the bias stretch component proportional to the product of the depth and the vertical depth dv_{z4}). It is not necessary to include the accelerometer uncertainties. They are without significance in the final result when the artificial logging speed measurement is used in the uncertainty estimation. Accelerations are generally small between two consecutive stations compared to the logging speed, and there are no accelerometer dependent singularities in equation *{8-14}*.

$$dD_{5,j} \approx \Delta t dv_{z1} \qquad \{8.1.1\text{-}20\}$$
$$dD_{6,j} \approx \Delta t dv_{z2} \qquad \{8.1.1\text{-}21\}$$
$$dD_{7,j} \approx \Delta t D_j dv_{z3} \qquad \{8.1.1\text{-}22\}$$
$$dD_{8,j} \approx \Delta t D_j D_{vj} dv_{z4} \qquad \{8.1.1\text{-}23\}$$

where D_j is the calculated or planned depth at measurement recording station j, and D_{vj} is the calculated or planned vertical depth at measurement recording station j given by

$$D_{vj} = l\left(\frac{\cos I_j}{2} + \Sigma_{k=1}^{j-1}\cos I_k\right) \qquad \{8.1.1\text{-}24\}$$

where l is the recording station separation.

The sensor dependent inclination uncertainty and the toolface uncertainty used in equation *{8.1.1-10}* are derived from accelerometer measurements. Equation *{8.1.1-10}* should therefore be substituted with seven uncorrelated accelerometer uncertainty components to avoid the problem with unknown correlation in the position uncertainty calculation.

$$dA_{7\_1,j} = dA_{7\_1,j-1} + \frac{\Delta t\Omega\cos\phi\cos I_j\cos A_j\sin\tau_j - \cos\tau_j\left(\Delta I_j - \Delta t\Omega\cos\phi\sin A_j\right)}{G} dg_{x1} \qquad \{8.1.1\text{-}25\}$$
$$dA_{7\_2,j} = dA_{7\_2,j-1} + \frac{\Delta t\Omega\cos\phi\cos I_j\cos A_j\sin\tau_j - \cos\tau_j\left(\Delta I_j - \Delta t\Omega\cos\phi\sin A_j\right)}{G} dg_{x2} \qquad \{8.1.1\text{-}26\}$$

$$dA_{7\_3,j} = dA_{7\_3,j-1} + \frac{\Delta t\Omega\cos\phi\cos I_j\cos A_j\cos\tau_j + \sin\tau_j\left(\Delta I_j - \Delta t\Omega\cos\phi\sin A_j\right)}{G} dg_{y1} \qquad \{8.1.1\text{-}27\}$$
$$dA_{7\_4,j} = dA_{7\_4,j-1} + \frac{\Delta t\Omega\cos\phi\cos I_j\cos A_j\cos\tau_j + \sin\tau_j\left(\Delta I_j - \Delta t\Omega\cos\phi\sin A_j\right)}{G} dg_{y2} \qquad \{8.1.1\text{-}28\}$$

$$dA_{7\_5,j} = dA_{7\_5,j-1} + \frac{\Delta t\Omega\cos\phi\sin I_j\cos A_j}{G} dg_{z1} \qquad \{8.1.1\text{-}29\}$$
$$dA_{7\_6,j} = dA_{7\_6,j-1} + \frac{\Delta t\Omega\cos\phi\sin I_j\cos A_j}{G} dg_{z2} \qquad \{8.1.1\text{-}30\}$$

$$dA_{7\_11,j} = dA_{7\_11,j-1} + \frac{\Delta t\Omega\cos\phi\sin I_j\cos A_j}{G} dg_{z4} \qquad \{8.1.1\text{-}31\}$$

Accelerometer uncertainties (dg_{x1}, dg_{x2}, dg_{y1}, dg_{y2}, dg_{z1}, dg_{z2} and dg_{z4}) are given in equations *{8.1.1-1}* to *{8.1.1-7}*.

dA_{7_1} through dA_{7_6} are systematic within surveys and random between surveys, and dA_{7_11} is random between stations.

The following error components should be treated as correlated errors in the position co-variance calculation if accelerometer uncertainties are used as input in the azimuth uncertainty calculation

- dI_1 and dA_{7_1} (Both caused by the *x*- accelerometer bias uncertainty)
- dI_2 and dA_{7_2} (Both caused by the *x*- accelerometer scale factor uncertainty)
- dI_3 and dA_{7_3} (Both caused by the *y*- accelerometer bias uncertainty)
- dI_4 and dA_{7_4} (Both caused by the *y*- accelerometer scale factor uncertainty)
- dI_5 and dA_{7_5} (Both caused by the *z*- accelerometer bias uncertainty)
- dI_6 and dA_{7_6} (Both caused by the *z*- accelerometer scale factor uncertainty)
- dI_{11} and dA_{7_11} (Both caused by axial accelerations)

8.1.2 *Stationary Uncertainties*

Stationary RIGS measurements are in normal operations only taken in connection with initialisation of continuous measurements. Stationary RIGS uncertainties are therefore to be handled as reference uncertainties in wellbore position uncertainty studies.

Stationary inclination and toolface uncertainties are given by the same uncertainty equations as continuous uncertainties (equations *{8.1.1-1}* to *{8.1.1-8}*) with exception the axial acceleration component (equation *{8.1.1-7}*), which is not applicable for stationary measurements.

The initial Rigs north seeking reference measurement can in uncertainty estimations without loss of estimation accuracy be substituted with an azimuth measurement near to 90°. It is given by

$$A = \arccos \frac{(\omega_x \sin\tau + \omega_y \cos\tau)\cos I + \omega_z \sin I}{\Omega \cos\phi} \qquad \{8.1.2\text{-}1\}$$

where ω_x, ω_y and ω_z are the three stationary ring laser gyro measurements (earth rotation rates around the three principal axis).

The reference azimuth uncertainty components are then given by the following set of equations (the azimuth is expected to be near 90°).

$$dA_7 = \frac{\partial A}{\partial I} dI + \frac{\partial A}{\partial \tau} d\tau \approx \frac{\sin\phi}{\cos\phi} dI - d\tau \qquad \{8.1.2\text{-}2\}$$

$$dA_{21} = \frac{\partial A}{\partial \phi} d\phi \approx 0 \qquad \{8.1.2\text{-}3\}$$

Page 144 Equation *{8.1.2-3}* $dA_7 = \frac{\partial A}{\partial I} dI + \frac{\partial A}{\partial \tau} d\tau \approx \frac{\sin\phi}{\cos\phi} dI - \cos I d\tau$

$$dA_{28} = \frac{\partial A}{\partial \omega_z} d\sigma_r = -\frac{\cos I \sin \tau}{\Omega \cos \phi \sin A} d\sigma_r \approx -\frac{\cos I \sin \tau}{\Omega \cos \phi} d\sigma_r \qquad \{8.1.2\text{-}4\}$$

$$dA_{29} = \frac{\partial A}{\partial \omega_z} d\eta_r \approx -\frac{\cos I \sin \tau}{\Omega \cos \phi} d\eta_r \qquad \{8.1.2\text{-}5\}$$

$$dA_{30} = \frac{\partial A}{\partial \omega_y} d\sigma_r \approx -\frac{\cos I \cos \tau}{\Omega \cos \phi} d\sigma_r \qquad \{8.1.2\text{-}6\}$$

$$dA_{31} = \frac{\partial A}{\partial \omega_y} d\eta_r \approx -\frac{\cos I \cos \tau}{\Omega \cos \phi} d\eta_r \qquad \{8.1.2\text{-}7\}$$

$$dA_{32} = \frac{\partial A}{\partial \omega_z} d\sigma_r \approx -\frac{\sin I}{\Omega \cos \phi} d\sigma_r \qquad \{8.1.2\text{-}8\}$$

$$dA_{33} = \frac{\partial A}{\partial \omega_z} d\eta_r \approx -\frac{\sin I}{\Omega \cos \phi} d\eta_r \qquad \{8.1.2\text{-}9\}$$

Equation *{8.1.2-2}* may, as for continuous gyros, be substituted with uncorrelated accelerometer uncertainty components.

$$dA_{7\_1} = \left(-\frac{\sin \phi \cos I_j \sin \tau_j}{G \cos \phi} + \frac{\cos \tau_j}{G \sin I_j} \right) dg_{x1} \qquad \{8.1.2\text{-}10\}$$

$$dA_{7\_2} = \left(-\frac{\sin \phi \cos I_j \sin \tau_j}{G \cos \phi} + \frac{\cos \tau_j}{G \sin I_j} \right) dg_{x2} \qquad \{8.1.2\text{-}11\}$$

$$dA_{7\_3} = \left(-\frac{\sin \phi \cos I_j \cos \tau_j}{G \cos \phi} - \frac{\sin \tau_j}{G \sin I_j} \right) dg_{y1} \qquad \{8.1.2\text{-}12\}$$

$$dA_{7\_4} = \left(-\frac{\sin \phi \cos I_j \cos \tau_j}{G \cos \phi} - \frac{\sin \tau_j}{G \sin I_j} \right) dg_{y2} \qquad \{8.1.2\text{-}13\}$$

$$dA_{7\_5} = -\frac{\sin \phi \sin I_j}{G \cos \phi} dg_{z1} \qquad \{8.1.2\text{-}14\}$$

$$dA_{7\_6} = -\frac{\sin \phi \sin I_j}{G \cos \phi} dg_{z2} \qquad \{8.1.2\text{-}15\}$$

Accelerometer uncertainties (dg_{x1}, dg_{x2}, dg_{y1}, dg_{y2}, dg_{z1} and dg_{z2}) are given in equations *{8.1.1-1}* to *{8.1.1-6}*.

dA_{7_1} through dA_{7_6} are systematic within surveys and random between surveys.

The following error components should be treated as correlated errors in the position co-variance calculation if accelerometer uncertainties are used as input in the azimuth uncertainty calculation

- dI_1 and dA_{7_1} (Both caused by the *x*- accelerometer bias uncertainty)
- dI_2 and dA_{7_2} (Both caused by the *x*- accelerometer scale factor uncertainty)
- dI_3 and dA_{7_3} (Both caused by the *y*- accelerometer bias uncertainty)
- dI_4 and dA_{7_4} (Both caused by the *y*- accelerometer scale factor uncertainty)
- dI_5 and dA_{7_5} (Both caused by the *z*- accelerometer bias uncertainty)
- dI_6 and dA_{7_6} (Both caused by the *z*- accelerometer scale factor uncertainty)

9 Summary

Basic Wellbore Positioning Error Propagation Theory

Errors associated with directional surveying can be divided into three fundamental classes, errors that are random between survey stations, errors that are systematic between a given number of stations, and errors that are systematic for all stations in a region (biases). Biases can usually be estimated and corrected for to avoid problems related to numerical quantification of skew uncertainties. Residual errors after bias correction will for a large number of surveys be transformed to systematic errors for a given number of stations.

The following error propagation relationships have been identified in connection with wellbore surveying

- The wellbore position uncertainties caused by random errors are near to proportional with the square root of the number of survey stations.
- The wellbore position uncertainties caused by systematic errors are near to proportional with the number of survey stations for traditional wellbore designs. Systematic error propagation is therefore far more critical than random error propagation.
- Systematic error propagation is dependent on wellbore geometry. The resultant effect of systematic errors may sometimes cancel out for example by azimuth reversal. Randomisation of systematic errors due to toolface rotations are also commonly seen.
- Systematic errors are usually systematic within and random between surveys, systematic within or random between wellbores, or systematic within fields.
- Random errors can in most cases be neglected as long as they are of the same magnitude or less than the systematic errors, and as long as not all systematic effects are cancelling out (will hardly never happen).
- The final wellbore position accuracy of a gyro survey can be significantly increased by splitting the entire wellbore profile into consecutive survey sections. Each section has to be surveyed independently with different instruments.
- MWD surveys will only be slightly improved by a similar approach.
- A statistical use of the redundant information in overlapping consecutive survey sections, or in multiple wellbore surveys, will improve the wellbore position accuracy significantly in addition to the searched security against gross errors.

Weighting Functions

Directional surveying uncertainties are related to sensor errors, different types of misalignments, and environmental effects like magnetic interference etc. Each error source propagates into the inclination-, the azimuth- and / or the toolface uncertainties, and further into the wellbore position uncertainties. Mathematical functions describing how the different error sources propagates into inclination-, azimuth- or toolface uncertainties are called weighting functions. They should reproduce any significant changes in sign and size of the angular uncertainties caused by wellbore geometry, geographic location, thermal gradients etc.

Wellbore Position Uncertainty Figures

Uncertainties associated with bias free wellbore positions can easily be communicated through well known statistical quantities like confidence intervals, uncertainty ellipses and uncertainty ellipsoids. Confidence intervals are convenient for vertical depth uncertainties and for minimum wellbore separation calculations. Error ellipses are most suited for horizontal- and normal plane uncertainties (normal to the wellbore axis), and error ellipsoids for full 3D uncertainties. Confidence intervals, error ellipses and error ellipsoids are directly linked to the position co-variance matrix at a survey station. It is, however, generally not any easy internal relationship between them, for example through the radius of the ellipsoid etc. Each alternative has usually to be calculated directly out of the position co-variance matrix. Intervals, ellipses and ellipsoids calculated out of a co-variance matrix can be scaled up to any confidence level. Scaling factors will be different for the three cases.

- The 95% confidence interval scaling factor is 1.96
- The 95% 2D uncertainty ellipse scaling factor is 2.49
- The 95% 3D uncertainty ellipsoid scaling factor is 2.80

Published Directional Surveying Error Propagation Theories

Three published directional surveying error propagation theories are currently available. It is the Walstrom model, the Wolff deWardt model and the Instrument performance model.

The Walstrom model is a pure random model. It was rejected as unsatisfactory many years ago, due to underestimation of uncertainties commonly seen in the field.

The Wolff deWardt model is a pure systematic model, which have been regarded as an industry standard for many years. A number of limitations have been identified. Some of them are critical enough to make the basic Wolff deWardt model unsuited for many present survey instruments and methods. Among the most serious limitations are

Page 147 Line 2 paragraph 3 *factor is 2.49* should be **factor is 2.45**

- Improper weighting functions that can lead to wrong conclusions.
- Neglecting of random errors in cases where the systematic errors are cancelling out.
- No method given for adequate connection of independent survey sections.
- No given confidence level.

The Instrument performance model is a combined random, systematic and bias model. It has already been available for some years, but has not been adopted as an industry standard. It has a different depth error handling compared to the standard within the directional surveying industry. This complicates position uncertainty analyses of inertial surveys and redundant survey programs.

Magnetic MWD Uncertainties

Wellbore position uncertainties in connection with magnetic surveys (MWD or EMS) are usually caused by environmental effects, but sensor errors are also important in cases where the mathematical azimuth solution has a singularity. Such singularities are found in these two cases.

- At the magnetic poles. The inclination uncertainty is proportional to $\frac{1}{\cos(mag.latitude)}$.
- For horizontal magnetic east / west wellbores when axial magnetic corrections are applied. The azimuth uncertainty is proportional to $\frac{1}{1-\left(\sin^2(inclination)*\sin^2(mag.azimuth)\right)}$.

The most significant environmental error sources in connection with magnetic surveys are

- Variations in the magnetic declination caused by "atmospheric"- and local crust effects. Similar variations in the magnetic dip and in the earth total field are also important when axial corrections are applied.
- Magnetic interference caused by axial drill string magnetisation for measurements without axial corrections. The cross axial component is usually without significance.
- Magnetic interference from existing casings when drilling close to them.
- Misalignments of the instrument within the collar, and misalignments of the collar within the borehole (sag).

Gyro Compassing Uncertainties

Both environmental- and sensor effects have to be taken into consideration in connection with north seeking gyro (gyro compassing) uncertainties. The following singularities caused by sensor errors are found in the mathematical azimuth solution.

- An inclination singularity for horizontal wellbores for two accelerometer systems. The inclination uncertainty is proportional to $\frac{1}{\cos(inclination)}$ ($\frac{1}{\cos(inclination+cant\_angle)}$ for canted systems).

- An azimuth singularity at the poles and for horizontal wellbores. The azimuth uncertainty is proportional to $\frac{1}{\cos(latitude)*\cos(inclination)}$.

The most significant gyro compassing errors are for rotor gyro instruments given by

- Accelerometer scale factor errors.
- Gyro scale factor errors.
- Spin axis mass unbalances. Some systems are also affected by input axis mass unbalances.
- Misalignments of the instrument within the instrument collar, and misalignments of the instrument collar within the borehole when run inside drill pipes.
- Uncertainties in input parameters such as local gravity and local latitude.

Continuous Gyro Uncertainties

Modern continuous high accuracy gyros are not discrete systems like traditional directional systems (magnetic- and gyro compassing instruments). They are designed for continuously surveying of the entire wellbore profile. They do therefore not fit directly into the survey station to station approach given by Wolff and deWardt. Current surveying practice is, however, only to record measurements taken at given intervals (every 10 meter or less in high curvatures). High accuracy gyros are therefore logically also discrete systems. This fact can be used in the derivation of weighting functions for an improved Wolff deWardt error propagation theory.

All available continuous gyro systems are affected by sensor dependent singularities. Different systems can suffer from different singularities. Possible singularities are

- An inclination singularity for canted systems. The inclination uncertainty is proportional to $\frac{1}{\cos(inclination-cant\_angle)}$.

- An azimuth singularity for vertical wellbores. The azimuth uncertainty is proportional to $\frac{1}{\sin(inclination)}$. Systems suffering from this singularity are used as stationary gyro compassing instruments at smaller inclinations (usually up to 15°).

The most significant error sources for continuous rotor gyro instruments are

- Accelerometer bias and scale factor errors.
- Gyro bias and scale factor errors.
- Spin- and input axis mass unbalances.
- Misalignments of the instrument within the instrument collar, and misalignments of the collar within the borehole when run inside drill pipes.
- Uncertainties in input parameters such as local gravity and local latitude.

Depth Uncertainties

Depth errors in connection with drill string- and wireline depth measurements suffer from many error sources, where the following are among the most dominant

- Reference point errors.
- Telescopic and drill string / wireline suspension effects.
- Measuring tape / wheel errors.
- Stretch and temperature effects.
- Pressure and mud flow effects.
- Wireline effects like twisting, inelastic stretch, buckling etc.

Input parameters needed in the estimation of these depth error components are usually not available during wellbore position uncertainty predictions. As a substitute for exact estimates of these depth errors, it is possible to create four empirical depth uncertainty components that together account for more than 80% off the total depth error. They are

- A random between stations reference error component.
- A systematic within surveys reference error component.
- A systematic within surveys scale error component (proportional to the measured depth).
- A bias stretch / temperature error component (proportional to the product of the measured depth and the vertical depth).

It is recommended that these four simplified depth weighting functions are used in wellbore position uncertainty predictions instead of the complete set of detailed depth weighting functions.

Inertial Navigation Systems Uncertainties

Modern inertial navigation systems (INS) are, like continuous gyro systems, designed for continuous surveying of entire wellbore profiles. They can, because of an discrete recording practice, logically be looked upon as discrete systems. This fact can be used to create weighting functions that fit into the framework of an improved Wolff deWardt theory.

There are currently two types of INS systems in use, wireline aided- and zero velocity update systems. Wireline aided systems are affected by three major uncertainty drivers, uncertainties in the wireline depth measurements, uncertainties in the initial angular reference determination and sensor dependent uncertainties. Zero velocity systems are only affected by the latter two.

Inertial systems do not show any sensor dependent singularities.

Error sources such as misalignments have usually very little significance on the wellbore position estimate due to specially designed filtering techniques.

10 Conclusions and Recommendations

Wellbore position surveying is affected by many different error sources. Both random errors, biases and other types of systematic errors are usually present. Random errors have more favourable error propagation characteristics (proportional with the square root of the number of survey stations) than biases and systematic errors (proportional with the number of survey stations), and are resulting in much smaller position uncertainties. It should therefore be focused on removal or reduction of biases and systematic errors in connection with accuracy improvement programs.

Biases result in skew uncertainties, which easily are misinterpreted. This problem can be avoided by correction for biases with a priori estimates. This correction, which always is recommended, transform a bias to a smaller systematic error. This leads to a reduction of the total uncertainty.

The effect of different error sources on the wellbore position are a function of wellbore geometry, geographical location etc. Many instrument types and surveying techniques do in certain cases suffer from mathematical singularities. It is therefore important to have a tool designed for planning of optimal survey programs with respect to required accuracy. Three published tools are currently available. It is the Walstrom-, the Wolff deWardt- (industry standard) and the Instrument performance error propagation models. There are identified problems with all of them, and it is concluded that they should be substituted with a new method. This new method should fulfil the following goals

- It should be an evolution of the Wolff deWardt theory (the industry standard) to reduce possible confusion and resistance within the oil industry.

- It should be comprehensive enough to give a realistic picture of the position uncertainty for all present and coming instruments and techniques such as continuous high accuracy gyros and inertial navigation systems.

- It should be accompanied by standard procedures on how to add new instruments and running procedures into this new method.

Such a error propagation theory is currently under development by the "Industry Steering Committee on Wellbore Survey Accuracy" (ISCWSA). The work presented in this theses is a major contribution to the steering committee work. A first version is currently under implementation in a leading well planning software.

The new method has to be accompanied by realistic uncertainty figures / predictions for all error sources which are identified as significant. It has to be distinguished between different running procedures and levels of quality control. It is recommended that these uncertainty figures are established in two steps. A first version data set based on current knowledge (best guess) should be established as soon as possible. A second version based

on laboratory measurements and redundant field data, should then be established when enough gross error free field data are collected. ISWCA has started the compilation of the first version of MWD figures. Depth uncertainty figures presented in this theses is a contribution to this work.

To secure the validity of uncertainty figures, they should be accompanied by a set of quality control procedures for each type of wellbore position surveying. The derivation of such procedures is regarded as one of the most important task for the near future.

Accurate depth error estimation involves twenty seven different error equations. They are dependent on varying parameters such as the mechanical properties of drill strings and wirelines, thermal gradients, mud pressure, and flow rates. Exact values will usually not be available during wellbore planning. It is shown that these equations can be replaced with four empirical depth uncertainty equations in uncertainty studies. A few angular error sources, such as sag and drill string magnetisation, are also dependent on drill string properties unknown during wellbore planning. It should be investigated whether it also for these error sources are possible to create simplified empirical uncertainty equations.

Modern extended reach and designer wellbores are often surveyed with independent consecutive survey sections overlapping each other. The redundant information present in these surveys are currently used only for gross error control. The redundant information can, however, also be used to improve the final wellbore position estimate significantly. It is therefore recommended that a statistical adjustment theory for redundant wellbore positioning survey programs is developed as soon as possible.

11 References

1. J. Holsen, "Landmåling" part two, Institute of Geodesy and Photogrammetry, Norwegian Institute of Technology, Trondheim, Norway, 1978

2. T. Torkildsen, "Minste kvadraters metode og hypoteseprøving", Institute of Geodesy and Photogrammetry, Norwegian Institute of Technology, Trondheim, Norway, 1978

3. J. M. Tienstra, "Het rekenen met gewichtsgetallen", Tijdschrift voor Kadaster en Landmeetkunde, The Netherlands, 1934

4. J. Holsen, "Das Mittlere Fehlerellipsoid", Vermessung Photogrammetrie Kulturtechnik, Switzerland, 1956

5. R. P Harvey, J. E. Walstrom, H. D. Eddy, "A Mathematical Analysis of Errors in Directional Survey Calculations", Journal of Petroleum Technology, November 1971

6. C. J. M. Wolff, J. P. de Wardt, " Borehole Position Uncertainty - Analysis of Measuring Methods and Derivation of Systematic Error Model", Journal of Petroleum Technology, December 1981

7. J. L. Thorogood, "Instrument Performance Models and Their Application to Directional Surveying Operations", SPE 18051, Society of Petroleum Engineers, 1988

8. J. I. Lange, G. D. N. Twilhaar, J. J. Pelgrom, "Accurate Surveying: An Operators Point of View", SPE 17213, Society of Petroleum Engineers, 1988

9. J. N. Truex, "Directional Surveys Problems, East Wilmington Oil Field, California", The American Association of Petroleum Geologists Bulletin V. 55 No. 4, 1971

10. J. L. Thorogood, "How to Get the Best Results from Well-Surveying Data", World Oil, 1986

11. B. Guo, R. L. Lee, S. Miska, "Constant-Curvature Equations Improve Design of 3-D Well Trajectory", Oil and Gas Journal, April 19, 1993

12. A. G. Brooks, H. Wilson, "An Improved Method for Computing Wellbore Position Uncertainty and its Application to Collision and Target Intersection Probability Analysis", SPE 36863, Society of Petroleum Engineers, 1995

13. T. Torkildsen, R. H. Sveen, J. Bang, "Geomagnetic Reference, Report No. 1 - Time Dependent Variations of Declination", IKU Petroleum Research, Trondheim, Norway, 1997

14. G. McElhinney, "Minutes of the 6th Industry Steering Committee on Wellbore Survey Accuracy in Vienna 24-25 June 1997 written by Hugh Williamson", 1997

15. O. Lotsberg, Marianne Stavland, Andy Brooks, "Measurements of Magnetization of BHA Components" (to be published), Baker Hughes INTEQ, Norway, 1997

16. M. Coles, "Method to Improve Directional Survey Accuracy", US Patent No. 4956921, 1990

17. H. Engebretson, "Error Reduction in Compensation of Drill String Interference For Magnetic Survey Tools", US Patent No. 5155916, 1992

18. A. W. Russell, R. F. Roesler, "Reduction of Nonmagnetic Drill Collar Length Through Magnetic Azimuth Correction Technique", SPE 13476, Society of Petroleum Engineers, 1985

19. D. Van Steenwyk, "Borehole Initial Alignment and Change Determination", US Patent No. 4706388, 1987

20. M. K. Russell, A. W. Russell, "Gyro-Stabilized Single-Axis Platform", US Patent No. 4071959, 1978

21. G. Uttecht, J. Brosnahan, E. Wright, G. Neubauer, "Rate Gyro Wells Survey System Including Nulling System", Canadian Patent No. 2165626, 1996

22. K. Noy, J. Leonard, "New Gyroscopic System Extends Wellbore-Survey Options", SPE 37664, Society of Petroleum Engineers, 1997

23. D. C. Brown, F. L. Watson, "Drill Steering in High Magnetic Interference Areas", US Patent No. 4909336, 1990

24. P. G. Savage, "Introduction to Strapdown Inertial Navigation Systems", Lecture Notes, Strapdown Associates Inc., Minnetonka, Minnesota, USA, 1991

25. R. Ekseth, E. I. Nakken, L. K. Jensen "Wellbore Position Uncertainty Calculation - A Tool for Risk Based Decision Making", Offshore Mediterranean Conference '97, Ravenna, Italy, 1997

26. Å. Kyllingstad, "Depth Correction Theory", DEA Report, Rogaland Research, Stavanger, Norway, 1992

27. P. Theys, "Log Data Acquisition and Quality Control", ISBN 2-7108 0601-0, Editions Technip, Paris, France, 1991

28. M. E. Ander, W. Kerr, C. L. V. Aitken, C. C. Glover, M. A. Zumberge, " An Absolute Wireline Calibration to Support a Test of Newton's Inverse Square Law", Geophysics V. 55 No. 7, 1990

29. F. L. Gibbons, U. Hense, "A Three-Axis Laser Gyro System for Borehole Wireline Surveying", SPE 16679, Society of Petroleum Engineers, 1987

30. D.H. Zijsling, R. A. Wilson, "Improved Magnetic Surveying Techniques: Field Experience", SPE 19239, Society of Petroleum Engineers, 1989

31. S. J. Grindrod, J. M. Wolff, "Calculation of NMDC Length Required for Various Latitudes Developed From Field Measurements of Drill String Magnetisation", SPE 11382, Society of Petroleum Engineers, 1983

32. C. K. Pratt, R. A. Hartmann, "A Magnetostatic Well Tracking Technique For Drilling of Horizontal Parallel Wells", SPE 28319, Society of Petroleum Engineers, 1994

12 Nomenclature

Symbol	Name
A	Azimuth
A_m	Magnetic azimuth
B	Local magnetic field strength
D	"Measured depth"
D_V	Vertical depth
E	East
E_w	Young's modulus of wirelines
E_Y	Young's modulus of steel
G	Local gravity
H	Angular momentum vector of a spinning mass
I	Inclination
M	Gyro mass unbalance
N	North
P_p	Stand pipe pressure
Q	Mud flow rate
T_c	Continuous rotor gyro measurement
T_g	Formation temperature gradient
T_n	Rotor gyro compassing measurement
T_t	Measuring tape temperature
V	Vertical
W	Load
a	Pipe cross sectional area
a_z	Axial accelerations
b	Magnetic measurement
$d...$	Uncertainty in ...
f_b	Ballooning factor
g	Gravity measurement

Symbol	Name
i_p	Pump on/off identification
i_s	Survey type indicator
k	Estimated constants
l	Pipe length
m	Misalignment angle
p_m	Magnetic pole strength
s	Sag misalignment angle
t	Time
v_s	Logging speed
$\Delta...$	Actual change in ...
Θ	Magnetic dip
ϕ	Local latitude
Γ	Observation co-variance matrix
Λ	Design matrix
Ψ	Annulus pressure loss
Σ	Position co-variance matrix
Ω	Earth angular rate
α	Temperature expansion constant
γ	Cant angle
δ	Magnetic declination
ε	Relative deformation
η	Bias
κ	Pressure loss factor
μ	Friction factor
ν_p	Poisson's ratio
ρ	Density
σ	Standard deviation
τ	High-side toolface
τ_A	Azimuth toolface
υ	Scale factor
ω	Ring laser gyro measurement
ω_H	Angular rotation vector perpendicular to $\boldsymbol{H}$

ISBN 82-471-0218-8
ISSN 0802-3271